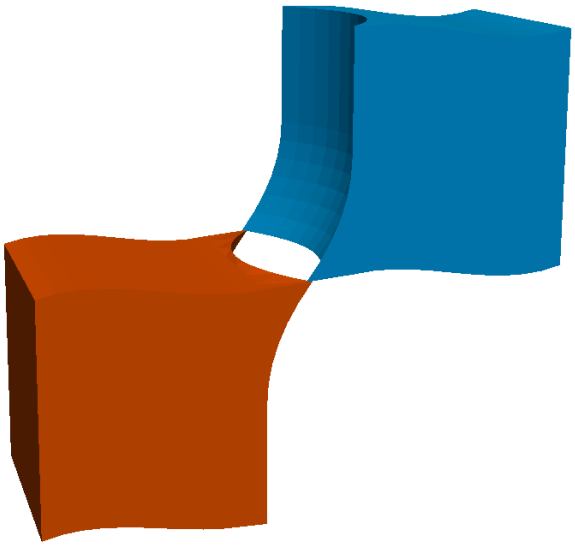

Adaptive FETI-DP and BDDC methods for highly heterogeneous elliptic finite element problems in three dimensions

inaugural-dissertation

zur
Erlangung des Doktorgrades
der Mathematisch-Naturwissenschaftlichen Fakultät
der Universität zu Köln

vorgelegt von
Martin Joachim Kühn
aus Dormagen

Köln, 2018

Berichterstatter: Prof. Dr. Axel Klawonn
(Universität zu Köln)

Prof. Dr. Oliver Rheinbach
(TU Bergakademie Freiberg)

Tag der letzten mündlichen Prüfung: 20.04.2018

Abstract

Numerical methods are often well-suited for the solution of (elliptic) partial differential equations (PDEs) modeling naturally occuring processes. Many different solvers can be applied to systems which are obtained after discretization by the finite element method.

Parallel architectures in modern computers facilitate the efficient use of diverse divide and conquer strategies. The intuitive approach, to divide a large (global) problem into subproblems, which are then solved in parallel, can significantly reduce the solution time. It is obvious that the solvers on the local subproblems then should deliver the contributions of the global solution restricted to the subdomains of computational region. The class of domain decomposition methods provides widely-used iterative algorithms for the parallel solution of implicit finite element problems. Often, an additional coarse space, which introduces a coupling between the subdomains, is used to ensure a global transport of information between the subdomains across the entire domain.

The FETI-DP and BDDC domain decomposition methods are highly scalable parallel algorithms. However, when the parameter or coefficient distribution in the underlying partial differential equation becomes highly heterogeneous, classical methods, with a priori chosen coarse spaces, might not converge in a limited number of iterations. A remedy is offered by problem-dependent coarse spaces. These coarse spaces can be provided by adaptive methods, which then can improve the convergence at the cost of additional constraints.

In this thesis, we introduce robust FETI-DP and BDDC methods for three-dimensional problems. These methods incorporate constraints, which are computed from local eigenvalue problems on faces and edges between subdomains, into the coarse space. The implementation of the constraints is performed by a deflation or balancing approach or by partial finite element assembly after a transformation of basis. For the latter, we introduce the generalized transformation-of-basis approach and show its correspondence to a deflation or balancing approach.

An efficient parallel implementation of adaptive FETI-DP is discussed in the last part of this thesis. We provide weak and strong parallel scalability results for our adaptive algorithm executed on the supercomputer magnitUDE of the University of Duisburg-Essen. For weak scaling, we can show very good results up to 4 096 cores. We can also present very good strong scaling results up to 864 cores.

Zusammenfassung

Numerische Verfahren sind häufig geeignete Verfahren zur Lösung (elliptischer) partieller Differentialgleichungen (PDGLen), welche natürlich auftretende Prozesse beschreiben. Viele unterschiedliche Löser können dabei auf Systeme angewandt werden, die zuvor durch eine Diskretisierung mittels der Finiten Elemente Methode enstanden.

Die parallelen Architekturen in modernen Computern ermöglichen die effiziente Verwendung verschiedenster Teile-und-herrsche-Verfahren. Der intuitive Ansatz, ein großes (globales) Problem in viele kleine Teilprobleme zu zerlegen und diese parallel zu lösen, kann die Rechenzeit immens reduzieren. Es ist klar, dass die lokalen Lösungen dann der globalen Lösung, eingeschränkt auf die zugehörigen Teilgebiete, entsprechen müssen. Die Klasse der Gebietszerlegungsverfahren bietet weitverbreitete iterative Algorithmen zur parallelen Lösung impliziter Finite Elemente Problemstellungen. Häufig werden Grobgitterräume, die die verschiedenen Teilgebiete koppeln, eingeführt, um einen globalen Informationsaustausch zwischen den Teilgebieten zu ermöglichen.

Die Gebietszerlegungsverfahren FETI-DP und BDDC sind hochskalierbare parallele Algorithmen. Allerdings ist die Konvergenz des iterativen Verfahrens, in einer begrenzten Anzahl Iterationen, nicht mehr zwangsläufig sichergestellt, wenn die Verfahren mit klassischen Grobgitterräumen auf Probleme mit stark heterogenen Parametern oder Koeffizienten in der zugrundeliegenden Differentialgleichung angewandt werden. Einen Ausweg bieten in diesen Fällen problemabhängige Grobgitterräume. Diese Grobgitterräume können in adaptiven Verfahren berechnet werden und ermöglichen, auf Kosten zusätzlicher Nebenbedingungen, eine schnelle Konvergenz des iterativen Lösers.

In dieser Arbeit führen wir robuste FETI-DP und BDDC Verfahren zur Lösung dreidimensionaler Problemstellungen ein. Diese Verfahren integrieren Nebenbedingungen aus lokalen Eigenwertproblemen auf Flächen und Kanten zwischen Teilgebieten in den Grobgitterraum. Die Nebenbedingungen werden entweder mithilfe eines Deflations- oder Balancing-Ansatzes oder mittels partieller Finite Elemente Assemblierung nach einer Transformation der Basis erzwungen. Für letzteres führen wir den verallgemeinerten Transformation-der-Basis Ansatz ein und zeigen seine Korrespondenz zum Deflations- und Balancing-Ansatz.

Eine effiziente parallele Implementierung des adaptiven FETI-DP Verfahrens wird im letzten Teil der Arbeit diskutiert. Wir stellen Ergebnisse der schwachen und starken parallelen Skalierbarkeit für unseren Algorithmus vor, der auf dem Supercomputer magnitUDE der Universität Duisburg-Essen ausgeführt wurde.

Wir können sehr gute Resultate der schwachen Skalierbarkeit bis hin zu 4096 Kernen zeigen. Zur starken Skalierbarkeit können sehr gute Ergebnisse für bis zu 864 Kerne gezeigt werden.

Acknowledgements

First of all, I owe special thanks to my advisor, Axel Klawonn, for giving me the opportunity to work on these interesting and highly topical matters. I also thank him for the encouragement in the more frustrating times at the beginning of my research and for the many hours of productive discussions on the theory that preceded and accompanied our submitted articles. I also like to thank Oliver Rheinbach for all his time dedicated to our joint work and his aid regarding the software which had built the base for my implementations.

I also owe thanks to my former colleague Patrick Radtke for the uncountable hours of theoretical and practical discussions on adaptive coarse spaces. I would like to thank my colleague Martin Lanser for all his patience, explaining me all the details of his parallel implementation, which also was essential for my parallel implementation of adaptive FETI-DP. I further want to thank my colleague and good friend Alexander Heinlein for all the discussions and help he provided, although, our fields of research are a little more remote. Of course, I also want to thank my colleagues Christian Hochmuth, Matthias Uran and Jascha Knepper for all their help and time spent on discussing things.

To test my implementations, different computing systems have been used. The use of the CHEOPS computing resources at the regional computing center (RRZK) of the University of Cologne is greatfully acknowledged. For the possibility to test my parallel implementation on up to four thousand cores, I particularly acknowledge the computing time granted by the Center for Computational Sciences and Simulation (CCSS) of the University of Duisburg-Essen and provided on the supercomputer magnitUDE (DFG grants INST 20876/209-1 FUGG, INST 20876/243-1 FUGG) at the Zentrum für Informations- und Mediendienste (ZIM). Of course, I also thank the PETSc and SLEPc developers for providing their high performance computing software.

I thank my friends Christoph and Christoph as well as my former fellow student Denis. Without them, all the studies would have been much harder. I further thank Jean-Claude, Vlad, Jacob, Abdou, Alex, Alex, Florent, and all the others for facilitating my stay abroad and studying in French at the Université de Montréal. Merci à vous tous!

I also thank my friends not involved in mathematics, in particular, Thilo and Martin, but also all the others, for the necessary disctraction and all the time we spent.

I deeply have to thank my parents. Without them and all their love, I would have never had all the opportunities I actually had. I also want to thank my

sister Ina and I am grateful for all the time I have spent with my entire family, without naming them all now, so far.

Last but not least, I want to thank my girlfriend Anna for all her loving support. Without ever being passionate about math, she now can speak on the transformation of basis, by putting the words in random order, however.

Being serious again: I should thank God. Stable political and personal circumstances are at least as important to achievements as personal abilities.

Danke!

To my parents. To Anna.

Contents

List of Tables

List of Figures

1 Introduction

Many naturally occuring processes can be modeled by partial differential equations (PDEs). Among others, popular applications of partial differential equations are flows in porous media, modeled by the diffusion equation, or the deformation of an elastic body under the application of volume and surface forces, modeled by the equilibrium equations of (linear) elasticity in solid and structural mechanics; see, e.g., [33, 19, 130, 13]. For most problems, classical solutions cannot be derived analytically; see [33].

Numerical algorithms can be used to compute approximate solutions. A widely-used technique is the discretization of the variational problem in *finite element spaces* by the ***f****inite* ***e****lement* ***m****ethod (FEM)*; see, e.g, [13, 136]. To an a priori defined precision, an accurate approximate solution can be computed using the finite element method. Though, an accurate numerical approximation to the solution of a given boundary value problem often requires a fine discretization of the computational domain. Direct methods such as Gaussian elimination are memory consuming and have a high computational complexity. For large-scale linear systems, also sparse direct solvers might be not suitable, anymore. Then, iterative methods such as Krylov subspace methods come into play. Commonly used Krylov subspace methods are the *preconditioned conjugate gradient (PCG)* and the *generalized minimal residual (GMRES)* method, where the convergence can be accelerated if adequate preconditioners are used; see, e.g., [114].

With the parallel architectures in modern computers and supercomputers, an intuitive approach to solve large-scale problems is a divide and conquer strategy to divide the global problem into smaller subproblems to be computed in parallel. The global solution then should be obtained from all the local solutions. *Domain decomposition methods* [119, 130, 96] are widely-used (iterative) methods for the parallel solution of implicit finite element problems. In these methods, the finite element problem is decomposed into decoupled or only slightly coupled local problems. As already stated in [61], domain decomposition methods can be classified by the presence or absence of a coarse problem. Although being (almost) perfectly parallelizable, methods lacking a coarse space lose their advantage over methods with a coarse space if the num-

ber of subdomains grows. The condition number of coarse space-free methods usually grows with the number of subdomains; see, e.g., [61, 40, 130]. In two- or multi-level domain decomposition methods, a coarse space ensures global transport of information to obtain scalability in the number of iterations (numerical scalability); see, e.g., [61, 40, 130].

Domain decomposition methods can also be categorized by the type of the decomposition itself, i.e., the decomposition can be overlapping or nonoverlapping; see, e.g., [61]. One-, two- or even multi-level *overlapping Schwarz* methods belong to the first group and have been studied extensively; see, e.g., [119, 130] and the references therein. In this thesis, however, we only consider nonoverlapping methods also referred to as (iterative) substructuring methods; see, e.g., [119, 130, 52] and the references therein.

The ***F**inite **E**lement **T**earing and **I**nterconnecting* (*FETI*; also denoted *FETI-1*) method is a dual nonverlapping method, which was introduced in [41]. The FETI method can be characterized as a Dirichet-Dirichlet type method enriched by a coarse space given by, at least, the null space of the subdomains without essential Dirichlet boundary conditions; see, e.g, [130]. The convergence properties of the FETI method were already studied in detail in [42, 40]. Additionally, comparisons between the FETI method and direct solvers for problem settings on finite element meshes of a high speed aircraft or a space antenna connector were carried out. In [34, 39, 35], studies of the FETI method applied to time-dependent, plate and shell problems were carried out and the two-level FETI method was introduced in [39]. A new preconditioner for the FETI method was then introduced in [81] such that the condition bound could be improved significantly.

The corresponding primal method to FETI is given by a balancing variant of a Neumann-Neumann method; see, e.g., [130]. For the first works on *Balancing Neumann-Neumann* (also denoted as ***B**alancing **D**omain **D**ecomposition* or *BDD*) methods, see [31, 90], which are based on, i.a., [11, 21].

Following the works on FETI and Balancing Neumann-Neumann, the methods *FETI-DP* (FETI-**D**ual-**P**rimal) and *BDDC* (BDD by **c**onstraints) were introduced. The FETI-DP method was originally introduced in [38, 37]. The BDDC method was proposed in different articles by different authors; see [20, 23, 43]. As FETI and BDD, the methods FETI-DP and BDDC are related (see, e.g., [81, 43, 53, 92, 89]) and many results, which have been found for one of the methods, can or could be transfered to the related other method. FETI-DP and BDDC are highly scalable domain decomposition methods tested extensively on thousands and even up to half a million of cores; see, i.a., [79, 2, 73, 131, 3, 134].

If the coefficients or parameters of the underlying partial differential equations become highly heterogeneous, standard FETI-DP and BDDC methods with classical coarse spaces might not converge anymore. Highly heterogeneous coefficient distributions can, e.g., occur when modeling composite materials in solid or structural mechanics, sometimes even combined with almost incompressible material behavior. To cope with such situations, the use of adaptive or automatic coarse spaces have been proposed. In methods using adaptive coarse spaces, spectral information of local matrices of pairs or more general sets of adjacent subdomains are used. To the best of our knowledge such adaptive coarse spaces have been introduced to domain decomposition in [9, 10], by integrating specific eigenvectors into the coarse space of Neumann-Neumann methods.

About a decade ago, in [93, 120], adaptive coarse spaces for FETI-DP and BDDC domain decomposition methods were proposed for two-dimensional problems, at this time without a theoretical bound. Later, in [44, 45], eigenvalue problems on complete subdomains, which replaced a Poincaré estimate, were proposed to set up adaptive coarse spaces for additive Schwarz methods. The authors of [94, 132, 122] implemented the adaptive coarse space introduced in [93, 120] in parallel and tested it with BDDC for chosen three-dimensional problems.

Based on local Dirichlet-to-Neumann maps, Schwarz preconditioners with adaptive coarse spaces were introduced and analyzed numerically and theoretically in [98, 99, 25]. The use of **gen**eralized **e**igenproblems in the **o**verlaps (*GenEO*) was then proposed and analyzed in [125, 126, 123]. This approach was also transfered to the nonoverlapping FETI and Balancing Neumann-Neumann domain decomposition methods; see [127, 123].

For FETI-DP and BDDC methods applied to two-dimensional problems, an adaptive coarse space replacing a Poincaré inequality and an extension theorem was introduced in [72]. The complete theory was given in [74, 109]. In [75, 109], this adaptive coarse space and those of [93, 120] and [22] were compared for two-dimensional problems, studying their strengths and weaknesses as well as their performance in numerical simulations. Additionally, in [75, 109], a condition number bound for FETI-DP using the coarse space of [93, 120] could be provided for two-dimensionsal problems. For BDDC, an adaptive coarse space for two-dimensional problems was introduced in [63].

In [64], it was shown that the coarse space of [93, 120] can lead to large condition numbers and iteration counts when considering highly heterogeneous three-dimensional problems. However, in [64], it was also shown that an en-

richment of the coarse space of [93, 120] by a small number of constraints from specific edge eigenvalue problems yields a theoretically and numerically robust method for all kinds of heterogeneities and almost incompressible materials. Moreover, different strategies were proposed to reduce the number of eigenvalue problems and the number of adaptive constraints. The publication [64] is based on Chapter 5 of this thesis.

Adaptive overlapping Schwarz preconditioners in two dimensions were considered in [46, 54]. For BDDC and three-dimensional problems, different authors considered related adaptive approaches at about the same time; see [7, 101, 17]. The author of [134] offered a highly scalable PETSc [4, 5] implementation of adaptive BDDC, with experimental support for FETI-DP, using the adaptive constraints from the face eigenvalue problems of [22] and a heuristical generalization thereof for edges in three dimensions; see also [135].

In [62], an adaptive coarse space was considered for BDDC and FETI-DP likewise. For FETI-DP, the adaptive coarse space was implemented as in [64] by a balancing approach. An overview on several approaches to adaptive coarse spaces for BDDC was given in [103]. Recently, adaptive coarse spaces for overlapping Schwarz methods in three dimensions were considered in [32].

Another adaptive approach, which does not set up any eigenvalue problem, was proposed in [124]. In this method, the constraints are computed directly inside the Krylov scheme. Scalability results can be found in [12].

In [67], it was shown that the use of a generalized approach to the transformation of basis with partial finite element assembly results in essentially the same spectrum as the use of a corresponding deflation or balancing approach, even when nondiagonal scalings are used or arbitrarily heterogeneous problems are considered. The adaptive coarse space of [64] was then implemented using the generalized transformation-of-basis approach; cf. [68]. The results of [67] are based on Section 4.5 of this thesis. The publication [68] is based on Chapter 6 of this thesis.

Using the generalized transformation-of-basis approach and the PETSc [4, 5] and SLEPc [56, 113] high performance libraries, preliminary parallel results for adaptive FETI-DP, excelling the standard FETI-DP method with a classical coarse space, were presented in [68]. Details on the efficient parallel implementation of adaptive FETI-DP and weak and strong scalability studies for our method can be found in Chapter 7 and will be published in [69].

The remaining part of this thesis is organized as follows. In the next chapter, we introduce three different model problems for which the algorithms presented in this thesis are studied theoretically and numerically. In Chapter 3, we outline

the widely-used domain decomposition methods FETI-DP and BDDC with a more detailed discussion of different scalings, which are commonly employed in these methods. In the first parts of Chapter 4, we shortly present popular techniques to implement coarse space enrichments for FETI-DP and BDDC. Then, in Section 4.5, the new and generalized transformation-of-basis approach is introduced. Chapter 5 introduces robust FETI-DP methods for three-dimensional problems using adaptive coarse spaces implemented by deflation or balancing. An extensive set of numerical results is provided. In Chapter 6, the adaptive coarse spaces are combined with the generalized transformation-of-basis approach. Within the numerical results, comparisons of the different scalings and different a priori chosen tolerances for the adaptive coarse spaces are considered. Subsequently, we explain necessary modifications for a scalable parallel implementation using the PETSc [4, 5] and the SLEPc [56, 113] high performance libraries in Chapter 7. We present results of weak and strong scaling for our parallel implementation of adaptive FETI-DP. Eventually, we draw a conclusion in Chapter 8.

2 Model problems

2.1 Preliminaries

In this chapter, we present three different model problems that are considered in this thesis. For a more detailed description and theoretical consideration of the model problems, see, e.g., [19, 15, 130, 14, 13], especially in the context of finite element based methods.

For all problems, let $\Omega \subset \mathbb{R}^d$, $d = 2, 3$, be a bounded polyhedral domain and let $\partial\Omega_D \subset \partial\Omega$ be a closed subset of nonvanishing measure where we prescribe Dirichlet boundary conditions. On the remaining part of the boundary $\partial\Omega_N := \partial\Omega \setminus \partial\Omega_D$, we prescribe Neumann boundary conditions.

We also define the Sobolev space $H_0^1(\Omega, \partial\Omega_D)^n := \{v \in H^1(\Omega)^n : v = 0 \text{ on } \partial\Omega_D\}$ of weakly differentiable functions on Ω. For the scalar diffusion problem, we have $n = 1$ regardless of the dimension d. For the case of linear elasticity, we have $n = d$ and vector valued functions.

Note that the ideas presented in this thesis can equally be adapted for $d = 2$ dimensions, in general, however, we consider the three-dimensional case.

2.2 Diffusion equation

The first model problem considered in this thesis is the well known *diffusion* equation. For a sufficiently smooth coefficient function $\rho : \Omega \to \mathbb{R}$ and adequate functions $f : \Omega \to \mathbb{R}$ and $g : \partial\Omega_N \to \mathbb{R}$, we have the boundary value problem

$$\begin{aligned} -\nabla \cdot (\rho \nabla u) &= f \quad \text{in } \Omega, \\ u &= 0 \quad \text{on } \partial\Omega_D, \\ \rho \nabla u \cdot n &= g \quad \text{on } \partial\Omega_N \end{aligned} \tag{2.1}$$

where n denotes the outer unit normal on Ω_N. For a piecewise constant parameter distribution $\rho \in L^\infty(\Omega)$ with $\rho \geq \rho_{\min} > 0$, $f \in L^2(\Omega)$, and $g \in L^2(\partial\Omega)$, we then study the weak formulation: Find $u \in H_0^1(\Omega, \partial\Omega_D)$ such that

$$a(u, v) = F(v) \quad \forall v \in H_0^1(\Omega, \partial\Omega_D),$$

where

$$a(u,v) := \int_\Omega \rho \nabla u \cdot \nabla v \mathrm{d}x \qquad \text{and} \qquad F(v) := \int_\Omega f v \mathrm{d}x + \int_{\partial\Omega} g v \mathrm{d}s. \tag{2.2}$$

For the numerical solution of diffusion problems, in this thesis, we use conforming $\mathcal{P}_1$ finite elements.

Parts of the description of this model problem have already been published in modified or unmodified form by the author of this thesis and his coauthors in [66, 67].

For details on the existence and uniqueness of the solution, derived from Lax-Milgram's theorem, we refer to, e.g., [130, 13].

2.3 Compressible linear elasticity

The second model problem is that of compressible linearized (in the following simply *linear*) *elasticity*. The domain Ω can then be regarded as a material body to be deformed under the application of a body force $f : \Omega \to \mathbb{R}^d$ and a surface force $g : \partial\Omega_N \to \mathbb{R}^d$. The sufficiently smooth solution $u : \Omega \to \mathbb{R}^d$ of the pure displacement model

$$\begin{aligned} -2\mu \mathrm{div}(\varepsilon(u)) - \lambda \nabla(\mathrm{div}(u)) &= f \text{ in } \Omega, \\ u &= 0 \text{ on } \partial\Omega_D, \\ \big(\lambda \mathrm{tr}(\varepsilon(u)) I + 2\mu\varepsilon(u)\big) \cdot n &= g \text{ on } \partial\Omega_N \end{aligned} \tag{2.3}$$

is called the *displacement* from the *reference configuration* to the *deformed configuration*. In (2.3), the linearized *strain tensor* $\varepsilon(v)$ is defined by the symmetric gradient

$$\varepsilon(v) := \frac{1}{2}\big(\nabla v + \nabla v^T\big) \quad \text{and} \quad \varepsilon_{ij}(v) := \frac{1}{2}\Big(\frac{\partial v_i}{\partial x_j} + \frac{\partial v_j}{\partial x_i}\Big),\ 1 \le i,j \le d, \tag{2.4}$$

and λ and μ are the material dependent *Lamé constants*. The Lamé constants can be calculated easily from *Young's modulus* $\mathrm{E} > 0$ and *Poisson's ratio* $\nu \in (0, \frac{1}{2})$ by

$$\lambda = \frac{\mathrm{E}\nu}{(1+\nu)(1-2\nu)} \quad \text{and} \quad \mu = \frac{\mathrm{E}}{2(1+\nu)}.$$

For piecewise constant and bounded material parameters E and ν, $f \in L^2(\Omega)$, and $g \in L^2(\partial\Omega)$, we obtain the variational formulation of compressible

linear elasticity: Find $u \in H_0^1(\Omega, \partial\Omega_D)^d$ such that

$$a(u,v) = F(v) \quad \forall v \in H_0^1(\Omega, \partial\Omega_D)^d, \tag{2.5}$$

where

$$\begin{aligned} a(u,v) :&= \int_\Omega 2\mu\varepsilon(u) : \varepsilon(v)\mathrm{d}x + \int_\Omega \lambda \mathrm{div}(u)\mathrm{div}(v)\mathrm{d}x \\ \text{and} \quad F(v) :&= \int_\Omega f \cdot v \mathrm{d}x + \int_{\partial\Omega_N} g \cdot v \mathrm{d}s. \end{aligned} \tag{2.6}$$

The product of the linearized strain tensor is given by $\varepsilon(u) : \varepsilon(v) = \sum_{i,j=1}^d \varepsilon_{ij}(u)\varepsilon_{ij}(v)$.

For the numerical consideration of compressible linear elastic materials, in this thesis, we use conforming $\mathcal{P}_1$ or $\mathcal{P}_2$ finite elements.

Parts of the description of this model problem have already been published in modified or unmodified form by the author of this thesis and his coauthors in [64, 65, 68, 70].

For more details on the derivation of the equations and the statements of existence and uniqueness of solutions of linear elasticity, see, e.g., [19, 130, 13].

2.4 Almost incompressible linear elasticity

Our third model problem is that of almost incompressible linear elasticity. Almost incompressible linear elasticity is strongly related to compressible linear elasticity since this model problem is obtained from (2.3) by introducing the pressure variable $p := \lambda \mathrm{div}(u)$. The reason to do so, is a locking phenomena that can occur for the low order standard finite element formulation when Poisson's ratio ν approaches 0.5, which corresponds to the fully incompressible limit. Typical for the occurence of locking is the absence of uniform convergence for the low order standard finite element formulation when $h \to 0$ and large errors might occur for $\nu \approx 0.5$; from the mathematical point of view, [13] then proposes to rather speak of a badly conditioned problem than of locking. To avoid this phenomenon, we derive the weak form of the mixed formulation in (u,p): Find $(u,p) \in H_0^1(\Omega, \partial\Omega_D)^d \times L^2(\Omega)$ such that

$$\begin{aligned} a(u,v) + b(v,p) &= F(v) \quad \forall v \in H_0^1(\Omega, \partial\Omega_D)^d, \\ b(u,q) - c(p,q) &= 0 \qquad \forall q \in L^2(\Omega), \end{aligned} \tag{2.7}$$

where

$$a(u,v) := \int_\Omega 2\mu\varepsilon(u) : \varepsilon(v)\mathrm{d}x, \quad b(v,p) := \int_\Omega p\,\mathrm{div}(v)\mathrm{d}x, \quad c(p,q) := \int_\Omega \frac{1}{\lambda} p\,q\mathrm{d}x, \tag{2.8}$$

and $F(v)$ as in (2.6). Special care has to be taken when choosing the finite elements for solving the mixed formulation. It has to be ensured that the chosen finite elements fulfill the discrete Ladyženskaya-Babuška-Brezzi condition to remain stable.

For the numerical consideration of almost incompressible linear elastic materials, in this thesis, we use $\mathcal{Q}_2 - \mathcal{P}_0$ finite elements with conforming $\mathcal{Q}_2$ and discontinuous pressure elements. These elements are inf-sup stable. We statically condensate the pressure variable elementwise.

Parts of the description of this model problem have already been published in modified or unmodified form by the author of this thesis and his coauthors in [64].

For more details on almost incompressible linear elasticity, we refer to, e.g., [14, 13, 130].

3 Standard FETI-DP and BDDC

3.1 Preliminaries

The FETI-DP (**F**inite **E**lement **T**earing and **I**nterconnection - **D**ual **P**rimal) and BDDC (**B**alancing **D**omain **D**ecomposition by **C**onstraints) methods are divide and conquer algorithms. To be more specific, they are nonoverlapping domain decomposition methods. Domain decomposition methods (see, e.g., [119, 130, 96]) are widely-used iterative methods for the parallel solution of discretized partial differential equations. In domain decomposition methods, the discretized problem is decomposed into overlapping or nonoverlapping local problems. In FETI-DP and BDDC, the local problems are finite element problems only coupled in a few degrees of freedom. In both methods, a coarse space ensures a global transport of information such that scalability in the number of iterations is obtained; see, e.g., [61, 40]. Fundamental for FETI-DP and BDDC are the previously developed methods FETI (also FETI-1) and Balancing Neumann-Neumann (also Balancing Domain Decomposition); see, e.g., [11, 41, 129, 31, 90, 42]. The FETI-DP method was originally introduced in [38, 37]. The BDDC method was proposed by different authors in [20, 23, 43].

In order to introduce the classical FETI-DP and BDDC methods, we first present some discretization and domain decomposition preliminaries which are essential for the following sections. For a more detailed introduction, we again refer to, e.g., [119, 130, 96]. Parts of this chapter have already been published in modified or unmodified form by the author of this thesis and his coauthors in [64, 65, 67, 68].

For a given domain $\Omega \subset \mathbb{R}^d$, $d = 2, 3$, we conduct a decomposition into N nonoverlapping subdomains Ω_i, $i = 1, \ldots, N$ such that $\overline{\Omega} = \bigcup_{i=1}^{N} \overline{\Omega}_i$ and where each Ω_i is discretized by the finite element method. In our case, each subdomain is an union of shape regular elements of diameter $\mathcal{O}(h)$. The diameter of a subdomain Ω_i is denoted by H_i or, generically, by H. Furthermore, we define the interface Γ as the set of values that belong to at least two subdomains, i.e., $\Gamma := \{x \in \left(\overline{\Omega}_i \cap \overline{\Omega}_j\right) \setminus \partial\Omega_D;\ i \neq j\}$ and always require that finite element nodes of neighboring subdomains match across the interface. We further define

Γ_h and $\partial\Omega_{i,h}$, $i = 1, \ldots, N$, as the set of finite element nodes on Γ and $\partial\Omega_i$, respectively.

Note that the ideas presented in this thesis can equally be adapted for $d = 2$ dimensions, in general, however, we consider the three-dimensional case.

For three-dimensional problems, the interface consists of vertices, edges, and faces; see, e.g., [77, Def. 2.1, Def. 2.2] and [82, Def. 3.1]. Note that vertices are sometimes also called corners or corner nodes. For the case of regular subdomains, these definitions coincide with our intuitive geometric understanding. In a regular decomposition, vertices are the endpoints of edges. In general, this also applies to irregular decompositions. However, in irregular decompositions, vertices not being the endpoint of an edge or edges with less than two vertices can appear. As already mentioned in [77], for automatic mesh partitioners such as METIS (see [60]) the situation can become quite complex. In these cases, it might be necessary to modify the definition slightly. We comment on this in detail and use a slightly modified definition, when it comes to the use of automatic mesh partitioners in combination with our adaptive methods; see Chapter 5. With both definitions, edges and faces are considered as open sets. We denote a face between the two subdomains Ω_i and Ω_j by $\mathcal{F}^{ij}$, an edge between Ω_i, Ω_j, Ω_k and possible other subdomains by $\mathcal{E}^{ik}$ and a vertex of Ω_i touching several subdomains by $\mathcal{V}^{il}$. Sometimes, we also use the generic index $\mathcal{F}$ for an arbitray face, $\mathcal{E}$ for an arbitrary edge, and $\mathcal{Z}$ for $\mathcal{Z}$ being either face or edge. Eventually, for an arbitrary face $\mathcal{F}$ and an arbitrary edge $\mathcal{E}$, we introduce the standard finite element cutoff functions $\theta_{\mathcal{F}}$ and $\theta_{\mathcal{E}}$, which are equal to one on $\mathcal{F}$ and $\mathcal{E}$, respectively, and which are zero otherwise.

Troughout the thesis, we use different kinds of finite elements. For the diffusion equation and the case of compressible linear elasticity in Chapters 5 and 6, we use conforming $\mathcal{P}_1$ finite elements. In Chapter 7, we only consider compressible linear elasticity and conforming $\mathcal{P}_2$ finite elements. For the case of almost incompressible linear elasticity, we use $\mathcal{Q}_2 - \mathcal{P}_0$ finite elements with conforming $\mathcal{Q}_2$ and discontinuous pressure elements. These elements are inf-sup stable. In our experiments, we statically condensate the pressure variable elementwise. The space of our finite elements on Ω_i is denoted by $W^h(\Omega_i \backslash \partial\Omega_D)$; independently of the choice of the finite elements. In all cases, the finite element functions vanish on $\partial\Omega_D$. For a part of the interface $\Gamma' \subset \Gamma$ with nonvanishing measure, we define the finite element trace space $W^h(\Gamma')$ and, in particular, $W_i := W^h(\partial\Omega_i)$. Finally, we define $W := \Pi_{i=1}^N W_i$ and denote by $\widehat{W} \subset W$ the space of functions in W that are continuous on Γ.

For FETI-DP and BDDC, we partition the degrees of freedom on the subdomains $\Omega_i \subset \Omega$, $i = 1, \ldots, N$, into interior, (a priori) dual, and (a priori) primal degrees of freedom, denoted by I, Δ', and Π', respectively. Interior degrees of freedom are all degrees of freedom belonging to nodes not touching the interface Γ. We have $\Gamma_h = \Delta' \cup \Pi'$. The choice of Π' is problem-dependent and then defines the remaining index set Δ'. In contrast to many other works on standard FETI-DP and BDDC, we use the notations Δ' and Π' instead of Δ and Π since the latter is reserved for the generalized transformation-of-basis approach; see Section 4.5. To avoid misunderstandings, we clearly differentiate between two kinds of primal variables: a priori primal (Π') and a posteriori primal (Π) variables. The sets of a priori and a posteriori dual (Δ' and Δ) degrees of freedom are the respective complementary sets on the interface. To conclude this preliminary section, we introduce the space $\widetilde{W}$, consisting of functions $w \in W$ that are continuous in the a priori primal variables. We thus have

$$\widehat{W} \subset \widetilde{W} \subset W. \tag{3.1}$$

3.2 Standard FETI-DP

As mentioned before, the FETI-DP method was introduced in [38, 37].

In a first step, we now compute the local stiffness matrices $K^{(i)}$ and the right hand sides $f^{(i)}$ for every subdomain Ω_i, $i = 1, \ldots, N$. The local solution vectors, e.g., the displacements for the case of linear elasticity (cf. Section 2.3), are denoted by $u^{(i)}$, $i = 1, \ldots, N$. Then, the local problems $K^{(i)}u^{(i)} = f^{(i)}$ are decoupled. Due to the absence of a global coupling or Dirichlet boundary conditions for subdomains Ω_i with $\partial\Omega_i \cap \partial\Omega_D = \emptyset$, these subdomains are also called floating subdomains. Consequently, the local solutions on floating subdomains are, in general, not unique and different from the solution u of the partial differential equation, restricted to the local subdomain $u_{|\overline{\Omega}_i}$. For problems of linear elasticity, the null space of the stiffness matrix of a floating subdomain consists of the rigid body modes, i.e., shifts of the entire subdomain as well as (linear approximations to) rotations of the entire subdomain. For the diffusion problem, the null space of the corresponding domains only consists of the constant functions. That means, for both problems, when solving the decoupled problems, we would obtain nonunique and discontinuous solutions; see Figure 3.1 (left). The FETI-DP domain decomposition approach tackles this issue as follows.

We use the subdivision of the degrees of freedom introduced in the previous section to assume the following partitioning of the local stiffness matrices $K^{(i)}$,

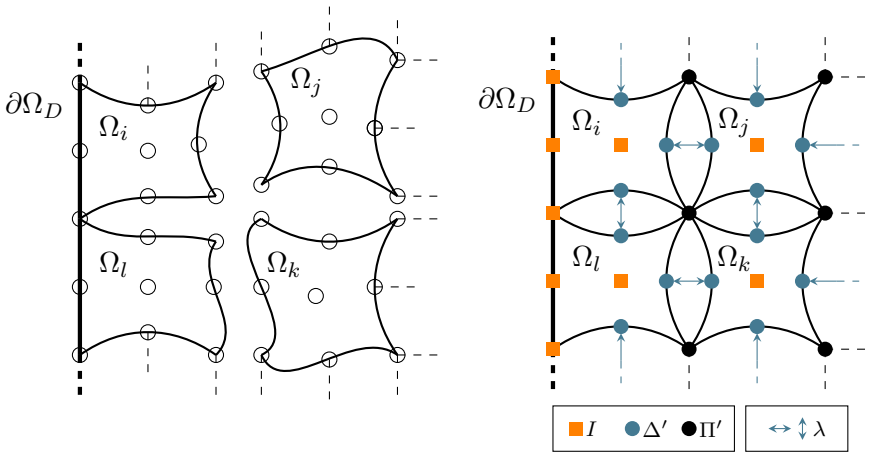

Figure 3.1: *Nonoverlapping domain decomposition, subdivision of the local degrees of freedom, and visualization of the FETI-DP approach:* Section of four subdomains Ω_i, Ω_j, Ω_k, $\Omega_l \subset \Omega$ for $\Omega \subset \mathbb{R}^2$, Dirichlet boundary conditions on $\partial\Omega_D$ on the left, and with nine exemplary nodes for each subdomain. Without global coupling, the local solutions on the floating subdomains Ω_j and Ω_k are not unique and detached from the solutions on Ω_i and Ω_l (left). The subdivision of the nodes and the coupling in the primal variables (black circles) attaches the solution on the floating subdomains to the unique solution on the nonfloating subdomains; for FETI-DP, continuity in the dual variables (blue circles) is enforced by Lagrange multipliers λ (blue arrows) (right). Continuity on the whole interface is only obtained at convergence of the iterative solver.

the local load vectors $f^{(i)}$, and the local solutions $u^{(i)}$:

$$K^{(i)} =: \begin{pmatrix} K_{II}^{(i)} & K_{\Delta' I}^{(i)T} & K_{\Pi' I}^{(i)T} \\ K_{\Delta' I}^{(i)} & K_{\Delta'\Delta'}^{(i)} & K_{\Pi'\Delta'}^{(i)T} \\ K_{\Pi' I}^{(i)} & K_{\Pi'\Delta'}^{(i)} & K_{\Pi'\Pi'}^{(i)} \end{pmatrix}, \quad u^{(i)} =: \begin{pmatrix} u_I^{(i)} \\ u_{\Delta'}^{(i)} \\ u_{\Pi'}^{(i)} \end{pmatrix}, \text{ and } f^{(i)} =: \begin{pmatrix} f_I^{(i)} \\ f_{\Delta'}^{(i)} \\ f_{\Pi'}^{(i)} \end{pmatrix}.$$

By grouping interior (I) and a priori dual (Δ') variables, denoted by the index B', we obtain

$$\begin{aligned} K_{B'B'}^{(i)} := \begin{pmatrix} K_{II}^{(i)} & K_{\Delta' I}^{(i)T} \\ K_{\Delta' I}^{(i)} & K_{\Delta'\Delta'}^{(i)} \end{pmatrix}, \; K_{\Pi' B'}^{(i)T} := \begin{pmatrix} K_{\Pi' I}^{(i)T} \\ K_{\Pi'\Delta'}^{(i)T} \end{pmatrix}, \\ u_{B'}^{(i)} := \begin{pmatrix} u_I^{(i)} \\ u_{\Delta'}^{(i)} \end{pmatrix}, \text{ and } f_{B'}^{(i)} := \begin{pmatrix} f_I^{(i)} \\ f_{\Delta'}^{(i)} \end{pmatrix}. \end{aligned} \tag{3.2}$$

By grouping a priori dual and a priori primal indices denoted by the index Γ, we obtain

$$\begin{aligned} K_{\Gamma\Gamma}^{(i)} := \begin{pmatrix} K_{\Delta'\Delta'}^{(i)} & K_{\Pi'\Delta'}^{(i)T} \\ K_{\Pi'\Delta'}^{(i)} & K_{\Pi'\Pi'}^{(i)} \end{pmatrix}, \; K_{\Gamma I}^{(i)} := \begin{pmatrix} K_{\Delta' I}^{(i)} \\ K_{\Pi' I}^{(i)} \end{pmatrix}, \\ u_{\Gamma}^{(i)} := \begin{pmatrix} u_{\Delta'}^{(i)} \\ u_{\Pi'}^{(i)} \end{pmatrix}, \text{ and } f_{\Gamma}^{(i)} := \begin{pmatrix} f_{\Delta'}^{(i)} \\ f_{\Pi'}^{(i)} \end{pmatrix}. \end{aligned} \tag{3.3}$$

We then can introduce the block diagonal matrices

$$\begin{aligned} K_{II} &:= \text{blockdiag}_{i=1}^{N} K_{II}^{(i)}, \\ K_{B'B'} &:= \text{blockdiag}_{i=1}^{N} K_{B'B'}^{(i)}, \\ \text{and } \; K_{\Gamma\Gamma} &:= \text{blockdiag}_{i=1}^{N} K_{\Gamma\Gamma}^{(i)} \end{aligned} \tag{3.4}$$

as well as the corresponding off-diagonal block $K_{\Gamma I}$. The global right hand side f and the global solution vector u can be partitioned accordingly.

As discussed before, the solution of the decoupled block diagonal system is not unique. Therefore, we now introduce the inter-subdomain assembly operator $R_{\Pi'}^T := \left(R_{\Pi'}^{(1)T}, \ldots, R_{\Pi'}^{(N)T}\right)$, which consists of values in $\{0, 1\}$ and performs the partial finite element assembly in the a priori primal variables $u_{\Pi'}^{(i)}$.

Traditionally, Π' was chosen to be the subdomain vertices (also corners or corner nodes) or as a subset of these, possibly enriched by edge averages or first order moments on edges if the considered problem required this; also face averages have been considered; see, e.g., [38, 107, 37, 84, 77, 82, 78]. The choice of an appropriate coarse space is a problem-dependent task. Since we mean to overcome this challenge by adaptive coarse spaces, we choose a minimal a priori coarse space, i.e., we set all vertices to be primal, and do not discuss in detail the advantages of other specific a priori coarse spaces. For more details on a priori coarse spaces; see, e.g., [77, 82, 78, 130] and the yet nonexhaustive enumeration at the end of this section on FETI-DP.

By assembly in the a priori primal variables, we obtain

$$\begin{aligned} \widetilde{K}_{\Pi'\Pi'} = \sum_{i=1}^{N} R_{\Pi'}^{(i)T} K_{\Pi'\Pi'}^{(i)} R_{\Pi'}^{(i)}, \; \widetilde{K}_{\Pi' B'} = \left(R_{\Pi'}^{(1)T} K_{\Pi' B'}^{(1)}, \ldots, R_{\Pi'}^{(N)T} K_{\Pi' B'}^{(N)}\right), \\ \widetilde{u}_{\Pi'} = \sum_{i=1}^{N} R_{\Pi'}^{(i)T} u_{\Pi'}^{(i)}, \text{ and } \widetilde{f}_{\Pi'} = \sum_{i=1}^{N} R_{\Pi'}^{(i)T} f_{\Pi'}^{(i)}. \end{aligned}$$

The assembly in the vertices is exemplarily shown by the black circles in Figure 3.1 (right).

In order to enforce continuity in the a priori dual degrees of freedom, we introduce a signed Boolean jump operator $B = \left(B^{(1)}, \ldots, B^{(N)}\right)$ with one +1 and one -1 per row such that $Bu = 0$ if and only if u is continuous on the interface. The operator $B_{B'} = \left(B^{(1)}_{B'}, \ldots, B^{(N)}_{B'}\right)$ is defined as the part of B where the columns corresponding to primal variables are removed. The restriction to the interface $B_\Gamma = [B^{(1)}_\Gamma, \ldots, B^{(N)}_\Gamma]$ is also obtained by elimination of trivial columns from B. Thus, B, $B_{B'}$, and B_Γ contain exactly one +1 and one −1 per row such that $Bu = 0$, $B_{B'}u_{B'} = 0$, and $B_\Gamma u_\Gamma = 0$ if and only if u, $u_{B'}$, and u_Γ are continuous on the interface. Related to the jump operator B are the Lagrange multipliers λ, which act between two degrees of freedom each. The Lagrange multipliers are exemplarily indicated by the blue arrows in Figure 3.1 (right).

Note that the jump operator B is not uniquely determined. In addition to the orientation of the Lagrange multipliers, i.e., the rows of B can be multiplied by -1, without changing the continuity constraint, the number of rows in B depends on the number of Lagrange multipliers introduced. For example, on an edge in three dimensions, which is shared by four subdomains, for each degree of freedom between a minimum of three and usually six Lagrange multipliers can be implemented without changing the solution; see Figure 3.2 for a nonredundant (three Lagrange multipliers) and the fully redundant (six Lagrange multipliers) choice. In practice, we always use the fully redundant implementation.

The dual part of the FETI-DP method corresponds to a Dirichlet-Dirichlet algorithm with continuous flux approximations at each step of the iterative solver while the local solution vectors corresponding to the iterates $\lambda^{(k)}$, $k = 1, 2, \ldots$, are continuous only at convergence; cf., e.g., [130, Sec. 1.3.5] for an elementary description of Dirichlet-Dirichlet methods.

The FETI-DP master system is then given by

$$\begin{pmatrix} K_{B'B'} & \widetilde{K}^T_{\Pi'B'} & B^T_{B'} \\ \widetilde{K}_{\Pi'B'} & \widetilde{K}_{\Pi'\Pi'} & 0 \\ B_{B'} & 0 & 0 \end{pmatrix} \begin{pmatrix} u_{B'} \\ \widetilde{u}_{\Pi'} \\ \lambda \end{pmatrix} = \begin{pmatrix} f_{B'} \\ \widetilde{f}_{\Pi'} \\ 0 \end{pmatrix}. \tag{3.5}$$

By block Gaussian elimination, we obtain the (unpreconditioned) standard FETI-DP system

$$F\lambda = d \tag{3.6}$$

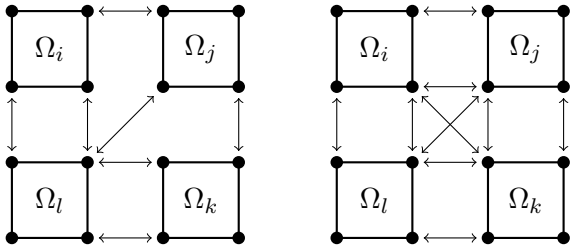

Figure 3.2: *Nonredundant and redundant choice of Lagrange multipliers for FETI-DP:* Cross-sectional view of four subdomains sharing an edge. Arrows symbolize Lagrange Multipliers in FETI-DP. Shown are a nonredundant choice of Lagrange multipliers (left) and the fully redundant choice (right).

with

$$\begin{aligned} F &:= B_{B'} K_{B'B'}^{-1} B_{B'}^T + B_{B'} K_{B'B'}^{-1} \widetilde{K}_{\Pi' B}^T \widetilde{S}_{\Pi'\Pi'}^{-1} \widetilde{K}_{\Pi' B'} K_{B'B'}^{-1} B_{B'}^T, \\ d &:= B_{B'} K_{B'B'}^{-1} f_{B'} + B_{B'} K_{B'B'}^{-1} \widetilde{K}_{\Pi' B'}^T \widetilde{S}_{\Pi'\Pi'}^{-1} \big(\widetilde{f}_{\Pi'} - \widetilde{K}_{\Pi' B'} K_{B'B'}^{-1} f_{B'} \big). \end{aligned} \tag{3.7}$$

Here, the Schur complement $\widetilde{S}_{\Pi'\Pi'}$ is defined as

$$\widetilde{S}_{\Pi'\Pi'} := \widetilde{K}_{\Pi'\Pi'} - \widetilde{K}_{\Pi' B'} K_{B'B'}^{-1} \widetilde{K}_{\Pi' B'}^T. \tag{3.8}$$

As can be seen from (3.7), the application of F can be divided into two additive parts. The first part can be executed completely in parallel while the expression $\widetilde{S}_{\Pi'\Pi'}^{-1}$ requires the solution of a coupled coarse problem. Consequently, $\widetilde{S}_{\Pi'\Pi'}$ represents the initial (or a priori) coarse space.

Based on the definition of the assembly operator $R_{\Pi'}^T$, we define R_Γ^T as the identity on Δ' and as the assembly operator $R_{\Pi'}^T$ on Π'. By computing the local Schur complements

$$S^{(i)} := K_{\Gamma\Gamma}^{(i)} - K_{\Gamma I}^{(i)} \big(K_{II}^{(i)} \big)^{-1} K_{\Gamma I}^{(i)T} \tag{3.9}$$

and by using the operator R_Γ^T introduced right before, we obtain the assembled Schur complement

$$\widetilde{S} := R_\Gamma^T S_{\Gamma\Gamma} R_\Gamma \;\text{ for }\; S_{\Gamma\Gamma} := \operatorname{blockdiag}_{i=1}^N S^{(i)}. \tag{3.10}$$

This enables the use of the identity

$$F = B_\Gamma \widetilde{S}^{-1} B_\Gamma^T. \tag{3.11}$$

Let us note that the expression (3.7) is needed for the implementation of FETI-DP while (3.11) might be a more convenient expression for an analytic examination of the method.

The considered system of equations (3.6) is then solved by a Krylov subspace method such as the (preconditioned) conjugate gradient algorithm (PCG). The error estimate of the conjugate gradient algorithm can be bounded from above by a function depending on the spectral condition number $\kappa(M^{-1}F)$, with M^{-1} an (adequate) preconditioner. Precisely, for λ^*, the solution of (3.6), and $\lambda^{(k)}$, the approximation at the k-step of the PCG algorithm, we have

$$\|\lambda^* - \lambda^{(k)}\|_F \leq 2 \left(\frac{\sqrt{\kappa(M^{-1}F)} - 1}{\sqrt{\kappa(M^{-1}F)} + 1} \right)^k \|\lambda^* - \lambda^{(0)}\|_F; \tag{3.12}$$

see, e.g., [108, 114]. Therefore, to speed up the convergence of the iterative solver, we now introduce a preconditioner for (3.6).

The standard Dirichlet preconditioner M_D^{-1} is commonly used in the FETI-DP method; see already the first works on FETI-DP [38, 37]. A key ingredient in this preconditioner are (diagonal) scaling matrices $D^{(i)} : \operatorname{range} B \to \operatorname{range} B$, $i = 1, \ldots, N$. In contrast to the original choice of diagonal matrices $D^{(i)}$ (see, e.g., [115, 112, 38, 81, 130, 78, 105] for FETI-DP and earlier related works on other domain decomposition methods), there are recent works using nondiagonal matrices; see, e.g., [24, 22, 6, 18, 16]. Nondiagonal scalings were initially introduced for BDDC (see [24]) but they are easily transferable and have already been used in FETI-DP methods; see, e.g., [18, 75, 62, 68].

Note that, in FETI-DP a degree of freedom based scaling $D_u^{(i)} : \partial\Omega_{i,h} \cap \Gamma_h \to \partial\Omega_{i,h} \cap \Gamma_h$ is also possible (see, e.g., the corresponding ideas for FETI-1 in [81, 130]). Then, the operator $B_{D,\Gamma}$ introduced in the following (see (3.18)) had to be defined differently. We do not further focus on this case here.

The diagonal scalings for FETI-DP are strongly related to the scalings already used in BDD and FETI-1 methods; see, e.g., [81, 130]. To define the range of diagonal scaling matrices, we define the set

$$\mathcal{N}_x = \{j \in \{1, \ldots, N\} \,:\, x \in \partial\Omega_j\} \tag{3.13}$$

for $x \in \Gamma_h$. The diagonal scaling matrices $D^{(i)}$, $i = 1, \ldots, N$, are then built from local weighting functions $d_u^{(i)} : \partial\Omega_{i,h} \cap \Gamma_h \to (0, 1)$ with the partition of unity feature

$$\sum_{i \in \mathcal{N}_x} d_u^{(i)}(x) = 1 \; \forall x \in \partial\Omega_{i,h} \cap \Gamma_h \tag{3.14}$$

such that

$$\left(D^{(i)}\right)_{rr} := d_u^{(j)}(x). \tag{3.15}$$

Here, r is the row index of the nontrivial row of $B^{(i)}$ corresponding to the Lagrange multiplier λ, which couples Ω_i and Ω_j at x.

The nondiagonal scaling matrices used in [24, 22, 6, 18, 75, 63, 16, 7, 101, 17, 134, 103, 62, 68] are, however, block diagonal with respect to the underlying geometry, i.e., the blocks are of the size of the edges and the faces. Consider either an (open) face $\mathcal{F}^{ij}$ shared by the two subdomains Ω_i and Ω_j or an (open) edge $\mathcal{E}^{ik}$ shared by the subdomains Ω_i, Ω_j, Ω_k. Multiplicities greater than three can be handled analogously. For the scaling matrices on the degrees of freedom u, i.e., $D^{(i)}_{u,\mathcal{F}^{ij}}, D^{(j)}_{u,\mathcal{F}^{ij}}$ defined on $\mathcal{F}^{ij}$ and $D^{(i)}_{u,\mathcal{E}^{ik}}, D^{(j)}_{u,\mathcal{E}^{ik}}, D^{(k)}_{u,\mathcal{E}^{ik}}$ defined on $\mathcal{E}^{ik}$, instead of (3.14), we require

$$D^{(i)}_{u,\mathcal{F}^{ij}} + D^{(j)}_{u,\mathcal{F}^{ij}} = I \text{ and } D^{(i)}_{u,\mathcal{E}^{ik}} + D^{(j)}_{u,\mathcal{E}^{ik}} + D^{(k)}_{u,\mathcal{E}^{ik}} = I \tag{3.16}$$

i.e., the respective sum of all blocks corresponding to a certain edge or face has to reduce itself to the identity.

For the scaling on the Lagrange multipliers, we have to distinguish two cases. In the simple case, the orientations of the Lagrange multipliers are chosen consistently between two subdomains. Then, if R is the set of row indices in B that couple $\Omega^{(i)}$ and $\Omega^{(j)}$ on either the face $\mathcal{F}^{ij}$ or the edge $\mathcal{E}^{ik}$, the corresponding part of the scaling matrix is given by

$$\left(D^{(i)}\right)_{RR} := \begin{cases} D^{(j)}_{u,\mathcal{F}^{ij}}, \text{ if } \mathcal{F}^{ij} \text{ is coupled by the rows } R, \\ D^{(j)}_{u,\mathcal{E}^{ik}}, \text{ if } \mathcal{E}^{ik} \text{ is coupled by the rows } R. \end{cases} \tag{3.17}$$

The other entries of $D^{(i)}$ as well as the entries of $D^{(j)}$ and $D^{(k)}$ are obtained correspondingly.

We speak of nonconsistent orientations of the Lagrange multipliers if the signs of the rows in B are not chosen consistently. An example is given by the following choice. Assume $R = [R_1, R_2]$ and that the Lagrange multipliers R_1 on a face or an edge coupling $\Omega^{(i)}$ and $\Omega^{(j)}$ are oriented such that their corresponding entries in $B^{(i)}$ have a positive sign. Assume on the other hand that the remaining Lagrange multipliers R_2 are oriented such that their corresponding entries in $B^{(i)}$ have a negative sign. In this case, the off-diagonal blocks $\left(D^{(i)}\right)_{R_1R_2}$ and $\left(D^{(i)}\right)_{R_2R_1}$ in $\left(D^{(i)}\right)_{RR}$ have to be scaled by -1. Again,

the other entries of $D^{(i)}$ as well as the entries of $D^{(j)}$ and $D^{(k)}$ are obtained correspondingly.

Note that (3.15) is obviously a special case of (3.17).

We can now define the scaled version of B_Γ,

$$B_{D,\Gamma} := \left(B_{D,\Gamma}^{(1)}, \ldots, B_{D,\Gamma}^{(N)}\right) := \left(D^{(1)T} B_\Gamma^{(1)}, \ldots, D^{(N)T} B_\Gamma^{(N)}\right) \tag{3.18}$$

and the standard FETI-DP Dirichlet preconditioner

$$M_D^{-1} := B_{D,\Gamma} R_\Gamma^T S_{\Gamma\Gamma} R_\Gamma B_{D,\Gamma}^T = B_{D,\Gamma} \widetilde{S} B_{D,\Gamma}^T. \tag{3.19}$$

An operator B_D could be obtained by inserting the zero columns corresponding to interior variables into $B_{D,\Gamma}$.

The standard FETI-DP method is the preconditioned conjugate gradient method applied to

$$M_D^{-1} F\lambda = M_D^{-1} d. \tag{3.20}$$

Remark 3.1. *Note that the columns of B can be reordered such that $B = \left(0,\ B_\Gamma\right)$. In order to simplify the notation and to avoid a proliferation of indices, we neglect the trivial part of B on the interior variables and set $B = B_\Gamma$ and $B_D = B_{D,\Gamma}$ for the rest of the thesis.*

Eventually, let us introduce the operator

$$P_D = B_D^T B \tag{3.21}$$

which is essential for the condition number estimate of FETI-DP. For arbitrary λ and $w := \widetilde{S}^{-1} B^T \lambda \in \widetilde{W}$, one has

$$\frac{\langle M_D^{-1} F\lambda, \lambda\rangle_F}{\langle \lambda, \lambda\rangle_F} = \frac{\langle B_D \widetilde{S} B_D^T\ B\widetilde{S}^{-1} B^T\lambda, B\widetilde{S}^{-1} B^T\lambda\rangle}{\langle \widetilde{S}^{-1} B^T\lambda, \widetilde{S}^{-1} B^T\lambda\rangle_{\widetilde{S}}} = \frac{\langle P_D w, P_D w\rangle_{\widetilde{S}}}{\langle w, w\rangle_{\widetilde{S}}} = \frac{|P_D w|_{\widetilde{S}}^2}{|w|_{\widetilde{S}}^2}.$$

The lower bound of this Rayleigh quotient is given by one and thus one is interested in constructing an upper bound of the type

$$|P_D w|_{\widetilde{S}} \leq C |w|_{\widetilde{S}} \quad \forall w \in \widetilde{W}; \tag{3.22}$$

see, e.g., [130].

At the end of this section on FETI-DP, we now give a short and nonexhaustive enumeration of results for standard FETI-DP with different a priori coarse

spaces obtained, in particular, for the diffusion problem and compressible linear elasticity.

In two dimensions, the preconditioned FETI-DP method with a standard vertex coarse space satisifies

$$\kappa(M_D^{-1}F) \leq C\left(1+\log\left(\frac{H}{h}\right)\right)^2 \tag{3.23}$$

with C independent of H and h; see [95].

In three dimensions, the preconditioned FETI-DP method with a standard vertex coarse space performs less well and cannot retain the condition number bound from (3.23); see [38] and [83]. Therefore, enforcing additional constraints such as continuous edge averages (and first-order moments on the edges) was proposed; cf. [37, 107, 83, 82]. Then, for heterogeneous coefficients that are constant on each subdomain, the estimate (3.23) holds with C independent of H, h, and the coefficients; see, e.g., [83] and [82]. For the diffusion equation with heterogeneous coefficients, primal edge averages are sufficient ([83]) while for linear elasticity additional first-order moments can be indispensable; cf. [82, 78]. Note that similar coarse space enrichments were proposed for other domain decomposition methods earlier; see, e.g., [30, 115, 29, 28, 36].

In [78], weighted edge averages for heterogeneities not aligned with the interface were studied numerically.

For materials with a stiff material at a minimum distance of $\eta > 0$ from the interface and included in a soft hull, a comparable condition number bound taking also η into consideration was given in [49, 48]. For the diffusion problem, related patch techniques and condition number bounds for one-level and all-floating FETI methods, depending only on the coefficient jumps in the neighborhood of the interface, were already considered in [104, 105].

In order to establish condition number bounds for the diffusion problem, Poincaré inequalities are used and constant coefficients on the subdomains are assumed. In [106] weighted Poincaré inqualities for quasi monotonous coefficient distributions (see [115, 29]) were considered.

For almost incompressible linear elasticity, a zero net flux condition has to be considered; without further going into detail, we refer to, e.g., [102, 49] for almost incompressible materials and FETI-DP and BDDC.

We end this section without going further into detail since the coefficient distributions considered in this thesis are in general arbitrarily heterogeneous and do not fulfill the previous assumptions on the coefficients. The condition

number bounds established in this thesis are based on adaptively computed coarse spaces.

3.3 Standard BDDC

As noted in the preliminary section, the BDDC method was proposed by different authors; see [20, 23, 43].

For BDDC, as for FETI-DP, we use the subdivision of the degrees of freedom introduced before.

On the dual interface nodes, the BDDC method corresponds to a Neumann-Neumann algorithm with continuous iterates and noncontinuous flux approximations which become continuous at convergence only; cf., e.g., [130, Sec. 1.3.4] for an elementary description of Neumann-Neumann methods. In this sense, the BDDC method is dual to FETI-DP and therefore both methods are related.

To define the BDDC method, it is convenient to introduce a modified ordering, i.e., $(u_{\Delta'}^T,\ u_{\Pi'}^T)^T := \left(u_{\Delta'}^{(1)T}, \ldots, u_{\Delta'}^{(N)T}, u_{\Pi'}^{(1)T}, \ldots, u_{\Pi'}^{(N)T}\right)^T$ instead of $\left(u_{\Delta'}^{(1)T}, u_{\Pi'}^{(1)T}, \ldots, u_{\Delta'}^{(N)T}, u_{\Pi'}^{(N)T}\right)^T$. Consequently, for theoretical considerations only, we have to assume a different ordering of the corresponding submatrices. We use calligraphic letters to distinguish matrices used in BDDC from the corresponding matrices used in FETI-DP. Instead of $K_{\Gamma\Gamma}$, we use

$$\mathcal{K}_{\Gamma\Gamma} := \begin{pmatrix} K^{(1)}_{\Delta'\Delta'} & 0 & \cdots & 0 & K^{(1)T}_{\Pi'\Delta'} & 0 & \cdots & 0 \\ 0 & \ddots & \ddots & \vdots & 0 & \ddots & \ddots & \vdots \\ \vdots & \ddots & \ddots & 0 & \vdots & \ddots & \ddots & 0 \\ 0 & \cdots & 0 & K^{(N)}_{\Delta'\Delta'} & 0 & \cdots & 0 & K^{(N)T}_{\Pi'\Delta'} \\ K^{(1)}_{\Pi'\Delta'} & 0 & \cdots & 0 & K^{(1)}_{\Pi'\Pi'} & 0 & \cdots & 0 \\ 0 & \ddots & \ddots & \vdots & 0 & \ddots & \ddots & \vdots \\ \vdots & \ddots & \ddots & 0 & \vdots & \ddots & \ddots & 0 \\ 0 & \cdots & 0 & K^{(N)}_{\Pi'\Delta'} & 0 & \cdots & 0 & K^{(N)}_{\Pi'\Pi'} \end{pmatrix}$$

and the corresponding off-diagonal block $\mathcal{K}_{\Gamma I}$ such that we can compute the Schur complement

$$\mathcal{S}_{\Gamma\Gamma} := \mathcal{K}_{\Gamma\Gamma} - \mathcal{K}_{\Gamma I} K_{II}^{-1} \mathcal{K}_{\Gamma I}^T$$

from the matrix

$$\begin{pmatrix} K_{II} & \mathcal{K}_{\Gamma I}^T \\ \mathcal{K}_{\Gamma I} & \mathcal{K}_{\Gamma\Gamma} \end{pmatrix}. \tag{3.24}$$

Note that we use the matrix K_{II} as defined in (3.4). The right hand side is obtained with the corresponding elimination of the interior degrees of freedom from f and is denoted by $\left(g_{\Delta'}^T,\ g_{\Pi'}^T\right)^T$; see below.

For BDDC, instead of the Boolean jump operator from FETI-DP, we use $R_{\Delta'}^T := \left(R_{\Delta'}^{(1)T}, \ldots, R_{\Delta'}^{(N)T}\right)$, which performs the finite element assembly in the dual variables $u_{\Delta'}^{(i)}$.

The (unpreconditioned) BDDC system corresponds to a primal Schur complement method. For $u_\Gamma^T = \left(u_{\Delta'}^T,\ u_{\Pi'}^T\right)^T$, the system writes

$$\mathcal{S}u_\Gamma := \begin{pmatrix} R_{\Delta'}^T & 0 \\ 0 & I_{\Pi'} \end{pmatrix} \begin{pmatrix} I_{\Delta'} & 0 \\ 0 & R_{\Pi'}^T \end{pmatrix} \mathcal{S}_{\Gamma\Gamma} \begin{pmatrix} I_{\Delta'} & 0 \\ 0 & R_{\Pi'} \end{pmatrix} \begin{pmatrix} R_{\Delta'} & 0 \\ 0 & I_{\Pi'} \end{pmatrix} u_\Gamma = g \tag{3.25}$$

with right hand side

$$g := \begin{pmatrix} R_{\Delta'}^T & 0 \\ 0 & R_{\Pi'}^T \end{pmatrix} \begin{pmatrix} g_{\Delta'} \\ g_{\Pi'} \end{pmatrix} := \begin{pmatrix} R_{\Delta'}^T & 0 \\ 0 & R_{\Pi'}^T \end{pmatrix} \begin{pmatrix} f_{\Delta'} - K_{\Delta' I} K_{II}^{-1} f_I \\ f_{\Pi'} - K_{\Pi' I} K_{II}^{-1} f_I \end{pmatrix}.$$

As in FETI-DP, we introduce a preconditioner to speed up the convergence of the iterative solver. A key ingredient in the standard preconditioner are again (diagonal) scaling matrices $D_u^{(i)} : \partial\Omega_{i,h} \cap \Gamma_h \to \partial\Omega_{i,h} \cap \Gamma_h$, $i = 1, \ldots, N$. The scaling in BDDC is very straight-forward, once the functions $d_u^{(i)} : \partial\Omega_{i,h} \cap \Gamma_h \to (0,1)$ from the previous section are defined; see (3.14).

For a diagonal scaling, if r is the local index of a degree of freedom on Γ, we obtain

$$\left(D_u^{(i)}\right)_{rr} := d_u^{(i)}(x). \tag{3.26}$$

The other entries of $D^{(i)}$ as well as the entries of $D^{(j)}$ and $D^{(k)}$ are obtained correspondingly.

The nondiagonal scaling matrices used in BDDC also consist of blocks of the size of the edges and the faces. Consider either an (open) face $\mathcal{F}^{ij}$ shared by the two subdomains Ω_i and Ω_j or an (open) edge $\mathcal{E}^{ik}$ shared by the subdomains Ω_i, Ω_j, Ω_k. Multiplicities greater than three can be handled analogously. Then, the scaling on Ω_i, restricted to $\mathcal{F}^{ij}$ and $\mathcal{E}^{ik}$, respectively, is easily given by

$$D_{u\,|\mathcal{F}^{ij}}^{(i)} := D_{u,\mathcal{F}^{ij}}^{(i)} \text{ and } D_{u\,|\mathcal{E}^{ik}}^{(i)} := D_{u,\mathcal{E}^{ik}}^{(i)}, \tag{3.27}$$

respectively, with $D^{(i)}_{u,\mathcal{F}^{ij}}$ and $D^{(i)}_{u,\mathcal{E}^{ik}}$ as introduced before equation (3.16). Again, the other entries of $D^{(i)}$ as well as the entries of $D^{(j)}$ and $D^{(k)}$ are obtained correspondingly.

As before, (3.27) is a generalization of (3.26).

With D_u defined, we can introduce the scaled assembly operator R^T_{Δ',D_u} in the a priori dual variables which results from scaling the operator $R^{(i)}_{\Delta'}$ by $D^{(i)}_u$, $i = 1, \ldots, N$. The standard BDDC preconditioner then writes

$$M^{-1}_{\mathrm{BDDC}} := \begin{pmatrix} R^T_{\Delta',D_u} & 0 \\ 0 & I_{\Pi'} \end{pmatrix} \widetilde{S}^{-1} \begin{pmatrix} R_{\Delta',D_u} & 0 \\ 0 & I_{\Pi'} \end{pmatrix} \tag{3.28}$$

and the preconditioned BDDC system is given by

$$M^{-1}_{\mathrm{BDDC}} \mathcal{S} u_\Gamma = M^{-1}_{\mathrm{BDDC}} g. \tag{3.29}$$

As in FETI-DP, the operator P_D is essential for establishing a condition number bound of the corresponding BDDC method. This comes from the fact, that the challenge of estimating the eigenvalues of $M^{-1}_{\mathrm{BDDC}}\mathcal{S}$ can be reduced to the problem of estimating the eigenvalues of

$$E_{D_u} := I - P_D; \tag{3.30}$$

see [81, 43, 53, 92, 89].

3.4 Scaling variants for FETI-DP and BDDC

For heterogeneous problems, the use of an appropriate scaling is important; see, e.g., [112]. To be effective, the scaling best depends on the coefficient distribution of the underlying PDE. The scaling is of equal importance in adaptive FETI-DP and BDDC methods since, for a bad scaling, the resulting adaptive coarse space can be very large; see, e.g., [74, 68].

In this thesis, we consider four different scalings and present an extensive numerical comparison of these for three-dimensional problems in Section 6.5.3.

ρ-Scaling. First, we introduce the standard ρ-scaling; see, e.g., [88, 31, 91, 115, 81, 130, 78, 105], also for domain decomposition methods other than FETI-DP and BDDC. For $i \in \{1, \ldots, N\}$ and $x \in \partial\Omega_i \cap \Gamma_h$, we introduce the local

ρ-coefficient or Young's modulus evaluation by

$$\widehat{\rho}_i(x) := \begin{cases} \sup\limits_{x \in \mathrm{supp}(\varphi_x) \cap \Omega_i} \rho(x), & \text{for diffusion,} \\ \sup\limits_{x \in \mathrm{supp}(\varphi_x) \cap \Omega_i} \mathrm{E}(x), & \text{for linear elasticity,} \end{cases} \tag{3.31}$$

where φ_x is the nodal finite element function at x and $\mathrm{supp}(\varphi_x)$ its support.

The functions $d_u^{(i)} : \partial\Omega_{i,h} \cap \Gamma_h \to (0,1)$ introduced generically before (3.14) are then defined as

$$d_u^{(i)}(x) := \frac{\widehat{\rho}_i(x)}{\sum_{k \in \mathcal{N}_x} \widehat{\rho}_k(x)}. \tag{3.32}$$

Let for example Ω_i and Ω_j share either a face or an edge and let $x \in \partial\Omega_i \cap \partial\Omega_j$. Then, in FETI-DP the corresponding nontrivial row of $B^{(i)}$, coupling Ω_i and Ω_j at x, is multiplied by the scaling $d_u^{(j)}(x) = \widehat{\rho}_j(x) / \Big(\sum_{k \in \mathcal{N}_x} \widehat{\rho}_k(x) \Big)$ to obtain the corresponding row of $B_D^{(i)}$; vice versa for Ω_j. On the other hand, in BDDC the degrees of freedom on $\partial\Omega_i$ are scaled by $d_u^{(i)} = \widehat{\rho}_i(x) / \Big(\sum_{k \in \mathcal{N}_x} \widehat{\rho}_k(x) \Big)$.

Stiffness-Scaling. Second, we introduce stiffness- (or K-, or super-lumped-) scaling (see, e.g., [21, 31, 91, 112]), which is a heuristic approximation of ρ-scaling. There, we replace the coefficient $\widehat{\rho}_i(x)$ by the corresponding diagonal element of the local stiffness matrix $K^{(i)}$. By replacing the definition in (3.31), we obtain stiffness-scaling with the same definitions of $d_u^{(i)}$, $D^{(i)}$ and $D_u^{(i)}$, $i = 1, \ldots, N$.

Multiplicity-Scaling. Third, we introduce multiplicity-scaling (see, e.g., [90, 42, 39, 112, 38]), which does not rely on the coefficients of the PDE. In multiplicity-scaling, the inverse of the multiplicity of a node is used. We obtain multiplicity-scaling from ρ-scaling by setting the coefficient evaluation to one, i.e., redefining

$$\widehat{\rho}_i(x) := 1$$

for all $x \in \partial\Omega_{i,h} \cap \Gamma_h$ and $i = 1, \ldots, N$. We can again use the same definitions of $d_u^{(i)}$, $D^{(i)}$ and $D_u^{(i)}$, $i = 1, \ldots, N$.

For coefficient jumps only along but not across subdomain boundaries, ρ-scaling reduces to multiplicity-scaling.

Deluxe-Scaling. Last, we consider deluxe-scaling, which was introduced recently; see [24] and, e.g, [22, 6, 18, 75, 16]. Deluxe-scaling is a nondiagonal scaling and therefore computationally more expensive.

Consider either a face $\mathcal{F}^{ij}$ shared by the two subdomains Ω_i and Ω_j or an edge $\mathcal{E}^{ik}$ shared by the subdomains Ω_i, Ω_j, and Ω_k. Multiplicities greater than three can be handled analogously.

The Schur complement $S^{(l)}$ can be partitioned as

$$S^{(l)} = \begin{pmatrix} S^{(l)}_{\mathcal{F}^{ij}\mathcal{F}^{ij}} & S^{(l)T}_{\mathcal{F}^{ij^C}\mathcal{F}^{ij}} \\ S^{(l)}_{\mathcal{F}^{ij^C}\mathcal{F}^{ij}} & S^{(l)}_{\mathcal{F}^{ij^C}\mathcal{F}^{ij^C}} \end{pmatrix}, \; l \in \{i,j\}, \tag{3.33}$$

$$\text{and } S^{(l)} = \begin{pmatrix} S^{(l)}_{\mathcal{E}^{ik}\mathcal{E}^{ik}} & S^{(l)T}_{\mathcal{E}^{ik^C}\mathcal{E}^{ik}} \\ S^{(l)}_{\mathcal{E}^{ik^C}\mathcal{E}^{ik}} & S^{(l)}_{\mathcal{E}^{ik^C}\mathcal{E}^{ik^C}} \end{pmatrix}, \; l \in \{i,j,k\}, \tag{3.34}$$

where the sets $\mathcal{F}^{ij^C}$ and $\mathcal{E}^{ik^C}$ are the complements of $\mathcal{F}^{ij}$ and $\mathcal{E}^{ik}$ with respect to the local interface; see, e.g., [75]. For $l \in \{i,j\}$, we define $S^{(l)}_{\mathcal{F}^{ij},0} := S^{(l)}_{\mathcal{F}^{ij}\mathcal{F}^{ij}}$, and for $l \in \{i,j,k\}$, we define $S^{(l)}_{\mathcal{E}^{ik},0} := S^{(l)}_{\mathcal{E}^{ik}\mathcal{E}^{ik}}$.

For the face $\mathcal{F}^{ij}$, deluxe-scaling is defined by

$$D^{(i)}_{u,\mathcal{F}^{ij}} := (S^{(i)}_{\mathcal{F}^{ij},0} + S^{(j)}_{\mathcal{F}^{ij},0})^{-1} S^{(i)}_{\mathcal{F}^{ij},0} \tag{3.35}$$

as well as (3.17) for FETI-DP and (3.27) for BDDC, respectively.

That means that nontrivial rows of $B^{(i)}$ corresponding to the Lagrange multipliers on this face are multiplied by $D^{(j)T}_{u,\mathcal{F}^{ij}} = \left((S^{(i)}_{\mathcal{F}^{ij},0} + S^{(j)}_{\mathcal{F}^{ij},0})^{-1} S^{(j)}_{\mathcal{F}^{ij},0}\right)^T$ if the orientation of the constraints in B is chosen consistently. Otherwise, certain entries have to be scaled by -1.

For the edge $\mathcal{E}^{ik}$, deluxe-scaling is defined by

$$D^{(i)}_{u,\mathcal{E}^{ik}} = (S^{(i)}_{\mathcal{E}^{ik},0} + S^{(j)}_{\mathcal{E}^{ik},0} + S^{(k)}_{\mathcal{E}^{ik},0})^{-1} S^{(i)}_{\mathcal{E}^{ik},0} \tag{3.36}$$

as well as (3.17) for FETI-DP and (3.27) for BDDC, respectively.

Again, that means that nontrivial rows of $B^{(i)}$ corresponding to the Lagrange multipliers coupling Ω_i and Ω_j on this edge are multiplied by $D^{(j)T}_{u,\mathcal{E}^{ik}} = \Big((S^{(i)}_{\mathcal{E}^{ik},0} + S^{(j)}_{\mathcal{E}^{ik},0} + S^{(k)}_{\mathcal{E}^{ik},0})^{-1} S^{(j)}_{\mathcal{E}^{ik},0}\Big)^T$ if a consistent orientation of the Lagrange multipliers is assumed.

4 An implementational view on coarse space enrichments for FETI-DP and BDDC

4.1 Preliminaries

In this chapter, we present different approaches to implement coarse space enrichments for FETI-DP and BDDC. The idea of an enrichment of the a priori coarse space of FETI-1 was already discussed in [36] and in one of the first works on FETI-DP; see [37]. Our specific choice of additional constraints to enrich the a priori coarse space is outlaid in the following chapters. Parts of this chapter have been published in modified or unmodified form by the author of this thesis and his coauthors in [64, 67, 68].

Theoretically elegant ways to enforce additional constraints in the FETI-DP method are given by the deflation and the balancing approach. Deflation (see [100]) is also known as projector preconditioning; see [26]. Deflation and balancing have already been used extensively in the context of domain decomposition methods; see, e.g., [97, 58, 80]. In this thesis, the deflation and the balancing approach are only considered for FETI-DP since the BDDC method using deflation is not equivalent to the BDDC method using a transformation of basis; see [80].

A second and intuitive way in the context of finite element methods, to enforce additional constraints, is the transformation-of-basis approach. In this approach, the nodal basis is transformed such that general constraints can be enforced by partial nodal assembly; see, e.g., [83, 89, 82, 77, 80]. The standard approach can be proven to be equivalent to a corresponding deflation approach if constant scaling on any face and any edge is assumed, e.g., multiplicity-scaling or ρ-scaling for certain coefficient distributions; see [80].

Third, we present a technique introduced in [82] to retain the sparsity of the matrix $K^{(i)}_{B'B'}$ which is otherwise affected by the explicit transformation of basis. Similar techniques using optional Lagrange multipliers and saddle point

formulations were also used in, e.g., [37, 51, 92, 93]. These techniques are not treated in detail in this thesis.

Last in this chapter, we present the generalized transformation-of-basis approach; see [67]. This generalized approach offers a remedy for arbitrary coefficient distributions and scalings where assumptions of the standard theory do not hold anymore. We prove that for every FETI-DP or BDDC method using the generalized transformation-of-basis approach, there is a corresponding FETI-DP method using the deflation or the balancing approach with essentially the same spectrum. On the other hand, for a given FETI-DP method using balancing or deflation (under a few assumptions, see Section 4.5), we can construct a FETI-DP method using the generalized transformation-of-basis approach, which again has essentially the same spectrum.

4.2 FETI-DP with deflation and balancing

In this section, we briefly explain the deflation and the balancing approach. These approaches provide a mechanism to enrich the coarse space by adding additional constraints. Parts of this section have already been published in modified or unmodified form by the author of this thesis and his coauthors in [64, 67].

For an introduction to deflation and balancing, in parts especially in the context of FETI-DP and other domain decomposition methods, see [100, 26, 27, 97, 80, 58] and the references therein.

For a matrix A, in the following, we denote by A^+ an arbitrary generalized inverse satisfying $AA^+A = A$ and $A^+AA^+ = A^+$. By elementary linear algebra, it can be shown that A^+A is a projection onto range A^+ with null space $\ker A$; cf., e.g., [8]. These properties are used (implicitly) in the following reasonings.

The following description is based on [80] extended to the case of a semidefinite matrix F. Note that F is symmetric.

In the context of deflation and balancing, we refer to $c_\lambda^T Bw = 0$ as a *constraint* while we refer to c_λ as a *constraint vector* for the Lagrange multipliers. Let $U = (c_{\lambda,1}, \dots, c_{\lambda,m})$ be given as the matrix where the constraint vectors are stored as columns.

Then, we define

$$P := U(U^T FU)^+ U^T F. \tag{4.1}$$

We have range $P = \text{range}\,(U(U^T FU)^+)$ and $\ker P = \ker(U^T FU)^+ U^T F)$. Next, we multiply the FETI-DP system (3.6) by $(I - P)^T$, which yields the deflated

system

$$(I-P)^T F\lambda = (I-P)^T d. \tag{4.2}$$

The deflated system is consistent. Moreover, range $U \subset \ker((I-P)^T F)$. By considering the orthogonal and complementary spaces, we still have range $(F(I-P)) \subset \ker U^T$ for a semidefinite matrix F. Since $(I-P)^T$ is also a projection, we can show that

$$(I-P)^T F = F(I-P) = (I-P)^T F(I-P). \tag{4.3}$$

Therefore, only components of the dual variable in range $(I-P)$ are relevant to the construction of the Krylov spaces. By λ^* we denote the solution of the original system $F\lambda = d$, which is unique only up to an element in $\ker B^T$. Let $\hat{\lambda} \in$ range $(I-P)$ be a solution of (4.2). Then, $\hat{\lambda}$ is identical to $(I-P)\lambda^*$ up to an element in $\ker B^T$. We have the decomposition

$$\lambda^* = P\lambda^* + (I-P)\lambda^* =: \bar{\lambda} + (I-P)\lambda^*,$$

where $\bar{\lambda}$ can be expressed by

$$\bar{\lambda} = P\lambda^* = U(U^T F U)^+ U^T F F^+ F\lambda^* = PF^+ d.$$

Since $B^T(I-P)\lambda^* = B^T\hat{\lambda}$, we can then show that the solution in terms of the displacements does not change if $(I-P)\lambda^*$ is replaced by $\hat{\lambda}$, i.e.,

$$u_\Delta = \widetilde{S}^{-1}\left(\widetilde{f}_\Delta - B^T\lambda^*\right) = \widetilde{S}^{-1}\left(\widetilde{f}_\Delta - B^T(\bar{\lambda}+\hat{\lambda})\right).$$

Preconditioning the resulting system of equations by the Dirichlet preconditioner M_D^{-1} gives

$$M_D^{-1}(I-P)^T F\lambda = M_D^{-1}(I-P)^T d.$$

Another multiplication with $I-P$ from the left gives the new symmetric preconditioner

$$M_{PP}^{-1} := (I-P)M_D^{-1}(I-P)^T, \tag{4.4}$$

which can also be denoted deflation preconditioner. As shown in [80, Theorem 6.1], we do not change the nonzero eigenvalues of the former left hand side when multiplying with $I-P$. Therefore, the deflated problem reads:

Find $\lambda \in \operatorname{range}(I - P)$, such that

$$M_{PP}^{-1} F \lambda = M_{PP}^{-1} d.$$

Instead of computing $\bar{\lambda}$ a posteriori, the computation can be included into each iteration. This leads to the balancing preconditioner

$$\widetilde{M}_{BP}^{-1} := M_{PP}^{-1} + P F^{+}.$$

Although the balancing preconditioner for a semidefinite matrix F is then of the form $\widetilde{M}_{BP}^{-1} = M_{PP}^{-1} + U(U^T F U)^{+} U^T F F^{+}$, we can equivalently use

$$M_{BP}^{-1} = M_{PP}^{-1} + U(U^T F U)^{+} U^T \tag{4.5}$$

since it is applied to $F\lambda = d$ and $FF^{+}F = F$ as well as $d \in \operatorname{range} F$.

Let us note that the Theorems 6.2 and 6.3 in [80] can be proven for a semidefinite matrix F by replacing F^{-1} by F^{+} and by following the arguments given in [80]. As a result, we obtain that the eigenvalues of $M_{BP}^{-1}F$ and $M_{PP}^{-1}F$ are essentially the same.

In order to provide a condition number bound for the deflation and the balancing approach let us first assume that a standard Rayleigh quotient estimate for the P_D-operator (see (3.21) and (3.22)) is given on the deflated space, i.e.,

$$\frac{\|P_D w\|_{\widetilde{S}}^2}{\|w\|_{\widetilde{S}}^2} \leq C \text{ for all } w \in \{w \in \widetilde{W} \,:\, U^T B w = 0\} \tag{4.6}$$

and $C = \text{const} > 0$. An estimate of this type is established in Lemma 5.5. Then, based on results of [80], it was shown in [75, Lemma 3.2] that the condition number of the FETI-DP operator preconditioned by deflation/projector preconditioning or balancing can be bounded from above by C.

Let us define

$$\widetilde{W}_U = \{w \in \widetilde{W} \,:\, U^T B w = 0\}, \tag{4.7}$$

then, with (3.1), we have

$$\widehat{W} \subset \widetilde{W}_U \subset \widetilde{W} \subset W. \tag{4.8}$$

Let us briefly comment on the computational cost. We use deflation or balancing as a second, independent mechanism (in addition to an initial coarse space from partial assembly; see (3.8)) to implement the coarse space con-

structed from our eigenvalue problems in Chapter 5. Other approaches to implement this coarse space would also be possible; see, e.g., Chapters 6 and 7. For the deflation or balancing approach, the coarse operator $U^T F U$ has to be formed as a sparse matrix and, during the iteration, the application of $(U^T F U)^+$ to a vector has to be computed. When forming the Galerkin product $U^T F U$, it is essential for the efficiency to exploit the sparsity of U and the structure of F. The generalized inverse $(U^T F U)^+$ can be computed at essentially the same cost as a sparse Cholesky factorization. However, for large adaptive coarse problems, the computational cost can still be large.

4.3 FETI-DP and BDDC with the (standard) transformation-of-basis approach

In this section, we recall the standard approach of the transformation of basis for FETI-DP and BDDC; see, e.g., [83, 89, 82, 77, 80]. Parts of this section have already been published in modified or unmodified form by the author of this thesis and his coauthors in [67, 68].

For this approach, we assume a constant scaling on any face and any edge, e.g., multiplicity-scaling or ρ-scaling for certain coefficient distributions. For an example violating the assumption of constant scaling per face or per edge, see Figure 4.3.

Using partial finite element assembly, continuity across the subdomain boundary on certain degrees of freedom of u can be enforced for the corresponding finite element basis function. However, when using a transformation of basis from a nodal to a different basis, also general constraints can be enforced using the same technique.

In order to simplify the visualization, we demonstrate the approach with the following two-dimensional example. Let the edge $\mathcal{E}$ be shared by the subdomains Ω_i and Ω_j. During the Krylov iteration, the iterates u now should fulfill a constraint involving the nodes of the edge $\mathcal{E}$. For the sake of simplicity, we further assume that this constraint is the only additional constraint to implement by a transformation of basis and partial assembly.

Suppose that the *constraint vector* for the transformation-of-basis approach is given by the normalized vector c_u defined on $\partial\Omega_i \cap \mathcal{E}$ and $\partial\Omega_j \cap \mathcal{E}$ (and equal on both sets). Then, the *constraint* writes

$$c_u^T \left(u_{\mathcal{E}}^{(i)} - u_{\mathcal{E}}^{(j)} \right) = 0 \quad \Leftrightarrow \quad c_u^T u_{\mathcal{E}}^{(i)} = c_u^T u_{\mathcal{E}}^{(j)} \tag{4.9}$$

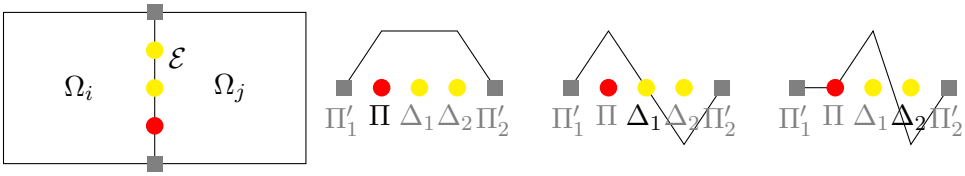

Figure 4.1: *Example of transformed, nonnodal basis functions:* Two subdomains Ω_i and Ω_j sharing the edge $\mathcal{E}$ (left). Transformed, nonnodal basis functions on the edge $\mathcal{E}$ belonging to the degrees of freedom Π, Δ_1, and Δ_2 (from second to left to right). In all images, a priori primal vertices (Π') are indicated by gray squares. A priori dual variables (Δ') are indicated by circles. The average constraint is enforced at the red degree of freedom (Π); yellow circles represent the remaining dual variables Δ_1 and Δ_2.

for $u_{\mathcal{E}}^{(l)} = u_{|\partial\Omega_l \cap \mathcal{E}}$, $l \in \{i, j\}$.

For instance, $c_u = \frac{1}{n_{\mathcal{E}}}(1, \ldots, 1)^T$ means a continuous edge average shared by Ω_i and Ω_j, where $n_{\mathcal{E}}$ is the length of c_u. This corresponds to the use of a nonnodal basis function; see Figure 4.1 for an edge with three degrees of freedom.

We then define a (square) transformation matrix

$$T_{\mathcal{E}}^{(l)} = \left(c_u,\ C_u^{(l)\perp}\right), \quad l \in \{i, j\} \tag{4.10}$$

where $C_u^{(l)\perp}$ is computed such that $T_{\mathcal{E}}^{(l)}$ is orthogonal. We then define the transformation matrix $T^{(l)}$, which acts on the complete subdomain, and which is identical to $T_{\mathcal{E}}^{(l)}$ on the edge $\mathcal{E}$ and the identity elsewhere.

We obtain the transformed variables $\overline{u}^{(l)}$, the transformed stiffness matrices $\overline{K}^{(l)}$, and the transformed load vectors $\overline{f}^{(l)}$ on Ω_l as

$$\overline{K}^{(l)} = T^{(l)T} K^{(l)} T^{(l)}, \quad \overline{u}^{(l)} = T^{(l)T} u^{(l)}, \quad \overline{f}^{(l)} = T^{(l)T} f^{(l)}, \quad l \in \{i, j\}. \tag{4.11}$$

After the transformation of basis has been performed, assembly in the new primal variables is used to enforce the given constraint.

This procedure indeed enforces our original constraint corresponding to c_u as follows. With (4.10) and (4.11), we have

$$c_u^T u_{\mathcal{E}}^{(l)} = c_u^T T_{\mathcal{E}}^{(l)} \overline{u}_{\mathcal{E}}^{(l)} = c_u^T \left(c_u,\ C_u^{(l)\perp}\right) \overline{u}_{\mathcal{E}}^{(l)} = (1, 0, \ldots, 0)\, \overline{u}_{\mathcal{E}}^{(l)} = \overline{u}_{\mathcal{E},1}^{(l)}, \quad l \in \{i, j\},$$

where $\overline{u}^{(l)}_{\mathcal{E},1}$ is the displacement at the first degree of freedom on the edge $\mathcal{E} \cap \partial\Omega_l$. Let us now reduce the variables $\overline{u}^{(i)}_{\mathcal{E},1}$ and $\overline{u}^{(j)}_{\mathcal{E},1}$ by using partial finite element assembly in the specific degree of freedom. For the transformed **and assembled** variables, we use $\widehat{u}$ instead of $\overline{u}$. Precisely, we have

$$\widehat{u}_{\mathcal{E},1} := \widehat{u}^{(i)}_{\mathcal{E},1} := \widehat{u}^{(j)}_{\mathcal{E},1} := \overline{u}^{(i)}_{\mathcal{E},1} + \overline{u}^{(j)}_{\mathcal{E},1} \tag{4.12}$$

by partial assembly in the first degree of freedom and $\widehat{u}^{(l)}_{\mathcal{E},k} := \overline{u}^{(l)}_{\mathcal{E},k}$ for $k > 1$. For the values transformed back to the initial basis, we now see by

$$c_u^T T^{(i)}_{\mathcal{E}} \widehat{u}^{(i)}_{\mathcal{E}} = \overline{u}^{(i)}_{\mathcal{E},1} + \overline{u}^{(j)}_{\mathcal{E},1} = c_u^T T^{(j)}_{\mathcal{E}} \widehat{u}^{(j)}_{\mathcal{E}} \quad \Leftrightarrow \quad c_u^T \left(T^{(i)}_{\mathcal{E}} \widehat{u}^{(i)}_{\mathcal{E}} - T^{(j)}_{\mathcal{E}} \widehat{u}^{(j)}_{\mathcal{E}} \right) = 0$$

that the constraint is enforced.

Note that it is not necessary for $T^{(l)}_{\mathcal{E}}$ of (4.10) to be orthogonal. The rows or columns only have to represent the basis of the transformation. Then, instead of T^T, T^{-1} would be necessary to realize the corresponding inverse transformation.

Faces in three dimensions can be handled completely analogously. However, it should be noted that explicit transformations on faces affect the sparsity pattern of the (transformed) stiffness matrices to a larger extent than explicit transformations on edges. For edges in three dimensions, only the additional transformation matrices $T^{(l)}_{\mathcal{E}}$ and $T^{(l)}$ ($l \notin \{i, j\}$) have to be defined accordingly and the partial assembly simply assembles more than two degrees of freedom.

4.4 An alternative formulation of the transformation of basis for FETI-DP and BDDC

In [82], a technique was introduced to avoid affecting the sparsity of the matrix $\overline{K}^{(i)}_{B'B'}$ by the explicit transformation of basis. This is important for face constraints. To resolve this issue, as in [82, Sec. 4.2.2], we can alternatively introduce additional, local Lagrange multipliers $\mu^{(i)}$ and consider local saddle point problems. Parts of this section have already been published in modified or unmodified form by the author of this thesis and his coauthors in [68].

Let us briefly consider this strategy. By applying the operator F with transformed stiffness matrices, the expression $B_{B'} \overline{K}^{-1}_{B'B'} \overline{v}_{B'}$ has to be evaluated locally, i.e., $B^{(i)}_{B'} \left(\overline{K}^{(i)}_{B'B'} \right)^{-1} \overline{v}^{(i)}_{B'}$ has to be computed. Obviously, the minimization of $\overline{u}^{(i)T}_{B'} \overline{K}^{(i)}_{B'B'} \overline{u}^{(i)}_{B'}$ leads to the same result as the minimization of

$$\begin{pmatrix} \overline{u}^{(i)T}_{B'} & 0 \end{pmatrix} \begin{pmatrix} \overline{K}^{(i)}_{B'B'} & \overline{K}^{(i)T}_{\Pi'B'} \\ \overline{K}^{(i)}_{\Pi'B'} & \overline{K}^{(i)}_{\Pi'\Pi'} \end{pmatrix} \begin{pmatrix} \overline{u}^{(i)}_{B'} \\ 0 \end{pmatrix}, \tag{4.13}$$

where the values at the a priori primal variables Π' are set to zero. This is admissible since the jump operator is applied afterwards and thus the values at the primal variables are set to zero.

Then, instead of minimizing the expression (4.13) in the transformed variables $\overline{u}_{B'}^{(i)}$, we introduce a corresponding constraint $Q^{(i)T}u^{(i)} = 0$ for the non-transformed variables. This consequently leads to the following saddle point problem

$$\begin{pmatrix} K_{II}^{(i)} & K_{\Gamma I}^{(i)T} & 0 \\ K_{\Gamma I}^{(i)} & K_{\Gamma\Gamma}^{(i)} & Q^{(i)} \\ 0 & Q^{(i)T} & 0 \end{pmatrix} \begin{pmatrix} u_I^{(i)} \\ u_\Gamma^{(i)} \\ \mu^{(i)} \end{pmatrix} = \begin{pmatrix} v_I^{(i)} \\ v_\Gamma^{(i)} \\ 0 \end{pmatrix}, \tag{4.14}$$

with additional local Lagrange mutipliers $\mu^{(i)}$ (cf. [82, Sec. 4.2.2] for more details) and where the right hand side $(v_I^{(i)T}, v_\Gamma^{(i)T})$ corresponds to $(\overline{v}_{B'}^T, 0)$ transformed back to the initial basis and restricted to the local subdomain.

Similar techniques of using saddle point problems to enforce (primal) constraints have been used by other authors in [37], the Lagrange multipliers are global; in [51, 92, 93], the saddle point problems are local, which is also the case in our approach. In the case presented here, however, the coarse Schur complement operator is assembled from the local subdomain contributions rather than built from a triple matrix product; see, e.g., [92, 93].

4.5 FETI-DP and BDDC with the generalized transformation-of-basis approach

Parts of Section 4.5 have already been published in modified or unmodified form by the author of this thesis and his coauthors in [67, 68]. This section, in particular, is essentially based on [67].

4.5.1 Preliminaries

When FETI-DP and BDDC methods are set up, an initial coarse space is defined to introduce sufficient coupling to obtain invertibility of the subdomain problems. A simple vertex coarse space can suffice as an initial coarse space. At the same time, an initial scaling is chosen; see Sections 3.2-3.4. For heterogeneous problems, the scaling used in the preconditioner is an important ingredient to obtain a robust iterative method. Then, if hard problems are considered, a second coarse space might be of interest to obtain fast convergence. To the first coarse space defined by the a priori primal variables we also refer as

a priori coarse space, and to the second coarse space, defined after the scaling had been chosen, we refer to as *a posteriori coarse space*.

As introduced in Section 3.1, we denote the index set of a priori primal variables by Π' and the index set of a priori dual variables by Δ'. The index set of a posteriori primal variables is denoted by Π, i.e., the final set of primal variables is $\widehat{\Pi} = \Pi' \cup \Pi$ and the remaining (or a posteriori) set of dual variables $\Delta = \Delta' \setminus \Pi$.

In adaptive FETI-DP and BDDC methods [93, 94, 22, 74, 75, 63, 64, 7, 101, 17, 134, 62, 103, 68], the a posteriori coarse space is highly dependent on the a priori scaling, i.e., the computation of the approximate eigenvectors for the a posteriori coarse space makes use of the a priori scaling. Indeed, the choice of an inappropriate a priori scaling (e.g., the use of multiplicity-scaling for heterogeneous problems) leads to an unnecessary large a posteriori coarse space. This can be observed in, e.g., [75, 68] and Section 6.5.3.

For FETI-DP, the implementation of a second coarse space by deflation or balancing (see, e.g., [80, 58]) is less critical in that context since partial finite element assembly is only used for nodal basis functions; for a combination of adaptive FETI-DP methods with deflation and balancing; cf., e.g. [75, 64, 62].

Though, using a transformation of basis, the a priori scaling might be transformed, too, since it was established for the nodal basis. The use of additional partial finite element assembly in the index set Π then makes the analysis of the new method quite complex.

However, for the different implementations of the constraints, a correspondence of the spectra is of interest. Then, the results of one method can be transfered to the other and vice versa.

Let us briefly illustrate the difference between the a priori and a posteriori coarse space by considering a corresponding deflation method. Assume that an initial coarse space and a scaling D have been defined. Let us assume further that a deflation vector $c_D := c(D)$, i.e., a constraint on the Lagrange multipliers, based on the a priori scaling has been chosen to further accelerate convergence. As an example, c_D could be defined by the solution of local eigenvalue problems, as they appear in adaptive domain decomposition methods (see, e.g., [93, 94, 22, 74, 75, 63, 64, 7, 101, 17, 134, 62, 103, 68]), where the a priori scaling enters the eigenvalue problems explicitly or implicitly. The deflated method using the constraint $c_D^T B w = 0$ may allow the construction of a bound

$$|P_D w|_{\widetilde{S}}^2 \leq C |w|_{\widetilde{S}}^2 \quad \forall w \in \{w \in \widetilde{W} \,:\, c_D^T B w = 0\}; \tag{4.15}$$

cf. Section 4.2. However, the estimate (4.15) depends on the use of the scaling D in combination with the constraint $c_D^T Bw = 0$ and may not be valid anymore if a different scaling $\widetilde{D}$ is used.

Departing from a deflation method with certain assumptions on the constraint set (see the following subsections), we derive the corresponding approach using a change of variables. Unfortunately, with the standard transformation-of-basis approach this correspondence could not be shown since necessary information between a posteriori primal and a posteriori dual variables are dropped within the standard approach. Though, a correspondence between deflation and a change-of-variables approach can be shown under certain assumptions on the constraints if the *generalized transformation-of-basis approach*, as introduced here, is used.

The assumptions on the constraints can be explained visually. In Figure 4.2, we see the difference between constraints in the deflation approach and an approach using partial assembly. To obtain an equivalence between both methods, we have to assume that the constraint from partial assembly is enforced for all Lagrange multipliers coupling the corresponding degree of freedom. Additionally, we assume that the constraints in the deflation approach do not span several edges or faces as in [50, 48].

In order to obtain a corresponding estimate to (4.15) for FETI-DP and BDDC using, both, a change of variables and partial assembly, we show how the scaling has to be transformed for heterogeneous problems. For the scaling in BDDC, see Definition 4.13. For FETI-DP, the scaling is transformed implicitly; see (4.38). This is different from the homogeneous context in [80], where it was shown that the scaling in the new basis is identical to that of the old basis. Note that the theory of [80] also covers specific heterogeneous cases, where, e.g., ρ-scaling reduces to multiplicity-scaling. A priori nondiagonal scaling matrices had not been yet introduced then.

Remark 4.1. *It is an important consequence that, after transformation, an a priori diagonal scaling may not be diagonal anymore and results in an a posteriori nondiagonal scaling. This occurs for nonnodal degrees of freedom, e.g., edge averages, if the scaling is different from multiplicity-scaling. For nodal degrees of freedom an interaction between dual and primal variables results if an a priori nondiagonal scaling such as deluxe-scaling or an a posteriori nondiagonal scaling is used. The interaction between dual and primal variables is not present in classical theory, and a standard argument used in the classical theory, i.e., that iterates are zero in the primal variables, cannot be used, anymore. In our theory, the use of Lemma 4.8 and Lemma 4.9 replaces this standard argument.*

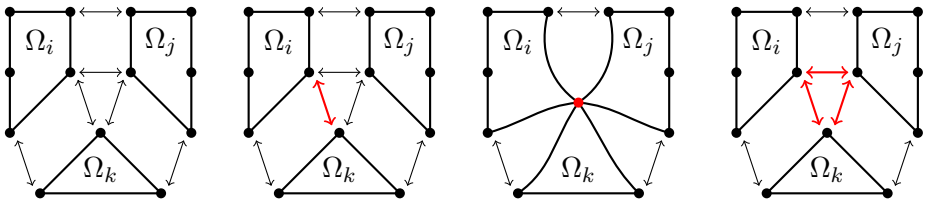

Figure 4.2: *Constraints of the direct deflation approach, the generalized transformation-of-basis approach, and the corresponding deflation approach:* Cross-sectional view of three subdomains sharing an edge. Arrows symbolize redundant Lagrange Multipliers in FETI-DP (left). Assume that, using deflation directly, one primal constraint is introduced, involving the Lagrange multiplier depicted in bold red color (second to left). Using partial assembly, after a transformation of the initial basis, the primal constraint is now enforced between all three subdomains, effectively involving all three Lagrange multipliers (second to right). The deflation or balancing approach corresponding to the generalized transformation-of-basis approach involves all three Lagrange multipliers depicted in bold red color with the same constraint vector (right). [67]

Constructing the scaling for the transformed displacements only in the remaining dual variables does, in general, not give the desired results; see Section 6.1.

This discussion is relevant for FETI-DP and BDDC methods with adaptive coarse spaces where first a scaling is chosen (e.g., ρ-, stiffness- or deluxe-scaling) and then a coarse space is constructed based on this scaling and using partial assembly. Several papers in the literature implicitly rely on the existence of a transformation-of-basis approach for FETI-DP corresponding to the method using deflation. This includes our own paper [68] as well as [7, 101, 17, 62, 103], where adaptive FETI-DP or BDDC methods are combined with, both, a change of variables and partial assembly. We discuss the implications for adaptive FETI-DP and BDDC methods in detail in Chapter 6.

Let us now revisit the classical theory considering an example where the assumption of diagonal and constant scaling on any face and any edge (as assumed in [80]) is not fulfilled anymore.

Example 4.1. In this example, we motivate that the transformation approach can lead to nonzero values in nonnodal primal variables; even if the a priori scaling is diagonal.

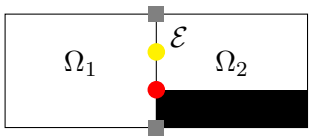

Figure 4.3: *Heterogeneous coefficient distribution to motivate the need for the generalized transformation-of-basis approach:* Decomposition of $\Omega = [0,1] \times [0,\frac{1}{2}]$ into two subdomains Ω_1, Ω_2 with given coefficient distribution. A nonhomogeneous coefficient distribution with $\rho_1 = 1$ (white) and $\rho_2 = 1e+6$ (black) is considered. Initial primal variables (Π') are indicated by gray squares. Initial dual variables are indicated by circles. The red circle represents an a posteriori primal variable (Π), where we enforce a scaling-dependent constraint by a change of variables and partial assembly. The yellow circle represents the remaining dual variable. [67]

Consider the edge $\mathcal{E}$ with first degree of freedom Π (red circle) and second degree of freedom Δ (yellow circle) between the two subdomains Ω_1 and Ω_2 as depicted in Figure 4.3.

The ρ-scaling for the degrees of freedom in the nodal basis is given by

$$D_u^{(1)} = \text{diag}\left(\frac{1}{1+1e6}, \frac{1}{2}\right), \text{ and } D_u^{(2)} = I - D_u^{(1)}.$$

Then, assuming a (nondiagonal) transformation T of the form

$$T = \begin{pmatrix} t_{rr} & t_{ry} \\ t_{yr} & t_{yy} \end{pmatrix} \tag{4.16}$$

with $t_{yr}, t_{ry} \neq 0$, $T^T T = I$, and where the first column is given by a (scaling dependent) constraint vector $c_D^T = (t_{rr}, t_{yr})^T$ enabling an estimate as of (4.15). The constraint is scaling-dependent in the way that the estimate in (4.15) can only be obtained if the constraint is used in combination with the given scaling. This is, e.g., typically the case in methods with adaptive coarse spaces. If the scaling in the adaptive methods is changed, e.g., by restriction (see below), the condition number bound of the adaptive method may not be valid anymore.

The indices r and y in (4.16) denote the relation to the nodes colored red and yellow in Figure 4.3.

In the new basis, the transformed ρ-scaling on the degrees of freedom (see Definition 4.13) is

$$\widehat{D}_u^{(1)} = \begin{pmatrix} \frac{1}{1+1e6}t_{rr}^2 + \frac{1}{2}t_{yr}^2 & \frac{1}{1+1e6}t_{rr}t_{ry} + \frac{1}{2}t_{yr}t_{yy} \\ \frac{1}{1+1e6}t_{rr}t_{ry} + \frac{1}{2}t_{yr}t_{yy} & \frac{1}{1+1e6}t_{ry}^2 + \frac{1}{2}t_{yy}^2 \end{pmatrix} =: \begin{pmatrix} \widehat{d}_{rr} & \widehat{d}_{ry} \\ \widehat{d}_{yr} & \widehat{d}_{yy} \end{pmatrix}$$
$$\text{and } \widehat{D}_u^{(2)} = I - \widehat{D}_u^{(1)} = \begin{pmatrix} 1-\widehat{d}_{rr} & -\widehat{d}_{ry} \\ -\widehat{d}_{yr} & 1-\widehat{d}_{yy} \end{pmatrix}.$$

After enforcing continuity in the a posteriori primal variable, we have with $w_\Pi = w_\Pi^{(1)} = w_\Pi^{(2)}$,

$$\begin{aligned}(\widehat{P}_D w)_\Pi^{(1)} = ((I - \widehat{E}_{D_u})w)_\Pi^{(1)} &= w_\Pi - (\widehat{d}_{rr}w_\Pi + \widehat{d}_{ry}w_\Delta^{(1)} + (1-\widehat{d}_{rr})w_\Pi - \widehat{d}_{ry}w_\Delta^{(2)}) \\ &= -\widehat{d}_{ry}(w_\Delta^{(1)} - w_\Delta^{(2)}).\end{aligned}$$

Since in general $\widehat{d}_{ry} \neq 0$ and $w_\Delta^{(1)} \neq w_\Delta^{(2)}$, we obtain a nonzero value in the a posteriori primal variables after $\widehat{P}_D = I - \widehat{E}_{D_u}$ is applied; this is contrary to the assumptions of the standard theory. The interaction of a posteriori primal and dual variables was also observed in [62].

Neither the use of the standard scaling $(D_u^{(1)})_\Delta = \frac{1}{2}$ nor the transformed and restricted scaling $(\widehat{D}_u^{(1)})_\Delta = \frac{1}{1+1e6}t_{ry}^2 + \frac{1}{2}t_{yy}^2$ on the remaining dual variables is adequate, here. In Section 6.1, we show for a minimal example of adaptive FETI-DP and BDDC that, for a cropped scaling such as $(\widehat{D}_u^{(1)})_\Delta$, i.e., setting $\widehat{d}_{ry} = 0$, the theory of the adaptive method is violated since the developed condition number bound does not hold anymore.

4.5.2 Correspondence of FETI-DP with the generalized transformation-of-basis approach to FETI-DP using deflation or balancing

4.5.2.1 Transformation and a posteriori assembly

In this section, we introduce the transformation matrices and the a posteriori assembly operator to afterwards discuss different (characterizations of) solution spaces.

For the sake of simplicity, we restrict ourselves to the transformation of one single face or edge. The transformation on all other faces and edges is assumed to be trivial, i.e., the identity matrix. Thus, let us consider an edge $\mathcal{Z}_1$ common to the three subdomains Ω_i, Ω_j, and Ω_k with a nontrivial transformation, i.e., we assume that a posteriori constraints are only associated with the edge $\mathcal{Z}_1$.

The calculations realized in the following can be transfered easily to the general case; just by accepting a notational and calculational overhead.

Without loss of generality, we can assume that the transformations $T^{(i)}_{\mathcal{Z}_{i_1}}$, $T^{(j)}_{\mathcal{Z}_{j_1}}$, and $T^{(k)}_{\mathcal{Z}_{k_1}}$ on the edge $\mathcal{Z}_{l_1} := \mathcal{Z}_1 \cap \partial\Omega_l$, $l \in \{i, j, k\}$, are identical. This implies that the numbering of the edge nodes is consistent for all three subdomains.

We implicitly use the assumption that a constraint vector does not span several faces and/or edges, which is not valid, e.g., for the FETI-DP method in [50, 48] for almost incompressible elasticity using only one deflation vector for each almost incompressible subdomain. For the important application of adaptive coarse spaces based on local eigenvalue problems where the constraints are already computed locally, this is no restriction to our method.

We describe all steps in detail and for general scalings. Our results are therefore also of interest for the adaptive BDDC methods in [7, 101, 17, 62] which combine deluxe-scaling with a transformation of basis and partial finite element assembly.

For simplicity, we always assume an initial (a priori) coarse space with all a priori constraints enforced by partial assembly as in [83, 89, 82, 77]. Then, our a posteriori coarse space consisting of a posteriori constraints is implemented using the generalized transformation-of-basis approach using additional partial assembly.

As motivated before, the construction of a transformation-of-basis approach with a posteriori constraints that yields the same condition number as the deflation approach requires some modifications of the theory compared to the standard approach where only a priori constraints are used. This results from the fact that the (a posteriori) primal components of $P_D w$ do, in general, not vanish – opposed to standard theory; cf. the motivation in Section 4.5.1.

Now consider an orthonormalized set of constraint vectors $(q^1_{\mathcal{Z}_{l_1}}, \dots, q^r_{\mathcal{Z}_{l_1}})$ on $\mathcal{Z}_{l,1}$. Then, introduce

$$T_{\mathcal{Z}_{l_1},\Pi_{\mathcal{Z}_{l_1}}} := \left(q^1_{\mathcal{Z}_{l_1}}, \dots, q^r_{\mathcal{Z}_{l_1}}\right). \tag{4.17}$$

Using an algorithm such as modified Gram-Schmidt, we compute $T_{\mathcal{Z}_{l_1},\Delta_{\mathcal{Z}_{l_1}}}$ so that $T_{\mathcal{Z}_{l_1}} := \left(T_{\mathcal{Z}_{l_1},\Pi_{\mathcal{Z}_{l_1}}},\ T_{\mathcal{Z}_{l_1},\Delta_{\mathcal{Z}_{l_1}}}\right)$ is a square matrix and $T^T_{\mathcal{Z}_{l_1}} T_{\mathcal{Z}_{l_1}} = I$, i.e., $T_{\mathcal{Z},\Delta_{\mathcal{Z}}}$ is orthogonal to the constraint space span $\left(q^1_{\mathcal{Z}_{l_1}}, \dots, q^r_{\mathcal{Z}_{l_1}}\right)$. For convenience, we order the primal variables in the whole section first.

For each subdomain Ω_l, we denote the faces and edges by $\mathcal{Z}_{l_1}, \dots, \mathcal{Z}_{l_s}$. Since we have assumed only one nontrivial transformation, for $n > 1$ the matrix $T_{\mathcal{Z}_{l_n},\Pi_{\mathcal{Z}_{l_n}}}$ is void and $T_{\mathcal{Z}_{l_n}} = \left(T_{\mathcal{Z}_{l_n},\,\Delta_{\mathcal{Z}_{l_n}}}\right) = I$, $2 \le n \le s$. Without loss of

generality, we assume that the degrees of freedom of all the corresponding faces and edges of Ω_l are ordered such that the degrees of freedom on $\mathcal{Z}_{l_1}$ are ordered first, those of $\mathcal{Z}_{l_2}$ are ordered second, etc. Then,

$$T_{\Delta_l'}^{(l)} := \left(T_{\Pi_l}^{(l)} \mid T_{\Delta_l}^{(l)}\right) := \left(\begin{array}{c|cccccc} T_{\mathcal{Z}_{l_1},\Pi_{\mathcal{Z}_{l_1}}} & T_{\mathcal{Z}_{l_1},\Delta_{\mathcal{Z}_{l_1}}} & 0 & \dots & \dots & 0 \\ 0 & 0 & I & 0 & \dots & 0 \\ \vdots & \vdots & 0 & \ddots & \ddots & \vdots \\ \vdots & \vdots & \vdots & \ddots & \ddots & 0 \\ 0 & 0 & 0 & \dots & 0 & I \end{array}\right) \tag{4.18}$$

represents the transformation on Δ_l' from the new basis to the old basis, i.e.,

$$w_{\Delta_l'}^{(l)} = T_{\Delta_l'}^{(l)} \overline{w}_{\Delta_l'}^{(l)}, \tag{4.19}$$

where the vectors in the new basis still lack an assembly operation. The identity matrices in (4.18) are of the size of the faces and edges $\mathcal{Z}_{l_2}, \dots, \mathcal{Z}_{l_n}$, $l \in \{i, j, k\}$.

As mentioned before, the transformations are chosen consistently, i.e., for the three subdomains, we have for the local transformations on $\mathcal{Z}_1$ (shared by Ω_i, Ω_j, and Ω_k) that

$$T_{\mathcal{Z}_{i_1},\Pi_{\mathcal{Z}_{i_1}}} = T_{\mathcal{Z}_{j_1},\Pi_{\mathcal{Z}_{j_1}}} = T_{\mathcal{Z}_{k_1},\Pi_{\mathcal{Z}_{k_1}}} \text{ and } T_{\mathcal{Z}_{i_1},\Delta_{\mathcal{Z}_{i_1}}} = T_{\mathcal{Z}_{j_1},\Delta_{\mathcal{Z}_{j_1}}} = T_{\mathcal{Z}_{k_1},\Delta_{\mathcal{Z}_{k_1}}}. \tag{4.20}$$

It also holds $T_{\Delta_l'}^{(l)T} T_{\Delta_l'}^{(l)} = I$, $l \in \{i, j, k\}$, and that the columns of $T_{\Pi_l}^{(l)}$ span the range of all a posteriori constraint vectors associated with Ω_l, $l \in \{i, j, k\}$. Therefore, using (4.18) and (4.19), we have

$$T_{\Pi_l}^{(l)T} w_{\Delta_l'}^{(l)} = \begin{pmatrix} I & 0 & \dots & 0 \end{pmatrix} \begin{pmatrix} \overline{w}_{\Pi_{\mathcal{Z}_{l_1}}}^{(l)} \\ \overline{w}_{\Delta_{\mathcal{Z}_{l_1}}}^{(l)} \\ \vdots \\ \overline{w}_{\Delta_{\mathcal{Z}_{l_s}}}^{(l)} \end{pmatrix} = \overline{w}_{\Pi_{\mathcal{Z}_{l_1}}}^{(l)} \text{ for } l \in \{i, j, k\}. \tag{4.21}$$

The global transformation matrix writes

$$T = \begin{pmatrix} I_{\Pi'} & 0 \\ 0 & \text{blockdiag}_{l=1,\dots,N}(T_{\Delta_l'}^{(l)}) \end{pmatrix}. \tag{4.22}$$

We often use T^T. Note that T^T has to be replaced by T^{-1} if the columns of T are not orthonormalized.

Remark 4.2. *Let us remark that the corresponding identity of* (4.20) *has to hold for all faces and all edges, i.e., the transformation matrices restricted to any particular face or edge have to be equal on all adjacent subdomains. This property is explicitly needed for the proof of Lemma 4.8 and can be assumed without loss of generality since the set of constraints can easily be modified or extended if the property did not yet hold.*

The transformed variables then still lack an assembly operation. In the following, we also use the simplified index $\mathcal{Z}_1$ instead of $\mathcal{Z}_{l_1}$ for $l \in \{i, j, k\}$ since this edge is shared by these three subdomains and since (4.20) holds. In order to enforce

$$\overline{w}^{(i)}_{\Pi_{\mathcal{Z}_1}} \stackrel{!}{=} \overline{w}^{(j)}_{\Pi_{\mathcal{Z}_1}} \stackrel{!}{=} \overline{w}^{(k)}_{\Pi_{\mathcal{Z}_1}}, \tag{4.23}$$

we introduce the global restriction operator R, which replicates the a posteriori primal degrees of freedom (given by the index set Π), and its transpose R^T, which sums a posteriori primal degrees of freedom.

The restriction operator R is of the form

$$R = \begin{pmatrix} I_{\Pi'} & 0 & 0 & \dots & \dots & 0 \\ 0 & (*)_{\Pi_1} & (*)_{\Delta_1} & 0 & \dots & 0 \\ \vdots & \vdots & 0 & \ddots & & \vdots \\ \vdots & \vdots & \vdots & & \ddots & 0 \\ 0 & (*)_{\Pi_N} & 0 & \dots & 0 & (*)_{\Delta_N} \end{pmatrix} \tag{4.24}$$

where the matrix $((*)_{\Pi_i}, (*)_{\Delta_i})$, $i = 1, \dots, N$, is a permutation of the columns of the identity matrix. The operator R replicates the a posteriori degrees of freedom to the different subdomains but does not change the a priori set of primal variables.

The multiplicity-weighted assembly operator for the a posteriori primal variables is defined as

$$R^T_\mu := (R^T R)^{-1} R^T \tag{4.25}$$

and therefore $R^T_\mu R = I$. Here, the index μ stands for multiplicity.

The local version of R^T, restricted to the considered edge $\mathcal{Z}_1$, is given by

$$R^T_{\mathcal{Z}_1} := \begin{pmatrix} R^T_{\Pi_{\mathcal{Z}_1}} \\ R^T_{\Delta_{\mathcal{Z}_1}} \end{pmatrix} := \begin{pmatrix} I_{i,\Pi_{\mathcal{Z}_1}} & 0 & I_{j,\Pi_{\mathcal{Z}_1}} & 0 & I_{k,\Pi_{\mathcal{Z}_1}} & 0 \\ 0 & I_{i,\Delta_{\mathcal{Z}_1}} & 0 & 0 & 0 & 0 \\ 0 & 0 & 0 & I_{j,\Delta_{\mathcal{Z}_1}} & 0 & 0 \\ 0 & 0 & 0 & 0 & 0 & I_{k,\Delta_{\mathcal{Z}_1}} \end{pmatrix},$$

and the local version of the multiplicity-weighted operator is

$$R^T_{\mathcal{Z}_1,\mu} := \begin{pmatrix} \frac{1}{3} R^T_{\Pi_{\mathcal{Z}_1}} \\ R^T_{\Delta_{\mathcal{Z}_1}} \end{pmatrix}.$$

For the variables, both, transformed to the new basis and assembled in the a posteriori primal variables, we then have

$$\widehat{w}^{(i)}_{\Pi_{\mathcal{Z}_1}} = \widehat{w}^{(j)}_{\Pi_{\mathcal{Z}_1}} = \widehat{w}^{(k)}_{\Pi_{\mathcal{Z}_1}}; \tag{4.26}$$

cf. (4.23) for the variables, which are only transformed, for which this property does not hold.

Note that R^T_μ is used in the FETI-DP Dirichlet preconditioner using the generalized transformation-of-basis approach and does not appear in the standard theory; cf. (3.19) and (4.36).

4.5.2.2 Solution spaces

For $w \in \widetilde{W}$, $\widehat{w} := R^T_\mu T^T w$ is also continuous in the a posteriori set of primal variables given by the index set Π as required by (4.26). We then introduce the corresponding space

$$\widetilde{W}_{T,a} := \{\widehat{w} = R^T_\mu T^T w \,:\, w \in \widetilde{W}\}. \tag{4.27}$$

In the space $\widetilde{W}_{T,a}$ all displacements are transformed to the new basis and are continuous in all primal variables, i.e., in the a priori (Π') as well as in the a posteriori (Π) primal variables. We also recall the definition of the space

$$\widetilde{W}_U := \{w \in \widetilde{W} \,:\, U^T B w = 0\}$$

from the context of deflation and balancing; see (4.7). Another characterization of the same space is given by

$$\widetilde{W}_Q := \{w \in \widetilde{W} \,:\, Q^T w = 0\} \tag{4.28}$$

with $Q = B^T U$, i.e., the constraint vectors for the degrees of freedom are stored in the columns of Q.

For our theoretical considerations, we would like to work with $\widetilde{W}_Q$, but in the implementation, the space is obtained via partial assembly and scattering of the corresponding continuous values, i.e., we iterate in $\widetilde{W}_{T,a}$. The two spaces correspond to different methods. The space $\widetilde{W}_{T,a}$ corresponds to a transformation-of-basis approach and $\widetilde{W}_Q$ corresponds to a deflation or balancing approach.

However, in general, we have

$$\widetilde{W}_{T,a} \subsetneq \widetilde{W}_Q. \tag{4.29}$$

This results from the assumption mentioned in Remark 4.2 and the fact that the deflation and balancing approach enforces the constraints on a Lagrange multiplier basis. For a better understanding, see Figure 4.2. Let an edge be shared by the three subdomains Ω_i, Ω_j, and Ω_k and assume that a deflation or balancing approach enforced one constraint on the Lagrange multiplier connecting Ω_i and Ω_k. Introducing the same constraint also for the other jumps on the edge and using partial assembly then involves all three Lagrange multipliers. Effectively, this corresponds to the deflation or balancing approach enforcing the constraint given on the jump $w^{(i)} - w^{(k)}$ for all other jumps across the edge; here, $w^{(i)} - w^{(j)}$ and $w^{(j)} - w^{(k)}$. Accordingly, $\widetilde{W}_{T,a}$ becomes a strict subset of $\widetilde{W}_Q$. On the other hand, we can always extend the columns of Q to $\widehat{Q} := \begin{pmatrix} Q, * \end{pmatrix}$ with $\operatorname{range} Q \subset \operatorname{range} \widehat{Q}$ such that it holds

$$\widetilde{W}_{T,a} = \widetilde{W}_{\widehat{Q}} = \{w \in \widetilde{W} \,:\, \widehat{Q}^T w = 0\} \subset \widetilde{W}_Q. \tag{4.30}$$

Another notation for the space $\widetilde{W}_{T,a}$ in the context of deflation and balancing is

$$\widetilde{W}_{\widehat{U}} := \{w \in \widetilde{W} : \widehat{U}^T B w = 0\}, \tag{4.31}$$

i.e., we have $\widehat{Q} = B^T \widehat{U}$ and $\widehat{U}$ then contains the constraint vectors for the Lagrange multipliers of the corresponding deflation or balancing approach; see Figure 4.2 (right).

Remark 4.3. *We refer to the deflation or balancing approach using $\widetilde{W}_U = \widetilde{W}_Q$ as the* **direct** deflation or balancing approach *and to the approach using $\widetilde{W}_{\widehat{U}} = \widetilde{W}_{\widehat{Q}}$ as the* **corresponding** deflation or balancing approach. *This results from the fact that $\widetilde{W}_{\widehat{U}}$ is obtained in correspondence to the generalized transforma-*

tion approach which generally enforces more constraints than a direct deflation approach in $\widetilde{W}_U$; cf. Figure 4.2.

We complete this subsection with a short résumé:

$$\widehat{W} \subset \widetilde{W}_{T,a} = \widetilde{W}_{\widehat{Q}} = \widetilde{W}_{\widehat{U}} \subset \widetilde{W}_Q = \widetilde{W}_U \subset \widetilde{W} \subset W. \tag{4.32}$$

4.5.2.3 FETI-DP in transformed and assembled operators

Note that our orthogonal transformation T performs the change of basis from a new, nonnodal basis, e.g., with explicit averages, to the standard nodal finite element basis. The inverse T^T then changes back to the nodal basis.

In the new basis, the assembled variables are given by

$$\widehat{w} := R_\mu^T T^T w = R_\mu^T \overline{w}; \tag{4.33}$$

see (4.27).

By construction, $\widehat{w}$ is continuous in the a posteriori set of primal variables given by Π and in the a priori set of primal variables given by Π'. For these transformed and assembled variables, we also define the transformed and assembled operators $\widehat{P}_D$ and $\widehat{\widetilde{S}}$ by

$$\widehat{P}_D := R_\mu^T T^T \, P_D \, T R \quad \text{and} \quad \widehat{\widetilde{S}} := R^T T^T \, \widetilde{S} \, T R, \tag{4.34}$$

where $P_D = B_D^T B$, i.e., the operator P_D corresponds to the jump operator B and the a priori scaling D used with the a priori coarse space corresponding to the index set Π'; see Section 3.2. For the theory, we also introduce

$$\widehat{B} := BTR \text{ and } \widehat{B}_D := B_D T R_\mu. \tag{4.35}$$

In practice, we do not implement a transformed version of B or B_D. Instead we use the applications of the transformation T and the scatters R and R_μ. With the new notation, we also have

$$\widehat{P}_D = \widehat{B}_D^T \widehat{B}.$$

The transformed, preconditioned FETI-DP system matrix, using the transformed Dirichlet preconditioner

$$\widehat{M_T^{-1}} := \widehat{B}_D \widehat{\widetilde{S}} \widehat{B}_D^T \tag{4.36}$$

for

$$\widehat{F} := \widehat{B}\widehat{\widetilde{S}}^{-1}\widehat{B}^T \tag{4.37}$$

is thus given by

$$\begin{aligned}\widehat{M_T}^{-1}\widehat{F} &= (\widehat{B}_D\widehat{\widetilde{S}}\widehat{B}_D^T)\,(\widehat{B}\widehat{\widetilde{S}}^{-1}\widehat{B}^T) \\ &= \Big(B_D \underbrace{TR_\mu\widehat{\widetilde{S}}R_\mu^T T^T}_{=\text{replaces } \widetilde{S}} B_D^T\Big)\,\Big(B\underbrace{TR\widehat{\widetilde{S}}^{-1}R^TT^T}_{=\text{replaces } \widetilde{S}^{-1}}B^T\Big).\end{aligned} \tag{4.38}$$

where $\widehat{\widetilde{S}} = R^TT^T\widetilde{S}TR$ is the transformed Schur complement assembled also in the a posteriori primal variables; see (4.34)

The preconditioned system (4.38) is different from the standard FETI-DP method using a transformation of basis, as, e.g., in [83, 89, 82, 77, 78, 80] which can be written, iterating in the transformed basis,

$$M_D^{-1}F = (B_{D,\Delta}\widehat{\widetilde{S}}B_{D,\Delta}^T)\,(B_\Delta\widehat{\widetilde{S}}^{-1}B_\Delta^T), \tag{4.39}$$

where the operator B_Δ only enforces continuity on the a posteriori dual variables and zeroes primal variables; $B_{D,\Delta}$ is its scaled variant, effectively scaling only a posteriori dual variables; cf., e.g., [83, 89].

Note that the expression (4.38) is missing an explicit transformed scaling $\widehat{D}$ but the scaling is transformed implicitly by applying T before B and B_D as well as T^T after B^T and B_D^T. In the next section, in a short digression, we show that an equivalent, explicitly transformed scaling $\widehat{D}$ exists. However, we do not see any advantages of building it explicitly.

4.5.2.4 Digression: Transformation in the space of the Lagrange multipliers and explicit scaling transformation for FETI-DP

In the previous section, we introduced the new preconditioned FETI-DP system matrix using the generalized transformation-of-basis approach. In the expression (4.38) the scaling is transformed implicitly. We now show that $T^TB_D^TBT$ could be written as $B_{\widehat{D}}^TB$ with transformed scaling $\widehat{D}$; see Definition 4.5.

For the case of nonredundant Lagrange multipliers, by [80, Theorem 6.5], we know that there exists a matrix T_λ so that $BT = T_\lambda B$. We now consider the case of redundant Lagrange multipliers.

Lemma 4.4 (Transformation in the space of Lagrange multipliers [67])**.** *Let us assume the case of redundant Lagrange multipliers and of transformation*

matrices $T^{(i)}$, $i = 1, \ldots, N$, such that $T^{(i)}_{|\mathcal{Z}} = T^{(s)}_{|\mathcal{Z}}$ for any face or any edge $\mathcal{Z}$ and any adjacent pair $\{\Omega_i, \Omega_s\}$, $1 \leq i, s \leq N$. Then, there exists a transformation of basis T_λ in the space of Lagrange multipliers such that

$$BT = T_\lambda B.$$

For the scaled jump operator, we only have

$$B_D T = (D^{(1),T} T_\lambda B^{(1)}, \ldots, D^{(N),T} T_\lambda B^{(N)}). \tag{4.40}$$

Proof. As in [80, Theorem 6.5], we state that the product BT can be considered face by face and edge by edge. This results from the form of B and T, i.e., T contains blocks $T_{\mathcal{Z}}$ of the size of the face or edge $\mathcal{Z}$.

The case of edges in two dimensions or faces in three dimensions (i.e., multiplicity of two) is already covered by [80, Theorem 6.5]. Here, we extend the proof to the case of multiplicities greater than two. For simplicity, let us consider an edge $\mathcal{Z}_1$ in three dimensions shared by three subdomains Ω_i, Ω_j, and Ω_k and its corresponding blocks in B and T. Other cases can be handled analogously. In the following, we just consider rows of B that belong to the Lagrange multipliers on the specific edge $\mathcal{Z}_1$.

We have

$$B^{(i)}_{\mathcal{Z}_1} = \begin{pmatrix} \widehat{I}_1 \\ \widehat{I}_2 \\ 0 \end{pmatrix}, \; B^{(j)}_{\mathcal{Z}_1} = \begin{pmatrix} -\widehat{I}_1 \\ 0 \\ \widehat{I}_3 \end{pmatrix}, \text{ and } B^{(k)}_{\mathcal{Z}_1} = \begin{pmatrix} 0 \\ -\widehat{I}_2 \\ -\widehat{I}_3 \end{pmatrix},$$

where $\widehat{I}_l$, $l \in \{1, 2, 3\}$, is a permutation of

$$\begin{pmatrix} I & 0 \\ 0 & -I \end{pmatrix}.$$

The sign reflects the orientation chosen in the construction of the Lagrange multiplier constraints.

Then, by $T_{u,\mathcal{Z}_1} := \underset{s \in \{i,j,k\}}{\text{blockdiag}}(T^{(s)}_{|\mathcal{Z}_1})$ and $T_{\mathcal{Z}_1} := T^{(i)}_{|\mathcal{Z}_1} = T^{(j)}_{|\mathcal{Z}_1} = T^{(k)}_{|\mathcal{Z}_1}$, we obtain

$$B_{\mathcal{Z}_1} T_{u,\mathcal{Z}_1} := \begin{pmatrix} B^{(i)}_{\mathcal{Z}_1} & B^{(j)}_{\mathcal{Z}_1} & B^{(k)}_{\mathcal{Z}_1} \end{pmatrix} \begin{pmatrix} T^{(i)}_{|\mathcal{Z}_1} & 0 & 0 \\ 0 & T^{(j)}_{|\mathcal{Z}_1} & 0 \\ 0 & 0 & T^{(k)}_{|\mathcal{Z}_1} \end{pmatrix}$$

$$
\begin{aligned}
&= \begin{pmatrix} \widehat{I}_1 & -\widehat{I}_1 & 0 \\ \widehat{I}_2 & 0 & -\widehat{I}_2 \\ 0 & \widehat{I}_3 & -\widehat{I}_3 \end{pmatrix} \begin{pmatrix} T_{\mathcal{Z}_1} & 0 & 0 \\ 0 & T_{\mathcal{Z}_1} & 0 \\ 0 & 0 & T_{\mathcal{Z}_1} \end{pmatrix} \\
&= \begin{pmatrix} \widehat{I}_1 T_{\mathcal{Z}_1} & -\widehat{I}_1 T_{\mathcal{Z}_1} & 0 \\ \widehat{I}_2 T_{\mathcal{Z}_1} & 0 & -\widehat{I}_2 T_{\mathcal{Z}_1} \\ 0 & \widehat{I}_3 T_{\mathcal{Z}_1} & -\widehat{I}_3 T_{\mathcal{Z}_1} \end{pmatrix} \\
&=: \begin{pmatrix} T_{\lambda,\mathcal{Z}_1,ij} & 0 & 0 \\ 0 & T_{\lambda,\mathcal{Z}_1,ik} & 0 \\ 0 & 0 & T_{\lambda,\mathcal{Z}_1,jk} \end{pmatrix} \begin{pmatrix} \widehat{I}_1 & -\widehat{I}_1 & 0 \\ \widehat{I}_2 & 0 & -\widehat{I}_2 \\ 0 & \widehat{I}_3 & -\widehat{I}_3 \end{pmatrix} \\
&=: T_{\lambda,\mathcal{Z}_1} \begin{pmatrix} B^{(i)}_{\mathcal{Z}_1} & B^{(j)}_{\mathcal{Z}_1} & B^{(k)}_{\mathcal{Z}_1} \end{pmatrix} \\
&= T_{\lambda,\mathcal{Z}_1} B_{\mathcal{Z}_1}
\end{aligned}
$$

where

$$
T_{\lambda,\mathcal{Z}_1,ij} = \begin{pmatrix} T_{\mathcal{Z}_1,ij,1,1} & -T_{\mathcal{Z}_1,ij,1,2} \\ -T_{\mathcal{Z}_1,ij,2,1} & T_{\mathcal{Z}_1,ij,2,2} \end{pmatrix}, \tag{4.41}
$$

where the blocks $T_{\mathcal{Z}_1,ij,1,1}$ and $T_{\mathcal{Z}_1,ij,2,2}$ and the corresponding off-diagonal blocks are determined by the blocks in $T_{\mathcal{Z}_1}$ and the size of I and $-I$ in $\widehat{I}_1$. This holds for $T_{\lambda,\mathcal{Z}_1,ik}$ and $T_{\lambda,\mathcal{Z}_1,jk}$, analogously.

By defining a global matrix T_λ from the local contributions on the faces and the edges, we obviously have

$$
\begin{aligned}
B_D T &= \left(D^{(1),T} B^{(1)} T^{(1)}, \ldots, D^{(N),T} B^{(N)} T^{(N)} \right) \\
&= \left(D^{(1),T} T_\lambda B^{(1)}, \ldots, D^{(N),T} T_\lambda B^{(N)} \right).
\end{aligned}
$$

□

Definition 4.5 (Transformed Lagrange multiplier scaling [67])**.** *For a scaling matrix $D^{(i)}$ the explicitly transformed scaling matrix $\widehat{D}^{(i)}$ is defined by*

$$
\widehat{D}^{(i)} := T_\lambda^T D^{(i)} T_\lambda \quad \textit{for} \quad i = 1, \ldots, N. \tag{4.42}
$$

For problems with constant coefficients on edges or faces the transformed scaling remains diagonal if the original scaling was diagonal. For heterogeneous problems this is not generally the case.

Let us eventually note that this transformed scaling is actually never formed. The intention of this section is to show that the implicitly transformed scaling

corresponds to an explicitly transformed scaling which, in general, is nondiagonal.

4.5.2.5 Eigenvalues of FETI-DP with the generalized transformation-of-basis approach

In this section, we show that FETI-DP using our generalized transformation-of-basis approach results in essentially the same eigenvalues as FETI-DP using the corresponding deflation or balancing approach, i.e., in both approaches eigenvalues of the preconditioned operator are the same, except, possibly, for eigenvalues zero and one.

Remark 4.6. *The generalized transformation-of-basis approach also results in the same number of zero eigenvalues as FETI-DP using deflation; cf. Figure 6.4, and analogously to* $(I-P)^T F U = 0$ *on* $\operatorname{range}(U^T F U)^+$*, we also have* $\widehat{F} U = 0$.

Note again that the FETI-DP and BDDC methods using a generalized transformation-of-basis approach are different from the ones using the standard approach [83, 89, 82, 77] in that it allows an interaction of dual and primal variables in the scaling.

To establish the equality of eigenvalues (greater than one) of FETI-DP (and BDDC) using the generalized transformation-of-basis approach and of FETI-DP using deflation, we show

$$\langle \widehat{M}_T^{-1} \widehat{F}\widehat{\lambda}, \widehat{F}\widehat{\lambda}\rangle = \langle \widehat{P}_D \widehat{u}, \widehat{P}_D \widehat{u}\rangle_{\widehat{\widetilde{S}}} \stackrel{!}{=} \langle P_D u_0, P_D u_0\rangle_{\widetilde{S}} = \langle M_{PP}^{-1} F(I-P)\widehat{\lambda}, F(I-P)\widehat{\lambda}\rangle \tag{4.43}$$

where $\widehat{u} \in \widetilde{W}_{T,a}$ and $u_0 \in \widetilde{W}_{\widehat{Q}}$; see Theorem 4.12.

For this, we show that for any assembled and transformed displacement $\widehat{w} \in \widetilde{W}_{T,a}$ we have a $w_0 = TR\widehat{w} \in \widetilde{W}_{\widehat{Q}}$ such that

$$|\widehat{P}_D \widehat{w}|^2_{\widehat{\widetilde{S}}} = |P_D w_0|^2_{\widetilde{S}}. \tag{4.44}$$

Vice versa, we show that for any $w_0 \in \widetilde{W}_{\widehat{Q}}$ a $\widehat{w} = R_\mu^T T^T w_0 \in \widetilde{W}_{T,a}$ exists such that (4.44) holds, too.

We therefore have, for arbitrary scalings and coefficients, the same eigenvalues (greater than one) for the generalized transformation-of-basis approach as for the corresponding deflation approach.

Remark 4.7. *In FETI-DP and BDDC theory, bounds of the form* $|P_D w|^2_{\widetilde{S}} \leq C|w|^2_{\widetilde{S}}$ *are established; cf. Section 3.2 and Section 4.2. For the adaptive coarse*

space approach in Chapter 5, we have $C = 4\max\{N_{\mathcal{F}}, N_{\mathcal{E}}M_{\mathcal{E}}\}^2\mathrm{TOL}$*, where* $N_{\mathcal{F}}$ *denotes the maximum number of faces of a subdomain,* $N_{\mathcal{E}}$ *the maximum number of edges of a subdomain,* $M_{\mathcal{E}}$ *the maximum multiplicity of an edge, and* TOL *an user-defined tolerance. For an application of the generalized transformation-of-basis approach in the context of adaptive domain decomposition methods, we refer the reader to Chapter 6 or [68].*

Using the definitions (4.33), (4.34), and (4.35), we have

$$\begin{aligned} |\widehat{P}_D\widehat{w}|^2_{\widehat{\widetilde{S}}} &= \widehat{w}^T\,(\widehat{B}^T\widehat{B}_D)\,\widehat{\widetilde{S}}\,(\widehat{B}_D^T\widehat{B})\,\widehat{w} \\ &= w^T T R_\mu\,(R^T T^T B^T B_D T R_\mu)\,R^T T^T \widetilde{S} T R\,(R_\mu^T T^T B_D^T B T R)\,R_\mu^T T^T w \end{aligned} \tag{4.45}$$

with $w \in \widetilde{W}$.

Given $w_0 \in \widetilde{W}_{\widehat{Q}}$, we would like to show $TRR_\mu^T T^T B_D^T B w_0 = B_D^T B w_0$. This, however, is not directly clear and is the subject of Lemma 4.8.

Classically, it is argued (see, e.g., [84, 89, 82, 130]) that the operator $TRR_\mu^T T^T$ reduces to the identity on the dual variables and that $R_\mu^T T^T B_D^T B w_0$ is zero in the primal variables; although the operator R_μ^T does not appear in classical theory. This latter argument, however, is not valid, here, since $R_\mu^T T^T B_D^T B w_0$ is not zero in the a posteriori set of primal variables if the transformation of basis and the partial assembly is established in the generalized way, corresponding to the deflation approach; cf. Example 4.1 and, for a combination with adaptive coarse spaces, Table 6.1. Lemma 4.8 essentially states that $TRR_\mu^T T^T$ can be seen as a projection onto span $\{B_D^T B w_0\}$ with w_0 given as before.

In the following lemma, we also show the identity $TRR_\mu^T T^T w_0 = w_0$, which is of use in Lemma 4.9.

Lemma 4.8 ([67])**.** *Given* $w_0 \in \widetilde{W}_{\widehat{Q}}$*, we have*

$$TRR_\mu^T T^T\, w_0 = w_0 \quad \text{and} \quad TRR_\mu^T T^T\, B_D^T B w_0 = B_D^T B w_0.$$

Proof. In the following, we use $u \in \{w_0, B_D^T B w_0\}$ in order to realize certain calculations for w_0 and $B_D^T B w_0$ simultaneously. The variable u is replaced by the corresponding function when necessary.

First, consider $TRR_\mu^T T^T u$. From $u^T = (u^{(1)T}, \ldots, u^{(N)T})^T$, we obtain the local functions $u^{(l)} \in W_l$, $l = 1, \ldots, N$, and for $l \in \{i, j, k\}$, we define $u^{(l)}_{\mathcal{Z}_1}$ as the values at the degrees of freedom on the edge $\mathcal{Z}_1$. For $l = \{i, j, k\}$, the values of

the local function $u^{(l)}$ on all remaining degrees of freedom on $(\partial\Omega_{l,h} \cap \Gamma_h) \setminus \mathcal{Z}_1$ are denoted by $u^{(l)}_{\mathcal{Z}_1^C}$. For $l \notin \{i,j,k\}$, we have $u^{(l)} = u^{(l)}_{\mathcal{Z}_1^C}$.

Thus,

$$T^T u = \begin{pmatrix} u_{\Pi'} \\ A^{(1)} \\ \vdots \\ A^{(N)} \end{pmatrix} \text{ with } A^{(l)} := \begin{cases} T_{\Delta_l}^{(l)^T} u^{(l)}_{\mathcal{Z}_1^C}, & l \notin \{i,j,k\}, \\ \begin{pmatrix} T_{\Pi_l}^{(l)^T} \begin{pmatrix} u^{(l)}_{\mathcal{Z}_1} \\ u^{(l)}_{\mathcal{Z}_1^C} \end{pmatrix} \\ T_{\Delta_l}^{(l)^T} \begin{pmatrix} u^{(l)}_{\mathcal{Z}_1} \\ u^{(l)}_{\mathcal{Z}_1^C} \end{pmatrix} \end{pmatrix}, & l \in \{i,j,k\}, \end{cases}$$

since $\Delta'_l = \Delta_l$ for $l \notin \{i,j,k\}$, and therefore, we also have

$$RR_\mu^T T^T u = \begin{pmatrix} u_{\Pi'} \\ \widehat{A}^{(1)} \\ \vdots \\ \widehat{A}^{(N)} \end{pmatrix}$$

with

$$\widehat{A}^{(l)} := \begin{cases} A^{(l)}, & l \notin \{i,j,k\}, \\ \begin{pmatrix} \frac{1}{3}\left(T_{\Pi_i}^{(i)^T} \begin{pmatrix} u^{(i)}_{\mathcal{Z}_1} \\ u^{(i)}_{\mathcal{Z}_1^C} \end{pmatrix} + T_{\Pi_j}^{(j)^T} \begin{pmatrix} u^{(j)}_{\mathcal{Z}_1} \\ u^{(j)}_{\mathcal{Z}_1^C} \end{pmatrix} + T_{\Pi_k}^{(k)^T} \begin{pmatrix} u^{(k)}_{\mathcal{Z}_1} \\ u^{(k)}_{\mathcal{Z}_1^C} \end{pmatrix} \right) \\ T_{\Delta_l}^{(l)^T} \begin{pmatrix} u^{(l)}_{\mathcal{Z}_1} \\ u^{(l)}_{\mathcal{Z}_1^C} \end{pmatrix} \end{pmatrix}, & l \in \{i,j,k\}. \end{cases}$$

Here, we have used (4.18), (4.24), and (4.25).

From (4.18) in compact form, we have

$$T^{(l)}_{\Delta'_l} = \begin{pmatrix} T^{(l)}_{\Pi_l} & T^{(l)}_{\Delta_l} \end{pmatrix} = \begin{pmatrix} T_{\mathcal{Z}_1,\Pi_{\mathcal{Z}_1}} & T_{\mathcal{Z}_1,\Delta_{\mathcal{Z}_1}} & 0 \\ 0 & 0 & T^{(l)}_{\mathcal{Z}_1^C} \end{pmatrix} = \begin{pmatrix} T_{\mathcal{Z}_1,\Pi_{\mathcal{Z}_1}} & T_{\mathcal{Z}_1,\Delta_{\mathcal{Z}_1}} & 0 \\ 0 & 0 & I \end{pmatrix} \tag{4.46}$$

for $l \in \{i,j,k\}$ and $T^{(l)}_{\Delta'_l} = T^{(l)}_{\Delta_l} = I$ otherwise.

We now apply T to $RR_\mu^T T^T u$ or, locally, $T^{(l)}_{\Delta'_l}$ to $\widehat{A}^{(l)}$. We restrict ourselves to the case of $l \in \{i,j,k\}$ since there is nothing to show for $l \notin \{i,j,k\}$, i.e.,

$T^{(l)}_{\Delta'_l}\widehat{A}^{(l)} = u^{(l)}_{\mathcal{Z}_1^C} = u^{(l)}$. Then, for $l \in \{i,j,k\}$, we obtain

$$
\begin{aligned}
T^{(l)}_{\Delta'_l}\widehat{A}^{(l)} &= \frac{1}{3}T^{(l)}_{\Delta'_l}\begin{pmatrix} {T^{(i)}_{\Pi_i}}^T \begin{pmatrix} u^{(i)}_{\mathcal{Z}_1} \\ u^{(i)}_{\mathcal{Z}_1^C} \end{pmatrix} \\ {T^{(l)}_{\Delta_l}}^T \begin{pmatrix} u^{(l)}_{\mathcal{Z}_1} \\ u^{(l)}_{\mathcal{Z}_1^C} \end{pmatrix} \end{pmatrix} + \frac{1}{3}T^{(l)}_{\Delta'_l}\begin{pmatrix} {T^{(j)}_{\Pi_j}}^T \begin{pmatrix} u^{(l)}_{\mathcal{Z}_1} \\ u^{(l)}_{\mathcal{Z}_1^C} \end{pmatrix} \\ {T^{(l)}_{\Delta_l}}^T \begin{pmatrix} u^{(l)}_{\mathcal{Z}_1} \\ u^{(l)}_{\mathcal{Z}_1^C} \end{pmatrix} \end{pmatrix} \\
&\qquad + \frac{1}{3}T^{(l)}_{\Delta'_l}\begin{pmatrix} {T^{(k)}_{\Pi_k}}^T \begin{pmatrix} u^{(k)}_{\mathcal{Z}_1} \\ u^{(k)}_{\mathcal{Z}_1^C} \end{pmatrix} \\ {T^{(l)}_{\Delta_l}}^T \begin{pmatrix} u^{(l)}_{\mathcal{Z}_1} \\ u^{(l)}_{\mathcal{Z}_1^C} \end{pmatrix} \end{pmatrix} \\
&\overset{(4.46)}{=} \frac{1}{3}T^{(l)}_{\Delta'_l}\begin{pmatrix} \begin{pmatrix} T^T_{\mathcal{Z}_1,\Pi_{\mathcal{Z}_1}} & 0 \end{pmatrix} \begin{pmatrix} u^{(i)}_{\mathcal{Z}_1} \\ u^{(i)}_{\mathcal{Z}_1^C} \end{pmatrix} \\ \begin{pmatrix} T^T_{\mathcal{Z}_1,\Delta_{\mathcal{Z}_1}} & 0 \\ 0 & I \end{pmatrix} \begin{pmatrix} u^{(l)}_{\mathcal{Z}_1} \\ u^{(l)}_{\mathcal{Z}_1^C} \end{pmatrix} \end{pmatrix} + \frac{1}{3}T^{(l)}_{\Delta'_l}\begin{pmatrix} \begin{pmatrix} T^T_{\mathcal{Z}_1,\Pi_{\mathcal{Z}_1}} & 0 \end{pmatrix} \begin{pmatrix} u^{(j)}_{\mathcal{Z}_1} \\ u^{(j)}_{\mathcal{Z}_1^C} \end{pmatrix} \\ \begin{pmatrix} T^T_{\mathcal{Z}_1,\Delta_{\mathcal{Z}_1}} & 0 \\ 0 & I \end{pmatrix} \begin{pmatrix} u^{(l)}_{\mathcal{Z}_1} \\ u^{(l)}_{\mathcal{Z}_1^C} \end{pmatrix} \end{pmatrix} \\
&\qquad + \frac{1}{3}T^{(l)}_{\Delta'_l}\begin{pmatrix} \begin{pmatrix} T^T_{\mathcal{Z}_1,\Pi_{\mathcal{Z}_1}} & 0 \end{pmatrix} \begin{pmatrix} u^{(k)}_{\mathcal{Z}_1} \\ u^{(k)}_{\mathcal{Z}_1^C} \end{pmatrix} \\ \begin{pmatrix} T^T_{\mathcal{Z}_1,\Delta_{\mathcal{Z}_1}} & 0 \\ 0 & I \end{pmatrix} \begin{pmatrix} u^{(l)}_{\mathcal{Z}_1} \\ u^{(l)}_{\mathcal{Z}_1^C} \end{pmatrix} \end{pmatrix}
\end{aligned}
$$

Without loss of generality, we consider $l = i$. Then, the last equation becomes

$$
\begin{aligned}
T^{(i)}_{\Delta_i'}\widehat{A}^{(i)} = &\frac{1}{3}\begin{pmatrix} T_{\mathcal{Z}_1,\Pi_{\mathcal{Z}_1}} & T_{\mathcal{Z}_1,\Delta_{\mathcal{Z}_1}} & 0 \\ 0 & 0 & I \end{pmatrix}\begin{pmatrix} T^T_{\mathcal{Z}_1,\Pi_{\mathcal{Z}_1}} & 0 \\ T^T_{\mathcal{Z}_1,\Delta_{\mathcal{Z}_1}} & 0 \\ 0 & I \end{pmatrix}\begin{pmatrix} u^{(i)}_{\mathcal{Z}_1} \\ u^{(i)}_{\mathcal{Z}_1^C} \end{pmatrix} \\
&+\frac{1}{3}\begin{pmatrix} T_{\mathcal{Z}_1,\Pi_{\mathcal{Z}_1}} & T_{\mathcal{Z}_1,\Delta_{\mathcal{Z}_1}} & 0 \\ 0 & 0 & I \end{pmatrix}\begin{pmatrix} T^T_{\mathcal{Z}_1,\Pi_{\mathcal{Z}_1}} & 0 & 0 & 0 \\ 0 & 0 & T^T_{\mathcal{Z}_1,\Delta_{\mathcal{Z}_1}} & 0 \\ 0 & 0 & 0 & I \end{pmatrix}\begin{pmatrix} u^{(j)}_{\mathcal{Z}_1} \\ u^{(j)}_{\mathcal{Z}_1^C} \\ u^{(i)}_{\mathcal{Z}_1} \\ u^{(i)}_{\mathcal{Z}_1^C} \end{pmatrix} \\
&+\frac{1}{3}\begin{pmatrix} T_{\mathcal{Z}_1,\Pi_{\mathcal{Z}_1}} & T_{\mathcal{Z}_1,\Delta_{\mathcal{Z}_1}} & 0 \\ 0 & 0 & I \end{pmatrix}\begin{pmatrix} T^T_{\mathcal{Z}_1,\Pi_{\mathcal{Z}_1}} & 0 & 0 & 0 \\ 0 & 0 & T^T_{\mathcal{Z}_1,\Delta_{\mathcal{Z}_1}} & 0 \\ 0 & 0 & 0 & I \end{pmatrix}\begin{pmatrix} u^{(k)}_{\mathcal{Z}_1} \\ u^{(k)}_{\mathcal{Z}_1^C} \\ u^{(i)}_{\mathcal{Z}_1} \\ u^{(i)}_{\mathcal{Z}_1^C} \end{pmatrix} \\
= &\frac{1}{3}\begin{pmatrix} u^{(i)}_{\mathcal{Z}_1} \\ u^{(i)}_{\mathcal{Z}_1^C} \end{pmatrix} + \frac{1}{3}\begin{pmatrix} T_{\mathcal{Z}_1,\Pi_{\mathcal{Z}_1}}T^T_{\mathcal{Z}_1,\Pi_{\mathcal{Z}_1}}u^{(j)}_{\mathcal{Z}_1} + T_{\mathcal{Z}_1,\Delta_{\mathcal{Z}_1}}T^T_{\mathcal{Z}_1,\Delta_{\mathcal{Z}_1}}u^{(i)}_{\mathcal{Z}_1} \\ u^{(i)}_{\mathcal{Z}_1^C} \end{pmatrix} \\
&+\frac{1}{3}\begin{pmatrix} T_{\mathcal{Z}_1,\Pi_{\mathcal{Z}_1}}T^T_{\mathcal{Z}_1,\Pi_{\mathcal{Z}_1}}u^{(k)}_{\mathcal{Z}_1} + T_{\mathcal{Z}_1,\Delta_{\mathcal{Z}_1}}T^T_{\mathcal{Z}_1,\Delta_{\mathcal{Z}_1}}u^{(i)}_{\mathcal{Z}_1} \\ u^{(i)}_{\mathcal{Z}_1^C} \end{pmatrix} \\
= &\begin{pmatrix} \frac{1}{3}\left(\left(I + 2T_{\mathcal{Z}_1,\Delta_{\mathcal{Z}_1}}T^T_{\mathcal{Z}_1,\Delta_{\mathcal{Z}_1}}\right)u^{(i)}_{\mathcal{Z}_1} + \sum_{n\in\{j,k\}} T_{\mathcal{Z}_1,\Pi_{\mathcal{Z}_1}}T^T_{\mathcal{Z}_1,\Pi_{\mathcal{Z}_1}}u^{(n)}_{\mathcal{Z}_1}\right) \\ u^{(i)}_{\mathcal{Z}_1^C} \end{pmatrix}.
\end{aligned}
\tag{4.47}
$$

This shows that we can focus on the degrees of freedom on the edge $\mathcal{Z}_1$ since $TRR_\mu^T T^T$ reduces to the identity on the degrees of freedom on $\Gamma \setminus \mathcal{Z}_1$, i.e., $u^T\widetilde{S}u = u^T TR_\mu\widetilde{\widetilde{S}}R_\mu^T T^T u$ for u with $u_{|_{\mathcal{Z}_1}} = 0$.

By a short computation, we obtain

$$
\begin{aligned}
&\left(I + 2T_{\mathcal{Z}_1,\Delta_{\mathcal{Z}_1}}T^T_{\mathcal{Z}_1,\Delta_{\mathcal{Z}_1}}\right)u^{(i)}_{\mathcal{Z}_1} + \sum_{n\in\{j,k\}} T_{\mathcal{Z}_1,\Pi_{\mathcal{Z}_1}}T^T_{\mathcal{Z}_1,\Pi_{\mathcal{Z}_1}}u^{(n)}_{\mathcal{Z}_1} \\
=&\left(I + 2T_{\mathcal{Z}_1,\Delta_{\mathcal{Z}_1}}T^T_{\mathcal{Z}_1,\Delta_{\mathcal{Z}_1}} + 2T_{\mathcal{Z}_1,\Pi_{\mathcal{Z}_1}}T^T_{\mathcal{Z}_1,\Pi_{\mathcal{Z}_1}}\right)u^{(i)}_{\mathcal{Z}_1} \\
&\qquad - 2T_{\mathcal{Z}_1,\Pi_{\mathcal{Z}_1}}T^T_{\mathcal{Z}_1,\Pi_{\mathcal{Z}_1}}u^{(i)}_{\mathcal{Z}_1} + \sum_{n\in\{j,k\}} T_{\mathcal{Z}_1,\Pi_{\mathcal{Z}_1}}T^T_{\mathcal{Z}_1,\Pi_{\mathcal{Z}_1}}u^{(n)}_{\mathcal{Z}_1} \\
=&3u^{(i)}_{\mathcal{Z}_1} + T_{\mathcal{Z}_1,\Pi_{\mathcal{Z}_1}}T^T_{\mathcal{Z}_1,\Pi_{\mathcal{Z}_1}}\left(u^{(j)}_{\mathcal{Z}_1} + u^{(k)}_{\mathcal{Z}_1} - 2u^{(i)}_{\mathcal{Z}_1}\right).
\end{aligned}
$$

Thus, (4.47) reduces to

$$T_{\Delta_l'}^{(l)}\widehat{A}^{(l)} = \begin{pmatrix} u_{\mathcal{Z}_1}^{(i)} + \frac{1}{3}T_{\mathcal{Z}_1,\Pi_{\mathcal{Z}_1}}T_{\mathcal{Z}_1,\Pi_{\mathcal{Z}_1}}^T\left(u_{\mathcal{Z}_1}^{(j)} + u_{\mathcal{Z}_1}^{(k)} - 2u_{\mathcal{Z}_1}^{(i)}\right) \\ u_{\mathcal{Z}_1^C}^{(i)} \end{pmatrix}. \tag{4.48}$$

In the two following parts of the proof, we have to distinguish between $u = w_0$ and $u = B_D^T B w_0$.

First, for $u = w_0$ with $w_{0,\mathcal{Z}_1}^{(l)} := w_{0|_{\partial\Omega_l\cap\mathcal{Z}_1}}$ for $l \in \{i,j,k\}$, it yields

$$\begin{aligned} u_{\mathcal{Z}_1}^{(j)} + u_{\mathcal{Z}_1}^{(k)} - 2u_{\mathcal{Z}_1}^{(i)} &= w_{0,\mathcal{Z}_1}^{(j)} + w_{0,\mathcal{Z}_1}^{(k)} - 2w_{0,\mathcal{Z}_1}^{(i)} \\ &= (w_{0,\mathcal{Z}_1}^{(j)} - w_{0,\mathcal{Z}_1}^{(i)}) + (w_{0,\mathcal{Z}_1}^{(k)} - w_{0,\mathcal{Z}_1}^{(i)}) \end{aligned}$$

Due to $w_0 \in \widetilde{W}_{\widehat{Q}} = \widetilde{W}_{T,a}$ (see (4.32)) we know from (4.21) and (4.26) that the jump across $\mathcal{Z}_1$ of $(w_0^{(r_1)}, w_0^{(r_2)})$ $(r_1, r_2 \in \{i,j,k\},\ r_1 \neq r_2)$ is orthogonal to the constraint vectors introduced before. Hence,

$$\begin{aligned} &T_{\mathcal{Z}_1,\Pi_{\mathcal{Z}_1}}T_{\mathcal{Z}_1,\Pi_{\mathcal{Z}_1}}^T\left(u_{\mathcal{Z}_1}^{(j)} + u_{\mathcal{Z}_1}^{(k)} - 2u_{\mathcal{Z}_1}^{(i)}\right) \\ =&T_{\mathcal{Z}_1,\Pi_{\mathcal{Z}_1}}T_{\mathcal{Z}_1,\Pi_{\mathcal{Z}_1}}^T((w_{0,\mathcal{Z}_1}^{(j)} - w_{0,\mathcal{Z}_1}^{(i)}) + (w_{0,\mathcal{Z}_1}^{(k)} - w_{0,\mathcal{Z}_1}^{(i)})) \\ =&T_{\mathcal{Z}_1,\Pi_{\mathcal{Z}_1}}\big(\underbrace{T_{\mathcal{Z}_1,\Pi_{\mathcal{Z}_1}}^T(w_{0,\mathcal{Z}_1}^{(j)} - w_{0,\mathcal{Z}_1}^{(i)})}_{=0} + \underbrace{T_{\mathcal{Z}_1,\Pi_{\mathcal{Z}_1}}^T(w_{0,\mathcal{Z}_1}^{(k)} - w_{0,\mathcal{Z}_1}^{(i)})}_{=0}\big) = 0. \end{aligned} \tag{4.49}$$

Second, consider $u = B_D^T B w_0$. Using $u_{\mathcal{Z}_1}^{(i)} = \left(B_D^T B w_0\right)_{|_{\partial\Omega_i\cap\mathcal{Z}_1}}$, we have

$$u_{\mathcal{Z}_1}^{(i)} = D_{u,\mathcal{Z}_1}^{(j)}(w_{0,\mathcal{Z}_1}^{(i)} - w_{0,\mathcal{Z}_1}^{(j)}) + D_{u,\mathcal{Z}_1}^{(k)}(w_{0,\mathcal{Z}_1}^{(i)} - w_{0,\mathcal{Z}_1}^{(k)});$$

cf. the general definition of the scaling in (3.17). With corresponding formulas for $u_{\mathcal{Z}_1}^{(j)}$ and $u_{\mathcal{Z}_1}^{(k)}$ and (3.16), we obtain

$$
\begin{aligned}
u_{\mathcal{Z}_1}^{(j)} + u_{\mathcal{Z}_1}^{(k)} - 2u_{\mathcal{Z}_1}^{(i)} = {} & D_{u,\mathcal{Z}_1}^{(i)}(w_{0,\mathcal{Z}_1}^{(j)} - w_{0,\mathcal{Z}_1}^{(i)}) + D_{u,\mathcal{Z}_1}^{(k)}(w_{0,\mathcal{Z}_1}^{(j)} - w_{0,\mathcal{Z}_1}^{(k)}) \\
& + D_{u,\mathcal{Z}_1}^{(i)}(w_{0,\mathcal{Z}_1}^{(k)} - w_{0,\mathcal{Z}_1}^{(i)}) + D_{u,\mathcal{Z}_1}^{(j)}(w_{0,\mathcal{Z}_1}^{(k)} - w_{0,\mathcal{Z}_1}^{(j)}) \\
& + 2D_{u,\mathcal{Z}_1}^{(j)}(w_{0,\mathcal{Z}_1}^{(j)} - w_{0,\mathcal{Z}_1}^{(i)}) + 2D_{u,\mathcal{Z}_1}^{(k)}(w_{0,\mathcal{Z}_1}^{(k)} - w_{0,\mathcal{Z}_1}^{(i)})
\end{aligned}
$$

$$
\begin{aligned}
= {} & (D_{u,\mathcal{Z}_1}^{(i)} + D_{u,\mathcal{Z}_1}^{(j)})(w_{0,\mathcal{Z}_1}^{(j)} - w_{0,\mathcal{Z}_1}^{(i)}) \\
& + (D_{u,\mathcal{Z}_1}^{(i)} + D_{u,\mathcal{Z}_1}^{(k)})(w_{0,\mathcal{Z}_1}^{(k)} - w_{0,\mathcal{Z}_1}^{(i)}) \\
& + D_{u,\mathcal{Z}_1}^{(k)}(w_{0,\mathcal{Z}_1}^{(j)} - w_{0,\mathcal{Z}_1}^{(k)}) + D_{u,\mathcal{Z}_1}^{(k)}(w_{0,\mathcal{Z}_1}^{(k)} - w_{0,\mathcal{Z}_1}^{(i)}) \\
& + D_{u,\mathcal{Z}_1}^{(j)}(w_{0,\mathcal{Z}_1}^{(k)} - w_{0,\mathcal{Z}_1}^{(j)}) + D_{u,\mathcal{Z}_1}^{(j)}(w_{0,\mathcal{Z}_1}^{(j)} - w_{0,\mathcal{Z}_1}^{(i)})
\end{aligned}
$$

$$
\begin{aligned}
= {} & \underbrace{\left(D_{u,\mathcal{Z}_1}^{(i)} + D_{u,\mathcal{Z}_1}^{(j)} + D_{u,\mathcal{Z}_1}^{(k)}\right)}_{=I}(w_{0,\mathcal{Z}_1}^{(j)} - w_{0,\mathcal{Z}_1}^{(i)}) \\
& + \underbrace{\left(D_{u,\mathcal{Z}_1}^{(i)} + D_{u,\mathcal{Z}_1}^{(j)} + D_{u,\mathcal{Z}_1}^{(k)}\right)}_{=I}(w_{0,\mathcal{Z}_1}^{(k)} - w_{0,\mathcal{Z}_1}^{(i)})
\end{aligned}
$$

$$
= (w_{0,\mathcal{Z}_1}^{(j)} - w_{0,\mathcal{Z}_1}^{(i)}) + (w_{0,\mathcal{Z}_1}^{(k)} - w_{0,\mathcal{Z}_1}^{(i)}). \tag{4.50}
$$

As before, the orthogonality to the constraint vectors of the jump across $\mathcal{Z}_1$ of $(w_0^{(r_1)}, w_0^{(r_2)})$, $r_1, r_2 \in \{i, j, k\}$, $r_1 \neq r_2$, implies with (4.50)

$$
T_{\mathcal{Z}_1,\Pi_{\mathcal{Z}_1}} T_{\mathcal{Z}_1,\Pi_{\mathcal{Z}_1}}^T \left(u_{\mathcal{Z}_1}^{(j)} + u_{\mathcal{Z}_1}^{(k)} - 2u_{\mathcal{Z}_1}^{(i)}\right) = 0; \tag{4.51}
$$

see (4.49).

Therefore, for $u = w_0$ and $u = B_D^T B w_0$, from (4.48) with (4.49) and (4.51) we likewise have

$$
T_{\Delta_l'}^{(l)} \widehat{A}^{(l)} = \begin{pmatrix} u_{\mathcal{Z}_1}^{(l)} \\ u_{\mathcal{Z}_1^C}^{(l)} \end{pmatrix},
$$

which finally yields

$$
T R R_\mu^T T^T u = u
$$

for any $w_0 \in \widetilde{W}_{\widehat{Q}}$ and $u = w_0$ or $u = B_D^T B w_0$. □

Let us now have a closer look at $\widehat{B}\widehat{w} = B T R R_\mu^T T^T w$.

Lemma 4.9 ([67]). *For $\widehat{w} \in \widetilde{W}_{T,a}$ there exists a $w_0 := TR\widehat{w} \in \widetilde{W}_{\widehat{Q}}$ with*

$$\widehat{B}\widehat{w} = Bw_0. \tag{4.52}$$

Vice versa, for $w_0 \in \widetilde{W}_{\widehat{Q}}$ there exists a $\widehat{w} := R_\mu^T T^T w_0 \in \widetilde{W}_{T,a}$ satisfying (4.52).

Proof. Let $\widehat{w} \in \widetilde{W}_{T,a}$ be given. We define

$$w_0 := TR\widehat{w} = TRR_\mu^T T^T w = T \begin{pmatrix} * \\ \frac{1}{3}\big(\overline{w}_{\Pi_i}^{(i)} + \overline{w}_{\Pi_j}^{(j)} + \overline{w}_{\Pi_k}^{(k)}\big) \\ \overline{w}_{\Delta_i}^{(i)} \\ * \\ \frac{1}{3}\big(\overline{w}_{\Pi_i}^{(i)} + \overline{w}_{\Pi_j}^{(j)} + \overline{w}_{\Pi_k}^{(k)}\big) \\ \overline{w}_{\Delta_j}^{(j)} \\ * \\ \frac{1}{3}\big(\overline{w}_{\Pi_i}^{(i)} + \overline{w}_{\Pi_j}^{(j)} + \overline{w}_{\Pi_k}^{(k)}\big) \\ \overline{w}_{\Delta_k}^{(k)} \\ * \end{pmatrix}. \tag{4.53}$$

By construction, we have $\widehat{B}\widehat{w} = BTR\widehat{w} = Bw_0$. Then, with $\widehat{w}_{0,\Pi} := \frac{1}{3}(\overline{w}_{\Pi_i}^{(i)} + \overline{w}_{\Pi_j}^{(j)} + \overline{w}_{\Pi_k}^{(k)})$ and

$$w_{0,\Delta_l'}^{(l)} := \begin{pmatrix} T_{\Pi_l}^{(l)} & T_{\Delta_l}^{(l)} \end{pmatrix} \begin{pmatrix} \widehat{w}_{0,\Pi} \\ \overline{w}_{\Delta_l}^{(l)} \end{pmatrix}, \quad l \in \{i,j,k\}, \tag{4.54}$$

we also have

$$\widehat{w}_{0,\Pi} = T_{\Pi_{r_1}}^{(r_1)T} w_{0,\Delta_{r_1}'}^{(r_1)} = T_{\Pi_{r_2}}^{(r_2)T} w_{0,\Delta_{r_2}'}^{(r_2)} \tag{4.55}$$

for $r_1, r_2 \in \{i,j,k\}$, $r_1 \neq r_2$. From the construction of $T_{\Pi_l}^{(l)}$, $l \in \{i,j,k\}$, it follows that the jump across $\mathcal{Z}_1$ of $(w_0^{(r_1)}, w_0^{(r_2)})$ is orthogonal to the constraint vectors; cf. (4.17), (4.21), and (4.26). Since the constraints are local and we have assumed that a posteriori constraints are only associated with the edge common to Ω_i, Ω_j, and Ω_k, also all other local combinations $(w_0^{(r_1)}, w_0^{(r_2)})$, $r_1 \neq r_2$, $r_1, r_2 \in \{1, \ldots, N\}$, satisfy the constraints. Thus, w_0 fulfills all constraints introduced before, i.e., $w_0 \in \widetilde{W}_{\widehat{Q}}$.

More general cases can be treated analogously.

The other direction is shown as follows. Let $w_0 \in \widetilde{W}_{\widehat{Q}}$ be given. By the first identity of Lemma 4.8, we have $w_0 = TRR_\mu^T T^T w_0$. Define

$\widehat{w} := R_\mu^T T^T w_0 \in \widetilde{W}_{T,a}$. Then, it yields

$$Bw_0 = BTRR_\mu^T T^T w_0 = \widehat{B}\widehat{w}.$$

Again, more general cases can be treated analogously. □

We now prove the main relation between the deflation or the balancing and the generalized transformation-of-basis approach; see equation (4.44).

Lemma 4.10 ([67])**.** *For $\widehat{w} \in \widetilde{W}_{T,a}$ there exists a $w_0 := TR\widehat{w} \in \widetilde{W}_{\widehat{Q}}$ such that*

$$|\widehat{P}_D\widehat{w}|^2_{\widehat{\widetilde{S}}} = |P_D w_0|^2_{\widetilde{S}} \tag{4.56}$$

holds. Vice versa, for $w_0 \in \widetilde{W}_{\widehat{Q}}$ there exists a $\widehat{w} := R_\mu^T T^T w_0 \in \widetilde{W}_{T,a}$ such that (4.56) *holds too.*

Proof. Let $\widehat{w} \in \widetilde{W}_{T,a}$ be given. Define $w_0 := TR\widehat{w}$. Then, by using the first part of Lemma 4.9, the second part of Lemma 4.8, and the definitions of the corresponding operators, we have

$$\begin{aligned}
|\widehat{P}_D\widehat{w}|^2_{\widehat{\widetilde{S}}} &= \widehat{w}^T\widehat{B}^T\widehat{B}_D\widehat{\widetilde{S}}\widehat{B}_D^T\widehat{B}\widehat{w} = w_0 B^T\widehat{B}_D\widehat{\widetilde{S}}\widehat{B}_D^T Bw_0 \\
&= w_0 B^T \underbrace{B_D T R_\mu}_{=\widehat{B}_D} \underbrace{R^T T^T \widetilde{S} T R}_{=\widehat{\widetilde{S}}} \underbrace{R_\mu^T T^T B_D^T}_{=\widehat{B}_D^T} Bw_0 \\
&= w_0 B^T B_D \widetilde{S} B_D^T Bw_0 = |P_D w_0|^2_{\widetilde{S}}
\end{aligned}$$

with $w_0 \in \widetilde{W}_{\widehat{Q}}$.

Let $w_0 \in \widetilde{W}_{\widehat{Q}}$ be given. Define $\widehat{w} := R_\mu^T T^T w_0$. Then, by using the second part of Lemma 4.8, the second part of Lemma 4.9, and the definitions of the corresponding operators, we have

$$|P_D w_0|^2_{\widetilde{S}} = w_0^T B^T B_D \widetilde{S} B_D^T Bw_0 = \widehat{w}^T\widehat{B}^T\widehat{B}_D\widehat{\widetilde{S}}\widehat{B}_D^T\widehat{B}\widehat{w} = |\widehat{P}_D\widehat{w}|^2_{\widehat{\widetilde{S}}}$$

with $\widehat{w} \in \widetilde{W}_{T,a}$. □

The following lemma is also needed in the condition number proof. It is essentially based on Lemma 4.9, Lemma 4.8, and [82, equation (8.1)].

Lemma 4.11 ([67])**.** *For $\widehat{w} \in \widetilde{W}_{T,a}$, we have $\widehat{B}\widehat{P}_D\widehat{w} = \widehat{B}\widehat{w}$.*

Proof. By the arguments from Lemma 4.9, Lemma 4.8, and the identity $BP_D w = Bw$ for $w \in \widetilde{W}$ from [82, equation (8.1)], for $w_0 := TR\widehat{w} \in \widetilde{W}_{\widehat{Q}} \subset \widetilde{W}$,

we have,

$$\begin{aligned}\widehat{B}\widehat{P}_D\widehat{w} &= \widehat{B}\widehat{B}_D^T\widehat{B}\widehat{w} = \widehat{B}\widehat{B}_D^T B w_0 \\ &= BTRR_\mu^T T^T B_D^T B w_0 = BB_D^T B w_0 = B w_0 = \widehat{B}\widehat{w}.\end{aligned}$$

□

Note that Lemma 4.10 and Lemma 4.11 provide all the tools to prove identical condition numbers for FETI-DP with the generalized transformation-of-basis approach and the corresponding FETI-DP method with deflation or balancing: From Lemma 4.10, we have $|\widehat{P}_D\widehat{w}|^2_{\widehat{\widetilde{S}}} = |P_D w_0|^2_{\widetilde{S}}$. The relation $|\widehat{w}|_{\widehat{\widetilde{S}}} = |w_0|_{\widetilde{S}}$ for $\widehat{w} \in \widetilde{W}_{T,a}$ and $w_0 \in \widetilde{W}_{\widehat{Q}}$ can also be proven. The standard Rayleigh quotient estimate, e.g., [110, Theorem 2.4.2], [75, Lemma 3.2], and [82, Theorem 8.2], then gives the desired bound. However, with Theorem 4.12, we give a more general statement on the equality of the eigenvalues of the preconditioned operators where the relation between $|w_0|_{\widetilde{S}}$ and $|\widehat{w}|_{\widehat{\widetilde{S}}}$ is not needed explicitly.

We can now formulate and proof the main theorem of our work.

Theorem 4.12 ([67])**.** *Let an a priori coarse space, which ensures the invertibility of the local problems, be given. Then,*

$$\sigma(\widehat{M}_T^{-1}\widehat{F}) = \sigma(M_{PP}^{-1}F), \tag{4.57}$$

i.e., the eigenvalues of the preconditioned FETI-DP system matrix $(\widehat{M}_T^{-1}\widehat{F})$ using the generalized transformation-of-basis approach are the same as for the preconditioned FETI-DP system matrix $(M_{PP}^{-1}F)$ using the deflation approach.

Furthermore,

$$\sigma(\widehat{M}_T^{-1}\widehat{F}) \setminus \{0\} \subset \sigma(M_{BP}^{-1}F), \tag{4.58}$$

i.e., all nontrivial eigenvalues of the preconditioned FETI-DP system matrix $(\widehat{M}_T^{-1}\widehat{F})$ using the generalized transformation-of-basis approach are equal to eigenvalues of the preconditioned FETI-DP system matrix $(M_{BP}^{-1}F)$ using the balancing approach.

Proof. For arbitrary $\widehat{\lambda}$, we define $\widehat{u} := \widehat{\widetilde{S}}^{-1}\widehat{B}^T\widehat{\lambda} \in \widetilde{W}_{T,a}$. Then, we have

$$\langle \widehat{M}_T^{-1}\widehat{F}\widehat{\lambda}, \widehat{F}\widehat{\lambda}\rangle = \langle \widehat{B}_D\widehat{\widetilde{S}}\widehat{B}_D^T\, \widehat{B}\widehat{\widetilde{S}}^{-1}\widehat{B}^T\widehat{\lambda}\,,\, \widehat{B}\widehat{\widetilde{S}}^{-1}\widehat{B}^T\widehat{\lambda}\rangle = \langle \widehat{P}_D\widehat{u}, \widehat{P}_D\widehat{u}\rangle_{\widehat{\widetilde{S}}} \tag{4.59}$$

as, e.g., in [82, Theorem 8.2]; cf. the definitions in (4.36), (4.37), (4.35), and (4.34).

With $u_0 := TR\widehat{u} \in \widetilde{W}_{\widehat{Q}}$ (cf. Lemma 4.9) consider

$$\underbrace{R^T T^T \widetilde{S} T R}_{=\widehat{\widetilde{S}}} R_\mu^T T^T u_0 = \widehat{\widetilde{S}}\widehat{u} = \widehat{B}^T\widehat{\lambda} = R^T T^T B^T \widehat{\lambda}. \tag{4.60}$$

Now, we argue as in the proof of [80, Theorem 6.8], only the operators are slightly adapted. So, equivalently to (4.60), we may solve the saddle point problem

$$\begin{pmatrix} \widetilde{S} & \widehat{Q} \\ \widehat{Q}^T & 0 \end{pmatrix} \begin{pmatrix} u_0 \\ \mu \end{pmatrix} = \begin{pmatrix} B^T\widehat{\lambda} \\ 0 \end{pmatrix} \tag{4.61}$$

where the assembly was replaced by the constraint $\widehat{Q}^T u_0 = 0$, i.e., we have $\widehat{Q}^T TR = 0$ which explicitly uses the matrix $\widehat{Q}$ of $\widetilde{W}_{\widehat{Q}} := \{w \in \widetilde{W} : \widehat{Q}^T w = 0\}$. Note that this is connected to the deflation constraint matrix $\widehat{U}$ by $\widehat{Q} = B^T\widehat{U}$; see Section 4.5.2.2. Note that we can split any $\mu = \mu_1 + \mu_2$ with $\mu_1 \in \operatorname{range}(\widehat{Q}^T\widetilde{S}^{-1}\widehat{Q})^+$ and $\mu_2 \in \ker(\widehat{Q}^T\widetilde{S}^{-1}\widehat{Q}) = \ker\widehat{Q}$. Thus, we can directly consider $\mu \in \operatorname{range}(\widehat{Q}^T\widetilde{S}^{-1}\widehat{Q})^+$. From solving the saddle point system (4.61), we obtain with $\mu \in \operatorname{range}(\widehat{Q}^T\widetilde{S}^{-1}\widehat{Q})^+$

$$\begin{aligned} u_0 &= (I - \widetilde{S}^{-1}\widehat{Q}(\widehat{Q}^T\widetilde{S}^{-1}\widehat{Q})^+\widehat{Q}^T)\widetilde{S}^{-1}B^T\widehat{\lambda} \\ &= (I - \widetilde{S}^{-1}B^T\widehat{U}(\widehat{U}^T B\widetilde{S}^{-1}B^T\widehat{U})^+\widehat{U}^T B)\widetilde{S}^{-1}B^T\widehat{\lambda}. \end{aligned}$$

Thus, we obtain

$$Bu_0 = (I - F\widehat{U}(\widehat{U}^T F\widehat{U})^+\widehat{U}^T)F\widehat{\lambda} = (I - \widehat{P})^T F\widehat{\lambda} = (I - \widehat{P})^T F(I - \widehat{P})\widehat{\lambda} \tag{4.62}$$

with $\widehat{P} := \widehat{U}(\widehat{U}^T F\widehat{U})^+\widehat{U}^T F$; see (4.1) and (4.3). Note that $\widehat{P}$ holds the same properties with respect to $\widehat{U}$ as P with respect to U.

Using Lemma 4.10, (4.59), and (4.62), we obtain

$$\begin{aligned} \langle \widehat{M}_T^{-1}\widehat{F}\widehat{\lambda}, \widehat{F}\widehat{\lambda}\rangle &\overset{(4.59)}{=} \langle \widehat{P}_D\widehat{u}, \widehat{P}_D\widehat{u}\rangle_{\widehat{\widetilde{S}}} \\ &\overset{\text{Lemma 4.10}}{=} \langle P_D u_0, P_D u_0\rangle_{\widetilde{S}} \overset{(4.4),(4.62)}{=} \langle M_{PP}^{-1}F(I - \widehat{P})\widehat{\lambda}, F(I - \widehat{P})\widehat{\lambda}\rangle. \end{aligned} \tag{4.63}$$

Then, using (4.63) and following the Courant-Fischer-Weyl min-max principle, we obtain for the eigenvalues of $\widehat{M}_T^{-1}\widehat{F}$ and $M_{PP}^{-1}F$, the equality

$$\begin{aligned}\mu_k(\widehat{M}_T^{-1}\widehat{F}) &= \min_{\dim(V)=k}\max_{\widehat{\lambda}\in V\,:\,\|\widehat{\lambda}\|=1} \langle \widehat{M}_T^{-1}\widehat{F}\widehat{\lambda}, \widehat{F}\widehat{\lambda}\rangle \\ &= \min_{\dim(V)=k}\max_{\widehat{\lambda}\in V\,:\,\|\widehat{\lambda}\|=1} \langle M_{PP}^{-1}F(I-P)\widehat{\lambda}, F(I-P)\widehat{\lambda}\rangle = \mu_k(M_{PP}^{-1}F)\end{aligned}$$

where $\mu_k(\widehat{M}_T^{-1}\widehat{F})$ and $\mu_k(M_{PP}^{-1}F)$ denote the k-th eigenvalue each, sorted in increasing order.

The relation between the eigenvalues of $M_{PP}^{-1}F$ and $M_{BP}^{-1}F$ can be found in [97] or, in our notation, in [80]. □

Note that we have $0 \in \sigma(\widehat{M}_T^{-1}\widehat{F})$ also for the case of nonredundant Lagrange multipliers if $\widehat{U}$ is not an empty matrix; cf. Remark 4.6. This is a difference to the classical FETI-DP methods using a transformation of basis and results from the fact that the Lagrange multiplier constraints in B are applied to vectors which are already continuous in the a posteriori primal variables. These Lagrange multipliers are not discarded since they allow to implement an interaction of a posteriori primal and a posteriori dual variables through the scaling in B_D; see the preconditioned system in (4.38).

4.5.3 Modified operators and eigenvalues of BDDC with the generalized transformation-of-basis approach

In the previous sections, we have shown that we can use the generalized transformation-of-basis approach in order to derive a FETI-DP approach using a change of variables and partial assembly with essentially the same eigenvalues as a corresponding FETI-DP method with the deflation or the balancing approach. Given the close relations between FETI-DP and BDDC methods, a corresponding BDDC method using a generalized transformation-of-basis approach can also be constructed.

We use the assembly operator $R_{\Delta'}^T$ assembling all degrees of freedom on $\Delta' = \Pi \cup \Delta$, i.e., all a posteriori primal (Π) and all a posteriori dual (Δ) degrees of freedom; cf. the presentation of standard BDDC in Section 3.3. Then, we introduce the short notation

$$R' := \begin{pmatrix} I_{\Pi'} & 0 \\ 0 & R_{\Delta'} \end{pmatrix}, \tag{4.64}$$

such that R'^T leaves the initial coarse space variables unchanged and performs the assembly in all other interface variables. The BDDC system matrix is thus given by the Schur complement on the interface

$$\mathcal{S} = R'^T \widetilde{S} R'; \tag{4.65}$$

cf. (3.25). Note that, since the transformations are chosen consistently for every face and every edge (cf. (4.20)), and since $R'R'^T$ assembles and redistributes information in both, a posteriori primal and remaining dual degrees of freedom, we have

$$TR'R'^T = R'R'^T T \text{ and } T^T R'R'^T = R'R'^T T^T. \tag{4.66}$$

We now use the scaling matrix D_u (see (3.27)) for the untransformed degrees of freedom u in BDDC corresponding to the untransformed scaling D of the Lagrange multipliers in FETI-DP.

Definition 4.13. *(Transformed degree of freedom scaling [67]) For a scaling matrix $D_u^{(i)}$ the transformed scaling matrix $\widehat{D}_u^{(i)}$ is defined by*

$$\widehat{D}_u^{(i)} := T^{(i)T} D_u^{(i)} T^{(i)} \text{ for } i = 1, \ldots, N. \tag{4.67}$$

The transformed BDDC scaling, then, is defined by $\widehat{D}_u := T^T D_u T$ and obtained from the local contributions. Note again, for problems with constant coefficients on edges or faces the transformed scaling remains diagonal if the original scaling was diagonal. For heterogeneous problems this is not generally the case.

The BDDC preconditioner for the system matrix (4.65) is defined by

$$\begin{aligned} \widehat{M}_{\mathrm{BDDC}}^{-1} :&= R'^T T \widehat{D}_u R \widehat{\widetilde{S}}^{-1} R^T \widehat{D}_u T^T R' \\ &= R'^T D_u T R \left(R^T T^T \widetilde{S} T R\right)^{-1} R^T T^T D_u R', \end{aligned} \tag{4.68}$$

where R' was introduced in (4.64) and R, defined in (4.24), replicates the a posteriori primal variables. Thus, the preconditioned BDDC system matrix is

$$\widehat{M}_{\mathrm{BDDC}}^{-1} \mathcal{S} = \left(R'^T T \widehat{D}_u R \widehat{\widetilde{S}}^{-1} R^T \widehat{D}_u T^T R'\right)\left(R'^T \widetilde{S} R'\right). \tag{4.69}$$

Since the scaling $\widehat{D}_u$ affects a posteriori dual and a posteriori primal variables likewise, the method is clearly different from BDDC with the standard transformation-of-basis approach and a transformed scaling, which can be writ-

ten as follows

$$M_{\mathrm{BDDC}}^{-1}\mathcal{S} = \begin{pmatrix} I_{\Pi'\cup\Pi} & 0 \\ 0 & R^T_{\Delta,\widehat{D}_{u,\Delta}} \end{pmatrix} \widehat{\widetilde{S}}^{-1} \begin{pmatrix} I_{\Pi'\cup\Pi} & 0 \\ 0 & R_{\Delta,\widehat{D}_{u,\Delta}} \end{pmatrix} \mathcal{S} \tag{4.70}$$

and where $\widehat{D}_{u,\Delta}$ is a transformed but restricted scaling acting only on the remaining (a posteriori) dual variables Δ and $I_{\Pi'\cup\Pi}$ is the identity on all primal variables $\Pi' \cup \Pi$. In our preconditioner, however, an interaction between a posteriori dual and primal variables can be implemented by using a nondiagonal $\widehat{D}_u$ and not neglecting the a posteriori primal part. This interaction can be necessary; cf. Example 4.1 and Section 6.1.

The operator E_{D_u} of (3.30), which is central to the condition number proof of BDDC, also writes $E_{D_u} = R'R'^T D_u$. We now define

$$\widehat{E}_{D_u} := R_\mu^T T^T R' R'^T D_u T R. \tag{4.71}$$

Lemma 4.14 ([67])**.** *For $\widehat{E}_{D_u} = R_\mu^T T^T R' R'^T D_u T R$, it holds*

$$\begin{array}{lll} i) & \widehat{E}_{D_u} & = R_\mu^T E_{\widehat{D}_u} R, \\ ii) & \widehat{P}_D & = I - \widehat{E}_{D_u}. \end{array} \tag{4.72}$$

Proof. i) By (4.66) and Definition 4.13, we obtain

$$\widehat{E}_{D_u} = R_\mu^T T^T R' R'^T D_u T R = R_\mu^T R' R'^T T^T D_u T R = R_\mu^T R' R'^T \widehat{D}_u R = R_\mu^T E_{\widehat{D}_u} R.$$

ii) Since $R_\mu^T = (R^T R)^{-1} R^T$, we have $R_\mu^T R = I$. Combining the definition of $\widehat{P}_D$ in (4.34), the standard relation $P_D = I - E_{D_u}$, again (4.66), and the previous statement, we also have

$$\widehat{P}_D = R_\mu^T T^T P_D T R = R_\mu^T (I - E_{\widehat{D}_u}) R = I - \widehat{E}_{D_u}.$$

□

Theorem 4.15 ([67])**.** *Let an a priori coarse space, which ensures the invertibility of the local problems, be given. Then,*

$$\sigma(\widehat{M}_{BDDC}^{-1}\mathcal{S}) \setminus \{0,1\} \subset \sigma(\widehat{M}_T^{-1}\widehat{F}) = \sigma(M_{PP}^{-1}F), \tag{4.73}$$

i.e., except for zeros and ones, the preconditioned BDDC system matrix $\widehat{M}_{BDDC}^{-1}\mathcal{S}$ has the same eigenvalues as the preconditioned FETI-DP system

matrix using either the generalized transformation-of-basis or the deflation approach.

Proof. The proof is based on the known relation between BDDC and FETI-DP; see [81, 43, 53, 92, 89]. The preconditioned BDDC system operator is given by

$$\widehat{M}^{-1}_{\mathrm{BDDC}}\,\mathcal{S} = (R'^T T \widehat{D}_u R \widehat{\widetilde{S}}^{-1} R^T \widehat{D}_u T^T R')\,(R'^T \widetilde{S} R')$$

which, except for zeros, has the same eigenvalues as

$$\widehat{\widetilde{S}}^{-1} R^T \widehat{D}_u T^T R' R'^T \widetilde{S} R' R'^T T \widehat{D}_u R.$$

From (4.66), Definition 4.13, (4.71), and $R R_\mu^T R' = R'$, we obtain

$$\begin{aligned}
&\widehat{\widetilde{S}}^{-1} R^T \widehat{D}_u T^T R' R'^T \widetilde{S} R' R'^T T \widehat{D}_u R \\
&\qquad = \widehat{\widetilde{S}}^{-1} \underbrace{R^T \widehat{D}_u R' R'^T R_\mu}_{=\widehat{E}_{D_u}^T} \underbrace{R^T T^T \widetilde{S} T R}_{=\widehat{\widetilde{S}}} \underbrace{R_\mu^T R' R'^T \widehat{D}_u R}_{\widehat{E}_{D_u}} \\
&\qquad = \widehat{\widetilde{S}}^{-1} \widehat{E}_{D_u}^T \widehat{\widetilde{S}} \widehat{E}_{D_u},
\end{aligned}$$

which then has the same eigenvalues as

$$\widehat{E}_{D_u} \widehat{\widetilde{S}}^{-1} \widehat{E}_{D_u}^T \widehat{\widetilde{S}}.$$

By using $\widehat{P}_D = I - \widehat{E}_{D_u}$ from Lemma 4.14 and the estimate from Theorem 4.12, we obtain that the eigenvalues (except for zero and one) of the BDDC method using the generalized transformation-of-basis approach are identical to that of FETI-DP using the generalized transformation-of-basis or the deflation approach. □

Implementational remarks for BDDC

Let us note that, as in the case of adaptive FETI-DP, the a posteriori set of primal degrees of freedom (given by the index set Π) have to be scaled by the transformed scaling $\widehat{D}_u$, too. Thus, compared to the standard BDDC preconditioner, we replace $\widetilde{S}^{-1}$ by $\widehat{\widetilde{S}}^{-1}$, D_u by $\widehat{D}_u$, and assemble, using R^T, the a posteriori primal degrees of freedom between the application of the scaling $\widehat{D}_u$ and the solution of the system of equations associated with $\widehat{\widetilde{S}}$. In other words, in the preconditioner, we solve systems of the form $\widehat{\widetilde{S}} x = R^T \widehat{D}_u w$ for the unknown $x \in \widetilde{W}_{T,a}$; see (4.69).

4.5.4 Conclusion on the relation of the generalized transformation-of-basis approach and deflation and balancing

To conclude this section, we summarize the established results.

For every FETI-DP or BDDC method using the generalized transformation-of-basis approach, a *corresponding* FETI-DP method using the deflation or the balancing approach exists with essentially the same eigenvalues; see Theorems 4.12 and 4.15. The reverse is true under certain conditions. First, a constraint vector should not span several faces and edges (which is not true, e.g., in [50, 48]). In case such constraints exist, they would have to be split up and the partial assembly would enforce more constraints than intended by the deflation or balancing approach; see the relation of the solution spaces in (4.32) and the discussion around Figure 4.2. Second, for any face and any edge, the local constraint vectors have to be identical for all adjacent subdomains. If the second assumption cannot be assumed, additional local constraint vectors have to introduced – without generally creating a larger coarse space. Note that the number of constraint vectors does not equal the size of the coarse space since the partial finite element assembly determines the size of the coarse space.

5 FETI-DP with adaptive coarse spaces using deflation and balancing

5.1 Preliminaries

In the past, different, sophisticated nonadaptive coarse spaces have been developed for FETI-DP and BDDC given different problems and specific heterogeneity; cf., e.g., [37, 107, 83, 84, 23, 89, 77, 82, 78, 102, 49, 48, 130]. However, if the heterogeneity becomes arbitrary, assumptions on the coefficients might not be valid anymore and the classical methods might not converge.

At the beginning of this section, we present a simple model problem where the FETI-DP (or BDDC) method with a traditional coarse space does not converge. We also discuss a basic idea to develop problem-dependent *adaptive* coarse spaces. The coarse spaces are established in a local fashion, exploiting the parallel structure of the underlying domain decomposition.

Parts of this chapter have already been published in modified or unmodified form by the author of this thesis and his coauthors in [64, 65, 66].

Let us consider two small examples of linear elasticity on the unit cube, partitioned into $N = 64$ and $N = 216$ subdomains, respectively. In these examples, $N^{2/3}$ (i.e., 16 and 36, respectively) beams of a stiff material with $\mathrm{E}_2 = 1e + 6$ span from the face with $x = 0$ to the face with $x = 1$ and are surrounded by a soft matrix material with $\mathrm{E}_1 = 1$; see Figure 5.1 (top). In a regular (domain) decomposition into cubes, we have precisely one centered beam per subdomain. In this thesis, we refer to this material as *composite material no. 1.*

On the face with $x = 0$, we enforce homogeneous Dirichlet boundary conditions, for all other faces on $\partial\Omega$, we enforce homogeneous Neumann boundary conditions. By using the METIS mesh partitioner (see [60]), we obtain arbitrary heterogeneity on the interface since the beams then cut through many different faces and edges; see Figure 5.1 (bottom). Consequently, although the problem is kept quite simple, the heterogeneity introduced by the partitioning leads to a complex problem.

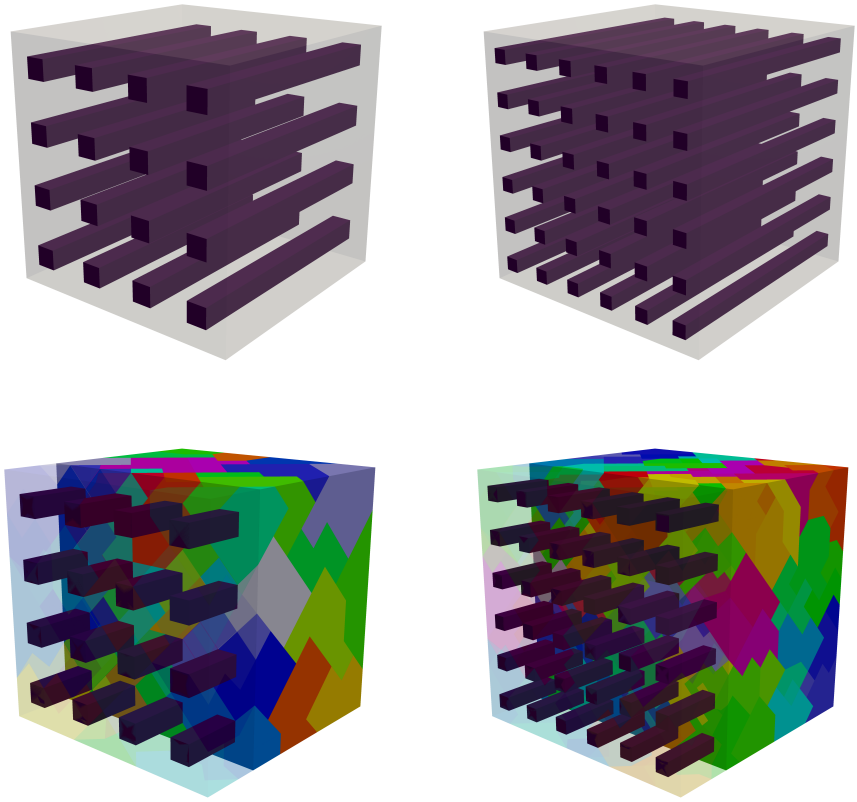

Figure 5.1: *Composite material no. 1 on the unit cube for 64 and 216 subdomains:* 16 and 36 beams of a stiff material with $E_2 = 1e + 6$, shown in dark purple, are surrounded by a soft matrix material with $E_1 = 1$, shown in light, half-transparent gray, (top). Irregular decomposition using METIS [60] for 64 and 216 subdomains; high coefficients are again shown in dark purple; subdomains shown in different colors; left quarter of the domain ($x > \frac{3}{4}$) made half-transparent (bottom). [64]

Table 5.1: *Standard FETI-DP with ρ-scaling and a classical (nonadaptive) vertex and edge average coarse space.* Compressible linear elasticity of composite material no. 1 with $E_1 = 1$ and $N^{2/3}$ beams with $E_2 = 1e+6$ on the unit cube; $\nu = 0.3$ for the whole domain; conforming $\mathcal{P}_1$ finite element discretization with $1/h = 6N^{1/3}$ and irregular partitioning of the domain; see Figure 5.1. N denotes the number of subdomains, $|\lambda|$ the size of the dual problem, $|\Pi'|$ the size of the nonadaptive coarse space, κ the condition number of the preconditioned operator (eigenvalue estimates from the underlying PCG iteration), *its* the number of iterations of the PCG algorithm, and $\|M_D^{-1}r\|_2$ the norm of the preconditioned residual after the last iteration (here: 2 000). [65]. Copyright Wiley-VCH Verlag GmbH & Co. KGaA. Reproduced with permission.

Standard FETI-DP with *Vertex and Edge Average Coarse Space*

$1/h = 6N^{1/3}$ – composite material no. 1 – irregular partitioning

N	$\lvert\lambda\rvert$	$\lvert\Pi'\rvert$	κ	*its*	$\|M_D^{-1}r\|_2$
4^3	20 991	2 367	1.10e+6	$> 2\,000$	5.37e-2
6^3	80 199	9 168	1.57e+6	$> 2\,000$	1.02e-0

As Table 5.1 shows, a standard FETI-DP method with a classical nonadaptive coarse space, in which all vertex variables and all edge averages are made primal, cannot ensure convergence in less than 2 000 iterations. The preconditioned residual then is still large.

Note that single heterogeneities, such as a discontinuity not aligned with a specific edge, can be controlled numerically by a weighted edge average; see [78].

For irregular decompositions, however, discontinuities on the interface are, in general, arbitrary and problem-dependent coarse spaces might be necessary. In the following sections, we present different problem-dependent coarse spaces. For one of them, we can prove a condition number bound not depending on the discontinuous material parameters. Two others are heuristical modifications thereof and the last two are from the literature.

5.2 A family of adaptive coarse spaces

Problem-dependent, adaptive coarse spaces have gained more and more interest over the last years. For FETI-DP and BDDC, different adaptive coarse spaces were introduced or considered in [93, 120, 94, 72, 22, 74, 109, 75, 63, 64, 7, 101, 17, 134, 103, 62, 68].

In the following, we present different sorts of adaptive constraints and then introduce adaptive algorithms based on the use of (subsets of) these constraints.

5.2.1 Various adaptive constraints

In order to guarantee the convergence of the iterative solver, we bound the condition number of the preconditioned FETI-DP system matrix, which is problem- and coarse space-dependent. In Sections 3.2 and 4.2, we mentioned the relation between the condition number estimate of the FETI-DP method and an estimate on the P_D-operator, i.e., we can reduce the problem of bounding the condition number to the problem of finding a constant $C \in \mathbb{R}$ such that

$$\frac{\|P_D w\|_{\widetilde{S}}^2}{\|w\|_{\widetilde{S}}^2} \leq C \text{ for all } w \in \widetilde{W}_U;$$

see the references given in these sections.

In order to bound C from above, a straightforward approach would then be to consider the generalized eigenvalue problem

$$\langle P_D v, \widetilde{S} P_D w \rangle = \mu \langle v, \widetilde{S} w \rangle \tag{5.1}$$

for all $v \in \widetilde{W} = \text{range}\, \widetilde{S}$. With an a priori coarse space ensuring the invertibility of the local problems, $\widetilde{S}$ is symmetric positive definite and thus $0 \leq \mu < \infty$. Assume $0 \leq \mu_1 \leq \ldots \leq \mu_n$ for the eigenvalues and denote the corresponding eigenvectors by $w_1, \ldots, w_n$. For an user-chosen tolerance TOL, let s be given such that $\mu_s \geq \text{TOL}$ and $\mu_{s-1} < \text{TOL}$. By defining the matrix

$$U := \left(B_D \widetilde{S} P_D w_s, \ldots, B_D \widetilde{S} P_D w_n \right), \tag{5.2}$$

it yields

$$\frac{\|P_D w\|_{\widetilde{S}}^2}{\|w\|_{\widetilde{S}}^2} \leq \text{TOL for all } w \in \widetilde{W}_U = \{ w \in \widetilde{W} \, : \, U^T B w = 0 \} \tag{5.3}$$

since the eigenvectors can be chosen to be orthogonal with respect to the (semi)inner products defined by $\langle \cdot, P_D^T \widetilde{S} P_D \, \cdot \rangle$ and $\langle \cdot, \widetilde{S} \, \cdot \rangle$. This can be proven by arguments from standard linear algebra and using (5.1).

In the context of domain decomposition methods, however, the solution of (5.1) is not feasible since this equation represents a global eigenvalue problem. Thus, we make use of the structure of the nonoverlapping decomposition and establish local versions of (5.1) on faces and on edges. This reduces the number

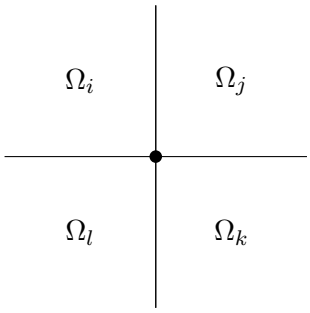

Figure 5.2: *Cross-sectional view of four subdomains sharing an edge (represented by the node) in a regular partition.* Ω_i shares faces $\mathcal{F}^{ij}$ and $\mathcal{F}^{il}$ with Ω_j and Ω_l, respectively, but only an edge $\mathcal{E}^{ik}$ with Ω_k. [64]

of subdomains affected by each local eigenvalue problem dramatically. In Section 5.3, we then prove a condition number bound for an adaptive algorithm based on local generalized eigenvalue problems. In the following, we consider the case of four cubic subdomains sharing an edge; see Figure 5.2 for a cross-sectional view. More general cases can be treated completely analogously. Note that this is already a more general case of the example considered in Section 4.5, which still satisfies the assumption of Ω_i, Ω_j, and Ω_k sharing an edge $\mathcal{E}^{ik}$.

In this chapter, we often use the expression *rigid body modes* when referring to the null space of Schur complements originated from the stiffness matrices. For the diffusion problem, the corresponding reasonings can be adapted easily. Note that for both problems we assume the existence of an a priori coarse space that ensures invertibility of the local problems, e.g., the coarse space where all vertices are made primal.

Note that adaptive coarse spaces for FETI-DP and BDDC are not always related to the P_D-operator. In [74], the eigenvalue problems replace a local extension theorem and local Poincaré inequalities.

As in [93, 120, 94], we first introduce local generalized eigenvalue problems on faces, based on a localized version of the P_D-operator. We extend this for three dimensions by some new edge eigenvalue problems of similar pattern; see [64].

Let us consider the following motivation of local generalized eigenvalue problems for linear elasticity problems. For the diffusion equation, only the arguments on the null space of the local matrices have to be adapted.

For the face eigenvalue problem based algorithm we proceed in the following sections as in [93] by using the notation from [75].

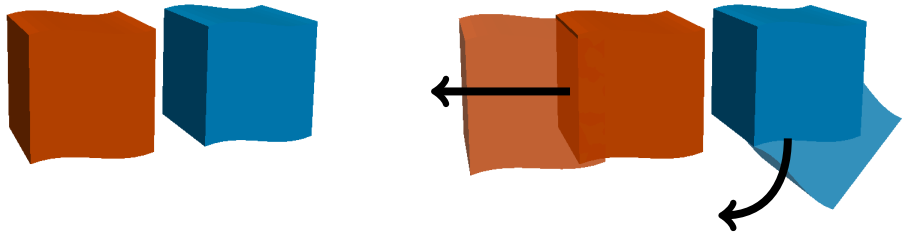

(a) *Two subdomains sharing a face (not coupled):* Ω_i (orange) and Ω_j (blue) share the face $\mathcal{F}^{ij}$ (left). Arbitrary rigid body modes of the single substructures indicated by black arrows and half-transparent copies of the cubic subdomains (right).

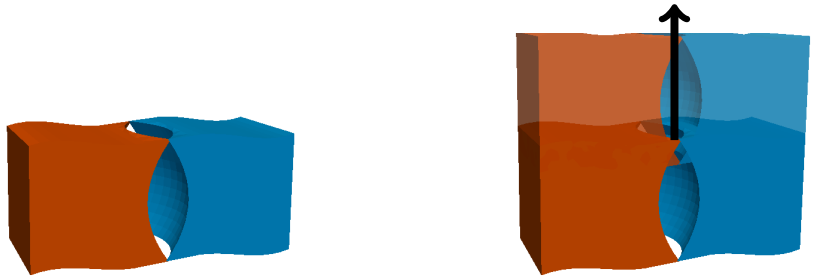

(b) *Two subdomains sharing a face (coupled in primal vertices):* Ω_i (orange) and Ω_j (blue) share the face $\mathcal{F}^{ij}$ and are coupled in the primal vertices (left). Arbitrary, common rigid body mode of the coupled substructures indicated by black arrow and half-transparent copies of the cubic subdomains (right).

Figure 5.3: *Two cubic subdomains sharing a face.*

Let us consider the face $\mathcal{F}^{ij}$ between the subdomains Ω_i and Ω_j as well as its closure $\overline{\mathcal{F}}^{ij}$; see Figure 5.3a (left). We define

$$B_{\overline{\mathcal{F}}^{ij}} := \left(B^{(i)}_{\overline{\mathcal{F}}^{ij}} \; B^{(j)}_{\overline{\mathcal{F}}^{ij}}\right) \tag{5.4}$$

as the submatrix of $\left(B^{(i)} \; B^{(j)}\right)$ consisting of all the rows that contain exactly one $+1$ and one -1. Analogously,

$$B_{D,\overline{\mathcal{F}}^{ij}} := \left(B^{(i)}_{D,\overline{\mathcal{F}}^{ij}} \; B^{(j)}_{D,\overline{\mathcal{F}}^{ij}}\right) \tag{5.5}$$

is the submatrix of $\left(B^{(i)}_D \; B^{(j)}_D\right)$, i.e., the scaled variant of $B_{\overline{\mathcal{F}}^{ij}}$. We then define

$$S_{ij} := \begin{pmatrix} S^{(i)} & 0 \\ 0 & S^{(j)} \end{pmatrix} \in \mathbb{R}^{(n_i+n_j)\times(n_i+n_j)} \quad \text{and} \quad P_{D,\overline{\mathcal{F}}^{ij}} := B^T_{D,\overline{\mathcal{F}}^{ij}} B_{\overline{\mathcal{F}}^{ij}}, \tag{5.6}$$

where n_l, $l \in \{i, j\}$, is the number of degrees of freedom on the local part of the interface.

Remark 5.1. *Let us note that the scalings used in the local generalized edge eigenvalue problems are the localized scalings from the FETI-DP algorithm, i.e., for a node on the edge between the four subdomains Ω_i, Ω_j, Ω_k, and Ω_l the scaling for the jump $w^{(i)} - w^{(j)}$ in the corresponding eigenvalue problem is $\widehat{\rho}_j/(\widehat{\rho}_i + \widehat{\rho}_j + \widehat{\rho}_k + \widehat{\rho}_l)$ if ρ-scaling is used. That means that although the face (or later also the edge) eigenvalue problems are established pairwise, information of the other subdomains sharing the edges is included. Thus, for deluxe-scaling, we (implicitly) need the Schur complements of Ω_j, Ω_k, and Ω_l; cf.* (3.17) *and* (3.36).

We then have the local generalized face eigenvalue problem: Find $w_{ij} \in \mathbb{R}^{n_i+n_j}$ such that

$$\langle P_{D,\overline{\mathcal{F}}^{ij}} v_{ij}, S_{ij} P_{D,\overline{\mathcal{F}}^{ij}} w_{ij} \rangle = \mu_{ij} \langle v_{ij}, S_{ij} w_{ij} \rangle \qquad \forall v_{ij} \in \mathbb{R}^{n_i+n_j}. \tag{5.7}$$

However, the solution and theoretical consideration of this problem then comprises the additional difficulty that neither the left hand side nor the right hand side operator is positive definite. Since the Schur complements originate from the local stiffness matrices, we know that both operators are at least symmetric positive semidefinite and that the null space of S_{ij} is given by the single rigid body modes of the two substructure interfaces; see Section 3.2 and Figure 5.3a (right).

As done for the a priori coarse space, we couple the two subdomains in the primal vertices; see Figure 5.3b (left). However, if neither Ω_i nor Ω_j have Dirichlet boundary conditions prescribed on an essential part of their boundary, e.g., $\partial\Omega_D \cap \big(\partial\Omega_i \cup \partial\Omega_j\big) = \emptyset$, the common rigid body modes (common shifts and common rotations) are still in the null space of the coupled right hand side operator; see Figure 5.3b (right).

We eventually remove the common rigid body modes and consider (5.7) on the subspace $\big(\ker S_{ij}\big)^{\perp}$: Find $w_{ij} \in \big(\ker S_{ij}\big)^{\perp}$ such that

$$\langle P_{D,\overline{\mathcal{F}}^{ij}} v_{ij}, S_{ij} P_{D,\overline{\mathcal{F}}^{ij}} w_{ij} \rangle = \mu_{ij} \langle v_{ij}, S_{ij} w_{ij} \rangle \qquad \forall v_{ij} \in \big(\ker S_{ij}\big)^{\perp}. \tag{5.8}$$

On the right hand side, we then have an inner product defined on a subspace, where S_{ij} is positive definite.

As seen in the preceding part of this section, this eigenvalue problem can be motivated by the localization of the global P_D-operator, which is at the center of the proofs on the condition number bound of FETI-DP and BDDC methods.

Another motivation, based on the upcoming estimate for faces (cf. (5.21)), can be found in [93, Sections 4 and 5] and [94, Section 3].

In practice, in order to obtain a positive definite operator on the right hand side, two separate projections are established to manage the single and common rigid body modes. By $\widetilde{W}_{ij}$, we denote the space of functions in $W_i \times W_j$ that are continuous in the primal variables shared by Ω_i and Ω_j and by Π_{ij}, we denote the ℓ_2-orthogonal projection from $W_i \times W_j$ to $\widetilde{W}_{ij}$. We introduce a second ℓ_2-orthogonal projection from $W_i \times W_j$ to range $(\Pi_{ij} S_{ij} \Pi_{ij} + \sigma(I - \Pi_{ij}))$, which is denoted by $\overline{\Pi}_{ij}$ and where σ is a positive constant used for stability reasons, e.g., the maximum of the diagonal entries of S_{ij}; see [93, 94].

Completely analogously to [109], we build Π_{ij} and $\overline{\Pi}_{ij}$. Note that Π_{ij} and $\overline{\Pi}_{ij}$ are set up so that they are symmetric.

By defining $R_{ij}^{(l)T}$, $l = i, j$, as the local part of the assembly operator of primal variables on $\partial\Omega_i \cap \partial\Omega_j$ and as the identity on the rest of $\left(\Gamma \cap \partial\Omega_i\right) \times \left(\Gamma \cap \partial\Omega_j\right)$, we obtain

$$R_{ij} := \begin{pmatrix} R_{ij}^{(i)} \\ R_{ij}^{(j)} \end{pmatrix}$$

and the orthogonal projection onto $\widetilde{W}_{ij}$,

$$\Pi_{ij} := R_{ij}(R_{ij}^T R_{ij})^{-1} R_{ij}^T. \tag{5.9}$$

We note that the inverse can be computed cheaply since R_{ij} contains a large identity block and a very small block of the size of the number of the primal degrees of freedom that are common to the two subdomains.

For the construction of $\overline{\Pi}_{ij}$ we exploit the fact that $I - \overline{\Pi}_{ij}$ is an orthogonal projection onto the rigid body modes that are continuous on $W_i \times W_j$. If $\{\tilde{r}_1, \ldots, \tilde{r}_s\}$ is the largest set of linear independent rigid body modes that are continuous on $W_i \times W_j$ we use a modified Gram-Schmidt method to create an orthonormal basis $\{r_1, \ldots, r_s\}$ and define

$$\overline{\Pi}_{ij} := I - \sum_{p=1}^{s} r_p r_p^T. \tag{5.10}$$

We now establish and solve the following generalized eigenvalue problems

$$\begin{aligned} &\overline{\Pi}_{ij}\Pi_{ij} P_{D,\overline{\mathcal{F}}^{ij}}^T S_{ij} P_{D,\overline{\mathcal{F}}^{ij}} \Pi_{ij}\overline{\Pi}_{ij} w_{ij} \\ &\qquad = \mu_{ij}(\overline{\Pi}_{ij}(\Pi_{ij} S_{ij} \Pi_{ij} + \sigma(I - \Pi_{ij}))\overline{\Pi}_{ij} + \sigma(I - \overline{\Pi}_{ij}))w_{ij}, \end{aligned} \tag{5.11}$$

for $\mu_{ij} \geq \text{TOL}$. Thus, for any of these eigenvalue problems with $w_{ij} \in W_i \times W_j$, we just consider the jumps $w^{(i)} - w^{(j)}$ across the closure $\overline{\mathcal{F}}^{ij}$ of the face $\mathcal{F}^{ij}$. We remark again that Π_{ij} removes the rigid body modes of each of the single substructures Ω_i and Ω_j while $I - \overline{\Pi}_{ij}$ is an orthogonal projection onto the space of rigid body modes that are continuous on $W_i \times W_j$ and move Ω_i and Ω_j as a connected entity; see Figure 5.3a (right) and Figure 5.3b (right). Consequently, the right hand side of the eigenvalue problem (5.11) is symmetric positive definite; cf. [93].

Note that the eigenvalue problems are defined for closed faces. As already proposed in [94, p.1819], we split the computed face constraint vectors. Assume $\mu_{ij}^r \geq \text{TOL}$, then the constraint vector $c_{\lambda,ij}^r := B_{D,\overline{\mathcal{F}}^{ij}} S_{ij} P_{D,\overline{\mathcal{F}}^{ij}} w_{ij}^r$ is split into several edge parts $c_{\lambda,ij,\mathcal{E}_m}^r$ and a part on the open face $c_{\lambda,ij,\mathcal{F}}^r$, all extended by zero to the closure of the face. We then enforce not only the open face constraint but all the constraints

$$c_{\lambda,ij,\mathcal{F}}^{r\,T} B_{\overline{\mathcal{F}}^{ij}} w_{ij} = 0, \tag{5.12}$$

$$c_{\lambda,ij,\mathcal{E}_m}^{r\,T} B_{\overline{\mathcal{F}}^{ij}} w_{ij} = 0, \quad m = 1, 2, \ldots. \tag{5.13}$$

We refer to the edge constraints in (5.13) as *edge constraints from face eigenvalue problems*; cf. also the definition of the different adaptive algorithms in Section 5.2.2.

Clearly, since $c_{\lambda,ij}^r = c_{\lambda,ij,\mathcal{F}}^r + \sum_m c_{\lambda,ij,\mathcal{E}_m}^r$, we then also have $c_{\lambda,ij}^{r\,T} B_{\overline{\mathcal{F}}^{ij}} w_{ij} = 0$. With this approach, we avoid a coupling of constraints across the closures of the faces which would spoil the block structure of the constraint matrix U; cf. [94]. In contrast to (5.2), coupling then only occurs between the degrees of freedom on the open faces and open edges. Thus, from a single eigenvector defined on a closed face, in case of a structured decomposition into cubes, we would obtain one face constraint and four edge constraints.

Considering again Figure 5.2, we also have to control the jumps $w^{(i)} - w^{(k)}$ across the edge $\mathcal{E}^{ik}$. Note that the jumps $w^{(i)} - w^{(j)}$ and $w^{(i)} - w^{(l)}$ across the edge $\mathcal{E}^{ik}$ are handled within the face eigenvalue problems considered on the closure of the corresponding faces. However, the jump $w^{(i)} - w^{(k)}$ across the edge cannot be assigned to any corresponding face eigenvalue problem since Ω_i and Ω_k do not share any face.

Remark 5.2. *Note that, in the following, we always assume that all vertices are chosen to be primal. If this was not the case, and certain corner nodes were not primal, the adjacent edge eigenvalue problems have to be extended to the closure of the edge. Additionally, a vertex eigenvalue problem might be*

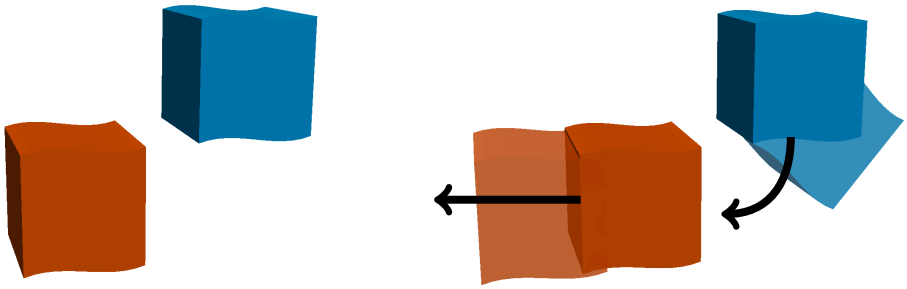

(a) *Two subdomains sharing an edge (not coupled):* Ω_i (orange) and Ω_k (blue) share the edge $\mathcal{E}^{ik}$ (left). Arbitrary rigid body modes of the single substructures indicated by black arrows and half-transparent copies of the cubic subdomains (right).

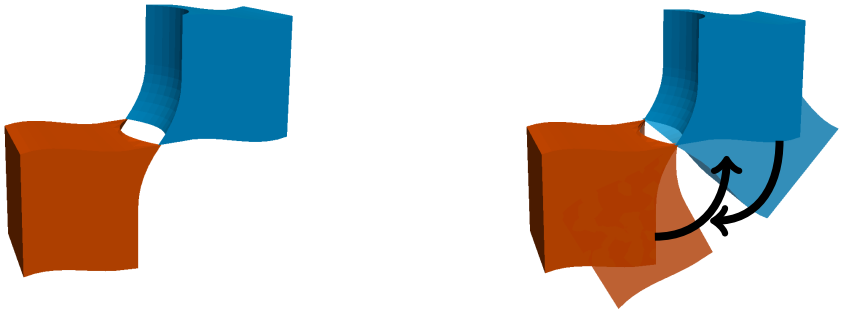

(b) *Two subdomains sharing an edge (coupled in primal vertices):* Ω_i (orange) and Ω_k (blue) share the edge $\mathcal{E}^{ik}$ and are coupled in the primal vertices (left). Arbitrary, common rigid body mode of the coupled substructures indicated by black arrows and half-transparent copies of the cubic subdomains (right).

Figure 5.4: *Two cubic subdomains sharing an edge.*

necessary; cf. Remark 5.6. However, since vertex eigenvalue problems had to be built and solved over the whole interface of the two connected subdomains they might be more expensive than choosing the vertex to be primal. By assuming all vertices to be primal, we can use the index $\mathcal{E}^{ik}$ *instead of* $\overline{\mathcal{E}}^{ik}$ *for the operators related to the edge eigenvalue problem on* $\mathcal{E}^{ik}$.

We define

$$B_{\mathcal{E}^{ik}} := \left(B^{(i)}_{\mathcal{E}^{ik}} \; B^{(k)}_{\mathcal{E}^{ik}}\right) \tag{5.14}$$

as the submatrix of $\left(B^{(i)} \; B^{(k)}\right)$ consisting of all the rows corresponding to $\mathcal{E}^{ik}$ that contain exactly one $+1$ and one -1. Analogously,

$$B_{D,\mathcal{E}^{ik}} := \left(B^{(i)}_{D,\mathcal{E}^{ik}} \; B^{(k)}_{D,\mathcal{E}^{ik}}\right) \tag{5.15}$$

is the submatrix of $\begin{pmatrix} B_D^{(i)} & B_D^{(k)} \end{pmatrix}$ corresponding to the Lagrange multipliers on $\mathcal{E}^{ik}$, i.e., the scaled variant of $B_{\mathcal{E}^{ik}}$. Note that Ω_i can share more than one edge eigenvalue problem with Ω_k when automatic mesh partitioners are used. Thus, not all the rows of $\begin{pmatrix} B^{(i)} & B^{(k)} \end{pmatrix}$ having one +1 and one -1 entry correspond to the eigenvalue problem on $\mathcal{E}^{ik}$. We then should rather write $\mathcal{E}^{ik,1}$, $\mathcal{E}^{ik,2}$, ... for the multiple edges. To avoid a proliferation of indices, we refrain from doing this.

Then, as for the face eigenvalue problems, we define

$$S_{ik} := \begin{pmatrix} S^{(i)} & 0 \\ 0 & S^{(k)} \end{pmatrix} \in \mathbb{R}^{(n_i+n_k)\times(n_i+n_k)}, \qquad P_{D,\mathcal{E}^{ik}} := B_{D,\mathcal{E}^{ik}}^T B_{\mathcal{E}^{ik}}, \tag{5.16}$$

where n_l, $l \in \{i,k\}$, is the number of degrees of freedom on the local part of the interface.

As for the face eigenvalue problems, we have the local generalized edge eigenvalue problem: Find $w_{ik} \in \mathbb{R}^{n_i+n_k}$ such that

$$\langle P_{D,\mathcal{E}^{ik}} v_{ik}, S_{ik} P_{D,\mathcal{E}^{ik}} w_{ik} \rangle = \mu_{ik} \langle v_{ik}, S_{ik} w_{ik} \rangle \qquad \forall v_{ik} \in \mathbb{R}^{n_i+n_k}. \tag{5.17}$$

Again, neither the left hand side nor the right hand side operator is positive definite. We know that both operators are at least symmetric positive semidefinite and that the null space of S_{ik} is given by the rigid body modes of the two subdomains; see Section 3.2 and Figure 5.4a (right).

Analogously to the face eigenvalue problems, we couple the two subdomains in the primal vertices; see Figure 5.4b (left). Though, in contrast to the face eigenvalue problems, if Ω_i or Ω_k has no Dirichlet boundary conditions prescribed on an essential part of its boundary, e.g., $\partial\Omega_D \cap \partial\Omega_i = \emptyset$, the common rigid body modes include an additional hinge mode around the shared edge; see Figure 5.4b (right).

We eventually remove the common rigid body modes and consider (5.17) on the subspace $\big(\ker S_{ik}\big)^\perp$: Find $w_{ik} \in \big(\ker S_{ik}\big)^\perp$ such that

$$\big(P_{D,\mathcal{E}^{ik}} v_{ik}, S_{ik} P_{D,\mathcal{E}^{ik}} w_{ik}\big) = \mu_{ik} \big(v_{ik}, S_{ik} w_{ik}\big) \qquad \forall v_{ik} \in \big(\ker S_{ik}\big)^\perp. \tag{5.18}$$

We thus obtain a formulation with symmetric positive definite right hand side. With the corresponding projections Π_{ik} and $\overline{\Pi}_{ik}$, (5.18) writes

$$\begin{aligned} &\overline{\Pi}_{ik}\Pi_{ik} P_{D,\mathcal{E}^{ik}}^T S_{ik} P_{D,\mathcal{E}^{ik}} \Pi_{ik}\overline{\Pi}_{ik} w_{ik} \\ &\qquad = \mu_{ik}(\overline{\Pi}_{ik}(\Pi_{ik} S_{ik} \Pi_{ik} + \sigma(I - \Pi_{ik}))\overline{\Pi}_{ik} + \sigma(I - \overline{\Pi}_{ik}))w_{ik}. \end{aligned} \tag{5.19}$$

Again, we are only interested in eigenvectors w_{ik} of eigenvalues $\mu_{ik} \geq$TOL. For edge eigenvalue problems without essential Dirichlet boundary the corresponding hinge mode is in fact a rigid body mode and is used to establish the projection $\overline{\Pi}_{ik}$. Note that for bent (i.e., nonstraight) edges we use a different treatment than for straight edges and that the hinge mode is eliminated in advance by making a third node on the edge primal; cf. Remark 5.3.

Clearly, the construction and solution of edge eigenvalue problems only has to be carried out for edges shared by more than three subdomains and in rare occasions where the open face does not contain any discretization nodes. We refer to [110] where experiments showed that typically more than 99% of the edges are common to exactly three subdomains when an automatic graph partitioner is used. Hence, for automatically partitioned domains, which we consider as the standard case, these new eigenvalue problems just come into play for either a small number of edges or a slightly larger number of small edges. Therefore, the extra work for solving the edge eigenvalue problems is small. We come back to this matter and discuss the cost and necessity of edge eigenvalue problems in practice in Section 5.4.

Finally, for all $\mu_{ik}^r \geq$ TOL, the constraints resulting from edge eigenvalue problems are

$$w_{ik}^{r\,T} P_{D,\mathcal{E}^{ik}}^T S_{ik} P_{D,\mathcal{E}^{ik}} w_{ik} = c_{\lambda,ik}^{r\,T} B_{\mathcal{E}^{ik}} w_{ik} = 0, \tag{5.20}$$

with w_{ik}^r the corresponding eigenvectors and $c_{\lambda,ik}^r := B_{D,\mathcal{E}^{ik}} S_{ik} P_{D,\mathcal{E}^{ik}} w_{ik}^r$ the corresponding constraint vectors.

Next, we consider the local estimates obtained by using the adaptively computed constraints. We can argue as in the two-dimensional case; see [76] for the face estimate analogon. From (5.11) and (5.19), we obtain the local estimates

$$w_{ij}^T \overline{\Pi}_{ij} \Pi_{ij} P_{D,\overline{\mathcal{F}}^{ij}}^T S_{ij} P_{D,\overline{\mathcal{F}}^{ij}} \Pi_{ij} \overline{\Pi}_{ij} w_{ij} \leq \text{TOL}\, w_{ij}^T \overline{\Pi}_{ij} \Pi_{ij} S_{ij} \Pi_{ij} \overline{\Pi}_{ij} w_{ij}, \tag{5.21}$$

$$w_{ik}^T \overline{\Pi}_{ik} \Pi_{ik} P_{D,\mathcal{E}^{ik}}^T S_{ik} P_{D,\mathcal{E}^{ik}} \Pi_{ik} \overline{\Pi}_{ik} w_{ik} \leq \text{TOL}\, w_{ik}^T \overline{\Pi}_{ik} \Pi_{ik} S_{ik} \Pi_{ik} \overline{\Pi}_{ik} w_{ik}, \tag{5.22}$$

for all $w_{ij} \in W_i \times W_j$ or $w_{ik} \in W_i \times W_k$, which satisfy the constraints (5.12) and (5.13) or (5.20). Obviously, (5.22) only appears for subdomains Ω_i where no common face $\mathcal{F}^{ik}$ but only an edge $\mathcal{E}^{ik}$ with Ω_k exists.

For $s \in \{j, k\}$, these estimates can be proven, by splitting $W_i \times W_s = \text{range}\,(\Pi_{is}) \oplus \text{range}\,(I - \Pi_{is})$ and $\text{range}\,(\Pi_{is}) = \text{range}\,(\Pi_{is|\text{range}\,(\overline{\Pi}_{is})}) \oplus \text{range}\,(\Pi_{is|\text{range}\,(I-\overline{\Pi}_{is})})$. The estimates (5.21) and (5.22) are derived separately for the complementary subspaces. Analogously to [76] (the more detailed technical report version of [75]), we use the orthogonal projection

property of Π_{is} and $\overline{\Pi}_{is}$, the fact that $\Pi_{is}(I-\overline{\Pi}_{is})w_{is} = (I-\overline{\Pi}_{is})w_{is}$, [8, Section 2.7], and consequently that Π_{is} and $\overline{\Pi}_{is}$ commute. Let us give some more details. The identity $\Pi_{is}(I-\overline{\Pi}_{is})w_{is} = (I-\overline{\Pi}_{is})w_{is}$ is obtained since $(I-\overline{\Pi}_{is})$ is an orthogonal projection onto the space of rigid body modes that are continuous on $W_i \times W_s$. For orthogonal projections P and Q, we can prove the equivalence of

i) $QP = P$,

ii) $PQ = P$,

iii) $\text{range}\,(P) \subset \text{range}\,(Q)$;

mentioned, e.g., in [8, Section 2.7]; by using elementary projection properties. By substituting $Q = \Pi_{is}$ and $P = I - \overline{\Pi}_{is}$, we have

$$I - \overline{\Pi}_{is} = \Pi_{is}(I - \overline{\Pi}_{is}) = (I - \overline{\Pi}_{is})\Pi_{is},$$

which implies

$$\Pi_{is} - \Pi_{is}\overline{\Pi}_{is} = \Pi_{is} - \overline{\Pi}_{is}\Pi_{is},$$

i.e., that Π_{is} and $\overline{\Pi}_{is}$ commute. Note that the same arguments can be used for face and edge eigenvalue problems likewise.

We now take a closer look at the local estimates from above for functions fulfilling the constraints and derived from a restriction of $w \in \widetilde{W}$ to $W_i \times W_s$. This is necessary for the use in the proof on the FETI-DP condition number bound. For $w \in \widetilde{W}$ we have

$$\begin{pmatrix} R^{(i)}w \\ R^{(s)}w \end{pmatrix} \in \widetilde{W}_{is}, \quad \text{and therefore} \quad \Pi_{is}\begin{pmatrix} R^{(i)}w \\ R^{(s)}w \end{pmatrix} = \begin{pmatrix} R^{(i)}w \\ R^{(s)}w \end{pmatrix}. \tag{5.23}$$

Exactly as in [75], only extended to edge eigenvalue problems in three dimensions, we argue as follows. Let $s \in \{j,k\}$ be as above, we now use the generic expression $P_{D,\overline{\mathcal{Z}}^{is}}$ representing $P_{D,\overline{\mathcal{F}}^{ij}}$ and $P_{D,\mathcal{E}^{ik}}$ likewise. Since $I-\overline{\Pi}_{is}$ is the projection onto the common rigid body modes, we have $\Pi_{is}(I-\overline{\Pi}_{is})w_{is} = (I-\overline{\Pi}_{is})w_{is}$. Both arguments together yield $P_{D,\overline{\mathcal{Z}}^{is}}(I-\overline{\Pi}_{is})w_{is} = 0$ and thus $S_{is}(I-\overline{\Pi}_{is})w_{is} = 0$. Since we can split any eigenvector w_{is}^r resulting from the local eigenvalue problem (5.11) or (5.19) as $w_{is}^r = (I-\overline{\Pi}_{is})w_{is}^r + \overline{\Pi}_{is}w_{is}^r$, it therefore holds

$$w_{is}^T\Pi_{is}P_{D,\overline{\mathcal{Z}}^{is}}^T S_{is}P_{D,\overline{\mathcal{Z}}^{is}}\Pi_{is}w_{is} \leq \text{TOL}\, w_{is}^T\Pi_{is}S_{is}\Pi_{is}w_{is} \tag{5.24}$$

for all w_{is} in $W_i \times W_s$ with ${w_{is}^r}^T P^T_{D,\overline{\mathcal{Z}}^{is}} S_{is} P_{D,\overline{\mathcal{Z}}^{is}} w_{is} = 0$ for all $\mu_{is}^r \geq \text{TOL}$.

Note that $P_{D,\overline{\mathcal{Z}}^{is}}(I - \overline{\Pi}_{is})w_{is} = 0$ also holds for a priori nondiagonal scalings since the common rigid body modes are continuous in all the interface variables. The situation therefore is different from Example 4.1, where we also considered nondiagonal scalings, in another context, however. Here, we have $\Big((I - \overline{\Pi}_{is})w_{is}\Big)^{(i)}_{\Delta} = \Big((I - \overline{\Pi}_{is})w_{is}\Big)^{(s)}_{\Delta}$.

Hence, the estimate (5.24) is valid for $w_{is} \in \widetilde{W}_{is}$, which satisfies the constraints; cf. [93].

Alternatively, to obtain (5.24), [93, Theorem 9] and [93, Theorem 11] can be used; see also [75, 109].

Remark 5.3. *In order to guarantee that* TOL *is finite, for all $w_{is} \in \widetilde{W}_{is}$, we have to treat the kernel of S_{is} correctly. As already mentioned in [93, Assumption 8] or [120, Assumption 29], we have to ensure that*

$$\forall w_{is} \in \widetilde{W}_{is} \,:\, S_{is} w_{is} = 0 \;\Rightarrow\; B_{is} w_{is} = 0. \tag{5.25}$$

As mentioned before, we have possibly to be aware of $\dim(\Pi_{is} \ker(S_{is})\Pi_{is}) = 7$ *if* $\ker S_{is} = 12$ *or* $\dim(\Pi_{is} \ker(S_{is})\Pi_{is}) = 1$ *if* $\ker S_{is} = 6$. *This results from an additional hinge mode, i.e., a rigid body rotation of the two subdomains around the common edge. In order to ensure the assumption in* (5.25)*, we select at least two primal vertices on straight edges. For nonstraight or bent edges we select a third primal vertex that is not located on the straight line between the other two vertices on the edge. Thus, hinge modes that violate* (5.25) *are eliminated. We remark that the existence of sufficient vertices on an edge is, in general, not ensured if we use a graph partitioner and a common understanding of edges and vertices; see, e.g., [77, Def. 2.1] and [82, Def. 3.1]. We thus transform arbitrary dual nodes that fulfill the given restrictions into primal vertices.*

Based on the previous paragraphs, we now introduce five different algorithms of adaptively preconditioned FETI-DP. The two heuristically optimized algorithms (Algorithm Ib and Algorithm Ic) are defined by similar strategies which can help to keep the number of eigenvalue problems as well as the size of the coarse problem small – while still obtaining an acceptable condition number. Algorithms II and III were proposed in in [93, 120, 94].

5.2.2 Various adaptive algorithms

In this section, we use (subsets of) the adaptively computed constraints introduced before to define five different algorithms of adaptive FETI-DP.

Algorithm Ia. In *Algorithm Ia*, compared to all subsequently introduced algorithms, we use of the largest number of eigenvalue problems. We use face eigenvalue problems on all faces $\mathcal{F}^{ij}$ as well as edge eigenvalue problems on all edges $\mathcal{E}^{ik}$, where the jumps across the edge cannot be assigned to any corresponding face eigenvalue problem. We enforce all constraints obtained by these eigenvalue problems, i.e., (5.12), (5.13), and (5.20). Consequently, Algorithm Ia also leads to the most generous coarse problem when compared to the other algorithms presented in this thesis. Though, all eigenvalue problems and constraints are necessary to prove the condition number bound in the upcoming Section 5.3 and Theorem 5.7. In Algorithm Ia, the local estimate (5.24) holds for all faces and all edges.

Algorithm Ib. In *Algorithm Ib*, we eliminate certain edge eigenvalue problems where neither homogeneously stiff materials nor heterogeneities are present. This can be conducted in different ways. In Chapters 5 and 6, we assume that the distribution of the coefficient ρ (for the diffusion equation) or E (for compressible linear elasticity) is known. In Chapter 7, we proceed to the more realistic assumption that these values are not known and use the diagonal elements of the stiffness matrices to infer the existence of heterogeneities.

The idea for the elimination of edge eigenvalue problems is based on slab techniques; see, e.g., [104, 105, 49, 48, 75]. If we imply a completely homogeneous, soft or diffusive material (for linear elasticity or the diffusion problem) within a distance of one element around the edge of the eigenvalue problem, we discard the whole eigenvalue problem with all possible constraints. Thus, all the constraints (5.12), (5.13) from the face eigenvalue problems are enforced, the constraints (5.20) are only computed and enforced if the edge eigenvalue problem is not discarded.

Let us note that, after reducing the number of edge eigenvalue problems, our explicit condition number bound of Theorem 5.7 might not hold anymore. Nevertheless, based on the theory of slab techniques (see, e.g., [104, 105, 49, 48, 75]), the condition number is expected to stay bounded independently of the coefficient jumps. This is confirmed by our numerical experiments.

If the Young modulus or the ρ-coefficient is known, the strategy can be implemented by traversing the nodes on the edge while evaluating the coefficient function. If no large heterogeneities are encountered then the edge eigenvalue problem can be discarded. If the coefficient function is not available the diagonal entries of the stiffness matrices are used, instead.

In presence of coefficient jumps combined with almost incompressible components, the technique based on the Young modulus E is not advisable since

constraints enforcing the essential zero net flux condition may be removed from the coarse space.

The number of coefficient jumps encountered while traversing the edge can also be used to define the number of eigenvectors to be used for the edge, i.e., as an alternative to defining a tolerance TOL. If a single heterogeneity is encountered, e.g., if a single channel with a high coefficient crosses the edge, then only one eigenvector (per dimension of the solution) is added to the coarse problem. This corresponds to the use of a single weighted edge average as first suggested in [78]. Of course, for a larger number of channels more eigenvectors have to be used. In the classical approach [78], it is then necessary to split the weighted edge average [78] into several weighted averages, defined on subsets of the edge, or to introduce additional primal vertex constraints.

Algorithm Ic. *Algorithm Ic* takes up the idea of Algorithm Ib in order to further reduce the size of the coarse problem. Here, the strategy explained for Algorithm Ib is used to additionally discard certain edge constraints from face eigenvalue problems. In detail, this means that edge constraints from face eigenvalue problems are not added to the coarse space if only low coefficients are detected in the neighborhood of the edge. Although, the coarse space of Algorithm Ic is usually already much smaller than that of Algorithms Ia and Ib, the numerical results show that the condition numbers of all three algorithms are comparable for all our test problems.

Summarized, all the constraints of (5.12) are enforced in Algorithm Ic. However, (5.13) and (5.20) are only enforced if high material parameters or heterogeneities are present in the neighborhood of the edge.

Note that the same number of eigenvalue problems is considered in Algorithms Ib and Ic.

Algorithm II. As *Algorithm II*, we denote the coarse space proposed in [93, 120, 94], where all edge constraints from face eigenvalue problems are enforced as additional constraints, i.e., the constraints of Algorithm II are those given in (5.12) and (5.13). No edge eigenvalue problems are considered and thus, (5.20) does not apply.

Algorithm III. As *Algorithm III*, we denote the "classical" adaptive approach already tested extensively in [93, 120, 94]. In this approach, all edge constraints from face eigenvalue problems are simply discarded, which results in a smaller coarse problem at the cost of losing robustness. The constraints of Algorithm III

are given by (5.12). The constraints given by (5.13) are not used. No edge eigenvalue problems are considered and thus, (5.20) does not apply either.

5.2.3 Further Strategies to reduce the computational overhead of the adaptive methods

We now describe two additional strategies to reduce the computational overhead introduced by the eigenvalue problems and to reduce the size of the coarse space of Algorithms Ia, Ib, Ic, II, and III further.

5.2.3.1 Reducing the number of edge eigenvalue problems on short edges

For a reasonable reduction of the number of eigenvalue problems, we consider all eigenvalue problems related to short edges. For short edges, we set all nodes as primal if there are not more than k dual nodes on the edge. Throughout this thesis, we consider edges as short if they consist of only a single node, i.e., in our experiments, we use $k = 1$. Possible edge eigenvalue problems on these edges then become superfluous.

This strategy can be used for all adaptive algorithms presented in Section 5.2.2. For Algorithm Ia, this strategy keeps the theoretical condition number bound. For all other algorithms, there are no condition number bounds available yet, the actual condition numbers are slightly reduced, however. This strategy is always used in our numerical experiments.

5.2.3.2 Reducing the number of eigenvalue problems based on the residual

The following reduction approach, first suggested for 2D in [74], is based on considering the preconditioned starting residual to detect critical edges (and faces). This strategy was proposed but not implemented in [74]. We assume that the residuals on faces and edges with homogeneous coefficients are several magnitudes smaller than those on faces and edges with jumps in the coefficients along or across the interface. Therefore, we compute the residual $r := M_D^{-1}(d - F\lambda^{(1)})$ (i.e., one iteration of the underlying PCG algorithm; but more iterations are also possible) and restrict the preconditioned residual to the closure of the faces and edges. Let the closure of any face or any edge generically be denoted by $\mathcal{Z}$.

For the restriction $r_{\mathcal{Z}} = r_{|\mathcal{Z}}$, we compute $r_{\mathcal{Z},2} := n^{-1/2}\|r_{\mathcal{Z}}\|_2$ to check its magnitude. Here, n represents the number of Lagrange multipliers on the closure of $\mathcal{Z}$. Another reasonable approach would be to compute the maximum norm of $r_{\mathcal{Z}}$, here denoted by $r_{\mathcal{Z},\infty}$. In our experiments, we take a combination

of these residual norms. For two user-chosen tolerances τ_2 and τ_∞, we check simultaneously for every face and every edge if $r_{\mathcal{Z},2} < \tau_2$ and $r_{\mathcal{Z},\infty} < \tau_\infty$. If this is the case, we do not consider the corresponding eigenvalue problem and discard it (with all possible constraints). Otherwise, we continue as before and compute the constraints from the corresponding eigenvalue problems. If the energy norm is used, this approach is remotely related to the computation of Rayleigh quotients in [124].

Note that this approach can significantly reduce the number of eigenvalue problems but often results in a coarse space of comparable size. Due to the smaller number of eigenvalue computations, the heuristic approach presented here is computationally less expensive. However, the heuristic choice of τ_2 and τ_∞ is not trivial and requires further studies.

5.3 Condition number estimate for adaptive FETI-DP

In the following section, we consider Algorithm Ia. The heuristically reduced algorithms Algorithm Ib and Algorithm Ic often result in the same condition number (see the numerical results in Sections 5.4 and 6.5) but in cases where they do not reduce to Algorithm Ia, they are not proven theoretically. Algorithm II and Algorithm III often result in higher condition numbers since jumps across edges require special treatment by edge constraints and/or edge eigenvalue problems; again, see Sections 5.4 and 6.5.

We now introduce the solution space for our adaptive FETI-DP method, Algorithm Ia, with deflation or balancing. Extending the constraint vectors $c^r_{\lambda,ij,\mathcal{F}}$, $c^r_{\lambda,ij,\mathcal{E}_m}$, $m = 1, 2, \ldots$, and $c^r_{\lambda,ik}$ of (5.12), (5.13), and (5.20) by zero to the space of the Lagrange multipliers, we obtain the columns of the constraint matrix U; see Section 4.2. We then have the solution space

$$\widetilde{W}_U = \{w \in \widetilde{W} \,:\, U^T B w = 0\}.$$

The subspace $\widetilde{W}_U$ of $\widetilde{W}$ then contains those elements $w \in \widetilde{W}$ satisfying the adaptive constraints and $Bw \in \ker U^T$.

Remark 5.4. *Note that we can equally define other matrices, generically denoted by U, by only using the columns corresponding to the constraints of Algorithm Ib, Ic, II, or III. These coarse matrices are used in the implementation but the corresponding solution space is not considered in this section.*

Before we are able to provide the theoretical bound on the condition number of the adaptively preconditioned FETI-DP operator with deflation or balancing,

we have to present an analytical expression for the application of the localized P_D-operator; cf. the definition of the P_D-operator at the end of Section 3.2 and the introduction of the localized versions in Section 5.2.1.

The local operators $P_{D,\overline{\mathcal{F}}^{ij}}$ and $P_{D,\mathcal{E}^{ik}}$ on the closure of the face $\overline{\mathcal{F}}^{ij}$ and the edge $\mathcal{E}^{ik}$, respectively, are

$$P_{D,\overline{\mathcal{F}}^{ij}} = \begin{pmatrix} B_{D,\overline{\mathcal{F}}^{ij}}^{(i)T} B_{\overline{\mathcal{F}}^{ij}}^{(i)} & B_{D,\overline{\mathcal{F}}^{ij}}^{(i)T} B_{\overline{\mathcal{F}}^{ij}}^{(j)} \\ B_{D,\overline{\mathcal{F}}^{ij}}^{(j)T} B_{\overline{\mathcal{F}}^{ij}}^{(i)} & B_{D,\overline{\mathcal{F}}^{ij}}^{(j)T} B_{\overline{\mathcal{F}}^{ij}}^{(j)} \end{pmatrix} \text{ and } P_{D,\mathcal{E}^{ik}} = \begin{pmatrix} B_{D,\mathcal{E}^{ik}}^{(i)T} B_{\mathcal{E}^{ik}}^{(i)} & B_{D,\mathcal{E}^{ik}}^{(i)T} B_{\mathcal{E}^{ik}}^{(k)} \\ B_{D,\mathcal{E}^{ik}}^{(k)T} B_{\mathcal{E}^{ik}}^{(i)} & B_{D,\mathcal{E}^{ik}}^{(k)T} B_{\mathcal{E}^{ik}}^{(k)} \end{pmatrix};$$

see [75].

For a face $\mathcal{F}^{ij}$ with edges $\mathcal{E}_1^{ij}, \ldots, \mathcal{E}_m^{ij}$, we define the cutoff function on the closure of the face

$$\vartheta_{\overline{\mathcal{F}}^{ij}} := \theta_{\mathcal{F}^{ij}} + \sum_{p=1}^{m} \theta_{\mathcal{E}_p^{ij}}. \tag{5.26}$$

We can use the cutoff function $\theta_{\mathcal{E}_p^{ij}}$ on the open edge since all vertices are chosen to be primal; cf. Remark 5.2.

For $w \in \widetilde{W}$, it yields

$$P_{D,\overline{\mathcal{F}}^{ij}} \begin{pmatrix} R^{(i)}w \\ R^{(j)}w \end{pmatrix} = \begin{pmatrix} I^h(\vartheta_{\overline{\mathcal{F}}^{ij}} D_{u,\overline{\mathcal{F}}^{ij}}^{(j)}(w^{(i)} - w^{(j)})) \\ I^h(\vartheta_{\overline{\mathcal{F}}^{ij}} D_{u,\overline{\mathcal{F}}^{ij}}^{(i)}(w^{(j)} - w^{(i)})) \end{pmatrix}, \tag{5.27}$$

where I^h is the finite element interpolation operator on Ω_i and Ω_j, respectively and $D_{u,\overline{\mathcal{F}}^{ij}}^{(j)}$ is built from the scaling of the Lagrange multipliers on the open face $D_{u,\mathcal{F}^{ij}}^{(j)}$ and the scaling of the Lagrange multipliers on the corresponding edges; cf. the definition of the scaling matrices in (3.15) and (3.17).

For the sake of simplicity, we assume that just $\mathcal{E}_1^{ij} = \mathcal{E}^{ik}$ has a multiplicity greater than three and equal to four with $w^{(i)} - w^{(k)}$ as the problematic jump between two subdomains sharing at least one edge but no face; see Figure 5.2. Other cases can be handled in the same way. The application of the local P_D-operator of the edge eigenvalue problem yields with the corresponding scaling on the edge

$$P_{D,\mathcal{E}^{ik}} \begin{pmatrix} R^{(i)}w \\ R^{(k)}w \end{pmatrix} = \begin{pmatrix} I^h(\theta_{\mathcal{E}^{ik}} D_{u,\mathcal{E}^{ik}}^{(k)}(w^{(i)} - w^{(k)})) \\ I^h(\theta_{\mathcal{E}^{ik}} D_{u,\mathcal{E}^{ik}}^{(i)}(w^{(k)} - w^{(i)})) \end{pmatrix}. \tag{5.28}$$

Lemma 5.5 ([64]). *Let $N_{\mathcal{F}}$ denote the maximum number of faces of a subdomain, $N_{\mathcal{E}}$ the maximum number of edges of a subdomain, $M_{\mathcal{E}}$ the maximum multiplicity of an edge, and* TOL *a given tolerance for solving the local generalized eigenvalue problems. We assume that all vertices are chosen to be primal. Then, for $w \in \widetilde{W}_U$, we have*

$$|P_D w|_{\widetilde{S}}^2 \leq 4 \max\{N_{\mathcal{F}}, N_{\mathcal{E}} M_{\mathcal{E}}\}^2 \mathrm{TOL} |w|_{\widetilde{S}}^2.$$

Proof. We first have a closer look at the global operator P_D and its restriction to a subdomain. Since all vertices are primal, we obtain

$$v_i := R^{(i)} P_D w = \sum_{\mathcal{F}^{ij} \subset \partial\Omega_i} I^h(\theta_{\mathcal{F}^{ij}} v_i) + \sum_{\mathcal{E}^{ik} \subset \partial\Omega_i} I^h(\theta_{\mathcal{E}^{ik}} v_i); \tag{5.29}$$

see, e.g., [130, Sec. 6.4.3].

In contrast to other proofs on the condition number of the FETI-DP system, where the additive terms of (5.29) are bounded separately, we now rearrange these additive terms. This is due to the fact that the face eigenvalue problems are solved on the closure of the faces.

Therefore, we introduce a global and N local sets of pairs of indices, where each index pair represents an edge eigenvalue problem on $\mathcal{E}^{ik}$ and vice versa, i.e.,

$$\begin{aligned} \mathcal{E}^* := \{\{r,s\} : 1 \leq r,s \leq N,\ \lambda_1(\partial\Omega_r \cap \partial\Omega_s) > 0,\ \lambda_2(\partial\Omega_r \cap \partial\Omega_s) = 0\} \\ \text{and, for } i = 1,\ldots,N, \quad \mathcal{E}_i^* := \{\{r,s\} \in \mathcal{E}^* : r = i \vee s = i\}. \end{aligned}$$

Here, λ_d is the d-dimensional Lebesgue measure. Thus, $\{r,s\} \in \mathcal{E}^*$ means that the subdomains Ω_r and Ω_s share at least one edge but no face. In general, for subdomains obtained from graph partitioners, these sets do not contain many elements as already mentioned before.

For a given face $\mathcal{F}^{ij}$, we denote the edges which are part of the closure of the face by $\mathcal{E}_1^{ij}, \ldots, \mathcal{E}_m^{ij}$. In order to avoid the proliferation of indices we take an arbitrary edge $\mathcal{E}^{ij} \in \{\mathcal{E}_1^{ij}, \ldots, \mathcal{E}_m^{ij}\}$ that is shared by Ω_i and $\Omega_{r_1}, \ldots, \Omega_{r_p}$ with $r_1, \ldots, r_p \in \{1,\ldots,N\} \setminus \{i\}$. We then have the interpolation operators

$$I^h(\theta_{\mathcal{F}^{ij}} v_i) = I^h(\theta_{\mathcal{F}^{ij}} D^{(j)}_{u,\mathcal{F}^{ij}}(w^{(i)} - w^{(j)})), \tag{5.30}$$

$$I^h(\theta_{\mathcal{E}^{ij}} v_i) = I^h(\theta_{\mathcal{E}^{ij}}(D^{(r_1)}_{u,\mathcal{E}^{ir_1}}(w^{(i)} - w^{(r_1)}) + \ldots + D^{(r_p)}_{u,\mathcal{E}^{ir_p}}(w^{(i)} - w^{(r_p)})). \tag{5.31}$$

Obviously, for each edge $\mathcal{E}^{ij} \in \{\mathcal{E}_1^{ij}, \dots, \mathcal{E}_m^{ij}\}$ the term $I^h(\theta_{\mathcal{E}^{ij}}(D^{(j)}_{u,\mathcal{E}^{ij}}(w^{(i)}-w^{(j)}))$ is part of (5.31). For each edge $\mathcal{E}^{ij}$, we subtract it from (5.31) and add it to (5.30). The remaining jumps in (5.31) can then either be added analogously to another corresponding face term

$$I^h(\theta_{\mathcal{F}^{ir_s}} D^{(r_s)}_{u,\mathcal{E}^{ir_s}}(w^{(i)} - w^{(r_s)}))$$

(cf. (5.30)), if such a face $\mathcal{F}^{ir_s}$ between Ω_i and Ω_{r_s} exists, or they remain in (5.31).

If this is carried out for all faces and edges analogously, (5.29) becomes

$$\begin{aligned} R^{(i)} P_D w = \sum_{\mathcal{F}^{ij} \subset \partial\Omega_i} & I^h(\vartheta_{\overline{\mathcal{F}}^{ij}} D^{(j)}_{u,\overline{\mathcal{F}}^{ij}}(w^{(i)} - w^{(j)})) \\ & + \sum_{\{i,k\} \in \mathcal{E}_i^*} I^h(\theta_{\mathcal{E}^{ik}} D^{(k)}_{u,\mathcal{E}^{ik}}(w^{(i)} - w^{(k)})). \end{aligned} \tag{5.32}$$

Note that we could also replace the cutoff functions for the open edges by those for the closure of these edges, that is, $\vartheta_{\overline{\mathcal{E}}} = 1$ at the endpoints of the edge and $\vartheta_{\overline{\mathcal{E}}} = \theta_{\mathcal{E}}$ for all other nodes of the mesh and also extend the scaling arbitrarily to the closure of the edge since all vertices are chosen to be primal.

We define the $S^{(s)}$-seminorm $|\cdot|_{S^{(s)}} := \langle \cdot, S^{(s)} \cdot \rangle$ for $s \in \{i,j,k\}$. Then, we estimate the face terms in (5.32) similar to the edge terms in two dimensions; see [75]. The remaining edge terms in (5.32) can be estimated by using the constraints obtained from the edge eigenvalue problems. For $w \in \widetilde{W}_U$, $w^{(s)} = R^{(s)} w$, $s \in \{i,j,k\}$, we have

$$\begin{aligned} |P_D w|^2_{\widetilde{S}} &= \sum_{i=1}^N |R^{(i)} P_D w|^2_{S^{(i)}} \\ &\overset{(5.32)}{=} \sum_{i=1}^N \Bigg| \sum_{\mathcal{F}^{ij} \subset \partial\Omega_i} I^h(\vartheta_{\overline{\mathcal{F}}^{ij}} D^{(j)}_{u,\overline{\mathcal{F}}^{ij}}(w^{(i)} - w^{(j)})) \\ &\qquad + \sum_{\{i,k\} \in \mathcal{E}_i^*} I^h(\theta_{\mathcal{E}^{ik}} D^{(k)}_{u,\mathcal{E}^{ik}}(w^{(i)} - w^{(k)})) \Bigg|^2_{S^{(i)}} \\ &\le 2 \max\{N_{\mathcal{F}}, N_{\mathcal{E}} M_{\mathcal{E}}\} \sum_{i=1}^N \Bigg(\sum_{\mathcal{F}^{ij} \subset \partial\Omega_i} |I^h(\vartheta_{\overline{\mathcal{F}}^{ij}} D^{(j)}_{u,\overline{\mathcal{F}}^{ij}}(w^{(i)} - w^{(j)}))|^2_{S^{(i)}} \\ &\qquad + \sum_{\{i,k\} \in \mathcal{E}_i^*} |I^h(\theta_{\mathcal{E}^{ik}} D^{(k)}_{u,\mathcal{E}^{ik}}(w^{(i)} - w^{(k)}))|^2_{S^{(i)}} \Bigg) \end{aligned}$$

$$
\begin{aligned}
&= 2\max\{N_{\mathcal{F}}, N_{\mathcal{E}}M_{\mathcal{E}}\}\left(\sum_{\mathcal{F}^{ij}\subset\Gamma}\left(|I^h(\vartheta_{\overline{\mathcal{F}}^{ij}}D^{(j)}_{u,\overline{\mathcal{F}}^{ij}}(w^{(i)}-w^{(j)}))|^2_{S^{(i)}}\right.\right.\\
&\qquad\left.+|I^h(\vartheta_{\overline{\mathcal{F}}^{ij}}D^{(i)}_{u,\overline{\mathcal{F}}^{ij}}(w^{(j)}-w^{(i)}))|^2_{S^{(j)}}\right)\\
&\quad+\sum_{\{i,k\}\in\mathcal{E}^*}\left(|I^h(\theta_{\mathcal{E}^{ik}}D^{(k)}_{u,\mathcal{E}^{ik}}(w^{(i)}-w^{(k)}))|^2_{S^{(i)}}\right.\\
&\qquad\left.\left.+|I^h(\theta_{\mathcal{E}^{ik}}D^{(i)}_{u,\mathcal{E}^{ik}}(w^{(k)}-w^{(i)}))|^2_{S^{(k)}}\right)\right)\\
&\overset{\substack{(5.27)\\(5.28)\\(5.23)}}{=} 2\max\{N_{\mathcal{F}}, N_{\mathcal{E}}M_{\mathcal{E}}\}\left(\sum_{\mathcal{F}^{ij}\subset\Gamma}\begin{pmatrix}w^{(i)}\\w^{(j)}\end{pmatrix}^T\Pi_{ij}P^T_{D,\overline{\mathcal{F}}^{ij}}\begin{pmatrix}S^{(i)}&0\\0&S^{(j)}\end{pmatrix}P_{D,\overline{\mathcal{F}}^{ij}}\Pi_{ij}\begin{pmatrix}w^{(i)}\\w^{(j)}\end{pmatrix}\right.\\
&\quad\left.+\sum_{\{i,k\}\in\mathcal{E}^*}\begin{pmatrix}w^{(i)}\\w^{(k)}\end{pmatrix}^T\Pi_{ik}P^T_{D,\mathcal{E}^{ik}}\begin{pmatrix}S^{(i)}&0\\0&S^{(k)}\end{pmatrix}P_{D,\mathcal{E}^{ik}}\Pi_{ik}\begin{pmatrix}w^{(i)}\\w^{(k)}\end{pmatrix}\right)\\
&\overset{(5.24)}{\leq} 2\max\{N_{\mathcal{F}}, N_{\mathcal{E}}M_{\mathcal{E}}\}\mathrm{TOL}\left(\sum_{\mathcal{F}^{ij}\subset\Gamma}\begin{pmatrix}w^{(i)}\\w^{(j)}\end{pmatrix}^T\Pi_{ij}\begin{pmatrix}S^{(i)}&0\\0&S^{(j)}\end{pmatrix}\Pi_{ij}\begin{pmatrix}w^{(i)}\\w^{(j)}\end{pmatrix}\right.\\
&\quad\left.+\sum_{\{i,k\}\in\mathcal{E}^*}\begin{pmatrix}w^{(i)}\\w^{(k)}\end{pmatrix}^T\Pi_{ik}\begin{pmatrix}S^{(i)}&0\\0&S^{(k)}\end{pmatrix}\Pi_{ik}\begin{pmatrix}w^{(i)}\\w^{(k)}\end{pmatrix}\right)\\
&\overset{(5.23)}{=} 2\max\{N_{\mathcal{F}}, N_{\mathcal{E}}M_{\mathcal{E}}\}\mathrm{TOL}\left(\sum_{\mathcal{F}^{ij}\subset\Gamma}\left(|w^{(i)}|^2_{S^{(i)}}+|w^{(j)}|^2_{S^{(j)}}\right)\right.\\
&\quad\left.+\sum_{\{i,k\}\in\mathcal{E}^*}\left(|w^{(i)}|^2_{S^{(i)}}+|w^{(k)}|^2_{S^{(k)}}\right)\right)\\
&\leq 2\max\{N_{\mathcal{F}}, N_{\mathcal{E}}M_{\mathcal{E}}\}\mathrm{TOL}\left(2\max\{N_{\mathcal{F}}, N_{\mathcal{E}}M_{\mathcal{E}}\}\sum_{i=1}^{N}|R^{(i)}w|^2_{S^{(i)}}\right)\\
&= 4\max\{N_{\mathcal{F}}, N_{\mathcal{E}}M_{\mathcal{E}}\}^2\mathrm{TOL}|w|^2_{\widetilde{S}}.
\end{aligned}
$$

□

Remark 5.6. *Note that if not all vertices were chosen to be primal, we had a more general form of* (5.29) *and for jumps across a vertex where the adjacent subdomains do not share either face or edge, a vertex eigenvalue problem of similar type as* (5.8) *and* (5.18) *might be introduced to bound the more general expression.*

In the next theorem, we provide a condition number bound for the preconditioned FETI-DP algorithm with all vertices being primal and additional, adaptively chosen edge and face constraints.

Theorem 5.7 ([64])**.** *Let $N_{\mathcal{F}}$ denote the maximum number of faces of a subdomain, $N_{\mathcal{E}}$ the maximum number of edges of a subdomain, $M_{\mathcal{E}}$ the maximum multiplicity of an edge, and* TOL *a given tolerance for solving the local generalized eigenvalue problems. Let all vertices be primal. Then, the condition number κ of the FETI-DP Algorithm Ia with adaptive constraints as described and enforced by the deflation preconditioner M_{PP}^{-1}, satisfies*

$$\kappa(M_{PP}^{-1}F) \leq 4\max\{N_{\mathcal{F}}, N_{\mathcal{E}}M_{\mathcal{E}}\}^2\text{TOL}.$$

Using the balancing preconditioner M_{BP}^{-1} the same condition number bound holds, i.e.,

$$\kappa(M_{BP}^{-1}F) \leq 4\max\{N_{\mathcal{F}}, N_{\mathcal{E}}M_{\mathcal{E}}\}^2\text{TOL}.$$

Proof. The condition number bound for the deflation preconditioner can be derived with Lemma 5.5 and [75, Lemma 3.2]. The relation between the eigenvalues of $M_{PP}^{-1}F$ and $M_{BP}^{-1}F$ can be found in [97], or, in our notation in [80]. □

Let us finally note that the constant in the condition number estimate provided by Theorem 5.7 is quite conservative. The geometrical quantities $N_{\mathcal{F}}$, $N_{\mathcal{E}}$, and $M_{\mathcal{E}}$ enter our estimate when the Cauchy-Schwarz inequality is used to estimate the product of functions supported on faces and edges. These functions are not S_i-orthogonal to each other, but, in practice, their mutual S_i-inner product is small. This is not exclusive to our approach since these quantities already appear implicitly, in a generic constant C, in the traditional (nonadaptive) FETI-DP and BDDC condition number estimates; see, e.g., [89, 82, 130]. It can be observed numerically that (5.24) often provides a more realistic indicator for the condition number, i.e., our results in Section 5.4 show that the condition number is at the order of TOL in our numerical experiments rather than at the order of $4\max\{N_{\mathcal{F}}, N_{\mathcal{E}}M_{\mathcal{E}}\}^2$TOL. This has already been observed in [93, 94], and the use of (5.24) (for faces) has been proposed as a condition number indicator; see also [120, 121, 122].

5.4 Numerical results for adaptive FETI-DP using the balancing approach

In this section, we show numerical results for problems of linear elasticity using FETI-DP with the adaptive coarse space strategies discussed before. We compare the coarse spaces introduced in [93, 94] and our new coarse spaces with edge constraints from edge eigenvalue problems presented in Section 5.2. We recall that by *edge constraints from face eigenvalue problems* we refer to edge constraints which result from splitting constraints originating from eigenvectors computed on the (closed) face; see (5.13) in Section 5.2.1.

We have implemented the new coarse space (Algorithm Ia) covered by our theory (see Theorem 5.7) and two modifications thereof (Algorithms Ib and Ic). Algorithm Ib uses the neighborhood approach to reduce the number of edge eigenvalue problems if they are not needed and Algorithm Ic makes use of the same neighborhood approach to further reduce the size of the coarse space by discarding edge constraints from face eigenvalue problems. For a more detailed description, see Section 5.2.2. In our tables, the three approaches are denoted by 'Algorithms Ia, Ib, and Ic' in a common column, with single rows 'a)', 'b)', and 'c)' refering to these algorithms. Although Algorithms Ib and Ic are both not covered by the theory outlined in this thesis, we show that in our experiments they give almost the same results as Algorithm Ia.

Furthermore, we have implemented two variants of the classical approach of [93, 94]. These approaches do not use edge eigenvalue problems. Algorithm II refers to the coarse space proposed in [93, 94], where all edge constraints from face eigenvalue problems are enforced as additional constraints. To the best of our knowledge, this approach has not been implemented and tested before; cf. [120, 121, 94, 122]. Algorithm III refers to the "classical" adaptive approach already tested extensively in [93, 94]. In this approach, all edge constraints from face eigenvalue problems are simply discarded, which results in a smaller coarse problem at the cost of losing robustness. For a more detailed description, see also Section 5.2.2. Algorithms II and III are not covered by the theory, and our numerical results indeed show that they cannot guarantee low condition numbers and iteration counts for all our test cases.

For all algorithms, the columns of U are orthogonalized blockwise (i.e., edge by edge and face by face) by a singular value decomposition with a drop tolerance of 1e-6.

In all cases, we use the edge eigenvalue reduction strategy from Section 5.2.3.1. For short edges with just one dual node, the corresponding edge eigenvalue problems then become superfluous.

In this chapter, we conduct the strategies of Algorithms Ib and Ic, to detect heterogeneities in the neighborhood of the edge, based on the diffusion coefficient ρ and the Young modulus E, respectively, and not based on the Poisson ratio ν. Thus, we do not use these strategies for our test problems of almost incompressible elasticity. For these problems, we only report on Algorithm Ia.

For simplicity, we always assume the parameters ρ and E and ν, respectively, to be constant on each fine element. In this chapter, as scaling we solely use ρ-scaling in form of patch-ρ-scaling, and we set the diffusion coefficient and the Young modulus, respectively, at a node to the maximum of all values over the support of the corresponding nodal basis function; cf. [78]. For different scalings and scaling comparisons, see the following chapters, in particular, Section 6.5.3.

In the experiments, regular as well as irregular (domain) decompositions are tested. The irregular decompositions are performed by the METIS graph partitioner [60] using the options `-ncommon=3` for the diffusion equation and compressible linear elasticity, `-ncommon=4` for incompressible elasticity and `-contig` for all problems to avoid noncontiguous subdomains as well as additional hinge modes inside single subdomains.

In the tables, κ denotes the condition number of the preconditioned FETI-DP operator, which is estimated from the Krylov process. In our tables, we mark (estimated) condition numbers (or largest eigenvalues) below 50 in bold face to indicate that a sufficiently large coarse space has been found by the adaptive method. In Sections 5.4.1 and 5.4.7, we report the estimates λ_{min} and λ_{max} instead of κ.

If not stated otherwise, the local generalized eigenvalue problems are solved by the MATLAB built-in `eig` function. In all tables, *its* is the number of iterations used by the PCG algorithm and $|U|$ denotes the size of the corresponding adaptive (or a posteriori) coarse space implemented by deflation or balancing; see Section 4.2. By N we denote the number of subdomains. For regular decompositions, we give H/h in order to measure the size of the local problems. For irregular decompositions, we give $1/h = mN^{1/3}$ where m reduces to H/h for a comparable regular decomposition.

For our new coarse spaces (Algorithms Ia, Ib, and Ic), we also give the number of edge eigenvalue problem as $\#\mathcal{E}_{evp}$ and in parentheses the percentage of these with respect to the total number of eigenvalue problems.

Except for Section 5.4.1, where we push the deflation and balancing approach to their limits, the stopping criterion for the PCG algorithm is set to a relative reduction of the preconditioned starting residual by a factor of 1e-10 and the maximum number of iterations is set to 500. If no convergence is reached, we simply write "500" instead of ">500" for the iterations. In Section 5.4.1, the chosen stopping criterion is denoted by tol_{cg} and the maximum number of iterations is set to 250.

In Section 5.4.1, we also report the preconditioned residual $\|M_{PP}^{-1}r\|_2$ and $\|M_{BP}^{-1}r\|_2$, respectively, as well as the error *err*, which is the relative difference between the solution of the adaptively preconditioned FETI-DP approach and a direct finite element solution obtained by assembling the stiffness matrix on the entire computational domain.

For the numerical experiments presented in this chapter, we solely use TOL = 10 to establish the adaptive coarse space. The resulting condition number then typically is at the order of TOL; cf. the remark at the end of Section 5.3 on the use of (5.24) as a condition number indicator and the numerical results. Note that, although our algorithm is algebraic and thus appears to be black-box, the efficiency of the method relies on properties of the underlying PDE. Therefore, in practice, TOL should be adapted to H/h, i.e., to the classical condition number bound $\kappa \leq C(1 + \log(H/h)^2$. Otherwise, for growing H/h, the coarse problem can become large. For a small tolerance, the adaptive FETI-DP method can even degenerate to a direct solver. For different choices of the tolerance, see the Chapters 6 and 7.

It is clear that Algorithms Ia, Ib, and II result in a larger coarse space than Algorithm III or Algorithm Ic. For simple examples, Algorithm Ic should reduce to Algorithm III. Our numerical results show that, in certain difficult cases, the larger coarse space is indeed necessary.

For all experiments in this section, we enforce homogeneous Dirichlet boundary conditions on the face with $x = 0$ and zero Neumann boundary conditions elsewhere. For compressible linear elasticity, we always apply the volume force $f := (0.1, 0.1, 0.1)^T$, for the diffusion equation, we choose $f := 0.1$. For almost incompressible linear elasticity, we change the volume force to $f := (-1, -1, -1)^T$, pushing the domain towards the Dirichlet boundary. We always use a structured fine mesh consisting of cubes. For the diffusion equation and the case of compressible linear elasticity, the fine cubes are each decomposed into five tetrahedral finite elements. For almost incompressible linear elasticity, we use brick elements for the whole domain.

For the case of compressible linear elasticity, we always use $\nu = 0.3$ for the entire computational domain.

Now, we give a short overview on the next subsections.

1. Section 5.4.1: **Deflation versus balancing**. In this section, we highlight differences in the convergence behaviour of adaptive FETI-DP with the balancing and the deflation approach. We explain our choice of adaptive FETI-DP with the balancing approach for the following sections by considering examples of compressible linear elasticity.

2. Section 5.4.2: **A composite material with a regular decomposition**. In this section, we consider a simple example of linear elasticity with a regular decomposition such that no heterogeneity is present around any edge. In this case, Algorithm Ic reduces to Algorithm III and the classical Algorithm III of [93, 94] can suffice. Since this simplified case is rarely on hand, we show the robustness of Algorithms Ia, Ib and Ic for arbitrary heterogeneity and/or irregular decompositions in the following sections.

3. Section 5.4.3: **Composite materials with irregular decompositions**. In this section, we consider composite materials with irregular decompositions into subdomains. We show for the diffusion equation and compressible linear elasticity that our extended coarse space of Algorithms Ia, Ib, and Ic is often indispensable if arbitrary heterogeneity is on hand.

4. Section 5.4.4: **Steel microstructure**. In this section, we consider a representative volume element (RVE) of a modern steel. We consider a regular as well as an irregular decomposition into subdomains.

5. Section 5.4.5: **Randomized coefficient distributions**. In this section, we consider random coefficient distributions (ρ and E) for the diffusion equation and compressible linear elasticity combined with irregular decompositions into subdomains. For compressible linear elasticity, we also vary the volume fraction of the stiff material. We always consider 100 random coefficient distributions with a comparable volume fraction of stiff material. We again see that our extended coarse space is indispensable.

6. Section 5.4.6: **Almost incompressible linear elasticity**. In this section, we consider different sample materials with almost incompressible components using irregular decompositions into subdomains. Here, for some examples, the classical adaptive approach of [93, 94] is sufficient but other examples require our enriched coarse space.

7. Section 5.4.7: **Heuristic approach based on the residual**. In this section, we consider examples from the previous sections, combined with the heuristic approach of Section 5.2.3.2. We show that our strategy can work well although Theorem 5.7 is not valid anymore.

8. Section 5.4.8: **Efficiently solving the eigenvalue problems**. In this section, we briefly consider the cost of building and solving the eigenvalue problems exactly and use favorable iterative solvers to show that approximate solutions of the eigenvectors also give low condition numbers and iteration counts.

Remark 5.8. *We always use the strategy described in Section 5.2.3.1, i.e., on short edges (i.e., one dual node) we never compute edge eigenvalue problems but rather set the corresponding edge node as primal. For the case of linear elasticity, we also have to take care of the issue described in Remark 5.3. This means that our initial coarse space for all algorithms, i.e., Algorithms Ia, Ib, Ic, II, and III, is richer than the standard vertex coarse space.*

5.4.1 A short comparison of deflation and balancing

In Section 5.3, we have shown equal condition number bounds for adaptive FETI-DP using either deflation or balancing.

In this section, we consider some small examples to show an exemplary convergence behaviour of adaptive FETI-DP with either deflation or balancing; cf. Section 4.2 for a detailed description. With this comparison, we want to highlight possible advantages and disadvantages of the particular approaches.

We conduct the comparison for the case of compressible linear elasticity. We consider the linear elastic and compressible material with $N^{2/3}$ beams with a Young modulus of $\mathrm{E}_2 = 1e+6$ inside a soft matrix material of $\mathrm{E}_1 = 1$. This material was introduced before as composite material no. 1; see Figure 5.1. In order to evaluate the potential of the two approaches, we stress the deflation and balancing approach up to convergence criterion of the iterative solver of $\mathrm{tol}_{cg} = 1e-13$. Consequently, in both tables, Table 5.2 and 5.3, we obtain results where the convergence criterion cannot be reached anymore, e.g., if the preconditioned residual reaches a plateau. In these cases, we report a second line with the corresponding values ($\lambda_{\min}$, $\lambda_{\max}$, *its*, $\|M_{PP}^{-1}r\|_2$, or $\|M_{BP}^{-1}r\|_2$, respectively, and *err*) in parentheses at the corresponding PCG iteration step before the preconditioned residual stagnates or even deteriorates.

Tables 5.2 and 5.3 show that mostly the same errors with respect to the global finite element solution are obtained. However, for really small toler-

Table 5.2: *Adaptive FETI-DP (Alg. Ia) with ρ-scaling and deflation approach with different convergence criteria for the conjugate gradient scheme.* Compressible linear elasticity of composite material no. 1 with $E_1 = 1$ and $N^{2/3}$ beams with $E_2 = 1e+6$ on the unit cube; $\nu = 0.3$ for the whole domain; conforming $\mathcal{P}_1$ finite element discretization with $1/h = 6N^{1/3}$ and irregular partitioning of the domain; see Figure 5.1. Coarse spaces for TOL = 10 for all generalized eigenvalue problems. N denotes the numer of subdomains, tol_{cg} the relative reduction of the preconditioned residual required for convergence of the PCG algorithm, $\lambda_{\min}$, $\lambda_{\max}$ the minimum and maximum eigenvalue estimates from the underlying PCG iteration (if the iterative scheme became unstable due to the not attained convergence criterion, the values before the occurence of the instabilities are given in parentheses), *its* the number of iterations until convergence or max_its=250 otherwise, $\|M_{PP}^{-1}r\|_2$ the 2-norm of the preconditioned residual in the deflation/projector preconditioning approach, *err* the relative difference between the domain decomposition solution and a direct finite element solution on the whole domain. Eigenvalues $\lambda_{\max}$ below 50 are marked in bold face.

Adaptive FETI-DP: *Algorithm Ia* (Deflation)

$1/h = 6N^{1/3}$ – composite material no. 1 – irregular partitioning

N	$\|U\|$	tol_{cg}	$\lambda_{\min}$	$\lambda_{\max}$	*its*	$\|M_{PP}^{-1}r\|_2$	*err*
2^3	86	1e-7	1.01	**8.66**	24	1.40e-8	2.38e-9
		1e-9	1.01	**8.66**	28	3.20e-8	1.33e-10
		1e-11	0.21 (1.00)	3.99e+4 (**8.66**)	250 (30)	6.47e-11 (6.66e-10)	3.00e-11 (4.14e-11)
		1e-13	0.21 (1.00)	3.99e+4 (**8.66**)	250 (30)	6.47e-11 (6.66e-10)	3.00e-11 (4.14e-11)
4^3	1761	1e-7	1.01 (1.01)	9.82e+7 (**9.74**)	250 (32)	2.54e-7 (2.54e-7)	1.16e-9 (1.11e-9)
		1e-9	1.01 (1.01)	9.82e+7 (**9.74**)	250 (32)	2.54e-7 (2.54e-7)	1.16e-9 (1.11e-9)
		1e-11	1.01 (1.01)	9.82e+7 (**9.74**)	250 (32)	2.54e-7 (2.54e-7)	1.16e-9 (1.11e-9)
		1e-13	1.01 (1.01)	9.82e+7 (**9.74**)	250 (32)	2.54e-7 (2.54e-7)	1.16e-9 (1.11e-9)
6^3	5514	1e-7	1.01	**10.01**	27	1.04e-7	4.54e-9
		1e-9	1.00 (1.00)	4.82e+5 (**10.05**)	250 (30)	9.38e-8 (9.40e-8)	1.27e-9 (1.53e-9)
		1e-11	1.00 (1.00)	4.82e+5 (**10.05**)	250 (30)	9.38e-8 (9.40e-8)	1.27e-9 (1.53e-9)
		1e-13	1.00 (1.00)	4.82e+5 (**10.05**)	250 (30)	9.38e-8 (9.40e-8)	1.27e-9 (1.53e-9)

Table 5.3: *Adaptive FETI-DP (Alg. Ia) with ρ-scaling and balancing approach with different convergence criteria for the conjugate gradient scheme.* Compressible linear elasticity of composite material no. 1 with $E_1 = 1$ and $N^{2/3}$ beams with $E_2 = 1e+6$ on the unit cube; $\nu = 0.3$ for the whole domain; conforming $\mathcal{P}_1$ finite element discretization with $1/h = 6N^{1/3}$ and irregular partitioning of the domain; see Figure 5.1. Coarse spaces for TOL = 10 for all generalized eigenvalue problems. $\|M_{BP}^{-1}r\|_2$ the 2-norm of the preconditioned residual in the balancing approach; all other notation as in Table 5.2.

Adaptive FETI-DP: *Algorithm Ia* (Balancing)

$1/h = 6N^{1/3}$ – composite material no. 1 – irregular partitioning

N	$\lvert U\rvert$	tol_{cg}	$\lambda_{\min}$	$\lambda_{\max}$	*its*	$\|M_{BP}^{-1}r\|_2$	*err*
2^3	86	1e-7	1.00	**8.66**	23	6.10e-8	6.19e-9
		1e-9	1.00	**8.66**	27	3.76e-10	2.05e-10
		1e-11	1.00	**8.66**	32	5.64e-12	4.39e-11
		1e-13	1.00	**8.66**	41	4.50e-14	4.42e-11
4^3	1761	1e-7	1.00	**9.74**	26	6.16e-8	6.71e-9
		1e-9	1.00	**9.74**	32	8.60e-10	1.92e-9
		1e-11	1.00	**9.74**	39	7.38e-12	1.91e-9
		1e-13	3.70e-15 (1.00)	1.20e+5 (**9.74**)	250 (42)	16.12 (1.19e-12)	2.59 (1.91e-9)
6^3	5514	1e-7	1.00	**9.98**	26	8.62e-8	8.81e-9
		1e-9	1.00	**10.04**	33	7.88e-10	1.01e-9
		1e-11	1.00	**10.04**	39	8.56e-12	1.01e-9
		1e-13	4.16e-16 (1.00)	13.47 (**10.05**)	250 (46)	3.60e-10 (5.46e-13)	0.25 (1.01e-9)

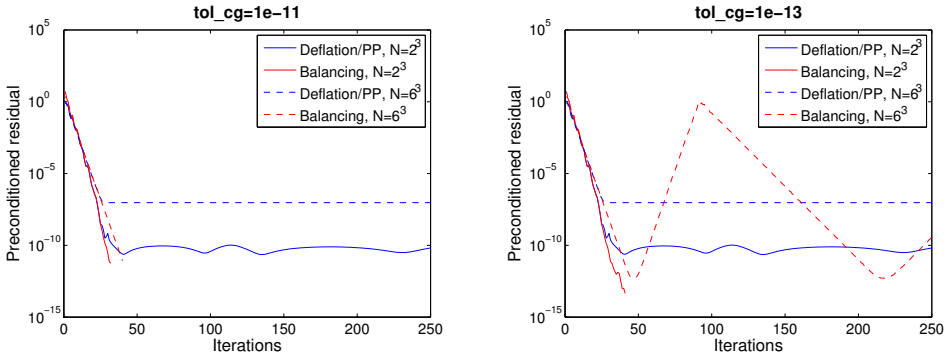

Figure 5.5: *Comparison of the convergence behaviour of adaptive FETI-DP (Alg. Ia) with deflation and balancing.* Plot of the history of the (log-scaled) 2-norm of the preconditioned residuals for the deflation and the balancing approach with $\text{tol}_{cg} = 1e-11$ (left) and $\text{tol}_{cg} = 1e-13$ (right) for $N = 2^3$ and $N = 6^3$ subdomains each; cf. Tables 5.2 and 5.3.

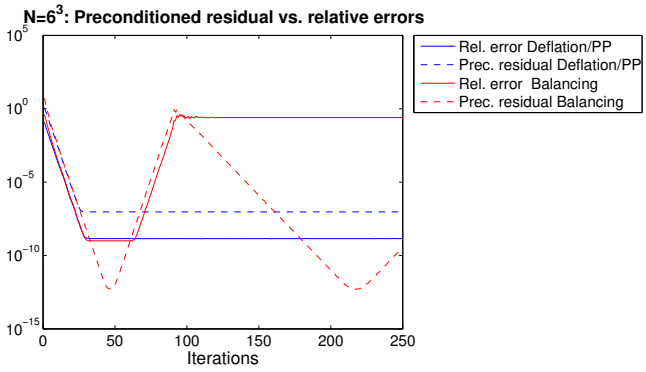

Figure 5.6: *Comparison of the preconditioned residuals and the relative errors for adaptive FETI-DP (Alg. Ia) with deflation and balancing.* Plot of the history of the (log-scaled) 2-norm of the preconditioned residuals and the corresponding relative error for the deflation and the balancing approach in each iteration step (until max_its=250) and $N = 6^3$ subdomains each; cf. Tables 5.2 and 5.3.

ances such as 1e-13 the balancing approach can converge to a wrong solution. Although the residual at convergence is really small, the error is large. We observed this behaviour for really small tolerances where the preconditioned residual develops as in Figure 5.5 (right); see Figure 5.6 for the simultaneous development of the error of the computed domain decomposition solution at each iteration step. In [80], it was already observed that the balancing approach might converge to the wrong solution if $(U^T F U)^+$ is solved approximately, although the preconditioned residual at the last step of the iterative solver indicates stable convergence. However, when using a tolerance of 1e-11 or smaller, the balancing approach remained stable with respect to the error. In order to validate our algorithm, the balancing approach seems more adequate since the eigenvalue estimates of the underlying conjugate gradient scheme deteriorate fast when a plateau for the preconditioned residual is reached. Thus, in this chapter, we use the balancing approach to implement the adaptively computed constraints; cf. Sections 4.2 and 5.2.1.

5.4.2 A simple example of a composite material with a regular decomposition

In this section, we consider a linear elastic and compressible material similar to the composite material no. 1 introduced before. In contrast to composite material no. 1, for *composite material no. 2*, we have $4N^{2/3}$ instead of $N^{2/3}$ beams of a stiff material.

The beams of composite material no. 2 are also arranged in a regular pattern and span from the face with $x = 0$ straight to the face with $x = 1$; see Figure 5.7 (top). The intersection of the beams with the face $x = 0$ represents 4/25th of the area of the face. In a regular decomposition four centered beams intersect the two corresponding faces of a considered subdomain; see Figure 5.7 (bottom).

If a regular decomposition is used with these coefficient configurations, already the classical approach from [93, 120] performs well. We see that for this simple case, where the jumps do not cut through edges, all approaches lead to low condition numbers and a low number of iterations. The most simple algorithm, i.e., Algorithm III performs well while resulting in the smallest coarse space. Algorithm Ic automatically reduces to Algoritm III, and therefore gives the same performance. This illustrates the effectiveness of the neighborhood strategies presented in Section 5.2.2. For this problem, the use of edge constraints can reduce the number of iterations further but not significantly. This shows that edge constraints from face eigenvalue problems (Algorithms Ia, Ib,

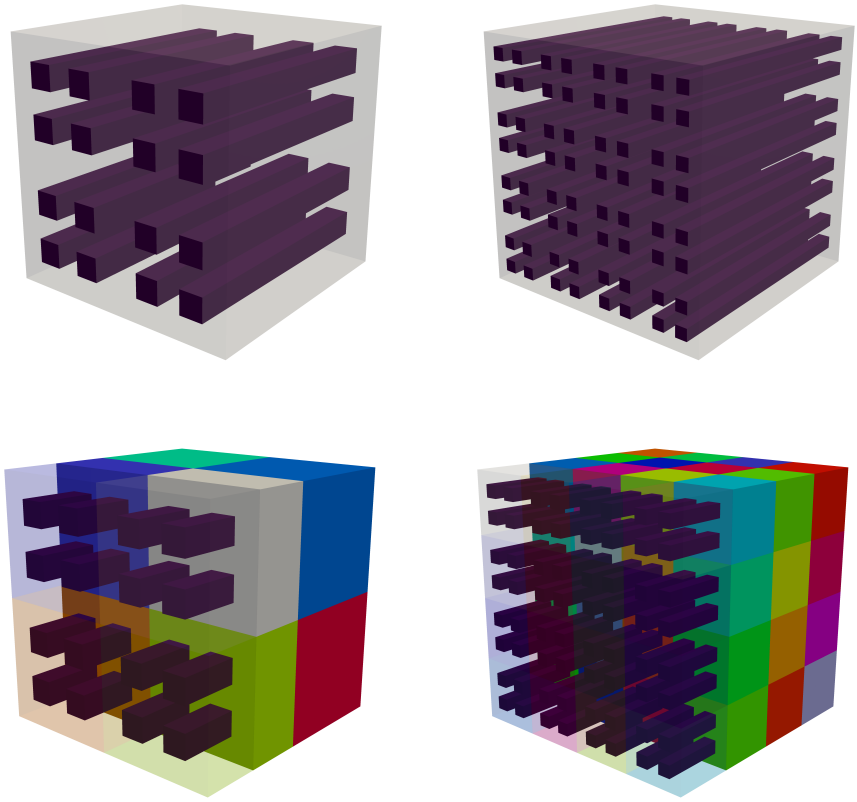

Figure 5.7: *Composite material no. 2 on the unit cube for 8 and 64 subdomains (coefficients and regular partitioning).* 16 and 64 beams of a stiff material with $E_2 = 1e+6$, shown in dark purple, are surrounded by a soft matrix material with $E_1 = 1$, shown in light, half-transparent gray, (top). Regular decomposition for 16 and 64 subdomains; high coefficients are again shown in dark purple; subdomains shown in different colors; left quarter of the domain ($x > \frac{3}{4}$) made half-transparent (bottom). [64]

Table 5.4: *Adaptive FETI-DP (Alg. Ia-III) with ρ-scaling and balancing approach.* Compressible linear elasticity of composite material no. 2 with $E_1 = 1$ and $4N^{2/3}$ beams with $E_2 = 1e+6$ on the unit cube; $\nu = 0.3$ for the whole domain; conforming $\mathcal{P}_1$ finite element discretization with $H/h = 10$ and regular partitioning of the domain; see Figure 5.7. Coarse spaces for TOL = 10 for all generalized eigenvalue problems. κ denotes the condition number estimates from the underlying PCG iteration and $\#\mathcal{E}_{evp}$ the number of eigenvalue problems computed (in parentheses the percentage of edge eigenvalue problems w.r.t. the total number of eigenvalue problems); all other notation as in Table 5.3. Condition numbers below 50 are marked in bold face. [64]

Adaptive FETI-DP: *Algorithms Ia, Ib, Ic, II, and III* (Balancing)
$H/h = 10$ – composite material no. 2 – regular partitioning

	Algorithms Ia, Ib, and Ic					*Algorithm II*			*Algorithm III*		
N		κ	*its*	$\lvert U\rvert$	$\#\mathcal{E}_{evp}$	κ	*its*	$\lvert U\rvert$	κ	*its*	$\lvert U\rvert$
3^3	a)	**3.37**	15	2548	72 (57.1%)						
	b)	**3.37**	15	2548	0 (0%)	**3.37**	15	2548	**3.55**	18	556
	c)	**3.55**	18	556	0 (0%)						
4^3	a)	**3.36**	15	7332	216 (60%)						
	b)	**3.36**	15	7332	0 (0%)	**3.36**	15	7332	**3.54**	18	1536
	c)	**3.54**	18	1536	0 (0%)						
5^3	a)	**3.39**	15	15896	480 (61.5%)						
	b)	**3.39**	15	15896	0 (0%)	**3.39**	15	15896	**3.55**	17	3272
	c)	**3.55**	17	3272	0 (0%)						

and II) are not needed, here. The same is true for the edge eigenvalue problems of Algorithm Ia.

In structured decompositions, we have a high number of edge eigenvalue problems in Algorithm Ia, i.e., around 50%; for our composite materials, if the strategy to reduce the number of edge eigenvalue problems from Algorithms Ib and Ic is applied, all edge eigenvalue problems are discarded while the results remain good; cf. Algorithms Ib and Ic and column 6 ($\#\mathcal{E}_{evp}$) in Table 5.4. This is possible in this simple setting where there are no cuts of coefficient jumps through any edges. Note that, in this case, we do not reduce the coarse problem size with Algorithm Ib. Only Algorithm Ic reduces to Algorithm III in these cases.

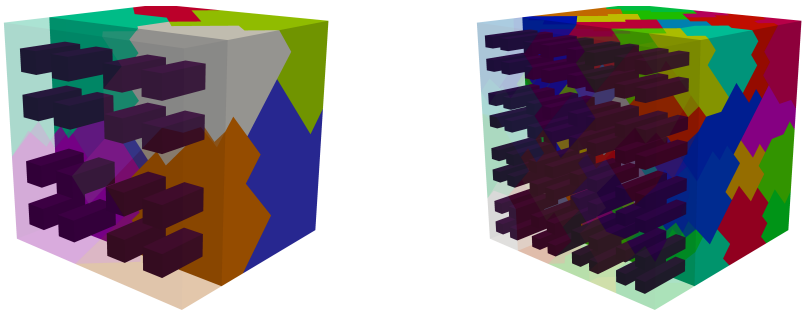

Figure 5.8: *Composite material no. 2 on the unit cube for 8 and 64 subdomains (irregular partitioning).* 16 and 64 beams of a stiff material with $E_2 = 1e+6$, shown in dark purple, are surrounded by a soft matrix material with $E_1 = 1$ (not shown); subdomains shown in different colors; left quarter of the domain ($x > \frac{3}{4}$) made half-transparent. [64]

5.4.3 Composite materials with irregular decompositions

In a next step, we consider adaptive FETI-DP with an irregular decomposition of the considered domain. We consider composite material no. 1 for compressible linear elasticity and different sizes of the local subdomains; see Figure 5.1 for 64 and 216 subdomains. Additionally, we test adaptive FETI-DP for composite material no. 2 and the diffusion equation as well as compressible linear elasticity; see Figure 5.7 (top) for the coefficient distribution and Figure 5.8 for the irregular decomposition for 8 and 64 subdomains. In all of these cases, jumps along and across subdomain edges are very likely to occur.

For the results on composite material no. 1, see Tables 5.5 and 5.6 for linear elasticity with $1/h = 3N^{1/3}$ and $1/h = 6N^{1/3}$.

For composite material no. 2, see Table 5.7 for the diffusion equation with $1/h = 5N^{1/3}$ and Tables 5.8 and 5.9 for linear elasticity with $1/h = 5N^{1/3}$ and $1/h = 10N^{1/3}$.

For all these test cases, discarding the edge constraints from face eigenvalue problems (Algorithm III) never seems to be a good option and often results in nonconvergence ($its = 500$); but also for Algorithm II large condition numbers and large number of iterations are observed. On the other hand, our Algorithm Ia, which makes use of our new coarse space, in accordance with the theory, results in small condition numbers for all cases – while, compared to Algorithm II, adding around or fewer than 5% of additional constraints to the coarse space. Algorithms Ib and Ic can reduce the number of edge eigenvalue

Table 5.5: *Adaptive FETI-DP (Alg. Ia-III) with ρ-scaling and balancing approach.* Compressible linear elasticity of composite material no. 1 with $E_1 = 1$ and $N^{2/3}$ beams with $E_2 = 1e+6$ on the unit cube; $\nu = 0.3$ for the whole domain; conforming $\mathcal{P}_1$ finite element discretization with $1/h = 3N^{1/3}$ and irregular partitioning of the domain; see Figure 5.1. Coarse spaces for TOL = 10 for all generalized eigenvalue problems. Notation as in Table 5.4. [64]

Adaptive FETI-DP: *Algorithms Ia, Ib, Ic, II, and III* (Balancing)

$1/h = 3N^{1/3}$ – composite material no. 1 – irregular partitioning

	Algorithms Ia, Ib, and Ic					*Algorithm II*			*Algorithm III*		
N		κ	*its*	$\lvert U\rvert$	$\#\mathcal{E}_{evp}$	κ	*its*	$\lvert U\rvert$	κ	*its*	$\lvert U\rvert$
3^3	a)	**8.55**	30	93	7 (11.9%)	**8.55**	30	90	8.43e+5	56	50
	b)	**8.55**	30	93	4 (7.1%)						
	c)	**8.55**	31	84	4 (7.1%)						
5^3	a)	**14.48**	37	278	14 (5.2%)	**14.48**	37	264	3.35e+5	211	153
	b)	**14.48**	37	278	8 (3.0%)						
	c)	**14.48**	37	227	8 (3.0%)						
7^3	a)	**14.08**	40	605	48 (6.0%)	2.97e+5	118	569	3.00e+5	434	358
	b)	**14.08**	41	602	21 (2.7%)						
	c)	**14.08**	41	506	21 (2.7%)						
9^3	a)	**16.45**	42	1076	90 (5.2%)	3.61e+5	115	1029	4.76e+5	500	704
	b)	**16.45**	42	1075	45 (2.7%)						
	c)	**16.45**	42	932	45 (2.7%)						
11^3	a)	**15.87**	43	1774	167 (5.2%)	2.69e+5	190	1668	3.72e+5	500	1174
	b)	**15.87**	43	1770	95 (3.0%)						
	c)	**15.87**	43	1580	95 (3.0%)						
13^3	a)	**17.32**	45	3070	303 (5.6%)	2.79e+5	345	2911	3.42e+5	500	2032
	b)	**17.32**	45	3068	171 (3.3%)						
	c)	**17.32**	45	2753	171 (3.3%)						

problems significantly, e.g., around 50%. However, for Algorithm Ib this still results in an almost identical coarse space. The coarse space of Algorithm Ic is always significantly smaller than the one of Algorithm Ib and Algorithm II. Nevertheless, condition numbers and iteration counts of Algorithm Ic are comparable to those of Algorithm Ia while Algorithm II cannot ensure this.

Let us highlight a subtle difference in the data reported for linear elasticity and the diffusion equation. Note that the number of edge eigenvalue problems for the diffusion equation (see Table 5.7) is larger than in the case of linear elasticity (see Table 5.8). This is due to the fact that, in case of elasticity, we select additional primal vertices to remove hinge modes on curved edges; cf. Remark 5.3. Then, edge eigenvalue problems on certain short edges become superfluous. Since this is not necessary for the diffusion equation, and since

Table 5.6: *Adaptive FETI-DP (Alg. Ia-III) with ρ-scaling and balancing approach.* Compressible linear elasticity of composite material no. 1 with $E_1 = 1$ and $N^{2/3}$ beams with $E_2 = 1e+6$ on the unit cube; $\nu = 0.3$ for the whole domain; conforming $\mathcal{P}_1$ finite element discretization with $1/h = 6N^{1/3}$ and irregular partitioning of the domain; see Figure 5.1. Coarse spaces for TOL = 10 for all generalized eigenvalue problems. Notation as in Table 5.4. [64]

Adaptive FETI-DP: *Algorithms Ia, Ib, Ic, II, and III* (Balancing)

$1/h = 6N^{1/3}$ – composite material no. 1 – irregular partitioning

	Algorithms Ia, Ib, and Ic					*Algorithm II*			*Algorithm III*		
N		κ	*its*	$\lvert U\rvert$	$\#\mathcal{E}_{evp}$	κ	*its*	$\lvert U\rvert$	κ	*its*	$\lvert U\rvert$
3^3	a)	**8.70**	34	642	2 (2.0%)	**8.70**	34	642	1.37e+6	81	188
	b)	**8.70**	34	642	1 (1.0%)						
	c)	**8.72**	34	405	1 (1.0%)						
5^3	a)	**9.78**	36	3323	25 (4.2%)	**11.43**	36	3316	5.54e+5	213	924
	b)	**9.78**	36	3323	12 (2.1%)						
	c)	**10.62**	36	2092	12 (2.1%)						
7^3	a)	**10.91**	37	9388	65 (3.6%)	**10.91**	37	9350	1.22e+6	455	2672
	b)	**10.91**	37	9388	27 (1.5%)						
	c)	**13.48**	39	6308	27 (1.5%)						

it enlarges the primal coarse space unnecessarily for the diffusion equation, we did not carry this out for the results in Table 5.7 and accept a higher number of eigenvalue problems.

For problems of linear elasticity and irregularly partitioned domains, we see that that the amount of edge eigenvalue problems is generally between 0% and 12% for Algorithm Ia while this can be reduced to 0 to 7% by Algorithms Ib and Ic. For Algorithm Ib, in the mean, we get about 2% to 3% edge eigenvalue problems and, compared to Algorithm II, 1% to 2% additional constraints; see Tables 5.5, 5.6, and 5.8, and 5.9. There are also cases, when Algorithms Ia, Ib and II coincide; see, e.g., Table 5.9.

For irregularly partitioned domains the computational overhead of Algorithm Ic, compared to the "classical" approach in Algorithm III, might be of up to 7% of extra eigenvalue problems and up to 2-3 times as many constraints but is then mostly mandatory for convergence and to reduce the condition number from approximately 1e+5 to approximately TOL = 10; see, Tables 5.5, 5.6 as well as 5.7, 5.8, and 5.9. However, compared to Algorithm II we can save up to 40% of the constraints by using Algorithm Ic.

We conclude that the additional edge eigenvalue problems and the resulting constraints are often necessary to obtain a small condition number and even

Table 5.7: *Adaptive FETI-DP (Alg. Ia-III) with ρ-scaling and balancing approach.* Diffusion equation of composite material no. 2 with $\rho_1 = 1$ and $4N^{2/3}$ beams with $\rho_2 = 1e+6$ on the unit cube; conforming $\mathcal{P}_1$ finite element discretization with $1/h = 5N^{1/3}$ and irregular partitioning of the domain; see Figure 5.8. Coarse spaces for TOL = 10 for all generalized eigenvalue problems. Notation as in Table 5.4. Adapted by permission from Springer International Publishing AG: [Springer] [Domain Decomposition Methods in Science and Engineering XXIII] [66] [COPYRIGHT] (2017).

Adaptive FETI-DP: *Algorithms Ia, Ib, Ic, II, and III* (Balancing)
$1/h = 5N^{1/3}$ – composite material no. 2 – irregular partitioning

	Algorithms Ia, Ib, and Ic					*Algorithm II*			*Algorithm III*		
N		κ	*its*	$\lvert U\rvert$	$\#\mathcal{E}_{evp}$	κ	*its*	$\lvert U\rvert$	κ	*its*	$\lvert U\rvert$
4^3	a)	**9.54**	36	1784	41 (14.9%)	**9.78**	37	1765	2.23e+6	500	609
	b)	**9.78**	36	1783	30 (11.3%)						
	c)	**10.68**	39	1475	30 (11.3%)						
6^3	a)	**11.72**	38	6455	166 (15.1%)	5.13e+5	98	6364	3.13e+6	500	2057
	b)	**11.72**	38	6455	134 (12.6%)						
	c)	**11.72**	39	5701	134 (12.6%)						
8^3	a)	**12.34**	39	15292	390 (14.1%)	2.27e+5	62	15120	2.99e+6	500	4921
	b)	**12.34**	39	15292	334 (12.4%)						
	c)	**12.34**	40	13682	334 (12.4%)						

mandatory if PCG is expected to converge in a small number of iterations. The only configurations when Algorithm III converged in fewer than 100 iterations were cases when coefficient jumps did not appear at subdomain edges, or in small examples with fewer subdomains, when the influence of the Dirichlet boundary was still strong.

5.4.4 A steel microstructure

In this section, we consider a representative volume element (RVE) representing the microstructure of a modern steel; see Figure 5.9.

The RVE has been obtained from the one in [87, Fig. 5.5], which again is a part of the structure in [117, Fig. 2], by resampling. As in [87], we use $\nu = 0.3$, $\mathrm{E}_1 = 210$, and $\mathrm{E}_2 = 210\,000$ as (artificial) material parameters. There, about 12% of the volume is covered by the high coefficient E_2. We have resampled the RVE from $64 \times 64 \times 64$ to $32 \times 32 \times 32$ voxels. Here, the coefficient is set to E_2 if at least three of the original voxels have a high coefficient. This procedure guarantees that the ratio of high and low coefficients is not changed.

Table 5.8: *Adaptive FETI-DP (Alg. Ia-III) with ρ-scaling and balancing approach.* Compressible linear elasticity of composite material no. 2 with $E_1 = 1$ and $4N^{2/3}$ beams with $E_2 = 1e+6$ on the unit cube; $\nu = 0.3$ for the whole domain; conforming $\mathcal{P}_1$ finite element discretization with $1/h = 5N^{1/3}$ and irregular partitioning of the domain; see Figure 5.8. Coarse spaces for TOL = 10 for all generalized eigenvalue problems. Notation as in Table 5.4. [64]

Adaptive FETI-DP: *Algorithms Ia, Ib, Ic, II, and III* (Balancing)
$1/h = 5N^{1/3}$ – composite material no. 2 – irregular partitioning

	Algorithms Ia, Ib, and Ic					*Algorithm II*			*Algorithm III*		
N		κ	*its*	$\lvert U\rvert$	$\#\mathcal{E}_{evp}$	κ	*its*	$\lvert U\rvert$	κ	*its*	$\lvert U\rvert$
3^3	a)	**14.12**	37	1312	0 (0%)	**14.12**	37	1312	2.39e+5	463	523
	b)	**14.12**	37	1312	0 (0%)						
	c)	**14.12**	37	1114	0 (0%)						
5^3	a)	**13.91**	39	5675	23 (4.1%)	**13.91**	39	5639	5.46e+5	500	2261
	b)	**13.91**	39	5675	19 (3.5%)						
	c)	**13.92**	39	4840	19 (3.5%)						
7^3	a)	**14.58**	42	15250	89 (5.5%)	1.81e+5	84	15104	4.93e+5	500	6420
	b)	**14.58**	42	15250	70 (4.4%)						
	c)	**14.58**	42	13336	70 (4.4%)						
9^3	a)	**16.24**	43	32083	165 (4.6%)	6.74e+3	66	31897	3.16e+5	500	13591
	b)	**16.24**	43	32083	138 (3.9%)						
	c)	**16.24**	43	28372	138 (3.9%)						

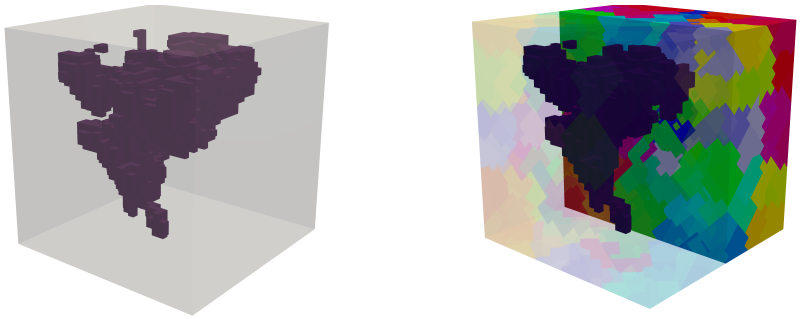

Figure 5.9: *Representative volume element (coefficients and irregular partitioning).* Resampled element of [87, Fig. 5.5], [117, Fig. 2]; (artificial) material parameters $E_1 = 210$, shown in light, half-transparent gray, and $E_2 = 210\,000$, shown in dark purple (left). Irregular decomposition for 512 subdomains; high coefficients are again shown in dark purple; subdomains shown in different colors; left half of the domain ($x > \frac{1}{2}$) made half-transparent (right). [64]. Data courtesy of Jörg Schröder.

Table 5.9: *Adaptive FETI-DP (Alg. Ia-III) with ρ-scaling and balancing approach.* Compressible linear elasticity of composite material no. 2 with $E_1 = 1$ and $4N^{2/3}$ beams with $E_2 = 1e+6$ on the unit cube; $\nu = 0.3$ for the whole domain; conforming $\mathcal{P}_1$ finite element discretization with $1/h = 10N^{1/3}$ and irregular partitioning of the domain; see Figure 5.8. Coarse spaces for TOL = 10 for all generalized eigenvalue problems. Notation as in Table 5.4. [64]

Adaptive FETI-DP: *Algorithms Ia, Ib, Ic, II, and III* (Balancing)

$1/h = 10N^{1/3}$ – composite material no. 2 – irregular partitioning

	Algorithms Ia, Ib, and Ic					*Algorithm II*			*Algorithm III*		
N		κ	*its*	$\lvert U\rvert$	$\#\mathcal{E}_{evp}$	κ	*its*	$\lvert U\rvert$	κ	*its*	$\lvert U\rvert$
3^3	a)	**9.86**	35	4441	1 (1.0%)						
	b)	**9.86**	35	4441	0 (0%)	**9.86**	35	4441	3.46e+5	243	1101
	c)	**11.25**	36	3364	0 (0%)						
4^3	a)	**9.60**	35	10524	0 (0%)						
	b)	**9.60**	35	10524	0 (0%)	**9.60**	35	10524	8.88e+5	379	2583
	c)	**11.57**	37	7417	0 (0%)						
5^3	a)	**9.90**	36	22704	13 (2.0%)						
	b)	**9.90**	36	22704	2 (0.3%)	**9.90**	36	22704	1.04e+6	500	5490
	c)	**11.12**	37	17219	2 (0.3%)						

We see from our results in Table 5.10 that Algorithms Ia, Ib, and II do behave quite the same. The amount of extra work for our modified coarse space in Algorithms Ia and Ib compared to Algorithm II is small. Algorithm Ic uses a reduced coarse space that still guarantees small condition numbers and convergence within a comparable number of PCG iterations while the smallest coarse space, represented by Algorithm III, gives larger condition numbers and iteration counts.

5.4.5 Randomly distributed coefficients

We turn towards randomly distributed coefficients and now perform 100 runs with different coefficients for every configuration. We consider the diffusion equation and a linear elastic and compressible material.

Besides N, the number of subdomains, we vary the number of tetrahedra with a high coefficient. We test a 50/50 and 80/20 ratio of low and high coefficients; see Figure 5.10.

In Tables 5.11, 5.12, and 5.13, we present the arithmetic mean $\overline{x}$, the median $\widetilde{x}$, the standard deviation σ, the minimum min and the maximum max over all 100 runs and for different numbers N of subdomains with $1/h = 5N^{1/3}$.

Table 5.10: *Adaptive FETI-DP (Alg. Ia-III) with ρ-scaling and balancing approach.* Compressible linear elasticity of representative volume element with $E_1 = 210$ and $E_2 = 210\,000$ on the unit cube; $\nu = 0.3$ for the whole domain; conforming $\mathcal{P}_1$ finite element discretization with $1/h = 4N^{1/3}$ for $N = 8^3$ and reg. and irregular partitioning of the domain; see Figure 5.9. Coarse spaces for TOL = 10 for all generalized eigenvalue problems. Notation as in Table 5.4. [64]. Data courtesy of Jörg Schröder.

Adaptive FETI-DP: *Algorithms Ia, Ib, Ic, II, and III* (Balancing)
$N = 8^3$ – $1/h = 4N^{1/3}$ – representative volume element – (ir)regular partitioning

	Algorithms Ia, Ib, and Ic					*Algorithm II*			*Algorithm III*		
part.		κ	*its*	$\lvert U\rvert$	$\#\mathcal{E}_{evp}$	κ	*its*	$\lvert U\rvert$	κ	*its*	$\lvert U\rvert$
reg.	a)	**10.04**	34	5950	2352 (63.6%)	**10.04**	35	5246	244.60	80	1066
	b)	**10.04**	34	5950	736 (35.4%)						
	c)	**10.06**	34	4769	736 (35.4%)						
irreg.	a)	**13.97**	37	700	114 (5.6%)	**13.97**	37	689	361.85	98	344
	b)	**13.97**	37	700	27 (1.4%)						
	c)	**13.97**	38	579	27 (1.4%)						

Since Algorithms Ia, Ib, and Ic behave almost identically for our test cases of randomized coefficients, we just report Algorithms Ia and Ic (as well as Algorithms II and III). Naturally, the results of Algorithm Ib are within the here small intervals of the only minimally differing results obtained by Algorithms Ia and Ic. In most of the runs, the three algorithms coincide. In Table 5.11, even all the results for the three algorithms are identical.

Again, we see that discarding the edge constraints resulting from face eigenvalue problems can result in large condition numbers and iteration counts; see the results for Algorithm III in Tables 5.11, 5.12, and 5.13. Nonetheless, keeping these edge constraints does, again, not always guarantee a small condition number and fast convergence, as the results for Algorithm II show. The number of extra eigenvalue problems for Algorithms Ia and Ic is either 0% or around 4% for our test cases of linear elasticity and between 10% and 15% for the diffusion problem; cf. the note on the higher number of eigenvalue problems for the diffusion equation in Section 5.4.3.

Since there are no edge eigenvalue problems for the linear elastic material on $N = 27$ subdomains Algorithms Ia, Ib and II coincide in that case. Moreover, since the edge eigenvalue problems always produce fewer or around 1% of additional constraints the computational overhead for Algorithms Ia, Ib and Ic is quite moderate compared to Algorithm II; see Tables 5.11, 5.12 and 5.13.

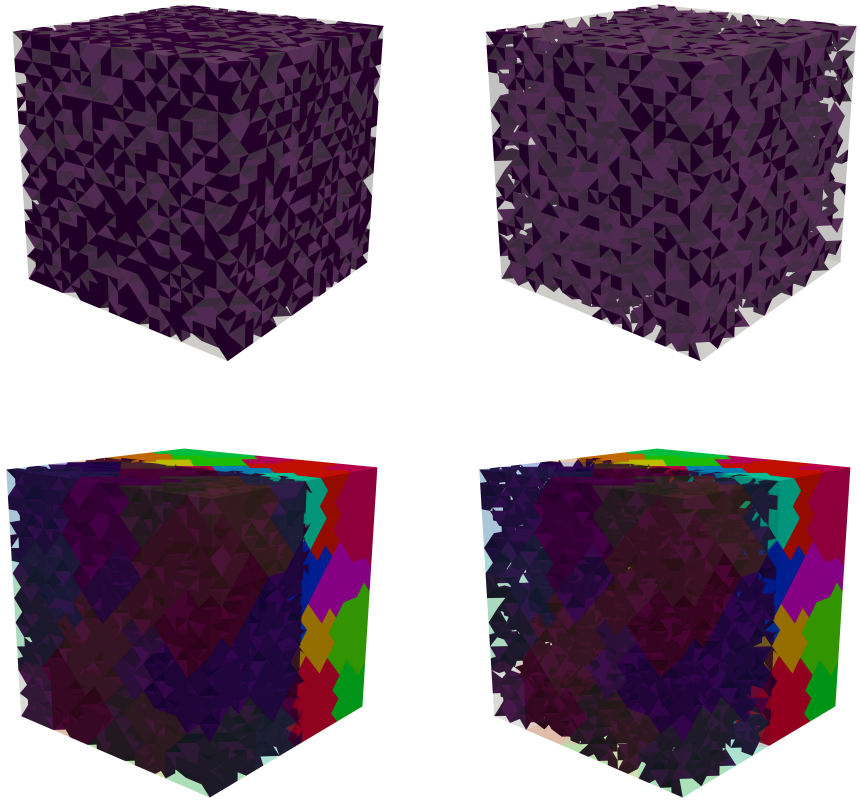

Figure 5.10: *Randomly distributed coefficients on the unit cube for 64 subdomains (coefficients and irregular partitioning).* 50% (top left) and 20% (top right) of the tetrahedra possess coefficient $\mathrm{E}_2 = 1e+6$ (or $\rho_2 = 1e+6$), shown in dark purple. The remaining numbers of tetrahedra possess coefficient $\mathrm{E}_1 = 1$ (or $\rho_1 = 1$), shown in light, half-transparent gray. Irregular decomposition for 64 subdomains with 50% (bottom left) and 20% high coefficients (bottom right), respectively; high coefficients are again shown in dark purple; subdomains shown in different colors; left half of the domain ($x > \frac{1}{2}$) made half-transparent. [64]

Table 5.11: *Adaptive FETI-DP (Alg. Ia, Ic, II, and III) with ρ-scaling and balancing approach.* Compressible linear elasticity of randomly distributed coefficients with 50% coefficients with $\mathrm{E}_1 = 1$ and 50% coefficients with $\mathrm{E}_2 = 1e+6$ on the unit cube; $\nu = 0.3$ for the whole domain; conforming $\mathcal{P}_1$ finite element discretization with $1/h = 5N^{1/3}$ and irregular partitioning of the domain; see Figure 5.10. Coarse spaces for $\mathrm{TOL} = 10$ for all generalized eigenvalue problems. $\overline{x}$ denotes the arithmetic mean, $\widetilde{x}$ the median, σ the standard deviation, min the minimum and max the maximum over all runs. All other notation as in Table 5.4. [64]

Adaptive FETI-DP: *Algorithms Ia, Ic, II, and III* (Balancing)
$1/h = 5N^{1/3}$ – random coefficients (50/50) – irregular partitioning

		Algorithm Ia				*Algorithm Ic*			
N		κ	*its*	$\lvert U\rvert$	$\#\mathcal{E}_{evp}$	κ	*its*	$\lvert U\rvert$	$\#\mathcal{E}_{evp}$
3^3	$\overline{x}$	**10.20**	35.17	180.94	0 (0%)	**10.20**	35.17	180.94	0 (0%)
	$\widetilde{x}$	**10.09**	35	179.5		**10.09**	35	179.5	0 (0%)
	min	**9.00**	34	136		**9.00**	34	136	0 (0%)
	max	**12.67**	37	248		**12.67**	37	248	0 (0%)
	σ	0.68	0.67	24.12	-	0.68	0.67	24.12	0.00
4^3	$\overline{x}$	**10.80**	36.09	383.77	9 (3.7%)	**10.80**	36.09	383.77	9 (3.7%)
	$\widetilde{x}$	**10.53**	36	381		**10.53**	36	381	9 (3.7%)
	min	**9.50**	35	310		**9.50**	35	310	9 (3.7%)
	max	**14.42**	37	450		**14.42**	37	450	9 (3.7%)
	σ	1.00	0.51	29.10	-	1.00	0.51	29.10	0.00
5^3	$\overline{x}$	**11.38**	36.70	721.46	23 (4.1%)	**11.38**	36.70	721.46	23 (4.1%)
	$\widetilde{x}$	**11.13**	37	717		**11.13**	37	717	23 (4.1%)
	min	**9.74**	36	595		**9.74**	36	595	23 (4.1%)
	max	**16.02**	39	855		**16.02**	39	855	23 (4.1%)
	σ	1.20	0.72	54.54	-	1.20	0.72	54.54	0.00

		Algorithm II			*Algorithm III*		
N		κ	*its*	$\lvert U\rvert$	κ	*its*	$\lvert U\rvert$
3^3	$\overline{x}$	**10.20**	35.17	180.94	7.53e+5	135.06	59.65
	$\widetilde{x}$	**10.09**	35	179.5	6.89e+5	134	59
	min	**9.00**	34	136	4.38e+5	72	44
	max	**12.67**	37	248	1.46e+6	204	85
	σ	0.68	0.66	24.12	2.19e+5	27.39	7.76
4^3	$\overline{x}$	6.85e+4	37.52	382.58	1.02e+6	222.96	137.37
	$\widetilde{x}$	**10.84**	36	380	1.01e+6	221	137
	min	**9.50**	35	309	5.33e+5	141	110
	max	7.99e+5	57	449	1.57e+6	294	164
	σ	1.83e+5	3.74	29.01	2.31e+5	30.70	11.43
5^3	$\overline{x}$	9.42e+5	39.35	719.27	8.54e+5	276.70	243.58
	$\widetilde{x}$	**11.62**	37	717	8.12e+5	269.5	241.5
	min	**9.97**	36	594	6.00e+5	187	194
	max	8.40e+5	67	851	1.84e+6	394	288
	σ	2.13e+5	5.64	54.47	1.90e+5	39.56	17.85

Table 5.12: *Adaptive FETI-DP (Alg. Ia, Ic, II, and III) with ρ-scaling and balancing approach.* Diffusion equation of randomly distributed coefficients with 80% coefficients with $\rho_1 = 1$ and 20% coefficients with $\rho_2 = 1e+6$ on the unit cube; conforming $\mathcal{P}_1$ finite element discretization with $1/h = 5N^{1/3}$ and irregular partitioning of the domain; see Figure 5.10. Coarse spaces for TOL = 10 for all generalized eigenvalue problems. Notation as in Table 5.11. Adapted by permission from Springer International Publishing AG: [Springer] [Domain Decomposition Methods in Science and Engineering XXIII] [66] [COPYRIGHT] (2017).

Adaptive FETI-DP: *Algorithms Ia, Ic, II, and III* (Balancing)
$1/h = 5N^{1/3}$ – random coefficients (80/20) – irregular partitioning

		Algorithm Ia				*Algorithm Ic*			
N		κ	*its*	$\lvert U\rvert$	$\#\mathcal{E}_{evp}$	κ	*its*	$\lvert U\rvert$	$\#\mathcal{E}_{evp}$
4^3	$\overline{x}$	**8.81**	30.64	1913.92	41 (14.9%)	**8.81**	30.64	1913.72	41 (14.9%)
	$\widetilde{x}$	**8.76**	31	1918		**8.76**	31	1918	41 (14.9%)
	min	**7.00**	27	1816		**7.00**	27	1816	41 (14.9%)
	max	**14.53**	34	2003		**14.53**	34	2003	41 (14.9%)
	σ	0.88	1.32	43.57	-	0.88	1.32	43.67	0.00
5^3	$\overline{x}$	**9.26**	32.19	3992.86	61 (10.3%)	**9.26**	32.19	3992.55	60.99 (10.3%)
	$\widetilde{x}$	**9.20**	32	3997.5		**9.20**	32	3996	61 (10.3%)
	min	**7.71**	30	3833		**7.71**	30	3833	60 (10.1%)
	max	**15.01**	35	4153		**15.01**	35	4153	61 (10.3%)
	σ	0.86	0.88	69.31	-	0.86	0.90	69.38	0.10

		Algorithm II			*Algorithm III*		
N		κ	*its*	$\lvert U\rvert$	κ	*its*	$\lvert U\rvert$
4^3	$\overline{x}$	3.92e+5	43.61	1889.83	2.62e+6	500	675.53
	$\widetilde{x}$	2.31e+5	42.5	1893.5	2.57e+6	500	676
	min	**7.91**	28	1795	1.29e+6	500	624
	max	3.61e+6	71	1977	5.65e+6	500	722
	σ	5.12e+5	10.41	43.25	7.42e+5	0	22.05
5^3	$\overline{x}$	2.29e+5	55.35	3954.50	2.96e+6	500	1357.53
	$\widetilde{x}$	2.01e+5	52.5	3955.5	2.79e+6	500	1359.5
	min	**8.34**	32	3796	1.57e+6	500	1279
	max	9.21e+5	100	4109	5.46e+6	500	1424
	σ	2.09e+5	15.05	68.58	7.52e+5	0	33.67

Table 5.13: *Adaptive FETI-DP (Alg. Ia, Ic, II, and III) with ρ-scaling and balancing approach.* Compressible linear elasticity of randomly distributed coefficients with 80% coefficients with $E_1 = 1$ and 20% coefficients with $E_2 = 1e+6$ on the unit cube; $\nu = 0.3$ for the whole domain; conforming $\mathcal{P}_1$ finite element discretization with $1/h = 5N^{1/3}$ and irregular partitioning of the domain; see Figure 5.10. Coarse spaces for TOL = 10 for all generalized eigenvalue problems. Notation as in Table 5.11. [64]

Adaptive FETI-DP: *Algorithms Ia, Ic, II, and III* (Balancing)
$1/h = 5N^{1/3}$ – random coefficients (80/20) – irregular partitioning

		Algorithm Ia				*Algorithm Ic*			
N		κ	*its*	$\lvert U\rvert$	$\#\mathcal{E}_{evp}$	κ	*its*	$\lvert U\rvert$	$\#\mathcal{E}_{evp}$
3^3	$\overline{x}$	**8.40**	30.74	1311.94	0 (0%)	**8.40**	30.74	1311.54	0 (0%)
	$\widetilde{x}$	**8.38**	31	1311.5		**8.38**	31	1311.5	0 (0%)
	min	**6.91**	29	1144		**6.91**	29	1144	0 (0%)
	max	**10.16**	32	1473		**10.16**	32	1473	0 (0%)
	σ	0.61	0.79	66.14	-	0.61	0.79	65.95	0.00
4^3	$\overline{x}$	**9.01**	32.68	2680.69	9 (3.7%)	**9.01**	32.68	2680.16	9 (3.7%)
	$\widetilde{x}$	**9.04**	33	2678		**9.04**	33	2678	9 (3.7%)
	min	**8.09**	31	2485		**8.09**	31	2479	9 (3.7%)
	max	**10.05**	34	2894		**10.05**	34	2894	9 (3.7%)
	σ	0.50	0.63	81.22	-	0.50	0.63	81.40	0.00
5^3	$\overline{x}$	**9.12**	32.96	6015.56	23 (4.1%)	**9.12**	32.96	6014.32	22.99 (4.1%)
	$\widetilde{x}$	**9.08**	33	6009		**9.08**	33	6005.5	23 (4.1%)
	min	**7.93**	32	5577		**7.93**	32	5571	22 (4.0%)
	max	**11.16**	34	6449		**11.16**	34	6449	23 (4.1%)
	σ	0.56	0.61	148.91	-	0.56	0.61	149.22	0.10

		Algorithm II			*Algorithm III*		
N		κ	*its*	$\lvert U\rvert$	κ	*its*	$\lvert U\rvert$
3^3	$\overline{x}$	**8.40**	30.74	1311.94	3.89e+5	486.03	499.76
	$\widetilde{x}$	**8.38**	31	1311.5	3.78e+5	500	501
	min	**6.91**	29	1144	1.99e+5	395	408
	max	**10.16**	32	1473	8.29e+5	500	579
	σ	0.61	0.79	66.14	1.21e+5	24.67	33.36
4^3	$\overline{x}$	6.93e+4	39.58	2663.58	5.57e+5	500	1100.85
	$\widetilde{x}$	2.90e+3	38	2661.5	5.22e+5	500	1103
	min	**8.16**	32	2473	2.97e+5	500	998
	max	5.93e+5	67	2875	1.34e+6	500	1201
	σ	1.16e+5	8.04	81.16	1.85e+5	0	42.15
5^3	$\overline{x}$	9.39e+4	58.14	5969.77	4.98e+5	500	2360.64
	$\widetilde{x}$	7.12e+4	55	5959.5	4.62e+5	500	2359
	min	**7.93**	32	5525	2.88e+5	500	2147
	max	4.32e+5	123	6392	1.07e+6	500	2570
	σ	9.33e+4	18.12	148.19	1.38e+5	0	70.92

For problems of linear elasticity, the median shows for $N \in \{64, 125\}$ (in Table 5.11) and $N = 64$ (in Table 5.13) subdomains that the majority of problems bears a condition number below 1e+4 when the coarse space of Algorithm II is used. However, the arithmetic mean points out that there are several problems with higher condition numbers if this coarse space is used. Let us just note that "several problems" for $N = 64$ subdomains and Table 5.13 even means 46 of 100 runs. Even worse, for $N = 125$ subdomains, Algorithm II exhibited in 21 and in 87 of 100 runs, respectively, a condition number of at least 1e+4; in 21 and in 33 cases, respectively, even a condition number of 1e+5 or higher is observed; see Tables 5.11 and 5.13.

Using Algorithm II for the diffusion equation leads in 71 ($N = 64$) and 73 ($N = 125$) of 100 runs to condition numbers of 1e+5 or larger. Except for the larger number of local eigenvalue problems, Algorithms Ia, Ib, and Ic perfom comparably for diffusion and linear elasticity. For the diffusion problem, the condition number of these algorithms is always lower than ≈ 15, and convergence is reached within 35 iterations.

We see that, by investing fewer or around 1% of additional constraints resulting from our edge eigenvalue problems, our Algorithms Ia, Ib, and Ic can guarantee a condition number around TOL. This shows that this additional amount of work is worthwile and can guarantee a small condition number and convergence within a reasonable number of PCG iterations.

5.4.6 Almost incompressible linear elasticity

In this section, we consider a linear elastic material which consists of compressible and almost incompressible parts. The compressible material parts have a Poisson ratio of $\nu = 0.3$ and for the almost incompressible parts we consider different values of Poisson's ratio with $0.45 \leq \nu < 0.5$. We also consider different distributions of Young's modulus in the material, allowing for large coefficient jumps, too. Let us note that such large coefficient jumps in the Young modulus, and simultaneously letting the Poisson ratio ν approach the incompressible limit 0.5, can lead to very ill-conditioned local matrices $K_{BB}^{(i)}$.

We use inf-sup stable $\mathcal{Q}_2 - \mathcal{P}_0$ finite elements for both, the compressible and the almost incompressible parts. We present numerical results for three different material distributions. Note that the decomposition by METIS (see [60]) is less irregular in these experiments since the irregular partitioning is performed based on brick elements instead of tetrahedrons; see Figure 5.11 (right).

In our first set of experiments, we consider a distribution of the Poisson ration in layers of ν_1 and ν_2. The layers have a thickness of two elements in x_3

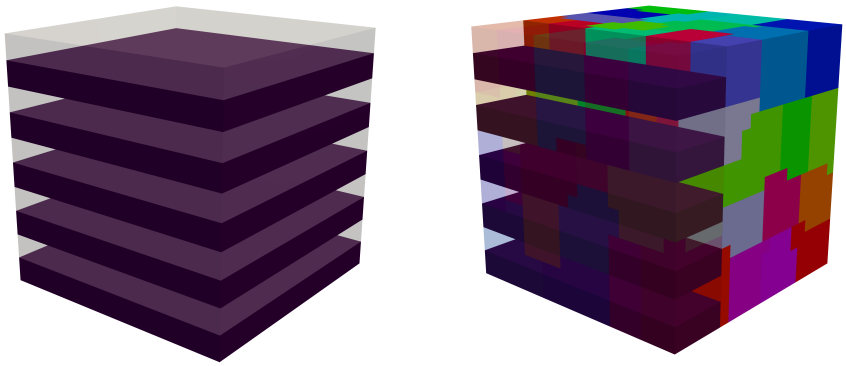

Figure 5.11: *Layered distribution on the unit cube for 64 subdomains (coefficients and irregular partitioning).* Layers of an almost incompressible material with varying ν_1, shown in dark purple, alternate with layers of a compressible material with $\nu_2 = 0.3$, shown in light, half-transparent gray (left). Irregular decomposition for 64 subdomains; higher values ν_1 are again shown in dark purple; subdomains shown in different colors; left quarter of the domain ($x > \frac{3}{4}$) made half-transparent (right). [64]

Table 5.14: *Adaptive FETI-DP (Alg. Ia, II, and III) with ρ-scaling and balancing approach.* Almost incompressible linear elasticity of layered distribution with layers of ν_1 as given alternating with layers of $\nu_2 = 0.3$ on the unit cube; E = 1 for the whole domain; $\mathcal{Q}_2 - \mathcal{P}_0$ finite element discretization with $1/h = 5N^{1/3}$ for $N = 4^3$ and irregular partitioning of the domain; see Figure 5.11 (right). Coarse spaces for TOL = 10 for all generalized eigenvalue problems. Notation as in Table 5.4. [64]

Adaptive FETI-DP: *Algorithms Ia, II, and III* (Balancing)

$N = 4^3$ – $1/h = 5N^{1/3}$ – layered distribution – irregular partitioning

	Algorithm Ia				*Algorithm II*			*Algorithm III*		
ν_1	κ	*its*	$\lvert U\rvert$	$\#\mathcal{E}_{evp}$	κ	*its*	$\lvert U\rvert$	κ	*its*	$\lvert U\rvert$
0.45	**6.83**	27	3804	15 (4.8%)	**6.83**	27	3800	**7.72**	29	712
0.499	**7.11**	28	4042	15 (4.8%)	**7.11**	28	4038	**8.41**	31	757
0.49999	**7.12**	28	4051	15 (4.8%)	**7.12**	28	4047	**8.62**	31	759
0.4999999	**7.12**	28	4051	15 (4.8%)	**7.12**	28	4047	**8.62**	31	759
0.499999999	**7.12**	28	4051	15 (4.8%)	**7.12**	28	4047	**8.62**	32	759

Table 5.15: *Adaptive FETI-DP (Alg. Ia, II, and III) with ρ-scaling and balancing approach.* Almost incompressible linear elasticity of composite material no. 2 with $E_1 = 1$ and $\nu_2 = 0.3$ surrounding $4N^{2/3}$ beams with $E_2 = 1e+3$ and ν_1 as given on the unit cube; $\mathcal{Q}_2 - \mathcal{P}_0$ finite element discretization with $1/h = 5N^{1/3}$ for $N = 4^3$ and irregular partitioning of the domain; see Figure 5.11 with different material parameters (right). Coarse spaces for TOL = 10 for all generalized eigenvalue problems. Notation as in Table 5.4. [64]

Adaptive FETI-DP: *Algorithms Ia, II, and III* (Balancing)

$N = 4^3$ – $1/h = 5N^{1/3}$ – composite material no. 2 – irregular partitioning

	Algorithm Ia				*Algorithm II*			*Algorithm III*		
ν_1	κ	*its*	$\|U\|$	$\#\mathcal{E}_{evp}$	κ	*its*	$\|U\|$	κ	*its*	$\|U\|$
0.45	**9.04**	31	6560	15 (4.8%)	**9.04**	31	6556	**12.27**	37	1239
0.499	**13.08**	34	7330	15 (4.8%)	**13.08**	34	7326	**34.71**	50	1402
0.49999	**8.84**	31	7571	15 (4.8%)	**8.84**	31	7564	589.80	98	1460
0.4999999	**8.80**	31	7576	15 (4.8%)	**8.80**	31	7569	796.50	106	1461
0.499999999	**8.80**	31	7576	15 (4.8%)	**8.80**	31	7569	799.90	120	1461

Table 5.16: *Adaptive FETI-DP (Alg. Ia, II, and III) with ρ-scaling and balancing approach.* Almost incompressible linear elasticity of homogeneous material with $E = 1$ and ν as given on the unit cube; $\mathcal{Q}_2 - \mathcal{P}_0$ finite element discretization with $1/h = 5N^{1/3}$ for $N = 4^3$ and irregular partitioning of the domain; see Figure 5.11 with different material parameters (right). Coarse spaces for TOL = 10 for all generalized eigenvalue problems. Notation as in Table 5.4. [64]

Adaptive FETI-DP: *Algorithms Ia, II, and III* (Balancing)

$N = 4^3$ – $1/h = 5N^{1/3}$ – homogeneous material – irregular partitioning

	Algorithm Ia				*Algorithm II*			*Algorithm III*		
ν	κ	*its*	$\|U\|$	$\#\mathcal{E}_{evp}$	κ	*its*	$\|U\|$	κ	*its*	$\|U\|$
0.45	**6.52**	27	4085	15 (4.8%)	**6.52**	27	4081	**7.69**	29	764
0.499	**7.34**	30	4736	15 (4.8%)	**7.34**	29	4732	**22.17**	43	892
0.49999	**6.81**	28	4909	15 (4.8%)	**12.18**	29	4900	1.98e+3	88	933
0.4999999	**6.81**	28	4913	15 (4.8%)	1.06e+3	38	4903	1.97e+5	119	934
0.499999999	**6.81**	28	4913	15 (4.8%)	1.06e+5	59	4903	1.97e+7	144	934

direction. Here, ν_1 takes different values whereas $\nu_2 = 0.3$; see Figure 5.11. We set $\mathrm{E} = 1$ on the complete domain Ω. For all three algorithms, the condition numbers and iteration counts are uniformly bounded, independently of ν_1 approaching 0.5. All algorithms also yield condition numbers and iteration counts of a comparable size; see Table 5.14. For the material distributions considered in this example, Algorithm III seems to be sufficient.

The second example is composite material no. 2; see Figure 5.7. Note again that, here, the irregular partitioning differs from the decomposition used in Section 5.4.3 (depicted in Figure 5.8) since the partitioning is performed based on brick elements instead of tetrahedrons. Here, we use $\mathrm{E}_1 = 1$ and $\mathrm{E}_2 = 1e+3$ instead 1e+6. We consider a variable Poisson ratio $\nu_1 \in [0.3, 0.5)$ for all finite elements with $\mathrm{E}_1 = 1$ and a fixed Poisson ratio $\nu_2 = 0.3$ for those finite elements with $\mathrm{E}_2 = 1e + 3$. Table 5.15 indicates uniformly bounded condition numbers and iteration counts for Algorithms Ia and II. For Algorithm III, the condition number and the iteration counts still seem to be bounded but at a higher level. Algorithms Ia and II perform as in the compressible case but at the cost of a larger coarse space.

In our third set of experiments, we consider an almost incompressible material with both, ν and $\mathrm{E} = 1$ constant on the complete domain. Table 5.16 shows that this becomes a hard problem for Algorithm III and also for Algorithm II. With ν approaching the incompressible limit, the condition number of the mentioned algorithms is several magnitudes larger than this of Algorithm Ia. In contrast to the other algorithms, Algorithm Ia can guarantee a small condition number and an almost constant number of PCG iterations.

Remark 5.9. *Note that the automatic coarse space constructed here for the almost incompressible case is slightly larger than the a priori coarse spaces constructed in [48] and [50], which introduce only a single (additional) constraint for each subdomain in 2D to cope with almost incompressible elasticity [48], or where all face constraints can be summed to a single constraint in 3D [50, 48].*

5.4.7 Reducing the number of eigenvalue problems based on the residual

We now consider the heuristic approach described in Section 5.2.3.2 to reduce the number of eigenvalue problems. We apply this approach to our Algorithm Ib for compressible elasticity and to Algorithm Ia for test problems with almost incompressible contributions. Note that this approach can equally be adopted for the coarse spaces of Algorithms Ic, II, or III.

Table 5.17: *Adaptive FETI-DP (Alg. Ib with residual heuristic) ρ-scaling and balancing approach.* Compressible linear elasticity of composite material no. 1 with $\mathrm{E}_1 = 1$ and $N^{2/3}$ beams with $\mathrm{E}_2 = 1e+6$ on the unit cube; $\nu = 0.3$ for the whole domain; conforming $\mathcal{P}_1$ finite element discretization with $1/h = 6N^{1/3}$ and irregular partitioning of the domain; see Figure 5.1. Coarse spaces for $\mathrm{TOL} = 10$ for all generalized eigenvalue problems. $\#\mathrm{EVP}_U$ denotes the number of solved eigenvalue problems, $\#\mathrm{EVP}_{\mathrm{disc\_res}}$ denotes the number of eigenvalue problems discarded by the residual heuristics, and $\#\mathrm{EVP}_{\mathrm{disc\_Ib}}$ denotes the number of eigenvalue problems discarded by the neighborhood strategy. All other notation as in Table 5.4. For the results without residual heuristic of Section 5.2.3.2, see Table 5.6. [64]

Adaptive FETI-DP: *Algorithm Ib* w/ residual heuristic (Balancing)
$1/h = 6N^{1/3}$ – composite material no. 1 – irregular partitioning

$\tau_2 = 0.01, \tau_\infty = 10\tau_2$							
N	λ_{min}	λ_{max}	*its*	$\lvert U\rvert$	$\#\mathrm{EVP}_U$	$\#\mathrm{EVP}_{\mathrm{disc\_res}}$	$\#\mathrm{EVP}_{\mathrm{disc\_Ib}}$
3^3	1.00	**8.79**	35	629	63	36	1
5^3	1.00	**15.71**	40	3229	312	267	13
7^3	1.00	120.10	72	9095	937	812	38
$\tau_2 = 0.001, \tau_\infty = 10\tau_2$							
N	λ_{min}	λ_{max}	*its*	$\lvert U\rvert$	$\#\mathrm{EVP}_U$	$\#\mathrm{EVP}_{\mathrm{disc\_res}}$	$\#\mathrm{EVP}_{\mathrm{disc\_Ib}}$
3^3	1.00	**8.79**	35	632	64	35	1
5^3	1.00	**10.63**	37	3260	326	253	13
7^3	1.00	**15.50**	40	9269	998	751	38

We report the number of eigenvalue problems solved and denoted by $\#\mathrm{EVP}_U$ as well the number of eigenvalue problems discarded by our heuristic approach of Section 5.2.3.2, denoted by $\#\mathrm{EVP}_{\mathrm{disc\_res}}$; see Tables 5.17, 5.18, and 5.19. For the cases, where Algorithm Ib is used, we also report the number of edge eigenvalue problems discarded inherently by this algorithm as $\#\mathrm{EVP}_{\mathrm{disc\_Ib}}$; cf. Section 5.2.2. Here, we report λ_{min} and λ_{max} instead of κ.

For the computation of the residual r (see Section 5.2.3.2), we use $\lambda^{(0)} = 0$ and conduct one iteration of the underlying conjugate gradient algorithm.

We also consider different values of τ_2, namely $\tau_2 \in \{0.01, 0.001\}$, each with $\tau_\infty = 10\tau_2$. Using a larger value of τ_2, e.g., setting $\tau_2 = 0.1$, does not give acceptable results anymore in about half of our test cases. We refrain from reporting the details.

Table 5.18: *Adaptive FETI-DP (Alg. Ib with residual heuristic) ρ-scaling and balancing approach.* Compressible linear elasticity of randomly distributed coefficients with 80% coefficients with $\mathrm{E}_1 = 1$ and 20% coefficients with $\mathrm{E}_2 = 1e+6$ on the unit cube; $\nu = 0.3$ for the whole domain; conforming $\mathcal{P}_1$ finite element discretization with $1/h = 5N^{1/3}$ and irregular partitioning of the domain; see Figure 5.10. Coarse spaces for $\mathrm{TOL} = 10$ for all generalized eigenvalue problems. Notation as in Table 5.11 and 5.17. For the results without heuristic of Section 5.2.3.2, see Table 5.13. [64]

Adaptive FETI-DP: *Algorithm Ib* w/ residual heuristic (Balancing)
$1/h = 5N^{1/3}$ – random coefficients (80/20) – irregular partitioning
$\tau_2 = 0.001, \tau_\infty = 10\tau_2$

N		λ_{min}	λ_{max}	*its*	$\lvert U\rvert$	$\#\mathrm{EVP}_U$	$\#\mathrm{EVP}_{\mathrm{disc\_res}}$	$\#\mathrm{EVP}_{\mathrm{disc\_Ib}}$
5^3	$\overline{x}$	1.00	**9.16**	32.97	6010.63	530.42	24.57	0.01
	$\widetilde{x}$	1.00	**9.09**	33	6005	530.5	24.5	0
	min	1.00	**8.02**	32	5574	520	17	0
	max	1.00	**11.16**	34	6441	538	34	1
	σ	0	0.55	0.64	149.97	4.35	4.33	0.10

The choice $\tau_\infty = 10\tau_2$ is heuristic and motivated from initial testing. The use of τ_∞ and τ_2 is motivated by the fact that localized high peaks and widespread heterogeneities with a (10 times) lower value should both trigger the adaptivity.

For our composite material no. 1, we observe good or acceptable behavior of our heuristics, and up to roughly 50% of the eigenvalue problems are saved; see Table 5.17. Nevertheless, to keep the condition number at the order of TOL, we have to use $\tau_2 = 0.001$.

We again turn towards randomly distributed cofficients which turned out to be the most challenging problem in the previous sections. For the corresponding Table 5.18, we additionally report that with $\tau_2 = 0.001$ the condition number is low in all runs, and the iteration number does not exceed 40. The heuristics works well but the savings are modest. Note that Algorithm Ib is identical to Algorithm Ia in 99 of the 100 runs for the randomized coefficients. Due to the high oscillation, high coefficients are likely to be present at all edges.

From our results in Table 5.19, we see that we can save a substantial number of eigenvalue problems when ν is still far away from the incompressible limit. As ν approaches the incompressible limit, the computational savings are more modest.

Table 5.19: *Adaptive FETI-DP (Alg. Ia with residual heuristic) ρ-scaling, and balancing approach.* Almost incompressible linear elasticity of composite material no. 2 with $\mathrm{E}_1 = 1$ and $\nu_2 = 0.3$ surrounding $4N^{2/3}$ beams with $\mathrm{E}_2 = 1e+3$ and ν_1 as given on the unit cube; $\mathcal{Q}_2 - \mathcal{P}_0$ finite element discretization with $1/h = 5N^{1/3}$ for $N = 4^3$ and irregular partitioning of the domain; see Figure 5.11 with different material parameters (right). Coarse spaces for $\mathrm{TOL} = 10$ for all generalized eigenvalue problems. Notation as in Table 5.17. For the results without heuristic of Section 5.2.3.2, see Table 5.15. [64]

Adaptive FETI-DP: *Algorithm Ia* w/ residual heuristic (Balancing)
$N = 4^3$ – $1/h = 5N^{1/3}$ – composite material no. 2 – irregular partitioning
$\tau_2 = 0.01, \tau_\infty = 10\tau_2$

ν_1	λ_{min}	λ_{max}	*its*	$\lvert U\rvert$	$\#\mathrm{EVP}_U$	$\#\mathrm{EVP}_{\mathrm{disc\_res}}$
0.45	1.00	**30.09**	55	4038	93	217
0.499	1.00	67.27	56	6535	253	57
0.49999	1.00	**37.98**	50	6988	272	38
0.4999999	1.00	**38.00**	50	6993	272	38

5.4.8 Approximate solutions of the local eigenvalue problems

The numerical solution of the local generalized eigenvalue problems can be expensive but their "exact" solution is required by the current theory. Additionally, the construction of the operators of the eigenvalue problem can also be expensive if an eigensolver is used that needs the matrices in explicit form. However, an approximation of the extreme eigenvectors by an iterative method is sufficient in practice. This was already reported to be successful for adaptive BDDC using LOBPCG; see [120, 121].

In Tables 5.20 and 5.21, we show results for $1/h = 15N^{1/3}$ using an iterative eigenvalue problem solver. We use an implementation of LOBPCG (see [86, 85]) with a block size of 10, preconditioned by a Cholesky decomposition of the right hand side of the eigenvalue problem. We conduct a given number of maximum iterations as indicated in the tables. If the smallest computed eigenvalue of the considered block exceeds the tolerance TOL, we proceed with another pass of the algorithm and search for 10 new eigenvectors in a subspace orthogonal to the previously computed eigenvector approximations. All approximate eigenvectors corresponding to approximate eigenvalues above TOL are added to the coarse space.

In Table 5.20, we consider a variable number of subdomains $N \in \{3^3, 4^3, 5^3\}$ and use a single iteration of LOBPCG. This already seems to work acceptably. For $N = 3^3$ subdomains, we also consider different values for the maximum

Table 5.20: *Adaptive FETI-DP (Alg. Ia-III with one iteration LOBPCG) with ρ-scaling and balancing approach.* Compressible linear elasticity of composite material no. 1 with $E_1 = 1$ and $N^{2/3}$ beams with $E_2 = 1e+6$ on the unit cube; $\nu = 0.3$ for the whole domain; conforming $\mathcal{P}_1$ finite element discretization with $1/h = 15N^{1/3}$ and irregular partitioning of the domain; see Figure 5.1. Coarse spaces for TOL = 10 for all generalized eigenvalue problems. Solution of the local eigenvalue problems by LOBPCG with one iteration. Notation as in Table 5.4. [64]

Adaptive FETI-DP: *Algorithms Ia, Ib, Ic, II, and III* (Balancing)
$1/h = 15N^{1/3}$ – composite material no. 1 – irregular partitioning

	Algorithms Ia, Ib, and Ic					*Algorithm II*			*Algorithm III*		
N		κ	*its*	$\lvert U\rvert$	$\#\mathcal{E}_{evp}$	κ	*its*	$\lvert U\rvert$	κ	*its*	$\lvert U\rvert$
3^3	a)	**26.74**	50	2360	0 (0%)						
	b)	**26.74**	50	2360	0 (0%)	**26.74**	50	2360	8.028e+5	150	462
	c)	**26.77**	50	1228	0 (0%)						
4^3	a)	**28.37**	54	4472	2 (0.7%)						
	b)	**28.37**	54	4472	0 (0%)	**28.37**	54	4472	4.315e+5	215	863
	c)	**28.39**	55	1962	0 (0%)						
5^3	a)	**43.87**	61	10178	8 (1.2%)						
	b)	**43.87**	61	10178	0 (0%)	**43.87**	61	10178	6.86e+5	288	1941
	c)	**43.93**	62	5334	0 (0%)						

iteration count, i.e., $\{1, 2, 5, 10, 200\}$ and with a requested tolerance for convergence of the LOBPCG solver of 1e-5; see Table 5.21. We see that, in terms of resulting global PCG iterations, exceeding a number of five LOBPCG iterations does not seem to be worthwhile. Note that the METIS decomposition for $N = 3^3$ subdomains here does not lead to any edge eigenvalue problem. Therefore, Algorithms Ia, Ib, and II behave identically. Note that in some cases, too many iterations of the LOBPCG solver might not be helpful and even lead to worse convergence behavior of the adaptive FETI-DP approach than just several iterations; for details see the numerical results in Chapter 6.

5.5 Conclusion on adaptive FETI-DP using balancing and deflation

In this chapter, we have presented an adaptive coarse space approach for FETI-DP methods (Algorithm Ia) including a condition number bound for general coefficient jumps inside subdomains and across subdomain boundaries as well as for almost incompressible elastic materials in 3D. The bound only depends

Table 5.21: *Adaptive FETI-DP (Alg. Ia-III with LOBPCG) with ρ-scaling and balancing approach.* Compressible linear elasticity of composite material no. 1 with $E_1 = 1$ and $N^{2/3}$ beams with $E_2 = 1e+6$ on the unit cube; $\nu = 0.3$ for the whole domain; conforming $\mathcal{P}_1$ finite element discretization with $1/h = 15^{1/3}$ for $N = 3^3$ and irregular partitioning of the domain; see Figure 5.1. Coarse spaces for TOL = 10 for all generalized eigenvalue problems. Solution of the local eigenvalue problems by LOBPCG with different maximum iteration numbers. Notation as in Table 5.4. [64]

Adaptive FETI-DP: *Algorithms Ia, Ib, Ic, II, and III* (Balancing)

$N = 3^3$ – $1/h = 15N^{1/3}$ – composite material no. 1 – irregular partitioning

	Algorithms Ia, Ib, and Ic					*Algorithm II*			*Algorithm III*		
LOBPCG max. its		κ	*its*	$\lvert U\rvert$	$\#\mathcal{E}_{evp}$	κ	*its*	$\lvert U\rvert$	κ	*its*	$\lvert U\rvert$
1	a)	**26.74**	50	2360	0 (0%)	**26.74**	50	2360	8.03e+5	150	462
	b)	**26.74**	50	2360	0 (0%)						
	c)	**26.77**	50	1228	0 (0%)						
2	a)	**17.65**	41	2623	0 (0%)	**17.65**	41	2623	7.76e+5	123	505
	b)	**17.65**	41	2623	0 (0%)						
	c)	**17.65**	42	1322	0 (0%)						
5	a)	**10.04**	37	2762	0 (0%)	**10.04**	37	2762	7.71e+5	126	531
	b)	**10.04**	37	2762	0 (0%)						
	c)	**12.86**	38	1374	0 (0%)						
10	a)	**12.61**	38	2782	0 (0%)	**12.61**	38	2782	7.70e+5	128	541
	b)	**12.61**	38	2782	0 (0%)						
	c)	**12.85**	40	1396	0 (0%)						
200	a)	**11.55**	38	3108	0 (0%)	**11.72**	38	3108	7.70e+5	113	686
	b)	**11.55**	38	3108	0 (0%)						
	b)	**12.86**	38	1665	0 (0%)						

on geometrical constants and a prescribed tolerance from local eigenvalue problems. Our approach is based on the classical adaptive approach from [93, 120] but we use a small number (fewer than 5 percent) of additional edge eigenvalue problems. Our experiments support our theory and show that the new method is able to cope with situations where the classical approach fails. We have also introduced two adaptive algorithms reducing the number of eigenvalue problems and constraints from Algorithm Ia which work very well, i.e., Algorithms Ib and Ic; see Section 5.2.2. Moreover, we have presented two additional strategies to further reduce the number of eigenvalue problems and adaptively computed constraints; see Sections 5.2.3.1 and 5.2.3.2.

We have seen in our numerical experiments that the classical coarse space of [93, 120] (Algorithm III) can be sufficient if coefficient jumps do only occur at subdomain faces. However, if jumps are present across or along subdomain

edges, in general, neither a small condition number nor a low count of Krylov iterations (or even convergence) can be guaranteed by Algorithm III, which does not use any edge constraints. For difficult coefficient distributions, at least the edge constraints resulting from face eigenvalue problems should be added to the coarse space. The resulting approach (Algorithm II) then can cope with a larger number of test problems. However, only Algorithms Ia, Ib, and Ic have been able to guarantee a low condition number for all our test cases. Although only Algorithm Ia is covered by our provable bound, Algorithm Ib performs almost identically. Algorithm Ic performs still comparably but can also save a considerable number of constraints; e.g., up to 40%. In simple cases, where Algorithm III is already successful, Algorithm Ic indeed reduces to Algorithm III.

Our experiments show that the condition number can quite precisely be controlled by the tolerance TOL even if the reduction strategies of Algorithm Ib or Ic are used.

For our problems from almost incompressible elasticity, among Algorithms Ia, II, and III, only Algorithm Ia performed well for all our test problems. Algorithms Ib and Ic have not been tested. If the neighborhood strategies of Algorithms Ib and Ic are adapted such that not only the Young modulus but also the Poisson ratio is considered, these algorithms are expected to cope with the situation, too.

For regular decompositions, the number of edge eigenvalue problems in Algorithm Ia is quite high, but can be reduced considerably by switching to Algorithms Ib and Ic. For irregular decompositions, which is the more relevant case, the number of additional edge eigenvalue problems to be computed by Algorithm Ia is often only in a low single-digit percentage range and can further be reduced by switching to Algorithms Ib and Ic.

Compared to Algorithm II, the number of additional constraints in Algorithms Ia and Ib is typically small, i.e., for our test problems, the mean is only between 1% to 3% of additional constraints. Furthermore, compared to Algorithm II, Algorithm Ic reduces the number of edge constraints from face eigenvalue problems. Comparing the computational overhead of Algorithms Ia, Ib, and Ic to Algorithm III is difficult in some way since the additional constraints are mostly necessary to obtain convergence.

Our heuristic strategy from Section 5.2.3.2 to reduce the number of eigenvalue problems can save a substantial amount of computational work but requires some tuning of tolerances. In our numerical experiments, selecting a

specific tolerance $0.001 \leq \tau_2 \leq 0.01$ with $\tau_\infty = 10\tau_2$ saved work while keeping the algorithm stable and reliable.

Considering the computational overhead for the solution of the eigenvalue problems, we have also shown that already an application of an iterative eigenproblem solver with just a few iterations results in a robust coarse space.

Altogether, the adaptive FETI-DP Algorithms Ia, Ib, and Ic with balancing or deflation can be used to solve hard problems which could not be solved with standard FETI-DP or even adaptive FETI-DP without edge eigenvalue problems (Algorithm II or III). Nevertheless, if a large and hard problem is considered, the adaptive coarse space can become large and an inexact solution of the coarse problem might be attractive. However, as shown in [80], the deflation or balancing approach is fragile with respect to inexactness of the coarse problem solution and the method can become unstable or even converge to a wrong solution. Therefore, the goal of the next chapter is to develop a corresponding FETI-DP approach using the generalized transformation-of-basis approach from Section 4.5. Then, the results can be also transfered to obtain an adaptive BDDC method.

6 FETI-DP and BDDC with adaptive coarse spaces using the generalized transformation-of-basis approach

6.1 Preliminaries

In this section, we revisit the adaptive FETI-DP method from the previous chapter and construct a corresponding method without using deflation or balancing. Central to this transition is the generalized transformation-of-basis approach presented in Section 4.5. By using the generalized transformation-of-basis approach, we also develop a corresponding adaptive BDDC method. Parts of this chapter have already been published in modified or unmodified form by the author of this thesis and his coauthors in [67, 68, 70].

In the previous chapter, in Section 5.1, we have reflected that for highly heterogeneous problems, the a priori coarse space might not be sufficient to ensure convergence and therefore adaptive strategies, as established in Section 5.2, are needed.

In this chapter, we explain how to define the new adaptive constraint vectors (in the space of displacements) for the generalized transformation-of-basis approach. We also relate those vectors to the deflation vectors for FETI-DP, which have been used in the previous chapter and which are defined in the Lagrange multiplier space.

In order to demonstrate the need of the generalized transformation-of-basis approach, we consider a preliminary example and anticipate results for adaptive FETI-DP and BDDC using the standard and the generalized transformation-of-basis approach. In the standard approach, we only have one set of primal constraints. In the generalized transformation-of-basis approach, we use two different sets of primal variables and we allow an interaction of a posteriori dual and a posteriori primal variables through the scaling.

Let us consider the diffusion equation on $\Omega = [0,1]^3$ partitioned into eight cubic subdomains and with homogeneous Dirichlet boundary for the face with $x = 0$ and homogeneous Neumann boundary elsewhere; see Figure 6.1 (Dirichlet

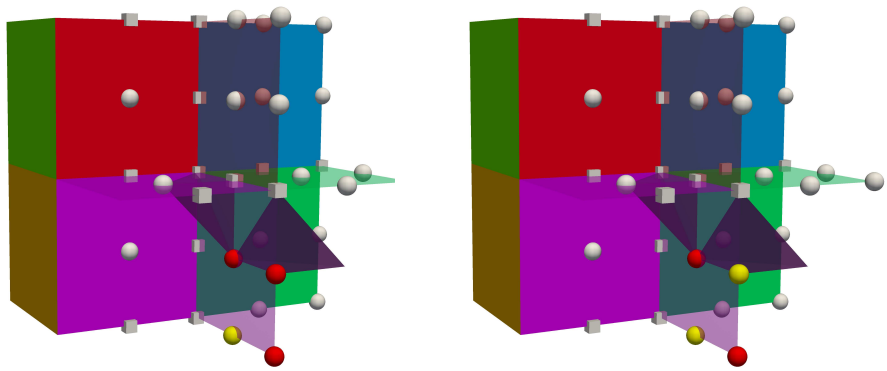

Figure 6.1: *Minimal example to motivate the need for the generalized transformation-of-basis approach (regular decomposition of the unit cube into eight subdomains).* On two tetrahedra, we have high coefficients $\mathrm{E}_2 = 1e+6$, shown in dark purple, all other tetrahedra have $\mathrm{E}_1 = 1$ and are not shown; of the front part of the domain ($y < \frac{1}{2}$) only the faces and edges are shown in half-transparent colors. Initial (or a priori) primal vertex constraints (Π') are indicated by gray cubes. Initial dual variables are indicated by spheres. Red spheres indicate a posteriori primal variables (Π) that are assembled for the transformed basis and yellow spheres represent the remaining dual variables. Adaptive approach for multiplicity-scaling (left) and ρ-scaling (right).

boundary on the left; face with $y = 0$ in front). We consider the closed face (the open face plus a bent edge on the Neumann boundary) with four dual variables (yellow and red spheres) that yielded three and two constraints, respectively, for multiplicity- (left) and ρ-scaling (right), respectively. After a transformation of basis, the variables at the red nodes are assembled and thus, made primal.

We present results for four different algorithms. The rows in Table 6.1 refer to the results for the algorithms described in the following enumeration. Note that the iteration counts are always small since we only consider a minimal example with a small number of eight subdomains and only 125 global nodes.

1. **Adaptive FETI-DP and BDDC with multiplicity-scaling**: If multiplicity-scaling is used, the scaling needs not to be transformed (even for heterogeneous coefficients) since the theory of [80] applies and the standard transformation-of-basis approach can be used. However, for

heterogeneous coefficients, the adaptive coarse space can become large and another scaling is advised; see, e.g., [75, 68] or Section 6.5.3.

2. **Adaptive FETI-DP and BDDC with ρ-scaling**:
   a) For ρ-scaling, we present results for the case if the scaling is not transformed and consequently no interaction between a posteriori dual and a posteriori primal variables is admitted.
   b) For ρ-scaling, we also present results for the case if the scaling is transformed but no interaction between a posteriori dual and a posteriori primal variables is admitted. This corresponds to the case described in Example 4.1 where $\widehat{d}_{ry} = 0$ is set. For the standard theory, $\widehat{d}_{ry} = 0$ has to be assumed since, otherwise, we would generally obtain continuous but nonzero values in the a posteriori primal variables after $\widehat{B}_D^T$ had been applied.
   c) Last, for ρ-scaling, we present results for the generalized transformation-of-basis approach to show the difference in the condition numbers of the generalized approach and of the approaches of the two previous items.

As can be seen from this example, although the convergence is fast for this small example, the incorrect handling of a posteriori primal variables can result in a high condition number. Thus, for arbitrary constraints from generalized eigenvalue problems based on an a priori scaling, which is not multiplicity-scaling, the standard theory cannot be applied.

6.2 A family of adaptive coarse spaces

As in the previous chapter, we now introduce local adaptive constraints for FETI-DP; see Section 6.2.1. As in Section 5.2.2, we can introduce adaptive methods with (almost) the same adaptive coarse space, only some minor restrictions on the constraints of the generalized transformation-of-basis approach have to be respected; see Sections 4.5 and 6.2.3. Additionally, we derive adaptive BDDC methods with essentially the same spectrum. We again refer to [93, 94, 72, 22, 74, 75, 63, 64, 7, 101, 17, 134, 103, 62] for (other) adaptive coarse spaces used in FETI-DP and BDDC methods.

6.2.1 Various adaptive constraints

Let us note that the local operators and the local generalized eigenvalue problems used in this chapter are identical to the ones from the previous chapter. To

Table 6.1: *Adaptive FETI-DP and BDDC (Alg. Ia) with multiplicity- and ρ-scaling and standard versus generalized transformation-of-basis approach.* Diffusion equation of material as in Fig. 6.1 with $\rho_1 = 1$ and $\rho_2 = 1e+6$ on the unit cube; conforming $\mathcal{P}_1$ finite element discretization with $1/h = 2N^{1/3}$ and regular partitioning of the domain. Coarse spaces for TOL $= 10$ for all generalized eigenvalue problems. 1.) untransformed multiplicity-scaling, 2a.) untransformed ρ-scaling without interaction of a posteriori dual and a posteriori primal variables, 2b.) transformed ρ-scaling without interaction, 2c.) transformed ρ-scaling with interaction (generalized transformation-of-basis appr.). Other notation as in Table 5.4.

Adaptive FETI-DP and BDDC:
(Standard and generalized transformation-of-basis approach)
$N = 2^3$ – $1/h = 2N^{1/3}$ – material as in Fig. 6.1 – regular partitioning

	FETI-DP			**BDDC**		
	$\lambda_{\min}$	$\lambda_{\max}$	*its*	$\lambda_{\min}$	$\lambda_{\max}$	*its*
1.)	1.00	**1.33**	7	1.00	**1.33**	7
2a.)	1.00	6.03e+3	10	1.00	6.03e+3	13
2b.)	1.00	1.42e+4	7	1.00	1.42e+4	12
2c.)	1.00	**1.38**	8	1.00	**1.38**	8

improve the readability of this section, we shortly rephrase the elementary operators already introduced in Section 5.2.1. For the motivation of the localized adaptive methods and detailed remarks, see Section 5.2. For the algorithms based on face eigenvalue problems, we also refer to [93, 120, 75].

We assume that all vertices of the decomposition are chosen to be primal and, additionally, that each nonstraight edge has at least three primal vertices; cf. Remark 5.3.

The face between the subdomains Ω_i and Ω_j is denoted by $\mathcal{F}^{ij}$ and its closure by $\overline{\mathcal{F}}^{ij}$. We define

$$B_{\overline{\mathcal{F}}^{ij}} := \left(B^{(i)}_{\overline{\mathcal{F}}^{ij}} \; B^{(j)}_{\overline{\mathcal{F}}^{ij}}\right) \tag{6.1}$$

as the submatrix of $\left(B^{(i)} \; B^{(j)}\right)$ consisting of all the rows that contain exactly one $+1$ and one -1. Analogously,

$$B_{D,\overline{\mathcal{F}}^{ij}} := \left(B^{(i)}_{D,\overline{\mathcal{F}}^{ij}} \; B^{(j)}_{D,\overline{\mathcal{F}}^{ij}}\right) \tag{6.2}$$

is the submatrix of $\begin{pmatrix} B_D^{(i)} & B_D^{(j)} \end{pmatrix}$, i.e., the scaled variant of $B_{\overline{\mathcal{F}}^{ij}}$. We then define

$$S_{ij} := \begin{pmatrix} S^{(i)} & 0 \\ 0 & S^{(j)} \end{pmatrix} \in \mathbb{R}^{(n_i+n_j)\times(n_i+n_j)} \quad \text{and} \quad P_{D,\overline{\mathcal{F}}^{ij}} := B^T_{D,\overline{\mathcal{F}}^{ij}} B_{\overline{\mathcal{F}}^{ij}}. \tag{6.3}$$

By removing all rigid body modes of either the single subdomains or the coupled pair of subdomains (cf. Figure 5.3), we obtain the local generalized eigenvalue problem: Find $w_{ij} \in \left(\ker S_{ij}\right)^{\perp}$ such that

$$\langle P_{D,\overline{\mathcal{F}}^{ij}} v_{ij}, S_{ij} P_{D,\overline{\mathcal{F}}^{ij}} w_{ij}\rangle = \mu_{ij}\langle v_{ij}, S_{ij} w_{ij}\rangle \qquad \forall v_{ij} \in \left(\ker S_{ij}\right)^{\perp}. \tag{6.4}$$

To obtain an explicit expression for the (positive definite) right hand side operator on the subspace $\left(\ker S_{ij}\right)^{\perp}$, we use the two separate projections Π_{ij} and $\overline{\Pi}_{ij}$. We denote the ℓ_2-orthogonal projection from $W_i \times W_j$ to $\widetilde{W}_{ij}$ by Π_{ij}. The space $\widetilde{W}_{ij}$ is the space of functions in $W_i \times W_j$ that are continuous in the primal variables shared by Ω_i and Ω_j. The ℓ_2-orthogonal projection from $W_i \times W_j$ to range $(\Pi_{ij} S_{ij} \Pi_{ij} + \sigma(I - \Pi_{ij}))$ is denoted by $\overline{\Pi}_{ij}$. Here, σ is a positive constant used for stability reasons; see [93, 94].

We then solve the following generalized eigenvalue problems

$$\begin{aligned} &\overline{\Pi}_{ij}\Pi_{ij} P^T_{D,\overline{\mathcal{F}}^{ij}} S_{ij} P_{D,\overline{\mathcal{F}}^{ij}} \Pi_{ij}\overline{\Pi}_{ij} w_{ij} \\ &\qquad = \mu_{ij}(\overline{\Pi}_{ij}(\Pi_{ij} S_{ij} \Pi_{ij} + \sigma(I - \Pi_{ij}))\overline{\Pi}_{ij} + \sigma(I - \overline{\Pi}_{ij}))w_{ij}, \end{aligned} \tag{6.5}$$

for $\mu_{ij} \geq \text{TOL}$.

To avoid a coupling of the different closed faces in the coarse matrix, we split the constraints on the similar to (5.12) and (5.13).

Assume $\mu^r_{ij} \geq \text{TOL}$, then the constraint vector $c^r_{u,ij} := P^T_{D,\overline{\mathcal{F}}^{ij}} S_{ij} P_{D,\overline{\mathcal{F}}^{ij}} w^r_{ij} = B^T_{\overline{\mathcal{F}}^{ij}} c^r_{\lambda,ij}$ is split into a part on the open face

$$c^r_{u,ij,\mathcal{F}} := B^T_{\overline{\mathcal{F}}^{ij}} c^r_{\lambda,ij,\mathcal{F}} \tag{6.6}$$

and several edge parts

$$c^r_{u,ij,\mathcal{E}_m} := B^T_{\overline{\mathcal{F}}^{ij}} c^r_{\lambda,ij,\mathcal{E}_m}, \quad m = 1, 2, \ldots, \tag{6.7}$$

all extended by zero to the closure of the face. We can then enforce the open face constraint and the edge constraints

$$c^{r\,T}_{u,ij,\mathcal{F}} w_{ij} = 0, \tag{6.8}$$

$$c^{r\,T}_{u,ij,\mathcal{E}_m} w_{ij} = 0, \quad m = 1, 2, \ldots. \tag{6.9}$$

Note that the constraint vectors in (6.8) and (6.9) differ from the constraint vectors in (5.12) and (5.13) since, here, we constrain degrees of freedom while in the previous chapter we constrained the Lagrange multipliers. However, the constraints are identical.

As before, we also want to control control the jumps $w^{(i)} - w^{(k)}$ across the edge $\mathcal{E}^{ik}$ between subdomains Ω_i and Ω_k that do not share any face. As in the previous chapter, we define

$$B_{\mathcal{E}^{ik}} := \left(B^{(i)}_{\mathcal{E}^{ik}} \; B^{(k)}_{\mathcal{E}^{ik}}\right) \tag{6.10}$$

as the submatrix of $\left(B^{(i)} \; B^{(k)}\right)$ consisting of all the rows, which correspond to $\mathcal{E}^{ik}$ and that contain exactly one $+1$ and one -1. Analogously,

$$B_{D,\mathcal{E}^{ik}} := \left(B^{(i)}_{D,\mathcal{E}^{ik}} \; B^{(k)}_{D,\mathcal{E}^{ik}}\right) \tag{6.11}$$

is the submatrix of $\left(B^{(i)}_D \; B^{(k)}_D\right)$, i.e., the scaled variant of $B_{\mathcal{E}^{ik}}$. As in the previous chapter, two subdomains, Ω_i and Ω_k, can share more than one edge eigenvalue problem. Consequently, not all the rows of $\left(B^{(i)} \; B^{(k)}\right)$ that contain exactly one $+1$ and one -1 correspond to Lagrange multipliers on $\mathcal{E}^{ik}$.

As for the face eigenvalue problems, we have

$$S_{ik} := \begin{pmatrix} S^{(i)} & 0 \\ 0 & S^{(k)} \end{pmatrix} \in \mathbb{R}^{(n_i+n_k)\times(n_i+n_k)} \quad \text{and} \quad P_{D,\mathcal{E}^{ik}} := B^T_{D,\mathcal{E}^{ik}} B_{\mathcal{E}^{ik}}. \tag{6.12}$$

By again introducing the two projections Π_{ik} and $\overline{\Pi}_{ik}$ to remove the single and common rigid body modes of the two subdomains, we solve

$$\begin{aligned} &\overline{\Pi}_{ik}\Pi_{ik}P^T_{D,\mathcal{E}^{ik}}S_{ik}P_{D,\mathcal{E}^{ik}}\Pi_{ik}\overline{\Pi}_{ik}w_{ik} \\ &\qquad = \mu_{ik}(\overline{\Pi}_{ik}(\Pi_{ik}S_{ik}\Pi_{ik} + \sigma(I-\Pi_{ik}))\overline{\Pi}_{ik} + \sigma(I-\overline{\Pi}_{ik}))w_{ik} \end{aligned} \tag{6.13}$$

for eigenvectors w_{ik} with eigenvalue $\mu_{ik} \geq$TOL.

As in the previous chapter, this only has to be carried out for edges shared by more than three subdomains and in rare occasions, where thin faces do not contain any interior discretization nodes.

For all $\mu^r_{ik} \geq$ TOL, the constraints resulting from the edge eigenvalue problems are

$$w^{r\,T}_{ik} P^T_{D,\mathcal{E}^{ik}} S_{ik} P_{D,\mathcal{E}^{ik}} w_{ik} = c^{r\,T}_{\lambda,ik} B_{\mathcal{E}^{ik}} w_{ik} =: c^{r\,T}_{u,ik} w_{ik} = 0, \tag{6.14}$$

where w_{ik}^r are the corresponding eigenvectors and $c_{u,ik}^r = P_{D,\mathcal{E}^{ik}}^T S_{ik} P_{D,\mathcal{E}^{ik}} w_{ik}^r$ are the corresponding constraint vectors.

Hence, for face and edge eigenvalue problems likewise, we obtain the constraint vectors in the displacement space by a multiplication of the constraint vector in the Lagrange multiplier space by the localized (and transposed) version of the jump operator B.

Properties of the adaptively computed constraint vectors. Due to the form of the given constraints (see (6.6)–(6.9), (6.14)) and the definition of the localized jump operators (see (6.1) and (6.10)), we have for $c_{u,ij,\mathcal{F}}^r$, $c_{u,ij,\mathcal{E}_m}^r$ ($m = 1, 2, \ldots$), and $c_{u,ik}^r$

$$\begin{aligned}
(w_{ij}, c_{u,ij,\mathcal{F}}^r) = 0 \quad &\Leftrightarrow \quad (B_{\overline{\mathcal{F}}^{ij}}^{(i)} w^{(i)}, c_{\lambda,ij,\mathcal{F}}^r) = -(B_{\overline{\mathcal{F}}^{ij}}^{(j)} w^{(j)}, c_{\lambda,ij,\mathcal{F}}^r), \\
(w_{ij}, c_{u,ij,\mathcal{E}_m}^r) = 0 \quad &\Leftrightarrow \quad (B_{\overline{\mathcal{F}}^{ij}}^{(i)} w^{(i)}, c_{\lambda,ij,\mathcal{E}_m}^r) = -(B_{\overline{\mathcal{F}}^{ij}}^{(j)} w^{(j)}, c_{\lambda,ij,\mathcal{E}_m}^r), \\
(w_{ik}, c_{u,ik}^r) = 0 \quad &\Leftrightarrow \quad (B_{\mathcal{E}^{ik}}^{(i)} w^{(i)}, c_{\lambda,ik}^r) = -(B_{\mathcal{E}^{ik}}^{(k)} w^{(k)}, c_{\lambda,ik}^r).
\end{aligned} \tag{6.15}$$

Since $B_{\overline{\mathcal{F}}^{ij}}^{(i)}$ and $B_{\overline{\mathcal{F}}^{ij}}^{(j)}$ are closely related, i.e., both operators only differ by their sign when restricted to the face (i.e., when all zero columns are removed), the constraint vector on the face is identical for both sides of the face. The same argument applies to the edge eigenvalue problems and the edge constraints from face eigenvalue problems, since, again, $B_{\mathcal{E}^{ik}}^{(i)}$ and $-B_{\mathcal{E}^{ik}}^{(k)}$ are identical if restricted to the jumps $w^{(i)} - w^{(k)}$ on the corresponding edge.

6.2.2 Coarse space adjustments for the generalized transformation-of-basis approach

For the generalized transformation-of-basis approach, minor restrictions on the set of constraints apply and, thus, the sets of adaptive constraint vectors might have to be enriched slightly. In this section, we explain how the computed sets have to be adjusted to satisfy the assumptions of the generalized transformation-of-basis approach.

Let us assume to have computed sets or a set of constraints on an open face $\mathcal{F}^{ij}$ and on its related edges $\mathcal{E}_m$ ($m = 1, 2, \ldots$) or just on an edge $\mathcal{E}^{ik}$. These constraints are orthonormalized edge by edge and separately for the open face. The orthonormalized results are denoted by $T_{\mathcal{F}^{ij},\Pi}$ and $T_{\mathcal{E}_m,\Pi}$, $m = 1, 2, \ldots$, and $T_{\mathcal{E}^{ik},\Pi}$. The matrices $T_{\mathcal{F}^{ij}} := \begin{pmatrix} T_{\mathcal{F}^{ij},\Pi} & T_{\mathcal{F}^{ij},\Delta} \end{pmatrix}$ and $T_{\mathcal{E}_m} := \begin{pmatrix} T_{\mathcal{E}_m,\Pi} & T_{\mathcal{E}_m,\Delta} \end{pmatrix}$, $m = 1, 2, \ldots$, and $T_{\mathcal{E}^{ik}} := \begin{pmatrix} T_{\mathcal{E}^{ik},\Pi} & T_{\mathcal{E}^{ik},\Delta} \end{pmatrix}$ then are computed such that they are orthogonal.

Given a face $\mathcal{F}^{ij}$, the sets of orthogonalized constraints $T_{\mathcal{F}^{ij},\Pi}$ and $T_{\mathcal{E}_m,\Pi}$ ($m = 1, 2, \ldots$) can then be used as constraint vectors for both subdomains Ω_i and Ω_j. This results from the form of B and that the constraint vector, restricted to one subdomain, equals the negative of the constraint vector, restricted to the other subdomain; cf. (6.15). Given an edge $\mathcal{E}^{ik}$, the same applies to the two subdomains considered in the edge eigenvalue problem.

In order to satisfy the assumptions of the generalized transformation-of-basis approach (see (4.20)), we also enforce the same constraints for all other jumps between two arbitrary subdomains at any considered edge (for a face, there are only two subdomains, of course). Then, for a face $\mathcal{F}^{ij}$ with jumps $w^{(i)} - w^{(j)}$ across the face and across the edges $\mathcal{E}_m$ ($m = 1, 2, \ldots$) or a single edge $\mathcal{E}^{ik}$ with jumps $w^{(i)} - w^{(s)}$ across the edge $\mathcal{E}^{ik}$, the local transformations have to be identical for all subdomains sharing the face or the edge. Precisely, we have

$$T^{(i)}_{|\mathcal{F}^{ij}} = T^{(j)}_{|\mathcal{F}^{ij}} = T_{\mathcal{F}^{ij}}, \qquad T^{(i)}_{|\mathcal{E}_m} = T^{(s)}_{|\mathcal{E}_m} = T_{\mathcal{E}_m}, \qquad T^{(i)}_{|\mathcal{E}^{ik}} = T^{(s)}_{|\mathcal{E}^{ik}} = T_{\mathcal{E}^{ik}}, \quad (6.16)$$

and all pairs of subdomains $\{\Omega_i, \Omega_s\}$ sharing the edges $\mathcal{E}_m$ or $\mathcal{E}^{ik}$. This equality is trivially true for our adaptive constraints on the faces; see (6.15). For the edges, this property analogously holds for the two subdomains considered in the eigenvalue problem. For other adjacent subdomains we just introduce a, generally, nonnodal constraint vector.

Thus, the constraint set obtained from the local eigenvalue problems can be extended such that the local transformations satisfy condition (6.16) of the generalized transformation-of-basis approach, as it has been introduced in Section 4.5 or [67].

6.2.3 Various adaptive algorithms

Subsequently to the previous section and as in Section 5.2.2, we can define the Algorithms Ia, Ib, Ic, II, and III for adaptive FETI-DP by respecting the necessary slight enrichment of the adaptive coarse spaces to satisfy the assumptions of the generalized transformation-of-basis approach. Corresponding algorithms can be defined for BDDC, too.

Algorithm Ia uses the coarse space for which the theoretical condition number bound is established, Algorithms Ib and Ic often yield the same numerical results but use a heuristic neighborhood strategy to discard edge eigenvalue problems (Algorithms Ib and Ic) and edge constraints from face eigenvalue problems (Algorithm Ic) if the edge is completely embedded in a soft material; for more details, see Section 5.2.2.

Algorithms II and III are the algorithms based on face eigenvalue problems as introduced in [93, 120]. Algorithm II uses all constraints from face eigenvalue problems, Algorithm III only enforces the constraints on the open face and discards all edge constraints (from face eigenvalue problems).

6.3 Adaptive FETI-DP and BDDC operators for the generalized transformation-of-basis approach

The adaptive constraints in the FETI-DP and BDDC method with a generalized transformation-of-basis approach are enforced by partial finite element assembly. Thus, we introduce the operator R^T that assembles in all a posteriori degrees of freedom to enforce the adaptive constraints and that leaves all other degrees of freedom (interior, a priori primal and remaining (or a posteriori) dual variables) unchanged. In accordance to the theory of the generalized transformation-of-basis approach, we also need a multiplicity-weighted assembly operator $R_\mu^T = (R^T R)^{-1} R^T$.

The adaptively preconditioned FETI-DP method is then given by

$$\begin{aligned}\widehat{M}_T^{-1}\widehat{F}\lambda &:= (\widehat{B}_D\widehat{\widetilde{S}}\widehat{B}_D^T)\,(\widehat{B}\widehat{\widetilde{S}}^{-1}\widehat{B}^T)\lambda \\ &:= (B_D T R_\mu (R^T T^T \widetilde{S} T R) R_\mu^T T^T B_D^T)\,(B T R (R^T T^T \widetilde{S} T R)^{-1} R^T T^T B^T)\lambda \\ &= \widehat{d}\end{aligned} \tag{6.17}$$

with the corresponding right hand side $\widehat{d}$. Now, the finite element vectors and matrices are, both, transformed and assembled in the a posteriori primal variables.

Introducing another operator R'^T which assembles in all a posteriori primal and all remaining (or a posteriori) dual variables (and leaves the a priori primal variables unchanged), the preconditioned adaptive BDDC method is given by

$$\begin{aligned}\widehat{M}_{\mathrm{BDDC}}^{-1}\mathcal{S}u &:= (R'^T T \widehat{D}_u R \widehat{\widetilde{S}}^{-1} R^T \widehat{D}_u T^T R')\,(R'^T \widetilde{S} R')u \\ &:= (R'^T D_u T R\,(R^T T^T \widetilde{S} T R)^{-1}\,R^T T^T D_u R')\,(R'^T \widetilde{S} R')u = \widehat{g}\end{aligned} \tag{6.18}$$

with the corresponding right hand side $\widehat{g}$. The BDDC scaling D_u scales the degrees of freedom and corresponds to the Lagrange multiplier scaling D of the FETI-DP method.

6.4 Condition number estimate for adaptive FETI-DP and BDDC

As in the previous chapter, where we have extended all the constraint vectors $c^r_{\lambda,ij,\mathcal{F}}$, $c^r_{\lambda,ij,\mathcal{E}_m}$, $m = 1, 2, \ldots$, and $c^r_{\lambda,ik}$ by zero to the space of the Lagrange multipliers to define the columns of the matrix U, we extend all the constraint vectors $c^r_{u,ij,\mathcal{F}}$, $c^r_{u,ij,\mathcal{E}_m}$, $m = 1, 2, \ldots$, and $c^r_{u,ik}$ by zero to $\widetilde{W}$. These vectors define the columns of the matrix Q.

Obviously, the spaces

$$\widetilde{W}_Q := \{w \in \widetilde{W} \,:\, Q^T w = 0\} \text{ and } \widetilde{W}_U = \{w \in \widetilde{W} \,:\, U^T B w = 0\} \tag{6.19}$$

are the same but their constraint vectors (given by Q and U) are defined differently. The space $\widetilde{W}_U$ corresponds to the solution space for deflation or balancing; cf. the previous chapter. The solution space for the generalized transformation-of-basis approach is, generally, a subset of this space. In order to define the solution space, we refer to our explanation on how to enrich the set of adaptively computed constraints to meet the requirements of the transformation approach; see Section 6.2.2. With the additionally introduced constraint vectors, we then have $\widehat{Q} := [Q, *]$ with $\operatorname{range} Q \subset \operatorname{range} \widehat{Q}$, thus, $\ker \widehat{Q}^T \subset \ker Q^T$ and the solution space

$$\widetilde{W}_{\widehat{Q}} = \{w \in \widetilde{W} \,:\, \widehat{Q}^T w = 0\} \subset \widetilde{W}_Q = \widetilde{W}_U. \tag{6.20}$$

In Section 4.5.2.2, we have given a detailed and generic explanation of the solution spaces.

In our implementation, the constrained elements of $\widetilde{W}_{\widehat{Q}}$ are represented by $\widetilde{W}_{T,a} = \{\widehat{w} = R_\mu^T T^T w \,:\, w \in \widetilde{W}\}$ where $R_\mu^T = (R^T R)^{-1} R^T$ and $T = \operatorname{blockdiag}_{i=1,\ldots,N} T^{(i)}$. The operator $T^{(i)}$ reduces to the identity on all interior degrees of freedom and is blockdiagonal on the interface with blocks $T_{\mathcal{F}^{ij}}$ and $T_{\mathcal{E}^{ik}}$ for all faces $\mathcal{F}^{ij}$ and edges $\mathcal{E}^{ik}$ shared by Ω_i; cf. (4.27) and Section 4.5.2.1.

Corollary 6.1. *Let $N_\mathcal{F}$ denote the maximum number of faces of a subdomain, $N_\mathcal{E}$ the maximum number of edges of a subdomain, $M_\mathcal{E}$ the maximum multiplicity of an edge, and* TOL *a given tolerance for solving the local generalized eigenvalue problems. Let all vertices be primal. Then, for $w \in \widetilde{W}_{\widehat{Q}}$, we have*

$$|P_D w|^2_{\widetilde{S}} \leq 4 \max\{N_\mathcal{F}, N_\mathcal{E} M_\mathcal{E}\}^2 \mathrm{TOL} |w|^2_{\widetilde{S}}.$$

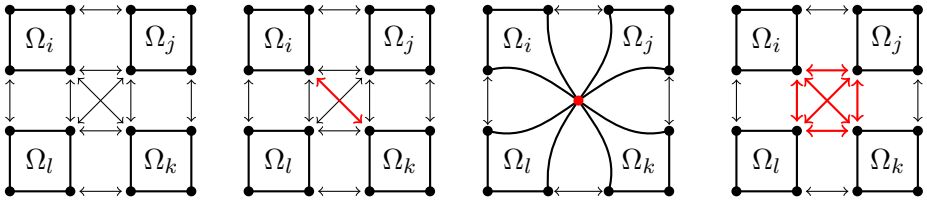

Figure 6.2: *Constraints of the direct deflation approach, the generalized transformation-of-basis, and the corresponding deflation approach:* Cross-sectional view of four subdomains sharing an edge. Arrows symbolize redundant Lagrange multipliers in FETI-DP (left). Assume that, using deflation directly, one constraint is introduced, involving the Lagrange multiplier depicted in bold red color (second to left). Using partial assembly, after a generalized transformation of basis, the primal constraint is now enforced between all four subdomains, effectively involving all six Lagrange multipliers (second to right). The deflation or balancing approach corresponding to the generalized transformation-of-basis approach constrains all six Lagrange multipliers depicted in bold red color with the same constraint vector (right). [68]. Copyright Electronic Transactions on Numerical Analysis.

Proof. The constraints are enforced by partial assembly; cf. Figure 6.2 for the examplary case of an edge $\mathcal{E}^{ik}$ shared by four subdomains. Thus, the solution space $\widetilde{W}_{\widehat{Q}}$ is in general a strict subset of the solution space $\widetilde{W}_U$ and we obtain our P_D-estimate from Lemma 5.5 for $\widetilde{W}_{\widehat{Q}}$. □

We can now formulate the following theorem for our adaptive Algorithm Ia using the generalized transformation-of-basis approach.

Theorem 6.2. *Let $N_{\mathcal{F}}$ denote the maximum number of faces of a subdomain, $N_{\mathcal{E}}$ the maximum number of edges of a subdomain, $M_{\mathcal{E}}$ the maximum multiplicity of an edge, and* TOL *a given tolerance for solving the local generalized eigenvalue problems. Furthermore, let all vertices be primal. Then, the condition number $\kappa(\widehat{M}_T^{-1}\widehat{F})$ of the FETI-DP Algorithm Ia, with adaptive constraints enforced by the generalized transformation-of-basis approach, satisfies*

$$\kappa(\widehat{M}_T^{-1}\widehat{F}) \leq 4\max\{N_{\mathcal{F}}, N_{\mathcal{E}}M_{\mathcal{E}}\}^2\text{TOL}.$$

The condition number $\kappa(\widehat{M}_{BDDC}^{-1}\mathcal{S})$ of the BDDC Algorithm Ia, with adaptive constraints enforced by the generalized transformation-of-basis approach, satis-

fies

$$\kappa(\widehat{M}_{BDDC}^{-1}\mathcal{S}) \leq 4\max\{N_{\mathcal{F}}, N_{\mathcal{E}}M_{\mathcal{E}}\}^2\text{TOL}.$$

Proof. The proof is complete by acknowledging that this is a special case of Theorem 4.12 for FETI-DP and Theorem 4.15 for BDDC if the transformations are built according to the assumptions of the generalized transformation-of-basis approach (i.e., they are identical for all sides of any considered edge; cf. Sections 4.5.2.1 and 6.2.2) and by using Corollary 6.1. □

Note that the bound in Theorem 6.2 is algebraic in the sense that the condition number bound holds under very weak assumptions. However, under unfavorable conditions, for small tolerances TOL, the coarse space can be so large that the method reduces to a direct solver.

Remark 6.3. *Note that the explicit condition number of the FETI-DP or BDDC method with our generalized transformation-of-basis approach is always smaller or equal to that of the direct deflation or balancing approach. This results from the fact that in our generalized transformation-of-basis approach, in the partial assembly, we often enforce additional constraints compared to the direct deflation or balancing approach – without creating a larger coarse space; cf.* (6.20)*,* (6.16)*, and Figure 6.2.*

Nevertheless, for every method using the generalized transformation-of-basis approach, we can always find an equivalent balancing or deflation method by expanding the constraint columns U such that all the constraints from $\widetilde{W}_{\widehat{Q}}$ are implemented and such that $\kappa(M_{PP}^{-1}F) = \kappa(\widehat{M}_T^{-1}\widehat{F})$; cf. Section 4.5.

6.5 Numerical results for adaptive FETI-DP and BDDC

As in Section 5.4, we consider examples of the diffusion equation and compressible linear elasticity on the unit cube $\Omega = [0,1]^3$. We present numerical results for the adaptive coarse spaces as defined in Section 6.2.3 with references to Section 5.2.2 and the description of the classical variants of [93, 120, 94], relying on face eigenvalue problems only. Here, we use the implementation of the coarse space by the generalized transformation-of-basis approach for FETI-DP and BDDC.

For the diffusion equation, we consider jumps of $\rho \in \{1, 1e{+}6\}$. For problems of linear elasticity, the Poisson ratio is set to $\nu = 0.3$ and the Young modulus is $\mathrm{E} \in \{1, 1e+6\}$. We assume constant values of ρ, E, and ν on each finite element.

The initial coarse space for all methods contains all vertex constraints. We then add several other nodes (turned into vertices) such that each nonstraight edge has at least three primal vertices. This choice is identical to that of Section 5. We consider irregular decompositions of the unit cube. These decompositions are obtained from the METIS graph partitioner (see [60]) using the options `-ncommon=3` and `-contig` to avoid noncontiguous subdomains and unwanted hinge modes between sets of tetrahedra inside single subdomains; again, cf. Chapter 5.

Except for Section 6.5.1 and 6.5.5, where we only study Algorithm Ia and Algorithms Ia, Ib, and Ic, respectively, we show results for all five adaptive algorithms defined before; see Section 6.2.3.

In all tables, we denote either by κ the condition number of the preconditioned FETI-DP and BDDC operator or by $\lambda_{\min}$ and $\lambda_{\max}$ the minimum and maximum eigenvalue. By *its*, we denote the number of preconditioned conjugate gradient (PCG) iterations that are needed until convergence. The iteration is also stopped if no convergence is observed within 500 iterations. We then simply write "500" instead of ">500" for the iterations. In Sections 6.5.2–6.5.5, we require a relative reduction of 1e-10 of the preconditioned residual of the PCG algorithm. In Section 6.5.1, we also use the deflation approach and therefore a moderate stopping criterion; cf. Section 5.4.1 for a short discussion on stopping criteria for deflation combined with FETI-DP. The condition numbers (or maximum and minimum eigenvalues), shown in the table, are the standard estimates obtained from PCG. The condition number estimates for FETI-DP and BDDC can differ to a minor degree since, in most cases, the estimates of the smallest eigenvalue differ slightly, typically starting in the second or third digit.

By $|\Pi'|$ we denote the size of the standard coarse space while by $|\Pi|$ we present the size of the corresponding adaptive coarse space implemented by the generalized transformation-of-basis approach; see the previous sections and, in particular, Section 4.5. For the deflation runs in Section 6.5.1, we denote the adaptive coarse space size by $|U|$. By N we denote the number of subdomains. For the Algorithms Ia, Ib, and Ic, we also present the number of edge eigenvalue problems as $\#\mathcal{E}_{evp}$ and in parentheses the percentage of these in the total number of eigenvalue problems.

For all runs, we highlight small condition number estimates (or maximum eigenvalue estimates) below 50 in bold face. If not stated otherwise, all eigenvalue problems are solved by the MATLAB built-in `eig` function. In Section 6.5.4, the eigenvalue problems are solved by the LOBPCG eigensolver [86,

85]. Except for Table 6.14, we always use TOL = 10. The resulting condition number is typically at the order of TOL.

If ρ-scaling is used, we apply the standard ρ-scaling, where the nodal coefficient values are given by the maximum value of the coefficient function on all neighboring tetrahedra inside the same subdomain.

For all test problems, we enforce zero Dirichlet boundary conditions for the face with $x = 0$ and zero Neumann boundary conditions elsewhere. We apply the body force $f = 0.1$ for the diffusion problem and $f = (0.1, 0.1, 0.1)^T$ for problems of linear elasticity.

We give short overview over the following sections.

1. Section 6.5.1: **Generalized transformation-of-basis approach and its equivalent deflation approach**. In accordance to our theory, for the diffusion equation, we show that for each adaptive approach using the generalized transformation-of-basis approach an equivalent deflation approach exists. In this section, we only test Algorithm Ia.

2. Section 6.5.2: **Comparison with the results of adaptive FETI-DP with the balancing approach**. In this section, we consider compressible linear elasticity and some of the materials already considered in Section 5.4 with the balancing approach.

3. Section 6.5.3: **Scaling comparisons**. In this section, we compare adaptive FETI-DP methods with four different scalings; cf. Section 3.4. Results for adaptive BDDC are not presented, but similar results are expected.

4. Section 6.5.4: **Approximate solutions of the local eigenvalue problems**: In this section, the influence of approximate solutions of the local generalized eigenvalue problems to the convergence of the adaptive method is studied; composite material no. 1 and randomly distributed coefficients are considered.

5. Section 6.5.5: **Preconditioners for iterative solvers of the local generalized eigenvalue problems**: Eventually, we study different local preconditioners for iterative solvers of the local generalized eigenvalue problems for composite material no. 2. Here, we only compare runs of Algorithms Ia, Ib, and Ic.

Remark 6.4. *In the first of the following sections, we construct the equivalent deflation approach for a the adaptive Algorithm Ia using the generalized*

Table 6.2: *Adaptive FETI-DP and BDDC (Alg. Ia) with ρ-scaling and the generalized transformation-of-basis approach and its equivalent deflation approach.* Diffusion equation of composite material no. 1 with $\rho_1 = 1$ and $N^{2/3}$ beams with $\rho_2 = 1e+6$ on the unit cube; conforming $\mathcal{P}_1$ finite element discretization with $1/h = 6N^{1/3}$ and irregular partitioning of the domain; see Figure 5.1. Coarse spaces for TOL = 10 for all generalized eigenvalue problems. $|\Pi'|$ denotes the size of a priori coarse space, $|\Pi|$ the number of adaptive, a posteriori constraints in the generalized transformation-of-basis approach, $|U|$ the number of adaptive constraints in the deflation approach. Other notation as in Table 5.4. [67]

Adaptive FETI-DP and BDDC:
(Generalized transformation-of-basis approach and equivalent deflation)
$1/h = 6N^{1/3}$ – composite material no. 1 – irregular partitioning

		Adaptive FETI-DP (Deflation)				**Adaptive FETI-DP** (Gen. t.-o.-b. appr.)				**Adaptive BDDC** (Gen. t.-o.-b. appr.)			
N	$\lvert\Pi'\rvert$	$\lambda_{\min}$	$\lambda_{\max}$	*its*	$\lvert U\rvert$	$\lambda_{\min}$	$\lambda_{\max}$	*its*	$\lvert\Pi\rvert$	$\lambda_{\min}$	$\lambda_{\max}$	*its*	$\lvert\Pi\rvert$
2^3	30	1.00	**7.59**	14	32	1.00	**7.59**	14	20	1.00	**7.59**	13	20
3^3	165	1.00	**8.19**	18	203	1.00	**8.19**	18	135	1.00	**8.19**	14	135
4^3	468	1.00	**10.27**	23	545	1.00	**10.27**	23	336	1.00	**10.27**	18	336
5^3	1066	1.00	**10.88**	23	1071	1.00	**10.88**	22	645	1.00	**10.88**	18	645
6^3	1878	1.00	**9.20**	23	1837	1.00	**9.20**	23	1099	1.00	**9.20**	18	1099

transformation-of-basis approach. In Sections 6.5.2–6.5.5, we only use the generalized transformation-of-basis approach. For these results, we do not construct an equivalent deflation or balancing approach. If these results are compared to an adaptive algorithm using balancing (see Section 5.4), the condition number of the approach using the generalized transformation-of-basis is always smaller or equal to that of the adaptive projection (deflation or balancing) method; cf. Section 6.2.2 (in particular, Figure 6.2) or, in a more general description, Section 4.5.

6.5.1 The generalized transformation-of-basis approach and its equivalent deflation approach

We now present results for the diffusion equation with highly varying coefficients $\rho \in [1, 1e+6]$ on the unit cube $\Omega = [0, 1]^3$ and an irregular METIS (see [59, 60]) decomposition for N subdomains. We consider two materials. First, we consider a soft matrix material with $\rho_1 = 1$ and an embedded stiff material in the form of $N^{2/3}$ beams with $\rho_2 = 1e + 6$ running from the face with $x = 0$ to the face

Table 6.3: *Adaptive FETI-DP and BDDC (Alg. Ia) with ρ-scaling and the generalized transformation-of-basis and its equivalent deflation approach.* Diffusion equation of 3D checkerboard distribution with $\rho_1 = 1$ and $\rho_2 = 1e+6$ on the unit cube; conforming $\mathcal{P}_1$ finite element discretization with $1/h = 6N^{1/3}$ and irregular partitioning of the domain; see Figure 6.3. Coarse spaces for TOL = 10 for all generalized eigenvalue problems. Notation as in Table 6.2. [67]

Adaptive FETI-DP and BDDC:
(Generalized transformation-of-basis approach and equivalent deflation)
$1/h = 6N^{1/3}$ – 3D checkerboard distribution – irregular partitioning

		Adaptive FETI-DP (Deflation)				**Adaptive FETI-DP** (Gen. t.-o.-b. appr.)				**Adaptive BDDC** (Gen. t.-o.-b. appr.)			
N	$\lvert\Pi'\rvert$	$\lambda_{\min}$	$\lambda_{\max}$	*its*	$\lvert U\rvert$	$\lambda_{\min}$	$\lambda_{\max}$	*its*	$\lvert\Pi\rvert$	$\lambda_{\min}$	$\lambda_{\max}$	*its*	$\lvert\Pi\rvert$
2^3	30	1.00	**7.31**	17	14	1.00	**7.31**	17	9	1.00	**7.31**	14	9
3^3	165	1.00	**8.35**	20	45	1.00	**8.35**	20	29	1.00	**8.35**	16	29
4^3	468	1.00	**8.93**	22	188	1.00	**8.93**	22	120	1.00	**8.93**	18	120
5^3	1066	1.00	**12.36**	22	245	1.00	**12.36**	22	150	1.00	**12.36**	18	150
6^3	1878	1.00	**9.72**	23	545	1.00	**9.72**	23	326	1.00	**9.72**	19	326

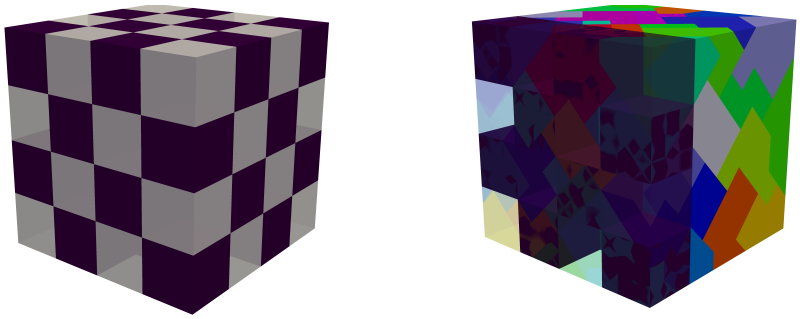

Figure 6.3: *Checkerboard on the unit cube for 64 subdomains (coefficients and irregular partitioning).* Cubes of high coefficients $E_2 = 1e+6$, shown in dark purple, and cubes of a soft material $E_1 = 1$, shown in light, half-transparent gray, are arranged in a 3D checkerboard pattern (left). Irregular decomposition using METIS [60] for 64 subdomains; high coefficients are again shown in dark purple; subdomains shown in different colors; left quarter of the domain ($x > \frac{3}{4}$) made half-transparent (right). [67]

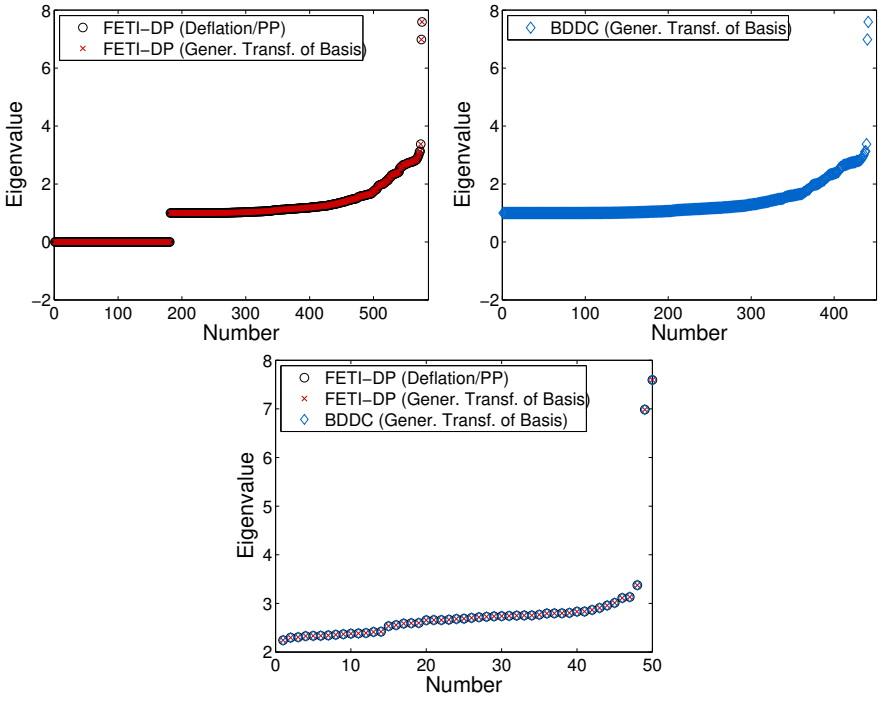

Figure 6.4: *Eigenvalues for the generalized transformation-of-basis approach and the equivalent deflation approach.* Eigenvalues of the preconditioned operators for FETI-DP with deflation ($M_{PP}^{-1}F$) and the generalized transformation-of-basis approach ($\widehat{M}_T^{-1}\widehat{F}$) (top left), BDDC with the generalized transformation-of-basis approach ($\widehat{M}_{BDDC}^{-1}\mathcal{S}$) (top right) and the largest 50 eigenvalues of the preconditioned operators (bottom center) for the composite material no. 1, an irregular decomposition of the unit cube into eight subdomains, and $1/h = 12$. The eigenvalues greater than one are identical for all three algoritms. [67]

with $x = 1$; see Figure 5.1. This material is denoted as composite material no. 1. In the second material, the Young modulus is distributed in a regular 3D checkerboard pattern; see Figure 6.3.

Our convergence criterion for the preconditioned conjugate gradient is a relative reduction of the preconditioned residual by a factor of 1e-6. Our results in Tables 6.2 and 6.3 show identical estimates for $\lambda_{\min}$ and $\lambda_{\max}$ for all three methods in accordance with the theory. In Figure 6.4, all eigenvalues of the three preconditioned operators were computed numerically for $1/h = 12$. We see that, indeed, all eigenvalues other than zero and one are identical, as predicted by the theory.

6.5.2 Comparison with the results of adaptive FETI-DP with the balancing approach

In this section, we test three different distributions of the Young modulus E; namely the composite material no. 1 (see Figure 5.1), the representative volume element (see Figure 5.9), and randomly distributed coefficients (see Figure 5.10). We also deliver an insight into the local spectra for the different materials; see Figure 6.5.

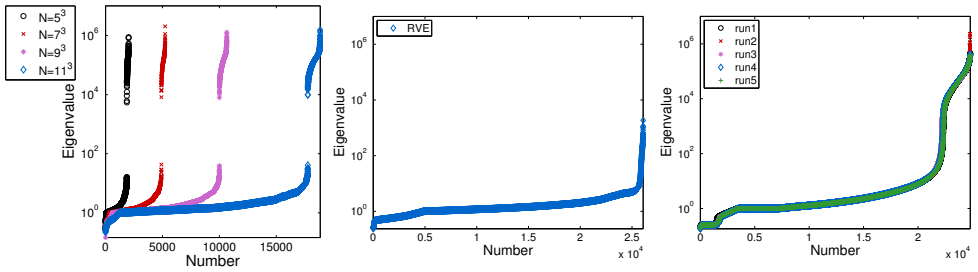

Figure 6.5: *Local eigenvalues greater 0.1 from all local generalized eigenvalue problems for selected runs and different materials.* The three materials are depicted in Figures 5.1, 5.9, and 5.10: composite material no. 1 for $N \in \{5^3, 7^3, 9^3, 11^3\}$ (left; cf. Table 6.4), representative volume element for $N = 8^3$ (center; cf. Table 6.6), and randomized coefficients for $N = 6^3$ and the first five runs (right; cf. Tables 6.7 and 6.8). [68]. Copyright Electronic Transactions on Numerical Analysis.

6.5.2.1 Composite materials

We first consider our composite material no. 1. The material consists of a soft matrix material with $\mathrm{E}_1 = 1$ that surrounds $N^{2/3}$ beams with $\mathrm{E}_2 = 1e+6$ that run in a straight line from the face with $x = 0$ to the face with $x = 1$ and that occupy $1/9$ of the cross-section of the material; cf. Figure 5.1 and Section 5.4.3 for the results of the adaptive methods with a direct balancing approach.

We see that FETI-DP and BDDC behave almost identically. Clearly, the coarse spaces for FETI-DP and BDDC are of the same size and the iteration count is almost the same for both methods. We see that the size of the second level coarse space is quite modest compared to the standard coarse space. Compared to the adaptive coarse space implemented by the balancing approach (cf. Chapter 5), the adaptive coarse space implemented by the generalized transformation-of-basis approach in Table 6.4 is up to twice the size of the first one. This is due to the fact that we always make all three degrees of freedom, which belong to a given node, primal, even if only one or two constraints are required. Nevertheless, the coarse spaces of Table 5.6 and Table 6.5 do have a comparable size, regardless of the implementation. For our parallel results, we have implemented a more efficient version by also making single degrees of freedom primal; cf. Chapter 7.

As expected, the adaptive Algorithms II and III cannot ensure small condition numbers and iteration counts, Algorithms Ia, Ib, and Ic, however, are robust and yield good results for all test problems.

For a more detailed consideration of the computational overhead of additional edge eigenvalue problems, see the detailed discussion in Chapter 5.

For a distribution of the local eigenvalues for some of the runs, see Figure 6.5 (left). We can observe a gap in the spectrum somewhere between the minimum and maximum value taken by the Young modulus.

6.5.2.2 A steel microstructure

In this section, we consider the representative volume element of a modern dual phase steel microstructure already considered with adaptive methods in Section 5.4.4. The RVE has been obtained from the one in [87, Fig. 5.5], which again is a part of the structure in [117, Fig. 2], by resampling. As in [87], we use $\nu = 0.3$, $\mathrm{E}_1 = 210$ and $\mathrm{E}_2 = 210\,000$ as artificial material parameters. The FETI-DP and BDDC algorithms tested here and the FETI-DP algorithm with a balancing approach show almost identical convergence behavior. The generalized transformation-of-basis approach gives a larger coarse space. As mentioned in the previous section this could be improved so that the balancing approach

Table 6.4: *Adaptive FETI-DP and BDDC (Alg. Ia-III) with ρ-scaling and generalized transformation-of-basis approach.* Compressible linear elasticity of composite material no. 1 with $E_1 = 1$ and $N^{2/3}$ beams with $E_2 = 1e+6$ on the unit cube; $\nu = 0.3$ for the whole domain; conforming $\mathcal{P}_1$ finite element discretization with $1/h = 3N^{1/3}$ and irregular partitioning of the domain; see Figure 5.1. Coarse spaces for TOL = 10 for all generalized eigenvalue problems. $|\Pi'|$: size of a priori coarse space, $|\Pi|$: number of additional a posteriori constraints in the generalized transformation-of-basis approach, other Notation as in Table 5.4. [68]. Copyright Electronic Transactions on Numerical Analysis.

Adaptive FETI-DP and BDDC: *Algorithms Ia, Ib, Ic, II, and III* (Gen. t.-o.-b. appr.)
$1/h = 3N^{1/3}$ – composite material no. 1 – irregular partitioning

Adaptive FETI-DP

		Algorithms Ia, Ib, and Ic				*Algorithm II*			*Algorithm III*		
N	$\lvert\Pi'\rvert$		κ	*its*	$\lvert\Pi\rvert$	$\#\mathcal{E}_{evp}$	κ	*its*	$\lvert\Pi\rvert$	κ	*its*	$\lvert\Pi\rvert$
5^3	3084	a)	**14.30**	36	459	14 (5.2%)						
		b)	**14.30**	36	459	8 (3.0%)	**14.30**	36	453	3.29e+5	187	303
		c)	**14.30**	37	375	8 (3.0%)						
7^3	8781	a)	**13.92**	40	1098	48 (6.0%)						
		b)	**13.92**	40	1089	21 (2.7%)	2.93e+5	84	1074	2.96e+5	373	780
		c)	**13.93**	41	942	21 (2.7%)						
9^3	19029	a)	**16.27**	41	2070	90 (5.2%)						
		b)	**16.28**	42	2067	45 (2.7%)	2.66e+5	71	2043	4.69e+5	482	1572
		c)	**16.28**	42	1812	45 (2.7%)						
11^3	35214	a)	**15.05**	43	3582	167 (5.2%)						
		b)	**15.05**	43	3570	95 (3.0%)	2.66e+5	142	3504	3.60e+5	500	2724
		c)	**15.05**	43	3192	95 (3.0%)						
13^3	58179	a)	**17.12**	44	5895	303 (5.6%)						
		b)	**17.12**	44	5889	171 (3.3%)	2.74e+5	225	5739	3.01e+5	500	4557
		c)	**17.13**	44	5346	171 (3.3%)						

Adaptive BDDC

		Algorithms Ia, Ib, and Ic				*Algorithm II*			*Algorithm III*		
N	$\lvert\Pi'\rvert$		κ	*its*	$\lvert\Pi\rvert$	$\#\mathcal{E}_{evp}$	κ	*its*	$\lvert\Pi\rvert$	κ	*its*	$\lvert\Pi\rvert$
5^3	3084	a)	**14.44**	35	459	14 (5.2%)						
		b)	**14.44**	35	459	8 (3.0%)	**14.44**	37	453	3.33e+5	241	303
		c)	**14.45**	36	375	8 (3.0%)						
7^3	8781	a)	**14.08**	40	1098	48 (6.0%)						
		b)	**14.08**	40	1089	21 (2.7%)	2.97e+5	98	1074	3.00e+5	459	780
		c)	**14.08**	41	942	21 (2.7%)						
9^3	19029	a)	**16.44**	41	2070	90 (5.2%)						
		b)	**16.44**	41	2067	45 (2.7%)	2.69e+5	76	2043	4.75e+5	500	1572
		c)	**16.44**	42	1812	45 (2.7%)						
11^3	35214	a)	**15.22**	40	3582	167 (5.2%)						
		b)	**15.22**	41	3570	95 (3.0%)	2.69e+5	162	3504	3.72e+5	500	2724
		c)	**15.22**	42	3192	95 (3.0%)						
13^3	58179	a)	**17.32**	41	5895	303 (5.6%)						
		b)	**17.32**	41	5889	171 (3.3%)	2.77e+5	250	5739	3.40e+5	500	4557
		c)	**17.32**	41	5346	171 (3.3%)						

Table 6.5: *Adaptive FETI-DP and BDDC (Alg. Ia-III) with ρ-scaling and generalized transformation-of-basis approach.* Compressible linear elasticity of composite material no. 1 with $\mathrm{E}_1 = 1$ and $N^{2/3}$ beams with $\mathrm{E}_2 = 1e+6$ on the unit cube; $\nu = 0.3$ for the whole domain; conforming $\mathcal{P}_1$ finite element discretization with $1/h = 6N^{1/3}$ and irregular partitioning of the domain; see Figure 5.1. Coarse spaces for $\mathrm{TOL} = 10$ for all generalized eigenvalue problems. Notation as in Table 6.4. [68]. Copyright Electronic Transactions on Numerical Analysis.

Adaptive FETI-DP and BDDC: *Algorithms Ia, Ib, Ic, II, and III* (Gen. t.-o.-b. appr.)
$1/h = 6N^{1/3}$ – composite material no. 1 – irregular partitioning

Adaptive FETI-DP

		Algorithms Ia, Ib, and Ic					*Algorithm II*			*Algorithm III*		
N	$\lvert\Pi'\rvert$		κ	*its*	$\lvert\Pi\rvert$	$\#\mathcal{E}_{evp}$	κ	*its*	$\lvert\Pi\rvert$	κ	*its*	$\lvert\Pi\rvert$
3^3	960	a)	**8.65**	34	699	2 (2.0%)						
		b)	**8.65**	34	699	1 (1.0%)	**8.65**	34	699	1.36e+6	68	243
		c)	**8.67**	34	450	1 (1.0%)						
4^3	2517	a)	**9.64**	36	1818	18 (6.6%)						
		b)	**9.64**	36	1818	7 (2.7%)	**9.64**	36	1818	6.94e+5	131	588
		c)	**9.65**	36	1059	7 (2.7%)						
5^3	5433	a)	**9.16**	35	3675	25 (4.2%)						
		b)	**9.16**	35	3675	12 (2.1%)	**9.16**	35	3669	5.50e+5	190	1242
		c)	**10.49**	36	2325	12 (2.1%)						
6^3	10110	a)	**9.89**	36	6156	32 (3.0%)						
		b)	**9.89**	36	6156	14 (1.3%)	**9.89**	36	6153	7.22e+5	252	2142
		c)	**12.97**	38	3996	14 (1.3%)						
7^3	16248	a)	**10.76**	37	10101	65 (3.6%)						
		b)	**10.76**	37	10101	27 (1.5%)	**10.76**	37	10089	1.21e+6	424	3606
		c)	**13.36**	39	6693	27 (1.5%)						

Adaptive BDDC

		Algorithms Ia, Ib, and Ic					*Algorithm II*			*Algorithm III*		
N	$\lvert\Pi'\rvert$		κ	*its*	$\lvert\Pi\rvert$	$\#\mathcal{E}_{evp}$	κ	*its*	$\lvert\Pi\rvert$	κ	*its*	$\lvert\Pi\rvert$
3^3	960	a)	**8.68**	32	699	2 (2.0%)						
		b)	**8.68**	32	699	1 (1.0%)	**8.68**	32	699	1.37e+6	77	243
		c)	**8.69**	32	450	1 (1.0%)						
4^3	2517	a)	**9.69**	33	1818	18 (6.6%)						
		b)	**9.69**	33	1818	7 (2.7%)	**9.69**	33	1818	6.98e+5	159	588
		c)	**9.69**	34	1059	7 (2.7%)						
5^3	5433	a)	**9.22**	33	3675	25 (4.2%)						
		b)	**9.22**	33	3675	12 (2.1%)	**9.22**	33	3669	5.53e+5	216	1242
		c)	**10.53**	34	2325	12 (2.1%)						
6^3	10110	a)	**9.95**	35	6156	32 (3.0%)						
		b)	**9.95**	35	6156	14 (1.3%)	**9.95**	35	6153	7.27e+5	285	2142
		c)	**13.04**	39	3996	14 (1.3%)						
7^3	16248	a)	**10.84**	35	10101	65 (3.6%)						
		b)	**10.84**	35	10101	27 (1.5%)	**10.84**	35	10089	1.22e+6	492	3606
		c)	**13.44**	38	6693	27 (1.5%)						

Table 6.6: *Adaptive FETI-DP and BDDC (Alg. Ia-III) with ρ-scaling and generalized transformation-of-basis approach.* Compressible linear elasticity of representative volume element with $E_1 = 210$ and $E_2 = 210\,000$ on the unit cube; $\nu = 0.3$ for the whole domain; conforming $\mathcal{P}_1$ finite element discretization with $1/h = 4N^{1/3}$ for $N = 8^3$ and irregular partitioning of the domain; see Figure 5.9. Coarse spaces for TOL = 10 for all generalized eigenvalue problems. Notation as in Table 6.4. [68]. Copyright Electronic Transactions on Numerical Analysis. Data courtesy of Jörg Schröder.

Adaptive FETI-DP and BDDC: *Algorithms Ia, Ib, Ic, II, and III* (Gen. t.-o.-b. appr.)
$N = 8^3$ – $1/h = 4N^{1/3}$ – representative volume element – irregular partitioning

Adaptive FETI-DP										
	Algorithms Ia, Ib, and Ic					*Algorithm II*			*Algorithm III*	
$\lvert\Pi'\rvert$		κ	*its*	$\lvert\Pi\rvert$	$\#\mathcal{E}_{evp}$	κ	*its*	$\lvert\Pi\rvert$	κ	*its*	$\lvert\Pi\rvert$
18888	a)	**13.75**	37	1275	114 (5.6%)	**13.75**	37	1263	354.30	98	699
	b)	**13.75**	37	1275	27 (1.4%)						
	c)	**13.75**	38	990	27 (1.4%)						
Adaptive BDDC										
	Algorithms Ia, Ib, and Ic					*Algorithm II*			*Algorithm III*	
$\lvert\Pi'\rvert$		κ	*its*	$\lvert\Pi\rvert$	$\#\mathcal{E}_{evp}$	κ	*its*	$\lvert\Pi\rvert$	κ	*its*	$\lvert\Pi\rvert$
18888	a)	**13.94**	31	1275	114 (5.6%)	**13.94**	31	1263	359.20	84	699
	b)	**13.94**	31	1275	27 (1.4%)						
	c)	**13.94**	33	990	27 (1.4%)						

does not have significant advantages over the transformation approach; we did not do so because of the ease of the implementation. However, in our parallel, high performance implementation, we have implemented the more efficient version; cf. Chapter 7.

For a distribution of the local eigenvalues, see Figure 6.5 (center). In contrast to composite material no. 1, we cannot observe any essential gap in the spectrum although the values of the Young modulus are well separated.

6.5.2.3 Randomly distributed coefficients

In this section, we test randomly distributed coefficients. We let 20% of the tetrahedra in the unit cube take the value $E_2 = 1e+6$ while the other tetrahedra take $E_1 = 1$; cf. Section 5.4.5. Both, FETI-DP and BDDC behave almost identically; see Tables 6.7 and 6.8. The coarse spaces implemented by the generalized transformation-of-basis and the balancing approach are of comparable size; cf. Table 5.13. Compared to the results using the balancing approach, we have also computed results for $N = 6^3$ where it can be seen that not only the

Table 6.7: *Adaptive FETI-DP (Alg. Ia, Ic, II, and III) with ρ-scaling and generalized transformation-of-basis approach.* Compressible linear elasticity of randomly distributed coefficients with 80% coefficients with $E_1 = 1$ and 20% coefficients with $E_2 = 1e+6$ on the unit cube; $\nu = 0.3$ for the whole domain; conforming $\mathcal{P}_1$ finite element discretization with $1/h = 5N^{1/3}$ and irregular partitioning of the domain; see Figure 5.10. Coarse spaces for TOL = 10 for all generalized eigenvalue problems. Notation as in Table 5.11. [68]. Copyright Electronic Transactions on Numerical Analysis.

Adaptive FETI-DP: *Algorithms Ia, Ic, II, and III* (Gen. t.-o.-b. appr.)

$1/h = 5N^{1/3}$ – random coefficients (80/20) – irregular partitioning

			Algorithm Ia				*Algorithm Ic*			
N		$\lvert\Pi'\rvert$	κ	*its*	$\lvert\Pi\rvert$	$\#\mathcal{E}_{evp}$	κ	*its*	$\lvert\Pi\rvert$	$\#\mathcal{E}_{evp}$
4^3	$\overline{x}$	2442	**8.83**	32.48	2421.99	9 (3.7%)	**8.83**	32.48	2421.39	9 (3.7%)
	$\widetilde{x}$		**8.78**	32	2421		**8.78**	32	2421	9 (3.7%)
	min		**7.48**	31	2268		**7.48**	31	2262	9 (3.7%)
	max		**9.92**	34	2553		**9.92**	34	2553	9 (3.7%)
	σ	-	0.48	0.63	59.68	-	0.48	0.63	59.76	0.00
5^3	$\overline{x}$	5058	**8.94**	32.76	5134.77	23 (4.1%)	**8.94**	32.76	5133.42	22.99 (4.1%)
	$\widetilde{x}$		**8.88**	33	5143.5		**8.88**	33	5140.5	23 (4.1%)
	min		**7.90**	31	4815		**7.90**	31	4809	22 (4.0%)
	max		**11.13**	35	5364		**11.13**	35	5364	23 (4.1%)
	σ	-	0.56	0.73	88.17	-	0.56	0.73	88.40	0.10
6^3	$\overline{x}$	9078	**9.18**	33.44	8797.38	57 (5.8%)	**9.18**	33.44	8795.94	56.95 (5.8%)
	$\widetilde{x}$		**9.12**	33	8812.5		**9.12**	33	8812.5	57 (5.8%)
	min		**8.40**	32	8454		**8.40**	32	8454	56 (5.7%)
	max		**10.93**	35	9015		**10.93**	35	9015	57 (5.8%)
	σ	-	0.48	0.57	114.73	-	0.48	0.57	114.84	0.22

			Algorithm II			*Algorithm III*		
N		$\lvert\Pi'\rvert$	κ	*its*	$\lvert\Pi\rvert$	κ	*its*	$\lvert\Pi\rvert$
4^3	$\overline{x}$	2442	6.42e+4	36.28	2420.10	5.57e+5	500	1317.60
	$\widetilde{x}$		**9.37**	33	2416.5	5.22e+5	500	1323
	min		**7.48**	31	2265	2.97e+5	500	1200
	max		5.93e+5	61	2553	1.34e+6	500	1425
	σ	-	1.17e+5	5.71	59.68	1.85e+5	0	46.06
5^3	$\overline{x}$	5058	8.40e+4	46.92	5128.53	4.98e+5	500	2831.28
	$\widetilde{x}$		5.40e+4	44	5139	4.61e+5	500	2830.5
	min		**7.90**	31	4806	2.88e+5	500	2583
	max		4.32e+5	87	5361	1.07e+6	500	3030
	σ	-	9.66e+4	11.99	88.32	1.37e+5	0	70.15
6^3	$\overline{x}$	9078	2.06e+5	76.19	8778.66	6.55e+5	500	4949.40
	$\widetilde{x}$		2.03e+5	74.5	8794.5	6.05e+5	500	4957.5
	min		1.72e+4	41	8442	3.53e+5	500	4686
	max		7.41e+5	139	8988	2.07e+6	500	5142
	σ	-	1.17e+5	20.60	115.27	2.54e+5	0	93.87

Table 6.8: *Adaptive BDDC (Alg. Ia, Ic, II, and III) with ρ-scaling and generalized transformation-of-basis approach.* Compressible linear elasticity of randomly distributed coefficients with 80% coefficients with $E_1 = 1$ and 20% coefficients with $E_2 = 1e+6$ on the unit cube; $\nu = 0.3$ for the whole domain; conforming $\mathcal{P}_1$ finite element discretization with $1/h = 5N^{1/3}$ and irregular partitioning of the domain; see Figure 5.10. Coarse spaces for TOL = 10 for all generalized eigenvalue problems. Notation as in Table 5.11. [68]. Copyright Electronic Transactions on Numerical Analysis.

Adaptive BDDC: *Algorithms Ia, Ic, II, and III* (Gen. t.-o.-b. appr.)
$1/h = 5N^{1/3}$ – random coefficients (80/20) – irregular partitioning

			Algorithm Ia				*Algorithm Ic*			
N		$\lvert\Pi'\rvert$	κ	*its*	$\lvert\Pi\rvert$	$\#\mathcal{E}_{evp}$	κ	*its*	$\lvert\Pi\rvert$	$\#\mathcal{E}_{evp}$
4^3	$\overline{x}$	2442	**8.82**	31.06	2421.99	9 (3.7%)	**8.82**	31.06	2421.39	9 (3.7%)
	$\widetilde{x}$		**8.78**	31	2421		**8.78**	31	2421	9 (3.7%)
	min		**7.48**	30	2268		**7.48**	30	2262	9 (3.7%)
	max		**9.91**	33	2553		**9.91**	33	2553	9 (3.7%)
	σ	-	0.48	0.71	59.68	-	0.48	0.71	59.76	0.00
5^3	$\overline{x}$	5058	**8.94**	31.59	5134.77	23 (4.1%)	**8.94**	31.61	5133.42	22.99 (4.1%)
	$\widetilde{x}$		**8.88**	32	5143.5		**8.88**	32	5140.5	23 (4.1%)
	min		**7.90**	30	4815		**7.90**	30	4809	22 (4.0%)
	max		**11.13**	33	5364		**11.13**	33	5364	23 (4.1%)
	σ	-	0.56	0.65	88.17	-	0.56	0.67	88.40	0.10
6^3	$\overline{x}$	9078	**9.18**	32.55	8797.38	57 (5.8%)	**9.18**	32.56	8795.94	56.95 (5.8%)
	$\widetilde{x}$		**9.12**	32	8812.5		**9.12**	32	8812.5	57 (5.8%)
	min		**8.40**	31	8454		**8.40**	31	8454	56 (5.7%)
	max		**10.93**	34	9015		**10.93**	34	9015	57 (5.8%)
	σ	-	0.48	0.66	114.73	-	0.48	0.66	114.84	0.22

			Algorithm II			*Algorithm III*		
N		$\lvert\Pi'\rvert$	κ	*its*	$\lvert\Pi\rvert$	κ	*its*	$\lvert\Pi\rvert$
4^3	$\overline{x}$	2442	6.41e+4	36.60	2420.10	5.57e+5	500	1317.60
	$\widetilde{x}$		**9.37**	32	2416.5	5.20e+5	500	1323
	min		**7.48**	30	2265	2.96e+5	500	1200
	max		5.93e+5	68	2553	1.34e+6	500	1425
	σ	-	1.17e+5	7.85	59.68	1.84e+5	0	46.06
5^3	$\overline{x}$	5058	8.40e+4	49.42	5128.53	4.94e+5	500	2831.28
	$\widetilde{x}$		5.40e+4	44.5	5139	4.59e+5	500	2830.5
	min		**7.90**	30	4806	2.87e+5	500	2583
	max		4.32e+5	94	5361	1.07e+6	500	3030
	σ	-	9.66e+4	14.48	88.32	1.37e+5	0	70.15
6^3	$\overline{x}$	9078	2.06e+5	83.36	8778.66	6.48e+5	500	4949.40
	$\widetilde{x}$		2.03e+5	81.5	8794.5	6.00e+5	500	4957.5
	min		1.72e+4	43	8442	3.51e+5	500	4686
	max		7.41e+5	156	8988	2.03e+6	500	5142
	σ	-	1.17e+5	24.33	115.27	2.49e+5	0	93.87

condition number but also the iteration count of Algorithm II deteriorates with a growing number of subdomains; we expect even worse results for $N > 6^3$. We conduct 100 runs for each algorithm and different coefficient distributions and present the arithmetic mean $\overline{x}$, the median $\widetilde{x}$, the minimum and maximum value and the standard deviation σ. For purposes of clarity, we refrain from reporting the results for Algorithm Ib since the results of Algorithms Ia and Ic are already almost identical.

For a distribution of the local eigenvalues for some of the runs, see Figure 6.5 (right). Although the coefficients only take two strongly separated values, the spectrum is continuous without showing any gap as it has been observed for the composite material no. 1.

6.5.3 Scaling comparisons

In this section, we compare the performance of the adaptive algorithms introduced before with four different kinds of scalings. Besides ρ-scaling, for which we already have given extensive perfomance results, we study deluxe-, stiffness/K-, and multiplicity-scaling.

We restrict ourselves to present results for adaptive FETI-DP but we can expect the same coarse space sizes and comparable convergence behavior for the corresponding BDDC methods.

6.5.3.1 Composite materials

First, we test the four different scalings for the composite material no. 1 and $1/h = 6N^{1/3}$ as in Section 6.5.2.1; cf. Table 6.9 and 6.10 for the different scaling results.

Except for one run with Algorithm II, Algorithms Ia, Ib, Ic, and II work well for all examples and all scalings, Algorithm III cannot be recommended for any scaling. As expected, the most expensive scaling (deluxe) also gives the smallest coarse space. However, the diagonal scalings ρ- and stiffness-scaling only result in an adaptive coarse space that is about 10-15% larger. Multiplicity-scaling cannot be recommended for any algorithm since it doubles the coarse space size compared to deluxe-scaling.

6.5.3.2 Randomly distributed coefficients

Second, we test the four different scalings for five different distributions of randomly distributed coefficients with 80% low and 20% high coefficients as in

Table 6.9: *Adaptive FETI-DP (Alg. Ia-III) with ρ- and deluxe-scaling and generalized transformation-of-basis approach.* Compressible linear elasticity of composite material no. 1 with $E_1 = 1$ and $N^{2/3}$ beams with $E_2 = 1e+6$ on the unit cube; $\nu = 0.3$ for the whole domain; conforming $\mathcal{P}_1$ finite element discretization with $1/h = 6N^{1/3}$ and irregular partitioning of the domain; see Figure 5.1. Coarse spaces for TOL = 10 for all generalized eigenvalue problems. Notation as in Table 6.4. [68]. Copyright Electronic Transactions on Numerical Analysis.

Adaptive FETI-DP: *Algorithms Ia, Ib, Ic, II, and III* (Gen. t.-o.-b. appr.)
$1/h = 6N^{1/3}$ – composite material no. 1 – irregular partitioning

		Algorithms Ia, Ib, and Ic					*Algorithm II*			*Algorithm III*		
N	$\lvert\Pi'\rvert$		κ	*its*	$\lvert\Pi\rvert$	$\#\mathcal{E}_{evp}$	κ	*its*	$\lvert\Pi\rvert$	κ	*its*	$\lvert\Pi\rvert$
ρ-scaling												
3^3	960	a)	**8.65**	34	699	2 (2.0%)	**8.65**	34	699	1.36e+6	68	243
		b)	**8.65**	34	699	1 (1.0%)						
		c)	**8.67**	34	450	1 (1.0%)						
5^3	5433	a)	**9.16**	35	3675	25 (4.2%)	**9.16**	35	3669	5.50e+5	190	1242
		b)	**9.16**	35	3675	12 (2.1%)						
		c)	**10.49**	36	2325	12 (2.1%)						
7^3	16248	a)	**10.76**	37	10101	65 (3.6%)	**10.76**	37	10089	1.21e+6	424	3606
		b)	**10.76**	37	10101	27 (1.5%)						
		c)	**13.36**	39	6693	27 (1.5%)						
9^3	35838	a)	**10.13**	36	19632	144 (3.6%)	**10.13**	36	19626	7.77e+5	500	7053
		b)	**10.13**	36	19632	52 (1.3%)						
		c)	**12.85**	39	12921	52 (1.3%)						
deluxe-scaling												
3^3	960	a)	**7.51**	20	603	2 (2.0%)	**7.51**	20	603	**7.52**	27	207
		b)	**7.51**	20	603	1 (1.0%)						
		c)	**7.51**	20	393	1 (1.0%)						
5^3	5433	a)	**9.61**	29	3129	25 (4.2%)	**9.61**	29	3126	9.98e+3	77	1002
		b)	**9.61**	29	3129	12 (2.1%)						
		c)	**9.63**	29	2004	12 (2.1%)						
7^3	16248	a)	**7.69**	30	8721	65 (3.6%)	**7.69**	30	8709	3.04e+4	178	2976
		b)	**7.69**	30	8721	27 (1.5%)						
		c)	**7.70**	30	5859	27 (1.5%)						
9^3	35838	a)	**10.76**	34	16671	144 (3.6%)	**10.76**	34	16656	8.57e+4	221	5718
		b)	**10.76**	34	16671	52 (1.3%)						
		c)	**10.77**	34	11022	52 (1.3%)						

Table 6.10: *Adaptive FETI-DP (Alg. Ia-III) with stiffness- and multiplicity-scaling and generalized transformation-of-basis approach.* Compressible linear elasticity of composite material no. 1 with $E_1 = 1$ and $N^{2/3}$ beams with $E_2 = 1e+6$ on the unit cube; $\nu = 0.3$ for the whole domain; conforming $\mathcal{P}_1$ finite element discretization with $1/h = 6N^{1/3}$ and irregular partitioning of the domain; see Figure 5.1. Coarse spaces for TOL $= 10$ for all generalized eigenvalue problems. Notation as in Table 6.4. [68]. Copyright Electronic Transactions on Numerical Analysis.

Adaptive FETI-DP: *Algorithms Ia, Ib, Ic, II, and III* (Gen. t.-o.-b. appr.)

$1/h = 6N^{1/3}$ – composite material no. 1 – irregular partitioning

		Algorithms Ia, Ib, and Ic					*Algorithm II*			*Algorithm III*		
N	$\lvert\Pi'\rvert$		κ	*its*	$\lvert\Pi\rvert$	$\#\mathcal{E}_{evp}$	κ	*its*	$\lvert\Pi\rvert$	κ	*its*	$\lvert\Pi\rvert$
stiffness-scaling												
3^3	960	a)	**7.84**	26	654	2 (2.0%)	**7.84**	26	654	7.23e+4	55	228
		b)	**7.84**	26	654	1 (1.0%)						
		c)	**7.85**	27	423	1 (1.0%)						
5^3	5433	a)	**11.16**	32	3393	25 (4.2%)	**11.16**	32	3390	3.45e+4	148	1107
		b)	**11.16**	32	3393	12 (2.1%)						
		c)	**11.19**	32	2151	12 (2.1%)						
7^3	16248	a)	**9.12**	33	9255	65 (3.6%)	**9.12**	33	9240	9.74e+4	342	3174
		b)	**9.12**	33	9255	27 (1.5%)						
		c)	**9.15**	34	6132	27 (1.5%)						
9^3	35838	a)	**9.92**	34	17718	144 (3.6%)	**9.92**	34	17712	1.04e+5	395	6138
		b)	**9.92**	34	17718	52 (1.3%)						
		c)	**9.93**	34	11583	52 (1.3%)						
multiplicity-scaling												
3^3	960	a)	**8.63**	33	1029	2 (2.0%)	5.51e+5	54	1026	1.36e+6	345	426
		b)	**8.63**	33	1029	1 (1.01%)						
		c)	**8.66**	35	696	1 (1.01%)						
5^3	5433	a)	**9.10**	35	5172	25 (4.2%)	**9.10**	35	5169	1.62e+6	500	2115
		b)	**9.10**	35	5172	12 (2.07%)						
		c)	**10.46**	36	3420	12 (2.07%)						
7^3	16248	a)	**10.73**	37	14625	65 (3.6%)	**10.73**	37	14619	1.72e+6	500	6183
		b)	**10.73**	37	14625	27 (1.54%)						
		c)	**13.34**	39	10023	27 (1.54%)						
9^3	35838	a)	**10.09**	36	29598	144 (3.6%)	**10.09**	36	29592	1.58e+6	500	12477
		b)	**10.09**	36	29598	52 (1.3%)						
		c)	**12.77**	39	20010	52 (1.3%)						

Table 6.11: *Adaptive FETI-DP (Alg. Ia-III) with ρ- and deluxe-scaling and generalized transformation-of-basis approach.* Compressible linear elasticity of randomly distributed coefficients with 80% coefficients with $E_1 = 1$ and 20% coefficients with $E_2 = 1e+6$ on the unit cube; $\nu = 0.3$ for the whole domain; conforming $\mathcal{P}_1$ finite element discretization with $1/h = 8N^{1/3}$ for $N = 4^3$ and irregular partitioning of the domain; see Figure 5.10. Coarse spaces for TOL = 10 for all generalized eigenvalue problems. Notation as in Table 6.4. [68]. Copyright Electronic Transactions on Numerical Analysis.

Adaptive FETI-DP: *Algorithms Ia, Ib, Ic, II, and III* (Gen. t.-o.-b. appr.)
$N = 4^3$ – $1/h = 8N^{1/3}$ – random coefficients (80/20) – irregular partitioning

		Algorithms Ia, Ib, and Ic				*Algorithm II*			*Algorithm III*		
run	$\lvert\Pi'\rvert$		κ	*its*	$\lvert\Pi\rvert$	$\#\mathcal{E}_{evp}$	κ	*its*	$\lvert\Pi\rvert$	κ	*its*	$\lvert\Pi\rvert$
ρ-scaling												
1	2646	a)	**9.24**	33	7350	8 (2.8%)	**12.21**	34	7347	5.00e+5	500	3543
		b)	**9.24**	33	7350	8 (2.8%)						
		c)	**9.24**	33	7350	8 (2.8%)						
2		a)	**9.40**	33	7278	8 (2.8%)	1.57e+5	52	7272	4.74e+5	500	3480
		b)	**9.40**	33	7278	8 (2.8%)						
		c)	**9.40**	33	7278	8 (2.8%)						
3		a)	**8.32**	33	7320	8 (2.8%)	6.52e+4	67	7308	4.72e+5	500	3525
		b)	**8.32**	33	7320	8 (2.8%)						
		c)	**8.32**	33	7320	8 (2.8%)						
4		a)	**9.44**	34	7230	8 (2.8%)	**9.44**	34	7227	4.67e+5	500	3408
		b)	**9.44**	34	7230	8 (2.8%)						
		c)	**9.44**	34	7230	8 (2.8%)						
5		a)	**9.26**	33	7416	8 (2.8%)	2.54e+5	73	7407	4.69e+5	500	3588
		b)	**9.26**	33	7416	8 (2.8%)						
		c)	**9.26**	33	7416	8 (2.8%)						
deluxe-scaling												
1	2646	a)	**6.08**	21	6174	8 (2.8%)	**7.09**	22	6171	1.86e+5	358	2769
		b)	**6.08**	21	6174	8 (2.8%)						
		c)	**6.08**	21	6174	8 (2.8%)						
2		a)	**5.65**	22	5997	8 (2.8%)	**5.65**	22	5997	6.90e+4	285	2643
		b)	**5.65**	22	5997	8 (2.8%)						
		c)	**5.65**	22	5997	8 (2.8%)						
3		a)	**4.89**	23	6069	8 (2.8%)	3.12e+4	42	6057	2.35e+5	433	2703
		b)	**4.89**	23	6069	8 (2.8%)						
		c)	**4.89**	23	6069	8 (2.8%)						
4		a)	**5.94**	24	5979	8 (2.8%)	**5.94**	24	5976	2.07e+5	336	2601
		b)	**5.94**	24	5979	8 (2.8%)						
		c)	**5.94**	24	5979	8 (2.8%)						
5		a)	**4.70**	22	6207	8 (2.8%)	3.14e+4	36	6201	1.37e+5	320	2799
		b)	**4.70**	22	6207	8 (2.8%)						
		c)	**4.70**	22	6207	8 (2.8%)						

Table 6.12: *Adaptive FETI-DP (Alg. Ia-III) with stiffness- and multiplicity-scaling and generalized transformation-of-basis approach.* Compressible linear elasticity of randomly distributed coefficients with 80% coefficients with $E_1 = 1$ and 20% coefficients with $E_2 = 1e+6$ on the unit cube; $\nu = 0.3$ for the whole domain; conforming $\mathcal{P}_1$ finite element discretization with $1/h = 8N^{1/3}$ for $N = 4^3$ and irregular partitioning of the domain; see Figure 5.10. Coarse spaces for TOL = 10 for all generalized eigenvalue problems. Notation as in Table 6.4. [68]. Copyright Electronic Transactions on Numerical Analysis.

Adaptive FETI-DP: *Algorithms Ia, Ib, Ic, II, and III* (Gen. t.-o.-b. appr.)
$N = 4^3$ – $1/h = 8N^{1/3}$ – random coefficients (80/20) – irregular partitioning

		Algorithms Ia, Ib, and Ic				*Algorithm II*			*Algorithm III*		
run	$\lvert\Pi'\rvert$	κ	*its*	$\lvert\Pi\rvert$	$\#\mathcal{E}_{evp}$	κ	*its*	$\lvert\Pi\rvert$	κ	*its*	$\lvert\Pi\rvert$
stiffness-scaling											
1	2646	a) **7.82**	29	6921	8 (2.8%)	**7.82**	29	6918	2.15e+5	500	3177
		b) **7.82**	29	6921	8 (2.8%)						
		c) **7.82**	29	6921	8 (2.8%)						
2		a) **7.40**	27	6876	8 (2.8%)	2.86e+4	43	6870	3.05e+5	500	3171
		b) **7.40**	27	6876	8 (2.8%)						
		c) **7.40**	27	6876	8 (2.8%)						
3		a) **9.97**	30	6903	8 (2.8%)	6.47e+4	61	6891	2.72e+5	500	3195
		b) **9.97**	30	6903	8 (2.8%)						
		c) **9.97**	30	6903	8 (2.8%)						
4		a) **7.80**	30	6738	8 (2.8%)	**7.80**	30	6735	2.19e+5	500	3033
		b) **7.80**	30	6738	8 (2.8%)						
		c) **7.80**	30	6738	8 (2.8%)						
5		a) **8.49**	29	6987	8 (2.8%)	3.63e+4	60	6978	2.15e+5	500	3228
		b) **8.49**	29	6987	8 (2.8%)						
		c) **8.49**	29	6987	8 (2.8%)						
multiplicity-scaling											
1	2646	a) **8.48**	32	12744	8 (2.8%)	6.12e+5	116	12732	9.70e+5	500	8574
		b) **8.48**	32	12744	8 (2.8%)						
		c) **8.48**	32	12744	8 (2.8%)						
2		a) **9.02**	33	12900	8 (2.8%)	9.69e+5	130	12885	1.31e+6	500	8721
		b) **9.02**	33	12900	8 (2.8%)						
		c) **9.02**	33	12900	8 (2.8%)						
3		a) **9.42**	33	13092	8 (2.8%)	6.32e+4	64	13080	1.42e+6		8922
		b) **9.42**	33	13092	8 (2.8%)						
		c) **9.42**	33	13092	8 (2.8%)						
4		a) **9.13**	33	13074	8 (2.8%)	2.69e+5	140	13059	1.35e+6	500	8895
		b) **9.13**	33	13074	8 (2.8%)						
		c) **9.13**	33	13074	8 (2.8%)						
5		a) **7.78**	31	12972	8 (2.8%)	2.48e+5	67	12963	1.85e+6	500	8805
		b) **7.78**	31	12972	8 (2.8%)						
		c) **7.78**	31	12972	8 (2.8%)						

Section 6.5.2.3 but with $1/h = 8N^{1/3}$ instead of $1/h = 5N^{1/3}$; cf. Tables 6.11 and 6.12 for the different scaling results.

Algorithms II and III are not robust for any scaling. Considering Algorithms Ia, Ib, and Ic, the coarse space for deluxe-scaling is again the smallest and the fewest iterations are needed for convergence, but deluxe-scaling is also far more costly than ρ- or stiffness-scaling and the latter two use an coarse space, which is only about 10-15% larger, to achieve similar convergence results. Once again, multiplicity-scaling cannot be recommended since it uses a coarse space that is about twice as large as that of deluxe-scaling.

6.5.4 Approximate solutions of the local eigenvalue problems

In this section, we present results for the adaptive FETI-DP and the adaptive BDDC algorithms in combination with the iterative eigenvalue solver LOBPCG; see [86, 85]. For LOBPCG, we choose a block size 10 and use a Cholesky decomposition of the right hand side of the eigenvalue problem as local preconditioner. We limit the number of maximum iterations of the iterative eigensolver in the following subsection as indicated in the tables and also study our methods for different random materials with just two iterations of LOBPCG. We use a stopping criterion of 1e-5 for LOBPCG which, in combination with highly ill-conditioned local matrices, can already lead to instability of the solver. The implementation of LOBPCG already states that "excessively small requested tolerance may result in often restarts and instability"; see [85]. On one hand, we see that for a maximum number of 200 iterations in LOBPCG, the global PCG algorithm can become unstable; see Table 6.13. On the other hand, it should be noted that convergence does not seem to be necessary since 2-5 iterations already seem to give a stable domain decomposition algorithm with fast convergence. In Figure 6.6, we present some insights into the convergence or nonvergence behavior of the residuals and given a posteriori error estimates in the LOBPCG eigensolver, preconditioned by a Cholesky decomposition of the right hand side, for 27 subdomains, $1/h = 15N^{1/3}$, composite material no. 1, and an irregular decomposition of the unit cube; see Tables 5.20 and 5.21 for the results of the corresponding runs of adaptive FETI-DP with balancing.

6.5.4.1 Composite materials

We test the larger example, i.e., $N = 5^3$, of Table 5.20 with different numbers of maximum iterations of the iterative eigensolver to show that a larger admissible number of iterations does not necessarily lead to faster convergence and can even lead to an instable global PCG scheme; see the results for LOBPCG with up

to 200 iterations in Table 6.13. Again, we also refer to Figure 6.6 for insights on the local convergence or nonconvergence of the residuals for the comparable test problem with just 27 subdomains.

6.5.4.2 Randomly distributed coefficients with different user-defined tolerances for the solution of the local eigenvalue problems

We test three different random coefficient distributions of a heterogeneous material composed out of seven different homogeneous materials. In these examples, 30% of the tetrahedra have a Young modulus of $\mathrm{E}_1 = 1$, 20% have a Young modulus of $\mathrm{E}_2 = 10$, and another 10% each have a Young modulus of $\mathrm{E}_3 = 100$, $\mathrm{E}_4 = 1000$, $\mathrm{E}_5 = 1e+4$, $\mathrm{E}_6 = 1e+5$, and $\mathrm{E}_7 = 1e+6$; see Figure 6.7 and Table 6.14. As can be seen from Figure 6.7 (right) the approximated spectrum of the local eigenvalue problems is continuous such that we can expect different results for different choices of the tolerance TOL.

We first observe that for all tolerances, convergence is achieved using just two iterations of the LOBPCG eigensolver.

Considering the different tolerances, for all runs the approximated condition number is of the size of the chosen tolerance TOL. We state that only TOL = 10 ensures convergence within less than 50 iterations but it also uses a coarse space that is three times as large as that of TOL = 100 and nine to ten times as large as that of TOL = 1000. A trade-off between fast convergence and a manageable size of the coarse space remains a problem- and facility-dependent task.

6.5.5 Preconditioners for iterative solvers of the local eigenvalue problems

Eventually, we present some results for different preconditioning choices for the iterative solution of the local generalized eigenvalue problems. As a test case, we use the composite material no. 2 with an irregular decomposition of the unit cube; cf. Figure 5.8. This section is essentially based on the results already published by the author of this thesis and his coauthors in [70].

In practice, when using two projections Π_{is} and $\overline{\Pi}_{is}$ to remove the rigid body modes from S_{is} for $\partial\Omega_i \cap \partial\Omega_s \neq \emptyset$, the matrix built from the local Schur complements $S^{(i)}$ and $S^{(s)}$, the right hand side of the eigenvalue problems writes

$$\overline{\Pi}_{is}(\Pi_{is}S_{is}\Pi_{is} + \sigma_{is}(I - \Pi_{is}))\overline{\Pi}_{is} + \sigma_{is}(I - \overline{\Pi}_{is}); \tag{6.21}$$

cf. (6.5) and (6.13). The projection $I - \overline{\Pi}_{is}$ consists of the sum of several rank one matrices, and we usually avoid to build the matrix explicitly.

Table 6.13: *Adaptive FETI-DP and BDDC (Alg. Ia-III with LOBPCG) with ρ-scaling and generalized transformation-of-basis approach.* Compressible linear elasticity of composite material no. 1 with $E_1 = 1$ and $N^{2/3}$ beams with $E_2 = 1e+6$ on the unit cube; $\nu = 0.3$ for the whole domain; conforming $\mathcal{P}_1$ finite element discretization with $1/h = 15N^{1/3}$ for $N = 5^3$ and irregular partitioning of the domain; see Figure 5.1. Coarse spaces for TOL = 10 for all generalized eigenvalue problems. Solution of the local eigenvalue problems by LOBPCG with different maximum iteration numbers. Notation as in Table 6.4. [68]. Copyright Electronic Transactions on Numerical Analysis.

Adaptive FETI-DP and BDDC: *Algorithms Ia, Ib, Ic, II, and III* (Gen. t.-o.-b. appr.)
$N = 5^3$ – $1/h = 15N^{1/3}$ – composite material no. 1 – irregular partitioning

Adaptive FETI-DP

		Algorithms Ia, Ib, and Ic				*Algorithm II*			*Algorithm III*		
LOBPCG max. its	$\lvert\Pi'\rvert$		κ	*its*	$\lvert\Pi\rvert$	$\#\mathcal{E}_{evp}$	κ	*its*	$\lvert\Pi\rvert$	κ	*its*	$\lvert\Pi\rvert$
1	6159	a)	**43.59**	59	10677	8 (1.2%)	**43.59**	59	10677	6.82e+5	269	2259
		b)	**43.59**	59	10677	0 (0%)						
		c)	**43.70**	59	5673	0 (0%)						
2		a)	**15.00**	42	12768	8 (1.2%)	**15.00**	42	12768	6.82e+5	189	2781
		b)	**15.00**	42	12768	0 (0%)						
		c)	**15.01**	42	6675	0 (0%)						
5		a)	**18.37**	40	13437	8 (1.2%)	**18.37**	40	13437	6.81e+5	184	2928
		b)	**18.37**	40	13437	0 (0%)						
		c)	**18.39**	41	6954	0 (0%)						
200		a)	4.77e+4	500	13734	8 (1.2%)	4.77e+4	500	13734	6.16e+5	500	3105
		b)	4.77e+4	500	13734	0 (0%)						
		c)	4.78e+4	500	7194	0 (0%)						

Adaptive BDDC

		Algorithms Ia, Ib, and Ic				*Algorithm II*			*Algorithm III*		
LOBPCG max. its	$\lvert\Pi'\rvert$		κ	*its*	$\lvert\Pi\rvert$	$\#\mathcal{E}_{evp}$	κ	*its*	$\lvert\Pi\rvert$	κ	*its*	$\lvert\Pi\rvert$
1	6159	a)	**43.72**	55	10677	8 (1.2%)	**43.72**	55	10677	6.84e+5	282	2259
		b)	**43.72**	55	10677	0 (0%)						
		c)	**43.79**	55	5673	0 (0%)						
2		a)	**15.05**	40	12768	8 (1.2%)	**15.05**	40	12768	6.84e+5	210	2781
		b)	**15.05**	40	12768	0 (0%)						
		c)	**15.05**	41	6675	0 (0%)						
5		a)	**18.43**	38	13437	8 (1.2%)	**18.43**	38	13437	6.83e+5	208	2928
		b)	**18.43**	38	13437	0 (0%)						
		c)	**18.42**	39	6954	0 (0%)						
200		a)	4.82e+4	500	13734	8 (1.2%)	4.82e+4	500	13734	6.55e+5	500	3105
		b)	4.82e+4	500	13734	0 (0%)						
		c)	4.81e+4	500	7194	0 (0%)						

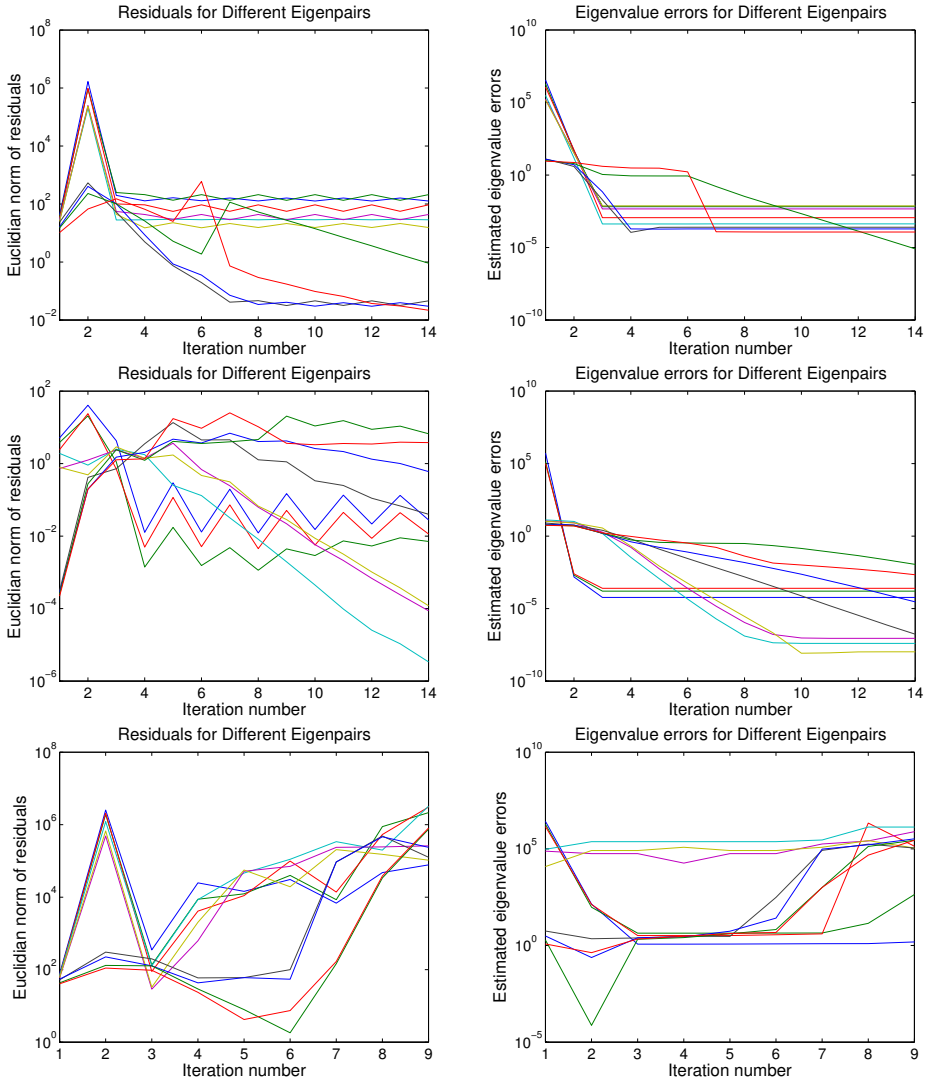

Figure 6.6: *Convergence or nonconvergence behavior of the residuals (left) and given a posteriori error estimates (right) of the local LOBPCG solver with a block size of 10 for compressible linear elasticity.* Residuals (left) and error estimates (right) for the first and significant iterations of the LOBPCG eigensolver and three local generalized eigenvalue problems. Compressible linear elasticity of composite material no. 1 with $E_1 = 1$ and $N^{2/3}$ beams with $E_2 = 1e+6$ on the unit cube; $\nu = 0.3$ for the whole domain; conforming $\mathcal{P}_1$ finite element discretization with $1/h = 15N^{1/3}$ for 27 subdomains and irregular partitioning of the domain; see Figure 5.1.

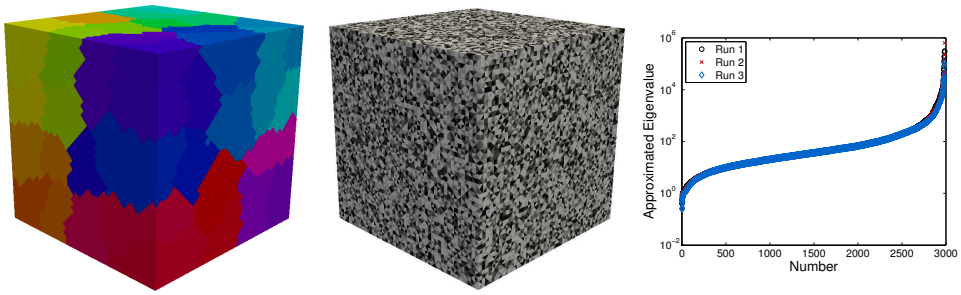

Figure 6.7: *Randomly distributed material coefficients with seven different coefficient values and an irregular decomposition of the unit cube.* Irregular decomposition of the unit cube into 64 subdomains (left), randomly distributed material coefficients from $\mathrm{E}_1 = 1e+0$ in lightgray to $\mathrm{E}_7 = 1e+6$ in black (center), and approximated local eigenvalues greater 0.1 from all generalized eigenvalue problems, i.e., estimates from two iterations with LOBPCG on the local eigenvalue problems (right). [68]. Copyright Electronic Transactions on Numerical Analysis.

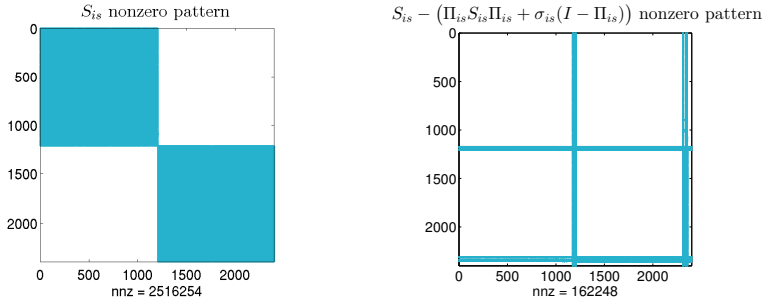

Figure 6.8: *Representative nonzero pattern of the matrices S_{is} (left) and $S_{is} - \left(\Pi_{is} S_{is} \Pi_{is} + \sigma_{is}(I - \Pi_{is})\right)$ (right).* Plot for two randomly chosen subdomains Ω_i, Ω_s and composite material no. 2 with an irregular decomposition of the unit cube, conforming $\mathcal{P}_2$ finite element discretization for $1/h = 6N^{1/3}$; see Figure 5.8. [70]

Table 6.14: *Adaptive FETI-DP and BDDC (Alg. Ia-III with LOBPCG) with ρ-scaling and balancing approach.* Compressible linear elasticity of a heterogeneous material with seven coefficient values from $E_1 = 1$ to $E_7 = 1e+6$ on the unit cube; $\nu = 0.3$ for the whole domain; conforming $\mathcal{P}_1$ finite element discretization with $1/h = 12N^{1/3}$ for $N = 4^3$ and irregular partitioning of the domain; see Figure 6.7. Coarse spaces for TOL $\in \{10, 100, 1000\}$ for all generalized eigenvalue problems. Solution of the local eigenvalue problems by LOBPCG with two iterations. Notation as in Table 6.4. [68]. Copyright Electronic Transactions on Numerical Analysis.

Adaptive FETI-DP: *Algorithms Ia, Ib, Ic, II, and III* (Gen. t.-o.-b. appr.)

$N = 4^3$ – $1/h = 12N^{1/3}$ – heterogeneous material with seven coefficient values
$E_1 = 1$ (30%), $E_2 = 10$ (20%), $E_i = 10^{i-1}$, $i = 3, \ldots, 7$ (10% each) – irregular partitioning

		Algorithms Ia, Ib, and Ic				*Algorithm II*			*Algorithm III*		
run	$\lvert\Pi'\rvert$		κ	*its*	$\lvert\Pi\rvert$	$\#\mathcal{E}_{evp}$	κ	*its*	$\lvert\Pi\rvert$	κ	*its*	$\lvert\Pi\rvert$
TOL=10												
1	2820	a)	**14.11**	41	12084	2 (0.7%)	**14.11**	41	12084	1.12e+5	500	4842
		b)	**14.11**	41	12084	2 (0.7%)						
		c)	**14.11**	41	12084	2 (0.7%)						
2		a)	**13.18**	40	12186	2 (0.7%)	**13.18**	40	12186	2.12e+5	500	4920
		b)	**13.18**	40	12186	2 (0.7%)						
		c)	**13.18**	40	12186	2 (0.7%)						
3		a)	**18.89**	42	12147	2 (0.7%)	**18.89**	42	12147	1.04e+5	500	4863
		b)	**18.89**	42	12147	2 (0.7%)						
		c)	**18.89**	42	12147	2 (0.7%)						
TOL=100												
1	2820	a)	107.26	113	4278	2 (0.7%)	107.26	113	4278	1.11e+5	500	987
		b)	107.26	113	4278	2 (0.7%)						
		c)	107.26	113	4278	2 (0.7%)						
2		a)	100.32	110	4299	2 (0.7%)	100.32	110	4299	2.11e+5	500	1041
		b)	100.32	110	4299	2 (0.7%)						
		c)	100.32	110	4299	2 (0.7%)						
3		a)	115.62	114	4329	2 (0.7%)	115.62	114	4329	1.04e+5	500	1041
		b)	115.62	114	4329	2 (0.7%)						
		c)	115.62	114	4329	2 (0.7%)						
TOL=1000												
1	2820	a)	970.55	321	1311	2 (0.7%)	970.55	321	1311	1.11e+5	500	321
		b)	970.55	321	1311	2 (0.7%)						
		c)	970.55	321	1311	2 (0.7%)						
2		a)	993.08	320	1260	2 (0.7%)	993.08	320	1260	2.08e+5	500	318
		b)	993.08	320	1260	2 (0.7%)						
		c)	993.08	320	1260	2 (0.7%)						
3		a)	1609.10	343	1158	2 (0.7%)	1609.10	343	1158	1.03e+5	500	273
		b)	1609.10	343	1158	2 (0.7%)						
		c)	1609.10	343	1158	2 (0.7%)						

The operator $\Pi_{is} S_{is} \Pi_{is} + \sigma_{is}(I - \Pi_{is})$, however, can be built cheaply by only scaling a few rows and columns of the Schur complements and adding some constants; see Figure 6.8 for the nonzero pattern of S_{is} and the difference $S_{is} - \Pi_{is} S_{is} \Pi_{is} + \sigma_{is}(I - \Pi_{is})$. The sparsity is only changed slightly and, here, the resulting sparsity is about 55%.

We test five different preconditioners for the iterative eigensolver. First, we take a Cholesky decomposition of the fully assembled right hand side (6.21) as the (expensive) base line to compare against. This choice has been used in all previously presented results using the iterative eigensolver LOBPCG. We also test an LU and ILU(0) decomposition of $\Pi_{is} S_{is} \Pi_{is} + \sigma_{is}(I - \Pi_{is})$ and use the projection $\overline{\Pi}_{is}$ to remove the corresponding kernel from the preconditioner, i.e., we apply the projection $\overline{\Pi}_{is}$ before and after the forward-backward substitution. If $\Pi_{is} S_{is} \Pi_{is} + \sigma_{is}(I - \Pi_{is})$ is only semidefinite, we automatically compute a generalized inverse by means of the MATLAB function.

The preconditioner using an LU decomposition, is denoted by

$$\overline{\Pi}_{is} \mathbf{LU}\Big(\Pi_{is} S_{is} \Pi_{is} + \sigma_{is}(I - \Pi_{is})\Big)\overline{\Pi}_{is}.$$

For the ILU(0) preconditioner, we write

$$\overline{\Pi}_{is} \mathbf{ILU(0)}\Big(\Pi_{is} S_{is} \Pi_{is} + \sigma_{is}(I - \Pi_{is})\Big)\overline{\Pi}_{is}.$$

Finally, we also test two different local lumped versions, i.e., an LU and an ILU(0) decomposition of $K_{\Gamma\Gamma,is} = \text{blockdiag}(K_{\Gamma\Gamma}^{(i)}, K_{\Gamma\Gamma}^{(s)})$ and also apply the projection Π_{is} before and after the forward-backward substitution. For the LU decomposition, we write

$$\overline{\Pi}_{is} \Pi_{is} \mathbf{LU}\Big(K_{\Gamma\Gamma,is}\Big)\Pi_{is}\overline{\Pi}_{is}$$

and for the ILU(0) preconditioner, we write

$$\overline{\Pi}_{is} \Pi_{is} \mathbf{ILU(0)}\Big(K_{\Gamma\Gamma,is}\Big)\Pi_{is}\overline{\Pi}_{is}$$

Obviously, the most expensive algorithm, the Cholesky decomposition of the assembled right hand side of the eigenvalue problem yields the best results with respect to the condition numbers and the iteration counts of the FETI-DP algorithm. In this case, only a few iterations (e.g., 1-5) of the LOBPCG solver are sufficient; cf. also our previous results. However, from Table 6.15, we also see that an LU or ILU(0)-factorization of $\Pi_{is} S_{is} \Pi_{is} + \sigma_{is}(I - \Pi_{is})$ with a few more iterations can suffice. The slight differences in the condition

Table 6.15: *Adaptive FETI-DP (Alg. Ia-Ic) with ρ-scaling and generalized transformation-of-basis approach.* Compressible linear elasticity of composite material no. 2 with $E_1 = 1$ and $4N^{2/3}$ beams with $E_2 = 1e+6$ on the unit cube; $\nu = 0.3$ for the whole domain; conforming $\mathcal{P}_1$ finite element discretization with $1/h = 10N^{1/3}$ and irregular partitioning of the domain; see Figure 5.8. Coarse spaces for TOL = 10 for all generalized eigenvalue problems. Notation as in Table 6.4. Adapted by permission from Springer International Publishing AG: [Springer] [Domain Decomposition Methods in Science and Engineering XXIV] [70] [COPYRIGHT] (2018).

Adaptive FETI-DP: *Algorithms Ia, Ib, Ic* (Gen. t.-o.-b. appr.)
$1/h = 10N^{1/3}$ – composite material no. 2 – irregular partitioning

Local Preconditioner: Chol$\Big(\overline{\Pi}_{is}(\Pi_{is}S_{is}\Pi_{is} + \sigma_{is}(I-\Pi_{is}))\overline{\Pi}_{is} + \sigma_{is}(I-\overline{\Pi}_{is})\Big)$.

			Algorithm Ia			*Algorithm Ib*			*Algorithm Ic*		
N	LOBPCG max. its	$\lvert\Pi'\rvert$	κ	*its*	$\lvert\Pi\rvert$	κ	*its*	$\lvert\Pi\rvert$	κ	*its*	$\lvert\Pi\rvert$
3^3	5	168	3.35	16	1905	3.35	16	1905	3.53	19	594
	25		8.89	18	2025	8.89	18	2025	9.12	21	684
	100		10.59	18	2013	10.59	18	2013	10.78	21	672
4^3	5	351	3.34	16	5259	3.34	16	5259	3.56	19	1674
	25		14.95	24	5535	14.95	24	5535	15.33	25	1869
	100		5.07	18	5496	5.07	18	5496	5.08	21	1848

Local Preconditioner: $\overline{\Pi}_{is}$**LU**$\Big(\Pi_{is}S_{is}\Pi_{is} + \sigma_{is}(I-\Pi_{is})\Big)\overline{\Pi}_{is}$.

			Algorithm Ia			*Algorithm Ib*			*Algorithm Ic*		
N	LOBPCG max. its	$\lvert\Pi'\rvert$	κ	*its*	$\lvert\Pi\rvert$	κ	*its*	$\lvert\Pi\rvert$	κ	*its*	$\lvert\Pi\rvert$
3^3	5	168	110.84	38	1872	110.84	38	1872	163.73	43	603
	25		3.84	18	1926	3.84	18	1926	3.84	20	660
	100		3.84	18	1938	3.84	18	1938	3.85	21	666
4^3	5	351	471.97	62	5074	471.97	62	5074	521.66	67	1647
	25		54.34	30	5259	54.34	30	5259	90.89	33	1830
	100		56.50	30	5328	56.50	30	5328	99.32	32	1884

Local Preconditioner: $\overline{\Pi}_{is}$**ILU(0)**$\Big(\Pi_{is}S_{is}\Pi_{is} + \sigma_{is}(I-\Pi_{is})\Big)\overline{\Pi}_{is}$.

			Algorithm Ia			*Algorithm Ib*			*Algorithm Ic*		
N	LOBPCG max. its	$\lvert\Pi'\rvert$	κ	*its*	$\lvert\Pi\rvert$	κ	*its*	$\lvert\Pi\rvert$	κ	*its*	$\lvert\Pi\rvert$
3^3	5	168	5.36	17	2088	5.36	17	2088	5.45	21	711
	25		3.82	20	1995	3.82	20	1995	3.84	21	678
	100		3.35	17	1998	3.35	17	1998	3.52	20	675
4^3	5	351	24.35	26	6225	24.35	26	6225	26.50	30	2394
	25		3.82	20	5964	3.82	20	5964	3.83	22	2277
	100		4.37	20	5850	4.37	20	5850	4.42	22	2181

Table 6.16: *Adaptive FETI-DP (Alg. Ia-Ic) with ρ-scaling and generalized transformation-of-basis approach.* Compressible linear elasticity of composite material no. 2 with $\mathrm{E}_1 = 1$ and $4N^{2/3}$ beams with $\mathrm{E}_2 = 1e+6$ on the unit cube; $\nu = 0.3$ for the whole domain; conforming $\mathcal{P}_1$ finite element discretization with $1/h = 10N^{1/3}$ and irregular partitioning of the domain; see Figure 5.8. Coarse spaces for $\mathrm{TOL} = 10$ for all generalized eigenvalue problems. Notation as in Table 6.4. Adapted by permission from Springer International Publishing AG: [Springer] [Domain Decomposition Methods in Science and Engineering XXIV] [70] [COPYRIGHT] (2018).

Adaptive FETI-DP: *Algorithms Ia, Ib, Ic* (Gen. t.-o.-b. appr.)

$1/h = 10N^{1/3}$ – composite material no. 2 – irregular partitioning

Local Preconditioner: $\overline{\Pi}_{is}\Pi_{is}\mathbf{LU}\left(K_{\Gamma\Gamma,is}\right)\Pi_{is}\overline{\Pi}_{is}$.

			Algorithm Ia			*Algorithm Ib*			*Algorithm Ic*		
N	LOBPCG max. its	$\lvert\Pi'\rvert$	κ	*its*	$\lvert\Pi\rvert$	κ	*its*	$\lvert\Pi\rvert$	κ	*its*	$\lvert\Pi\rvert$
3^3	5	168	1.81e+6	500	0	1.81e+6	500	0	1.81e+6	500	0
	25		3.83e+4	500	441	3.83e+4	500	441	1.56e+5	500	102
	100		452.95	126	442	452.95	126	442	468.46	129	81
4^3	5	351	1.06e+6	500	0	1.06e+6	500	0	1.06e+6	500	0
	25		5.97e+4	500	1254	5.97e+4	500	1254	1.72e+5	500	273
	100		677.56	181	936	677.56	181	936	685.30	183	213

Local Preconditioner: $\overline{\Pi}_{is}\Pi_{is}\mathbf{ILU(0)}\left(K_{\Gamma\Gamma,is}\right)\Pi_{is}\overline{\Pi}_{is}$.

			Algorithm Ia			*Algorithm Ib*			*Algorithm Ic*		
N	LOBPCG max. its	$\lvert\Pi'\rvert$	κ	*its*	$\lvert\Pi\rvert$	κ	*its*	$\lvert\Pi\rvert$	κ	*its*	$\lvert\Pi\rvert$
3^3	5	168	1.81e+6	500	0	1.81e+6	500	0	1.81e+6	500	0
	25		3.26e+4	500	462	3.26e+4	500	462	8.40e+4	500	111
	100		197.47	108	324	197.47	108	324	200.09	110	75
4^3	5	351	1.06e+6	500	0	1.06e+6	500	0	1.06e+6	500	0
	25		4.56e+4	500	1236	4.56e+4	500	1236	8.51e+4	500	282
	100		2.54e+4	316	978	2.54e+4	316	978	6.15e+4	329	222

numbers and iteration counts result from the larger coarse space size for the ILU preconditioner. The results for the lumped preconditioner, an LU or ILU decomposition of $K_{\Gamma\Gamma,is}$ are given for completeness and to show that the results are not satisfactory; cf. Table 6.16.

6.6 Conclusion on adaptive FETI-DP and BDDC with the generalized transformation-of-basis approach

In Chapter 5, an adaptive coarse space for the FETI-DP domain decomposition method applied to heterogeneous elliptic problems in three dimension has been introduced. The method is based on numerically solving local generalized eigenvalue problems on faces and edges of subdomains and on using these eigenvectors as deflation vectors. The condition number of the resulting preconditioned operator using deflation is bounded independently of the heterogeneity.

In Section 4.5, for heterogeneous problems and general scalings, a correspondence is shown between FETI-DP methods using deflation and FETI-DP and BDDC methods using the generalized transformation-of-basis approach with partial finite element assembly.

In this chapter, we have combined the adaptive approach with the generalized transformation-of-basis approach to obtain FETI-DP and BDDC methods with a condition number bound independent of heterogeneities but using a generalized transformation-of-basis approach instead of deflation or balancing.

For the new approach, it will be easier to extend the parallel scalability to a large number of subdomains on large supercomputers, also for heterogeneous problems, by solving the coarse problem inexactly. This is not possible in projection approaches like deflation or balancing, which are fragile with respect to inexact solves of the coarse problem; see, e.g., [80].

We have presented comparisons of the adaptive method with different scalings such as ρ-, deluxe-, stiffness-, and multiplicity-scaling. For our test cases, we state that ρ-scaling only needs about 10-15% of additional constraints compared to deluxe-scaling. The findings of stiffness-scaling are comparable to those of ρ-scaling. Multiplicity-scaling on the other hand gives significantly larger coarse spaces.

We have again shown that, also for hard problems including those with random coefficients with seven different materials, a few iterations of an iterative eigensolver on the local eigenvalue problems can be sufficient to obtain fast convergence of the overall method.

We have also shown that the use of an LU or ILU decomposition of $\Pi_{is} S_{is} \Pi_{is} + \sigma_{is}(I - \Pi_{is})$, instead of a Cholesky decomposition of the fully assembled right hand side of the eigenvalue problem, is a reasonable choice since this matrix can be built easily but just manipulating a few rows and columns of S_{is}.

7 A parallel implementation of FETI-DP with adaptive coarse spaces using the generalized transformation-of-basis approach

7.1 Preliminaries

In this chapter, we describe our parallel implementation of adaptive FETI-DP. We discuss and present details for an efficient implementation of the adaptive FETI-DP Algorithms Ia and Ic using the generalized transformation-of-basis approach; cf. Sections 6.2.3 and 4.5.

The FETI-DP algorithms are implemented in C/C++ using PETSc 3.8.0 [4, 5] and MPI. Direct solves are generally carried out by means of the PARDISO solver [116] from the Intel MKL [57]. The local generalized eigenvalue problems are solved by the SLEPc software library 3.8.0 [56, 113]. In some cases, we also use the SLEPc interface to LAPACK [1]. However, since the assembly and direct solution are memory- and time-consuming, we also present strategies for the alternative handling of these cases. We use nonblocking point-to-point MPI communication to set up the eigenvalue problems and to collect the computed constraints. The adaptive software is implemented based on the parallel implementation of standard FETI-DP of [73].

The data and index sets used in the standard FETI-DP implementation are sufficient to construct the generalized eigenvalue problems in the adaptive version. To store the data of each eigenvalue problem, we define a data structure *EigenvalueProblem*. It then consists of an `std::vector` *subdomains* which stores the two corresponding subdomains in the eigenvalue problem, an `std::vector` *subdomain_neighbors* that stores additional neighbors for edge eigenvalue problems and is empty for face eigenvalue problems. We also need an `std::vector` *edges* that holds the edges in the eigenvalue problem in a local numbering and an integer corresponding to the face in the eigenvalue problem (or -1 if the eigenvalue problem is based on an edge); see Figure 7.1. In order

`struct` *EigenvalueProblem*

- `int` *comm_tag*: individual communication tag
- `std::vector` *subdomains*: pair of subdomains in the eigenvalue problem
- `std::vector` *subdomain_neighbors*: other adjacent subdomains on the edge (empty for face eigenvalue problems)
- `int` *face*: face index (in local list of faces; or -1 for edge eigenvalue problem)
- `std::vector` *edges*: edges' indices (in local list of edges)

Figure 7.1: *Data structure* EigenvalueProblem *which holds the elementary information of the eigenvalue problems.*

to build these structures, for each face and each edge, we have to know the adjacent subdomain indices. For these latter sets, we make use of the categorization of nodes, which is already necessary in standard FETI-DP to set up the application of the jump operator B. In order to communicate the data, we have to create a consistent ordering of the eigenvalue problems and set up an individual communication tag.

In Section 7.2, we present details of the process to set-up and solve the local generalized eigenvalue problems using PETSc, plain MPI, and SLEPc. In Section 7.3, we discuss the obligatory modifications from the standard FETI-DP implementation to adaptive FETI-DP using the generalized transformation-of-basis approach.

Before discussing the parallel implementation in detail, let us shortly comment on another optimization for adaptive FETI-DP and BDDC if Neumann boundary conditions are used.

Remark 7.1 (Edges on the Neumann boundary and adaptive FETI-DP)**.** *According to the commonly used definitions of faces, edges and vertices in three dimensions (see, e.g., [77, Def. 2.2] and [82, Def. 3.1]), the degrees of freedom on the Neumann boundary with multiplicity two form edges on the Neumann boundary. However, when splitting up the face constraints as mentioned in* (5.12) *and* (5.13) *(or in* (6.8) *and* (6.9)*) the coarse space is enlarged unnecessarily if an edge in a face eigenvalue problem lies on the Neumann boundary and its nodes only have multiplicity two. By using the constraint on the face and the Neumann edge without splitting, no additional coupling is introduced and the size of the adaptive coarse space can be kept smaller. In our parallel implementation, we use this strategy and consequently reduce the coarse space size of Algorithm Ia significantly. For Algorithm Ic, this has made no differ-*

- local and global numbering for all a priori primal variables Π' on $\partial\Omega_s$
- local (in the space of the degrees of freedom) and global (one-to-one from the corresp. degree of freedom to the space of Lagrange multipliers) for all a priori dual variables Δ' on $\partial\Omega_s$
- a mapping from the local edges to the primal indices on the closure of the edge
- the Schur complement $S^{(s)}$
- the degrees of freedom on $\partial\Omega_s \cap \partial\Omega_D$ (to detect the common rigid body modes incl. possible hinge modes)
- the coordinates of the nodes on $\partial\Omega_s$ (to detect the rigid body modes incl. possible hinge modes)
- the edge(s) and the possible face considered in the eigenvalue problem (one send per eigenvalue problem between two adjacent subdomains!)

Figure 7.2: *Data sent from the rank of Ω_s to the rank of Ω_i (for $i < s$).*

ence for our test examples since we have never set high coefficients next to the boundary of the domain.

7.2 Parallel implementation details of the local generalized eigenvalue problems

Before the set-up of the local generalized eigenvalue problems can take place, certain information have to be interchanged between adjacent pairs of subdomains. The send and receive processes are executed with nonblocking point-to-point communication using `MPI_Isend` and `MPI_IRecv`. For each adjacent pair of subdomains $\{\Omega_i, \Omega_s\}$, the data is sent from the rank with the higher index to the rank with the lower index. Integers and doubles are sent separately. In most cases, two subdomains only share one eigenvalue problem. However, it can occur that two subdomains share more than one edge eigenvalue problem. In these cases, one additional send and receive process is initiated per additional eigenvalue problem between these two subdomains. Otherwise, we cannot extract the correct subset of corresponding rows from the jump operator B.

Let us assume $i < s$. The data sent, in the current implementation, from the rank of Ω_s to the rank of Ω_i is illustrated in Figure 7.2. Note that for deluxe-scaling, for any edge and any adjacent subdomain Ω_k, we also need to communicate the Schur complement $S^{(k)}$ from the processes of Ω_k to the process of Ω_i. This applies likewise to edges in face eigenvalue problems as to edges in edge eigenvalue problems.

We use $P_{D,\overline{\mathcal{Z}}^{is}}$ as a generic representation for $P_{D,\overline{\mathcal{F}}^{ij}}$ and $P_{D,\mathcal{E}^{ik}}$. The SLEPc built-in Krylov-Schur eigensolver is then applied to the local generalized eigenvalue problem

$$Ax = \mu Bx$$

with $A = \overline{\Pi}_{is}\Pi_{is}P^T_{D,\overline{\mathcal{Z}}^{is}}S_{is}P_{D,\overline{\mathcal{Z}}^{is}}\Pi_{is}\overline{\Pi}_{is}$ and $B = \overline{\Pi}_{is}(\Pi_{is}S_{is}\Pi_{is} + \sigma(I - \Pi_{is}))\overline{\Pi}_{is} + \sigma(I - \overline{\Pi}_{is})$; cf. (6.5) and (6.13).

The left hand side, A, is not formed explicitly, only the local Schur complements are assembled. For each application of A, we need one matrix-vector multiplication with $S^{(i)}$ and $S^{(s)}$ each. We apply both projections by several vector operations and just use two matrix-vector multiplications with the localized B_D- and B-operator.

For the right hand side B, after successful reception of the data from Ω_s, we assemble the matrix $S_{is} - \big(\Pi_{is}S_{is}\Pi_{is} + \sigma_{is}(I - \Pi_{is})\big)$ as a sparse sequential matrix. For assembling this matrix, we use the arrays of the dense Schur complements which are in column-major order and exploit the symmetry of the resulting matrix to set the column entries as row entries. Within this process only several rows and columns of S_{is} have to be manipulated to obtain $S_{is} - \big(\Pi_{is}S_{is}\Pi_{is} + \sigma_{is}(I - \Pi_{is})\big)$; cf. the representative nonzero pattern in Figure 6.8. In case of sufficient Dirichlet boundary conditions to prevent Ω_i or Ω_s from moving as a rigid body, the corresponding block in $\overline{\Pi}_{is}$ is empty. Otherwise, we exploit the fact that $I - \overline{\Pi}_{is}$ is an orthogonal projection onto the rigid body modes that are continuous on $W_i \times W_s$. Thus, the application of the right hand side operator of the generalized eigenvalue problem can be executed with just one matrix-vector multiplications with $S_{is} - \big(\Pi_{is}S_{is}\Pi_{is} + \sigma_{is}(I - \Pi_{is})\big)$ and several vector-vector or scalar-vector operations.

Inside the SLEPc `EPS` (Eigenvalue Problem Solver) object, the `ST` (Spectral Transformation) object handles the spectral transformations. Since we do not use any shift of the eigenvalues, the generalized problem is internally handled as $B^{-1}Ax = \mu x$ where the solution of the linear system defined by B is executed via the `KSP` object inside the spectral transformations object; see [113] and Figure 7.3. In our case, we set the preconditioner of the `KSP` to an LU decomposition of the (approximated) right hand side. The LU decomposition is performed inplace by Intel MKL PARDISO [57, 116]. If the two subdomains have sufficient Dirichlet boundary, the matrix $S_{is} - \big(\Pi_{is}S_{is}\Pi_{is} + \sigma_{is}(I - \Pi_{is})\big)$ is positive definite and an LU decomposition can be computed. If this is not the case, we conduct an LU factorization of $S_{is} - \big(\Pi_{is}S_{is}\Pi_{is} + \sigma_{is}(I - \Pi_{is})\big) + \varepsilon I$ with a standard choice of $\varepsilon = 1e - 4$ in order to prevent zero pivots.

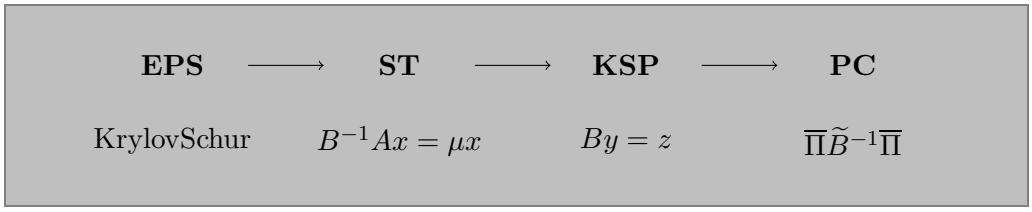

Figure 7.3: *Chosen settings for the object structure in the SLEPc* `EPS` *solver.* The `ST` object is used to build a basis for the Krylov decomposition. $\overline{\Pi}$ removes the common rigid body modes, $\widetilde{B}^{-1}$ represents an LU-decomposition of $S_{is} - \left(\Pi_{is} S_{is} \Pi_{is} + \sigma_{is}(I - \Pi_{is})\right) + \varepsilon I$. The solution of the Ritz problem is performed by a direct solver and not illustrated, here.

Inside the Krylov-Schur method, a Krylov decomposition is established before applying the Rayleigh-Ritz procedure; see [128]. As [55] states, in the symmetric case, the Krylov-Schur method is equivalent to the *thick-restart* Lanczos method; see [133]. Consequently, in SLEPc, a Lanczos factorization is computed by using the left hand side A and the `ST`-owned `KSP` object for the right hand side B. The orthogonalization of the basis vectors is carried out via a (modified) Gram-Schmidt algorithm with respect to the inner product $\langle \cdot, B \cdot \rangle$; see [55]. We always use the modified Gram-Schmidt algorithm. Though, due to highly ill-conditioned right hand sides B, the local iterative solver of the preconditioned `KSP` object might not converge or even break down if large coefficient jumps of 1e+6, irregular decompositions, the preset divergence tolerance, and a relative convergence tolerance of 1e-5 for the `KSP` object are used. The breakdown mostly occurs due to large jumps in the residual. However, we have already documented a similar behavior for LOBPCG in Figure 6.6. Note that the condition number of the local right hand sides B can exceed the condition number of the global system matrix by several orders of magnitude.

For cases, when the iterative solver of the `KSP` object breaks down, we offer two workarounds. The first workaround consists of an assembly of the left and the right hand side of the eigenvalue problem and the use of a direct solver via the SLEPc interface to LAPACK; see [1]. The SLEPc interface then calls `LAPACKgetrf` to solve the generalized eigenvalue problem by an LU decomposition with partial pivoting. A second workaround is obviously offered by (re)starting the iterative solver wit a very rough convergence criterion and a very high divergence tolerance `dtol` for the `KSP` object. If the workaround fails, we can still make a large part (e.g., every second or third degree of freedom) of the face or edge primal. We factually deactivate the breakdown test of the

`KSP` object via `dtol` by setting it to, e.g., 1e12. We refer to [121, Fig. 5.1] and Figure 6.6, where large jumps in the residual of the first steps of the iterative solver have already been observed, even if an adequate preconditioner is used. The iterative solver is only used to build the Lanczos factorization. Bad approximations to eigenvectors of large eigenvalues, i.e., approximations that do not point into the direction of the eigenvector, are removed after the Ritz-values have been computed by a direct solver and when the Krylov decomposition is truncated; cf. [128, 55]. The promising results of Tables 5.20, 5.21, 6.13, 6.14, and 6.15 proposed to use only very rough approximations to the eigenvectors.

We use a block Krylov-Schur method with a block size of 10. If the smallest eigenvalue in the computed block of (approximate) eigenvalues is still larger than our choice of TOL, we use the SLEPc functionality `EPSSetDeflationSpace` to compute another block of eigenvalues and -vectors in a deflated search space.

For some test cases, we let the Krylov-Schur algorithm iterate until a relative reduction of the residual of 1e-5 or until a maximum number of 100 iterations is attained. For other cases, we only allow five iterations of the iterative eigensolver and use the rough approximations to the eigenvectors to compute the adaptive constraints. Similar settings have been used in our experiments with LOBPCG (see [85]) in Section 6.5.5.

After all eigenvalue problems are solved, we collect the number of constraints and their global indices by one call to `MPI_Allgather` and `MPI_Allgatherv` each. The more expensive communication of the constraints itself is performed by nonblocking point-to-point communication. They are then orthogonalized edge by edge and face by face with the modified Gram-Schmidt algorithm with a drop tolerance of 1e-1 and redistributed point-to-point.

7.3 Parallel implementation details of adaptive FETI-DP

7.3.1 General adaptive method

For theoretical considerations of FETI-DP as it is done in the previous chapters, it is often more handy to consider the equations based on the Schur complements and the jump operator on the interface, i.e.,

$$F = B_\Gamma \widetilde{S}^{-1} B_\Gamma^T;$$

cf. (3.11). However, in the implementation, the identity

$$F = B_{B'} K_{B'B'}^{-1} B_{B'}^T + B_{B'} K_{B'B'}^{-1} \widetilde{K}_{\Pi' B}^T \widetilde{S}_{\Pi'\Pi'}^{-1} \widetilde{K}_{\Pi' B'} K_{B'B'}^{-1} B_{B'}^T$$

comes into play; cf. (3.7). Thus, in order to define an adaptive version of (3.7) and to describe the efficient parallel implementation of adaptive FETI-DP, we have to redefine the operators introduced for the generalized transformation-of-basis approach. This redefination is only based on the introduction of additional identity matrices to fit the dimension (and a reordering of the submatrices). Hence, the equivalent definitions can be carried over into one another easily. For the ease of understanding, we refrain from introducing new operator symbols or additional indices.

Let us recall the index sets $B' = (I,\, \Delta')$ and $\Delta' = (\Delta,\, \Pi)$ with Δ denoting the a posteriori dual and Π the a posteriori primal variables. Using the representation $B' = (I,\, \Delta')$, the system matrix of the FETI-DP master system as given in (3.5) writes

$$\begin{pmatrix} K_{II} & K_{\Delta' I}^T & \widetilde{K}_{\Pi' I}^T & 0 \\ K_{\Delta' I} & K_{\Delta'\Delta'} & \widetilde{K}_{\Pi'\Delta'}^T & B_{\Delta'}^T \\ \widetilde{K}_{\Pi' I} & \widetilde{K}_{\Pi'\Delta'} & \widetilde{K}_{\Pi'\Pi'} & 0 \\ 0 & B_{\Delta'} & 0 & 0 \end{pmatrix}. \tag{7.1}$$

Note that a further subdivision of $K_{\Delta'\Delta'}$ does not make much sense since the constraints in the transformation matrix are columns defined on $\Delta' = (\Delta,\, \Pi)$.

The global transformation matrix from (4.22), reordered and extended by the identity to the interior variables, is

$$T = \begin{pmatrix} I_I & 0 & 0 & 0 \\ 0 & T_\Delta & T_\Pi & 0 \\ 0 & 0 & 0 & I_{\Pi'} \end{pmatrix} \tag{7.2}$$

where T_Π is defined by all adaptively computed constraint vectors and T_Δ can be obtained by blockwise orthogonalization (i.e., edge by edge and face by face) of the identity matrix against the constraint vectors.

The global restriction operator R and the corresponding second level assembly operator R^T are given by

$$R = \begin{pmatrix} I_I & 0 & 0 & 0 \\ 0 & I_\Delta & 0 & 0 \\ 0 & 0 & R_\Pi & 0 \\ 0 & 0 & 0 & I_{\Pi'} \end{pmatrix}, \tag{7.3}$$

where R_Π^T assembles the a posteriori degrees of freedom; cf. (4.24). We also define the multiplicity-scaled variant of R_Π^T by $R_{\Pi,\mu}^T$. The operator R_μ is obtained from R by replacing R_Π with $R_{\Pi,\mu}$.

To obtain the system matrix of the adaptive FETI-DP master system, the leading 3×3 block of (7.1) has to be transformed and assembled, i.e., $R^T T^T$ has to be applied from the left and TR has to be applied from the right. Correspondingly, we also have to adapt the application of the jump operator B to be in the correct basis; cf. the definition in (4.35). Note that for several submatrices, the multiplication with the submatrices of T and the application of R is trivial and has not be carried out.

With the transformation, the assembly, and the restriction applied to (7.1) as well as the adaptation of the jump operator, the system matrix of the adaptive FETI-DP master system is

$$\left(\begin{array}{cc|c|cc} K_{II} & K_{\Delta' I}^T T_\Delta & K_{\Delta' I}^T T_\Pi R_\Pi & \widetilde{K}_{\Pi' I}^T & 0 \\ T_\Delta^T K_{\Delta' I} & T_\Delta^T K_{\Delta'\Delta'} T_\Delta & T_\Delta^T K_{\Delta'\Delta'} T_\Pi R_\Pi & T_\Delta^T \widetilde{K}_{\Pi'\Delta'}^T & T_\Delta^T B_{\Delta'}^T \\ \hline R_\Pi^T T_\Pi^T K_{\Delta' I} & R_\Pi^T T_\Pi^T K_{\Delta'\Delta'} T_\Delta & R_\Pi^T T_\Pi^T K_{\Delta'\Delta'} T_\Pi R_\Pi & R_\Pi^T T_\Pi^T \widetilde{K}_{\Pi'\Delta'}^T & R_\Pi^T T_\Pi^T B_{\Delta'}^T \\ \widetilde{K}_{\Pi' I} & \widetilde{K}_{\Pi'\Delta'} T_\Delta & \widetilde{K}_{\Pi'\Delta'} T_\Pi R_\Pi & \widetilde{K}_{\Pi'\Pi'} & 0 \\ \hline 0 & B_{\Delta'} T_\Delta & B_{\Delta'} T_\Pi R_\Pi & 0 & 0 \end{array}\right). \tag{7.4}$$

Equivalently, we can write

$$\left(\begin{array}{c|c|c} \widehat{K}_{BB} & \widehat{\widetilde{K}}_{\widehat{\Pi}B}^T & \widehat{B}_B^T \\ \hline \widehat{\widetilde{K}}_{\widehat{\Pi}B} & \widehat{\widetilde{K}}_{\widehat{\Pi}\widehat{\Pi}} & \widehat{B}_{\widehat{\Pi}}^T \\ \hline \widehat{B}_B & \widehat{B}_{\widehat{\Pi}} & 0 \end{array}\right) \tag{7.5}$$

if grouping interior and a posteriori dual variables to $B := (I, \Delta)$ and a priori and a posteriori primal variables to $\widehat{\Pi} := (\Pi, \Pi')$, i.e., merging the denoted submatrices inside the horizontal and vertical delimiters to the new notations. Note that $\widehat{B}_\Pi$ is only nontrivial on the a posteriori primal degrees of freedom and enables the necessary interaction between these and the a posteriori dual variables as explained in Section 4.5 for the generalized transformation-of-basis approach.

Thus, after solving the local generalized eigenvalue problems and distributing the computed constraints, the second step of the adaptive algorithm consists of establishing the new operators and matrices. The assembly in the primal variables is realized by setting up two `VecScatter`s. The first scatter is necessary to assemble in all primal variables $\widehat{\Pi}$ and, for the preconditioner, the second

scatter is needed to assemble only the a posteriori primal variables Π; cf. the subsequent paragraphs.

In a next step, the transformed matrices

- $T_\Delta^T K_{\Delta' I}$
- $T_\Pi^T K_{\Delta' I}$
- $T_\Delta^T K_{\Delta'\Delta'} T_\Delta$
- $T_\Delta^T K_{\Delta'\Delta'} T_\Pi$
- $T_\Pi^T K_{\Delta'\Delta'} T_\Pi$
- $K_{\Pi'\Delta'} T_\Delta$
- $K_{\Pi'\Delta'} T_\Pi$

are obtained block by block, where the blocks are local submatrices of $T^{(i)T} K^{(i)} T^{(i)}$. Note that $\widetilde{K}_{\Pi'\Delta'} T_\Delta$ and $\widetilde{K}_{\Pi'\Delta'} T_\Pi$ can be obtained from $K_{\Pi'\Delta'} T_\Delta$ and $K_{\Pi'\Delta'} T_\Pi$ since the order of the first level scatter (defined by R_Π) and the transformation T can be inversed. The first level scatter and the transformation act on disjoint sets.

By Gaussian elimination, we then obtain from (7.5)

$$\begin{aligned} \widehat{F} :&= \widehat{B}_B \widehat{K}_{BB}^{-1} \widehat{B}_B^T - \big(\widehat{B}_{\widehat{\Pi}} - \widehat{B}_B \widehat{K}_{BB}^{-1} \widehat{\widetilde{K}}_{\widehat{\Pi}B}^T\big) \widehat{\widetilde{S}}_{\widehat{\Pi}\widehat{\Pi}}^{-1} \big(\widehat{B}_{\widehat{\Pi}}^T - \widehat{\widetilde{K}}_{\widehat{\Pi}B} \widehat{K}_{BB}^{-1} \widehat{B}_B^T\big) \\ \text{with } \widehat{\widetilde{S}}_{\widehat{\Pi}\widehat{\Pi}} &:= \widehat{\widetilde{K}}_{\widehat{\Pi}\widehat{\Pi}} - \widehat{\widetilde{K}}_{\widehat{\Pi}B} \widehat{K}_{BB}^{-1} \widehat{\widetilde{K}}_{\widehat{\Pi}B}^T. \end{aligned} \tag{7.6}$$

In (7.6), the first part of $\widehat{F}$, i.e., $\widehat{B}_B \widehat{K}_{BB}^{-1} \widehat{B}_B^T$, remains perfectly parallelizable. Furthermore, as in standard FETI-DP, we need one coarse solve per iteration.

The scatter to realize the application of the jump operator does not need any new set-up. Only the application has to be changed by applying the local (transposed) transformation matrices before and after the scatter, respectively. By using the scatter structure of $B_{\Delta'}$ and $B_{\Delta'}^T$ already established a priori, a posteriori dual and a posteriori primal variables are processed simultaneously. Thus, the application of $\widehat{F}$ gets a bit tricky. For instance, for the solution of the linear system

$$\widehat{K}_{BB} x = \widehat{B}_B^T \widehat{\lambda}$$

the values $\widehat{B}_B^T \widehat{\lambda} = T_\Delta^T B_{\Delta'}^T \widehat{\lambda}$ are extracted from $T_{\Delta'}^T B_{\Delta'}^T \widehat{\lambda}$ (note the additional prime!). The complementary (and assembled) part, i.e., $\widehat{B}_{\widehat{\Pi}}^T \widehat{\lambda} = R_\Pi^T T_\Pi^T B_{\Delta'}^T \widehat{\lambda}$

is added afterwards to the vector $-\widehat{\widetilde{K}}_{\widehat{\Pi}B}x$. The assembly in the a posteriori primal variables is naturally performed by the scatter operation. Then, the coarse solve can be executed. Before the application of $B_{\Delta'}$, the values in the a posteriori dual and a posteriori primal variables have to be collected.

Note that $\Delta' \cap \widehat{\Pi} = \Pi$. As a consequence, in the iterative scheme, we always work with two vectors $u_{\Delta'}$ and $u_{\widehat{\Pi}}$. The values in the a posteriori primal variables have to be transfered from one to the other, depending on the next matrix-vector multiplication or `KSPSolve` process to execute.

The Dirichlet preconditioner of adaptive FETI-DP writes

$$\widehat{M}_T^{-1} := B_D T\, R_\mu \underbrace{R^T\, T^T S T\, R}_{=\widehat{\widetilde{S}}} R_\mu^T\, T^T B_D^T. \tag{7.7}$$

The preconditioner then is the sum of local operators with communication between neighboring subdomains via B, as before, and minimal additional communication via the scatter $R_\Pi R_{\Pi,\mu}^T$ (inside RR_μ^T). For the definition of $\widehat{M}_T^{-1}$, see also (4.36) and (3.19), respectively, for the related Dirichlet preconditioner M_D^{-1} for standard FETI-DP. In the application of $R_{\Pi,\mu}$, the conducted multiplicity-scaling is independent of the actually chosen scaling in B_D; cf. Section 4.5. Our numerical experiments show that the runtime of the Krylov process in total, and therefore also the time consumption of the additional communication process, is negligible.

7.3.2 Computation of the solution in the displacement variables

Given the appropriately transformed right hand side $\widehat{f} = (\widehat{f}_B^T,\ \widehat{\widetilde{f}}_{\widehat{\Pi}}^T,\ 0)^T$, assembled in the primal variables, the master system of adaptive FETI-DP reads

$$\begin{pmatrix} \widehat{K}_{BB} & \widehat{\widetilde{K}}_{\widehat{\Pi}B}^T & \widehat{B}_B^T \\ \widehat{\widetilde{K}}_{\widehat{\Pi}B} & \widehat{\widetilde{K}}_{\widehat{\Pi}\widehat{\Pi}} & \widehat{B}_{\widehat{\Pi}}^T \\ \widehat{B}_B & \widehat{B}_{\widehat{\Pi}} & 0 \end{pmatrix} \begin{pmatrix} \widehat{u}_B \\ \widehat{\widetilde{u}}_{\widehat{\Pi}} \\ \widehat{\lambda} \end{pmatrix} = \begin{pmatrix} \widehat{f}_B \\ \widehat{\widetilde{f}}_{\widehat{\Pi}} \\ 0 \end{pmatrix}; \tag{7.8}$$

cf. (7.5). When computing the solution in the displacement variables, we have to keep in mind that $\widehat{B}_{\widehat{\Pi}} \neq 0$. In contrast to standard FETI-DP, the Gaussian elimination then yields

$$\widehat{\widetilde{u}}_{\widehat{\Pi}} = \widehat{\widetilde{S}}_{\widehat{\Pi}\widehat{\Pi}}^{-1}\big(\widehat{\widetilde{f}}_{\widehat{\Pi}} - \widehat{\widetilde{K}}_{\widehat{\Pi}B}\widehat{K}_{BB}^{-1}\widehat{f}_B - \widehat{B}_{\widehat{\Pi}}^T\widehat{\lambda} + \widehat{\widetilde{K}}_{\widehat{\Pi}B}\widehat{K}_{BB}^{-1}\widehat{B}_B^T\widehat{\lambda}\big), \tag{7.9}$$

$$\widehat{u}_B = \widehat{K}_{BB}^{-1}\big(\widehat{f}_B - \widehat{B}_B^T\widehat{\lambda} - \widehat{\widetilde{K}}_{\widehat{\Pi}B}^T\widehat{\widetilde{u}}_{\widehat{\Pi}}\big). \tag{7.10}$$

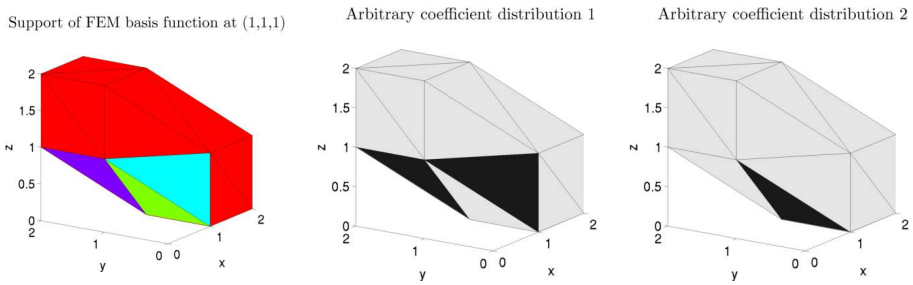

Figure 7.4: *24 tetrahedra forming the support of the finite element basis function φ_x at $x = (1,1,1)^T$.* View of an irregular domain decomposition restricted to the support of φ_x with Ω_i (turquois), Ω_j (green), Ω_k (purple), and Ω_l (red) sharing a nonstraight edge $\mathcal{E}$, where x is an inner node (left). Two arbitrary coefficient distributions restricted to the support of the basis function φ_x (center and right).

Thus, the term $-\widehat{\widetilde{S}}_{\widehat{\Pi}\widehat{\Pi}\widehat{\Pi}}^{-1}\widehat{B}_{\widehat{\Pi}}^T\widehat{\lambda}$ adds to the solution in the primal variables.

7.3.3 Parallel implementation details of Algorithm Ic with unknown coefficient values and based on stiffness-scaling

In this short section, we want to discuss the parallel implementation of the neighborhood strategy of Algorithm Ic (see Section 5.2.2) if the exact coefficient distribution is not available and stiffness-scaling is used. Let us consider structured or "relatively structured" meshes, where the ratio between the largest and the smallest element is close to one. For unstructured meshes, where we cannot give a parameter h, which is close to the diameter of all tetrahedral elements, the situation becomes more complex.

Let us consider an irregular domain decomposition and an edge eigenvalue problem between Ω_i and Ω_k on an edge $\mathcal{E}$ with interior node $(1,1,1)^T$; see Figure 7.4. Assume that this node is shared by these two subdomains as well as Ω_j and Ω_l. Now, the neighborhood strategy is applied to this edge. In Figure 7.4, we have depicted the situation by visualizing the support of the finite element basis function φ_x at $x = (1,1,1)^T$. In the first image (left), a selected, irregular domain decomposition is shown. Only a single tetrahedron of the support belongs to Ω_i (turquois), Ω_j (green), and Ω_k (purple) each. The remaining 21 tetrahedra belong to Ω_l (red). The other two pictures show two different coefficient distributions with high (black) and low (light-gray)

coefficients on the specific tetrahedra. In a structured mesh with six tetrahedra per cube, a node lies on the boundary of at most 24 tetrahedra.

There are several difficulties to be addressed if the coefficients are not know but Algorithm Ic should be used. The first difficulty is given by the fact that only the diagonal entry of the stiffness matrix $k_x^{(i)}$ and not the coefficient $\rho^{(i)}(x)$ is available. Additionally, we may avoid to send the entries of the stiffness matrices of Ω_j and Ω_l to the rank of Ω_i. If the Schur complements are sent for the set-up of the local eigenvalue problem between Ω_i and Ω_k (which has been found to be faster than to send the local stiffness matrices), the entries of the stiffness matrix of Ω_k are not available, either. Another difficulty results from the fact that the entries of the stiffness matrices are obtained by integration over the local support of the finite element basis functions. For the second distribution (Figure 7.4 (right)), for instance, the entry $k_x^{(l)}$ is 21 times larger than $k_x^{(i)}$ although the corresponding coefficient is actually identical.

We now want to argue on how to decide that the eigenvalue problem between Ω_i and Ω_k is not discarded.

The first coefficient distribution represents the simple case; see Figure 7.4 (center). We have a large entry $k_x^{(i)}$ in the stiffness matrix on Ω_i and if, e.g., $k_x^{(i)} \geq 1000h^3$ is satisfied, we do not discard the eigenvalue problem since, at least, one large jump exists in the neighborhood of the edge.

Now, consider the second coefficient distribution; see Figure 7.4 (right). We see that $k_x^{(i)}$ is small. We always keep the eigenvalue problem if the ratio between the largest and the smallest diagonal entry of $K^{(i)}$, which correspond to nodes in the neighborhood of the edge, is larger than 24. If this is not the case, our last check relies on the scaling. However, except for the entries of the stiffness matrix of Ω_i, we only have the communicated scaling values

$$d_x^{(i)} = \frac{k_x^{(k)}}{k_x^{(i)} + k_x^{(j)} + k_x^{(k)} + k_x^{(l)}} \quad \text{and} \quad d_x^{(k)} = \frac{k_x^{(i)}}{k_x^{(i)} + k_x^{(j)} + k_x^{(k)} + k_x^{(l)}}$$

at each local interface node x. Thus, we do not have direct access to the other stiffness matrix entries in the nominator or denominator on the rank of Ω_i. Let us denote by $k_{\max,\mathcal{E}}^{(i)}$ the largest diagonal entry of the stiffness matrix $K^{(i)}$, which corresponds to a node in the neighborhood of the edge. Assume that we already know that an homogeneous coefficient distribution is given in the entire neighborhood of the edge $\mathcal{E}$ in subdomain Ω_i. Otherwise, we keep the eigenvalue problem anyway.

For the maximum support of φ_x of 24 tetrahedra and a homogeneous, low coefficient distribution on all adjacent subdomains, it holds

$$k_x^{(s)} \leq 24 k_{\max,\mathcal{E}}^{(i)} \text{ for } s \in \{j,k,l\} \text{ as well as } \frac{1}{24} \leq \frac{k_x^{(i)}}{k_{\max,\mathcal{E}}^{(i)}} \leq 1.$$

If the minimum jump of the coefficients in the PDE is larger than just one or two orders of magnitude, we have an equivalence between these bounds and a homogeneous coefficient distribution with low coefficients around the nodes x of the edge.

The bound

$$d_x^{(k)} = \frac{\frac{k_x^{(i)}}{k_{\max,\mathcal{E}}^{(i)}}}{\frac{k_x^{(i)}+k_x^{(j)}+k_x^{(k)}+k_x^{(l)}}{k_{\max,\mathcal{E}}^{(i)}}} \geq \frac{\frac{1}{24}}{1+24(M_{\mathcal{E}}-1)} = \frac{1}{24+24^2(M_{\mathcal{E}}-1)} \tag{7.11}$$

holds for all edge nodes x. Here, $M_{\mathcal{E}}$ denotes the multiplicity of the edge. For heterogeneous problems with jumps of several orders of magnitude, this bound is broken if coefficients jumps are present around the edge.

Note that the bound (7.11) is very conservative and smaller jumps of 100 or 1000 are not detected by it. A more accurate heuristic using smaller constants might be more adequate. On the other hand, for a structured mesh with six tetrahedra per voxel and a regular domain decomposition the constant 24 can be replaced by 6, without using any heuristic.

7.4 Numerical results

In this section, we present numerical results for our parallel implementation of adaptive FETI-DP and compressible linear elasticity.

We have implemented the new coarse space (Algorithm Ia) covered by our theory (see Theorem 6.2) and a modified variant (Algorithm Ic). Algorithm Ic uses the neighborhood approach to reduce the number of edge eigenvalue problems as well as the number of constraints by also discarding edge constraints from face eigenvalue problems. For a more detailed description, see Section 5.2.2.

For all algorithms, the constraint vectors are orthogonalized blockwise (i.e., edge by edge and face by face) by a modified Gram-Schmidt algorithm with a drop tolerance of 1e-1. Note that, already in MATLAB, we observed better convergence properties with less strict drop tolerances than with tolerances of, e.g., 1e-7. We have observed a certain influence of the drop tolerance on

the obtainable precision of the global PCG algorithm. In any case, the condition number estimates from the Krylov scheme are good error indicators. If a requested convergence criterion cannot be attained by the algorithm, the eigenvalue estimate $\lambda_{\min}$ fast deteriorates.

For short edges consisting of only one dual node, we convert the single dual node into a primal node, to make the corresponding edge eigenvalue problem superfluous; see Section 5.2.3.1.

In this chapter, we always use stiffness-scaling and we follow the strategy of Algorithm Ic to detect heterogeneities in the neighborhood of the edge, based on the scaling; see Section 7.3.3.

For simplicity, we always assume the parameters E and ν to be constant on each finite element.

In the tables, κ denotes the estimated condition number of the preconditioned FETI-DP operator. The condition number estimates are obtained from the Krylov scheme. By N we denote the number of subdomains. Additionally, we report the number of iterations of the PCG algorithm by *its*, by $|\Pi'|$ the size of the a priori and by $|\Pi|$ the size of the adaptive coarse space, respectively. All a posteriori constraints are implemented using the generalized transformation-of-basis approach; see Section 4.5. We also list the number of nonzeros in the final coarse matrix as *nnz*. For the regular decompositions, we report H/h. For irregular decompositions, we only list $1/h$ and N in order to measure the mean size of the local problems. We also report the number of the global degrees of freedom as *d.o.f.* and the total *time* needed by the algorithm. A more detailed breakdown of the time needed for the single phases, e.g., the set-up and the solution time for the eigenvalue problems or the solution time of the global PCG algorithm can be found in some corresponding diagrams.

In the experiments, regular as well as irregular decompositions are tested. The irregular decompositions are set up by the METIS graph partitioner [60] using the options `-ncommon=3` and `-contig` for all problems to avoid noncontiguous subdomains as well as additional hinge modes inside single subdomains. The regular decompositions are directly performed by our C/C++ software, the irregular decompositions are imported after being exported from our MATLAB software. In these cases, the corresponding total *time*, which is given in the tables, does not include the basic set-up of the geometry. In Section 7.4.1, we also present the norm of the preconditioned residual at the last step of the PCG scheme as $\|M^{-1}r\|$.

The local generalized eigenvalue problems are set up and solved via the PETSc [4, 5] and SLEPc [56, 113] high-performance computing libraries v3.8.0; see Section 7.2.

In a few number of larger runs, we observed that a relative reduction of the preconditioned residual by a factor of 1e-10 was slightly missed. Thus, the stopping criterion for the PCG algorithm is set to a relative reduction of the preconditioned residual by a factor of 1e-8. The maximum number of iterations is set to 10 000 to show that the standard approach does not even converge after several thousands of iterations.

For the numerical experiments presented in this chapter, we use TOL $= 50\log(H/h)$ for regular decompositions. For the irregular decompositions, we use TOL $= 50\log\left(N/n_i\right)^{1/3}$, with n_i denoting the number of local nodes on Ω_i. The tolerance is therefore adapted to the estimate of edge terms in standard FETI-DP; see, e.g., [130]. It is slightly increased compared to most results from the previous chapters. See Table 6.14, for a comparison of the algorithms with different tolerances. Similar adaptations of the tolerance were already used for another adaptive coarse space; see [62]. See also [12], for detailed study of the influences of the a priori tolerances on the coarse space dimension for another adaptive approach.

For all experiments with a regular decomposition, we enforce homogeneous Dirichlet boundary conditions on the whole boundary $\partial\Omega$ of the computational domain Ω. For irregular decompositions and composite material no. 1, we enforce homogeneous Dirichlet boundary conditions on the face with $x = 0$ and zero Neumann boundary conditions elsewhere. For the hemisphere considered in Section 7.4.4, we enforce homogeneous Dirichlet boundary conditions on the upper part, satisfying $z = 0$, and, on the remaining part of the boundary, we enforce zero Neumann boundary conditions. We always apply the volume force $f := (0.1, 0.1, 0.1)^T$. Except for the last example, we always use a structured fine mesh consisting of cubes. The fine cubes are each decomposed into five (irregular decomp.) and six (reg. decomp.) tetrahedra, respectively.

We always use $\nu = 0.3$ for the entire computational domain.

All computations are conducted with one subdomain per core on the supercomputer magnitUDE at the Center for Computational Sciences and Simulation (CCSS) of the University of Duisburg-Essen. The supercomputer magnitUDE has 14 976 cores (Xeon E5-2650v4 12C 2.2GHz; 624 nodes with 24 cores each). All computing nodes hold, at least, 64 GB of main memory. Intel compilers v17.0.1 with the corresponding MKL are used.

The remaining part of the section is organized as follows.

1. **Adaptive FETI-DP versus standard FETI-DP in parallel**: In Section 7.4.1, we consider composite material no. 1 and consider different convergence criteria for the solution of the local generalized eigenvalue problems. We also show that our parallel implementation is able to excel standard FETI-DP methods.

2. **Weak scaling on irregular decompositions**: In Section 7.4.2, we consider irregular decompositions and weak scalability of our parallel implementation with a very rough convergence criterion for the solution of the local generalized eigenvalue problems.

3. **Weak scaling on regular decompositions**: In Section 7.4.3, we consider regular decompositions and weak scalability of our parallel implementation with a very rough convergence criterion for the solution of the local generalized eigenvalue problems. For regular decompositions, the a priori coarse can be chosen much smaller and the adaptive method can be tested on a larger number of subdomains.

4. **Strong scaling on irregular decompositions**: In Section 7.4.4, we consider the strong scaling of our parallel implementation on an irregularly decomposed cubic domain and an unstructured mesh on a hemisphere.

7.4.1 Adaptive FETI-DP versus standard FETI-DP in parallel

In this section, we consider composite material no. 1 and compare our parallel implementation of adaptive FETI-DP Algorithms Ia and Ic and a standard FETI-DP algorithm with a coarse space of primal vertices and edge averages. In Table 5.1, we have already shown that the classical approch does not converge within 2 000 iteratios. The results of our MATLAB implementation on composite material no. 1 and $H/h = 6$ can be found in Table 6.5. Compared to our MATLAB implementation, the size of the coarse space of Algorithm Ia is reduced; see Remark 7.1. Also note that the tolerance is not fixed to TOL = 10, here. The geometry is exported from MATLAB and imported by our C/C++ implementation. Then, the index sets of the local eigenvalue problems are collected and the eigenvalue problems are solved as described in Section 7.2. The results of the nonadaptive method have already been published as preliminary results by the author of this thesis and his coauthors in [68]. The preliminary results of our adaptive methods in [68] have been improved with respect to the timings. We only report the improved results, here.

We consider different solution strategies for the eigenvalue problems. For Algorithm Ia, we set maximum iteration number of the Krylov-Schur solver to

Table 7.1: *Standard (Vert.+edge av.) and adaptive (Algorithms Ia and Ic) FETI-DP in parallel with stiffness-scaling and generalized transformation-of-basis approach.* Compressible linear elasticity of composite material no. 1 with $\mathrm{E}_1 = 1$ and $N^{2/3}$ beams with $\mathrm{E}_2 = 1e+6$ on the unit cube; $\nu = 0.3$ for the whole domain; conforming $\mathcal{P}_2$ finite element discretization with $1/h = 6N^{1/3}$ and irregular partitioning of the domain; see Figure 5.1. Coarse spaces for $\mathrm{TOL} = 50 \log\left(N/n_i\right)^{1/3}$ for each generalized eigenvalue problem. N denotes the numer of subdomains, κ the condition numer estimates from the underlying PCG iteration, *its* the number of iterations until convergence or at cancellation of the process at the maximum wall time of 60 minutes (max_its=10 000), $\|M^{-1}r\|$ the norm of the preconditioned residual after the last step of PCG, $|\Pi'|$ the size of the a priori and (for adaptive) $|\Pi|$ the size of the adaptive coarse space. The number of nonzeros in the coarse matrix is given by *nnz* and the total runtime in minutes is denoted by *time (min)*. [68]. Copyright Electronic Transactions on Numerical Analysis.

Standard and adaptive FETI-DP:
Standard: vertices+edge averages, adaptive: Algorithms Ia and Ic (Gen. t.-o.-b. appr.)
$1/h = 6N^{1/3}$ – composite material no. 1 – irregular partitioning

$N = 64$, #cores=64, *d.o.f.*=3.11e+5							
	κ	*its*	$\lvert\Pi'\rvert$	$\lvert\Pi\rvert$	*nnz*	*time (min)*	$\|M^{-1}r\|$
Standard FETI-DP	2.06e+6	>6373	2346	-	8.59e+5	>60	5.22e-5
Adaptive Alg. Ia	83.90	51	2277	981	1.38e+6	16.65	3.78e-9
Adaptive Alg. Ic	83.89	51	2277	972	1.37e+6	16.66	3.63e-9
Adaptive Alg. Ic (loc. inex)	83.84	50	2277	998	1.39e+6	12.32	2.24e-9
$N = 216$, #cores=216, *d.o.f.*=1.02e+6							
	κ	*its*	$\lvert\Pi'\rvert$	$\lvert\Pi\rvert$	*nnz*	*time (min)*	$\|M^{-1}r\|$
Standard FETI-DP	2.09e+6	>6033	9828	-	4.46e+6	>60	7.56e-4
Adaptive Alg. Ia	55.08	62	9483	4144	7.39e+6	25.35	6.93e-9
Adaptive Alg. Ic	55.11	62	9483	4132	7.38e+6	25.30	7.01e-9
Adaptive Alg. Ic (loc. inex)	54.82	60	9483	4252	7.49e+6	18.95	7.65e-9

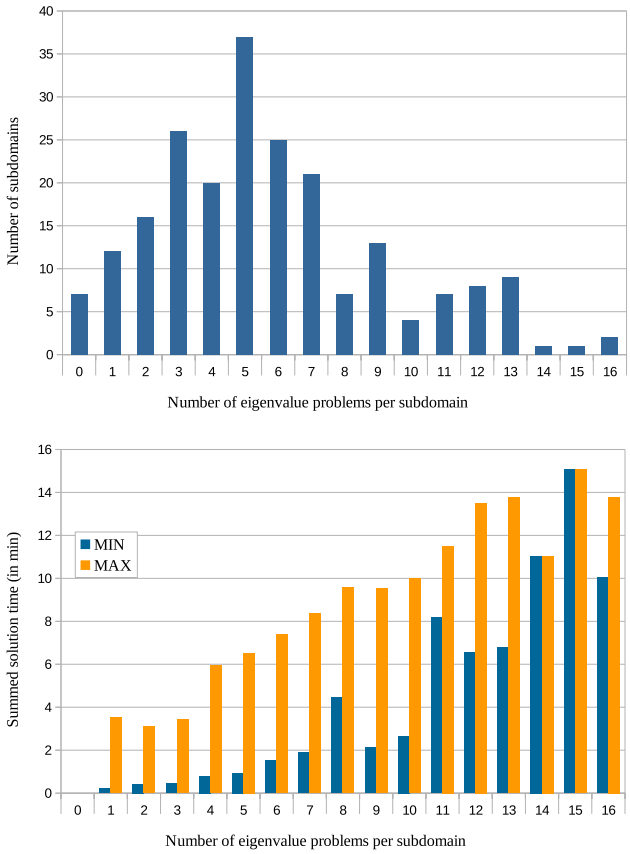

Figure 7.5: *Number of subdomains (top) and summed solution time (bottom) per number of local eigenvalue problems on one subdomain for Algoritm Ic (loc. inex.) and 216 subdomains and cores.* Plot of the distribution of the number of the local eigenvalue problems (top) and the summed solution time (bottom) for composite material no. 1 and an irregular decomposition of the unit cube; cf. Figure 5.1 and Table 7.1.

100 and require a relative reduction of the residual by a factor of 1e-5. When the iterative solver of the `ST`-owned `KSP` object breaks down, we make use of the SLEPc interface to LAPACK and solve the eigenvalue problem after assembly of the left and the right hand side operators by means of LAPACK; see Section 7.2. For the `KSP` solver, we also require a relative reduction of the residual by a factor of 1e-5 and allow up to 200 iterations. For Algorithm Ic, we first present results with the same settings. Additionally, we consider Algorithm Ic with very rough requirements on the accuracy of the approximated solution of the eigenvalue problems. We still require a relative reduction of the residual by a factor of 1e-5 for the Krylov-Schur algorithm, however, we only allow a maximum of five iterations. If the fifth iteration is attained, we use the current approximations regardless of convergence at that point. For the internal `KSP` object, we practically deactivate the divergence check via `dtol`, set it to 1e12, and only require a relative reduction of the residual by a factor of 1e-2. By this, we minimize or even eliminate the need for re-set-ups of the `EPS` object, restarts of the `KSP` solver with modified options, and the utilization of LAPACK for the solution of the eigenvalue problems to speed up our method. Note that the convergence behavior of the iterative eigensolver might not be straightforward for the highly ill-conditioned problems considered here and that large jumps in the residual can appear; see Figure 6.6. If the local solver does not converge anyway, we make every second node of the corresponding face or edge primal. This almost never occurs. In all our examples, we have found three faces where this occured. The condition numbers in the numerical results show that the final set of constraints remains comparable if this workaround, with roughly approximated eigenvectors, is used.

To distinguish the results of Algorithm Ic with accurate and with rough approximations to the eigenvectors, we write *Algorithm Ic (loc. inex.)* for the results with only rough convergence requirements for the local iterative solvers.

The maximum wall time for all algorithms is set to one hour. Within this time the classical method with a standard vertex and edge average coarse space does not converge.

From the results in Table 7.1, we see that all adaptive methods excel the standard approach, which does not converge to the required tolerance. We also see that the locally inexact version of Algorithm Ic can still reduce the runtime by about 25%, only a very low number of additional constraints (about 2% compared to the adaptive coarse space and even less compared to the total coarse space size) is (accidentally) incorporated. Compared to the preliminary results in [68], the adaptive algorithms have been speeded up significantly.

In Figure 7.5, we see that the number of local generalized eigenvalue problems is not distributed evenly and that a certain load imbalance exists. Though, Figure 7.5 (bottom) also shows that the number of eigenvalue problems per subdomain and the expected solution time for the entire set of local eigenvalue problems per subdomains is not necessarily correlated. Thus, it remains a difficult task to establish a load balance a priori. More elaborated strategies to distribute the local eigenvalue problems will be focussed.

7.4.2 Weak parallel scaling for adaptive FETI-DP on irregular decompositions

In this section, we present weak scaling results for our parallel implementation of adaptive FETI-DP Algorithm Ic with a very rough solution of the local eigenvalue problems, i.e., Algorithm Ic (loc. inex.). As before, we consider composite material no. 1, which means that the results for $N = 64$ and $N = 216$ are identical to those of Table 7.1. In Table 7.2, we present the results from 64 to 512 subdomains and cores. Figure 7.6 gives detailed information on the weak scaling for the most expensive stages of the adaptive algorithm.

In Table 7.2, we recognize good weak scalability from 64 to 512 irregular subdomains. We have a certain drop in the efficiency from 100% to 67% when increasing the number of subdomains from 64 to 125, from 125 to 512 subdomains, however, we then have very good scaling behavior.

7.4.3 Weak parallel scaling for adaptive FETI-DP on regular decompositions

In the previous section, we have presented weak scaling results for our parallel implementation and irregular decompositions into subdomains. For irregular decompositions our a priori coarse space is already quite large (cf. Remark 5.3 and Table 7.2) and the current implementation, which uses exact coarse solves, is limited by the available memory. Thus, the method runs out of memory for irregular decompositions and, e.g., thousand cores or more.

In this section, we consider a regular decomposition into subdomains, where the a priori coarse space is significantly smaller. We then present weak scaling results up to 4096 cores and subdomains; see Table 7.3 and Figure 7.8. The material considered here is a composite material denoted as *composite material no. 3*, which is similar to material no. 1. In composite material no. 3, the $N^{2/3}$ beams are cut at the interface. Then, they arranged with an offset as depicted in Figure 7.7 (left). This is performed in order to obtain coefficient

Table 7.2: *Weak parallel scaling for adaptive FETI-DP (Algorithm Ic (loc. inex.)) with one subdomain per core, stiffness-scaling and generalized transformation-of-basis approach.* Compressible linear elasticity of composite material no. 1 with $E_1 = 1$ and $N^{2/3}$ beams with $E_2 = 1e+6$ on the unit cube; $\nu = 0.3$ for the whole domain; conforming $\mathcal{P}_2$ finite element discretization with $1/h = 6N^{1/3}$ and irregular partitioning of the domain; see Figure 5.1. Coarse spaces for $\mathrm{TOL} = 50 \log\left(N/n_i\right)^{1/3}$ for each generalized eigenvalue problem. The efficiency is given by *eff.*. All other notation as in Table 7.1.

Adaptive FETI-DP: Algorithm Ic (loc. inex.) (Gen. t.-o.-b. appr.)
$1/h = 6N^{1/3}$ – composite material no. 1 – irregular partitioning

N (#cores)	κ	*its*	$\lvert\Pi'\rvert$	$\lvert\Pi\rvert$	*nnz*	*d.o.f.*	*time (min)*	*eff.*
64	83.84	50	2277	998	1.39e+6	3.11e+5	12.32	**100%**
125	72.08	59	5127	2247	3.71e+6	6.00e+5	18.37	67%
216	54.82	60	9483	4252	7.49e+6	1.02e+6	18.95	65%
343	75.41	64	15579	7349	1.30e+7	1.62e+6	24.64	50%
512	60.58	65	24705	10811	2.10e+7	2.41e+6	26.92	46%

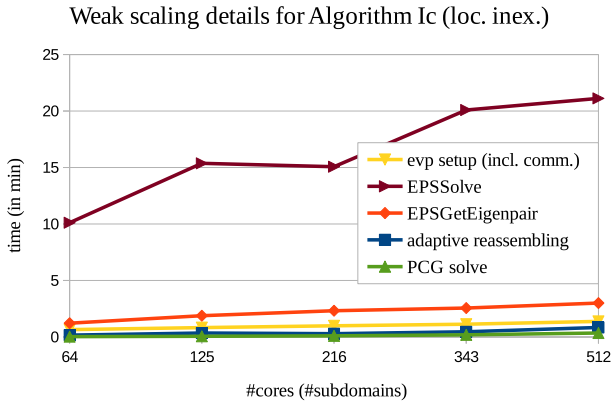

Figure 7.6: *Weak scaling details for Algoritm Ic (loc. inex.) with one subdomain per core, stiffness-scaling, and generalized transformation-of-basis approach for compressible linear elasticity (composite material no. 1; irregular partitioning).* Plot of the weak scaling of the most expensive code parts of adaptive FETI-DP for composite material no. 1 with an irregular decomposition of the unit cube (cf. Figure 5.1 and Table 7.2). The parts `EPSSolve` and `EPSGetEigenpair` refer to the multiple calls of the corresponding SLEPc functions (timed in total per subdomain).

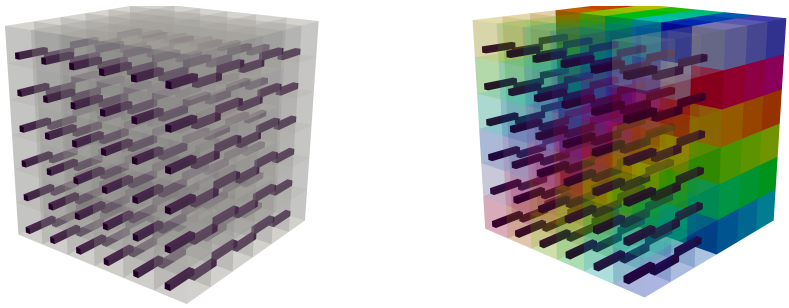

Figure 7.7: *Composite material no. 3 on the unit cube for 216 subdomains (coefficients and regular partitioning).* 36 beams of a stiff material with $\mathrm{E}_2 = 1e{+}6$, shown in dark purple, are cut at the interface and arranged with offset. The surrounding material is a soft matrix material with $\mathrm{E}_1 = 1$, shown in light, half-transparent gray, (left). Regular decomposition for 216 subdomains; high coefficients are again shown in dark purple; subdomains shown in different colors; left half of the domain ($x > \frac{1}{2}$) made half-transparent (right).

jumps also on edges in a regular decomposition; see Figure 7.7 (right). Note that the edge eigenvalue problems on the other edges are discarded by Algoritm Ic.

For the regular decomposition, our adaptive algorithm shows very good weak scalability from 216 to 4096 subdomains; see Table 7.3.

7.4.4 Strong parallel scaling for adaptive FETI-DP on irregular decompositions

Eventually, we now present strong scaling results for irregularly decomposed domains. We consider two different geometries and coefficient distributions. The strong scaling is conducted with one subdomain per core. The numbers of cores are all multiples of 24 in order to exploit the structure of the supercomputer magnitUDE with 24 cores per node.

The first example is that of composite material no. 1 with 64 beams of high coefficients with $\mathrm{E}_2 = 1e{+}6$ (see the corresp. run in Table 7.1 for $N = 216$). The global geometry consists of 1 027 083 degrees of freedom and 233 280 tetrahedral elements.

The second example is motivated by [78]. We consider the hemisphere $\Omega := \{(x, y, z) \in \mathbb{R}^3 \ : \ 0.8 < \|(x, y, z)^T\|_2 < 1,\ z < 0\}$ with different layers of a stiff and a soft material; see Figure 7.10 (left). The geometry and the unstructured surface mesh are created by means of SALOME v8.3.0 [111] and the NETGEN 1D-2D [118] algorithm. The surface mesh still retains a certain structure. For

Table 7.3: *Weak parallel scaling for adaptive FETI-DP (Algorithm Ic (loc. inex.)) with one subdomain per core, stiffness-scaling and generalized transformation-of-basis approach.* Compressible linear elasticity of composite material no. 3 with $\mathrm{E}_1 = 1$ and $N^{2/3}$ beams arranged with offset with $\mathrm{E}_2 = 1e+6$ on the unit cube; $\nu = 0.3$ for the whole domain; conforming $\mathcal{P}_2$ finite element discretization with $1/h = 6N^{1/3}$ and regular partitioning of the domain; see Figure 7.7. Coarse spaces for $\mathrm{TOL} = 50 \log\left(N/n_i\right)^{1/3}$ for each generalized eigenvalue problem. Notation as in Table 7.2.

Adaptive FETI-DP: Algorithm Ic (loc. inex.) (Gen. t.-o.-b. appr.)

$1/h = 6N^{1/3}$ – composite material no. 3 – regular partitioning

N (#cores)	κ	*its*	$\lvert\Pi'\rvert$	$\lvert\Pi\rvert$	*nnz*	*d.o.f.*	*time (min)*	*eff.*
216	11.25	32	375	1813	2.30e+5	1.17e+6	7.23	**100%**
512	14.97	34	1029	4581	6.18e+5	2.74e+6	7.87	92%
1000	18.85	37	2187	9479	1.35e+6	5.31e+6	7.97	91%
1728	22.50	41	3993	17214	2.57e+6	9.15e+6	8.08	89%
2744	25.69	44	6591	28430	4.36e+6	1.45e+7	8.93	81%
4096	28.34	47	10125	43694	6.84e+6	2.16e+7	9.57	76%

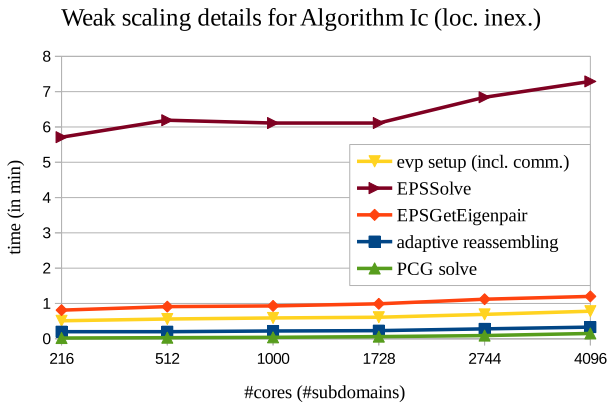

Figure 7.8: *Weak scaling details for Algoritm Ic (loc. inex.) with one subdomain per core, stiffness-scaling, and generalized transformation-of-basis approach for compressible linear elasticity (composite material no. 3; regular partitioning).* Plot of the weak scaling of the most expensive code parts of adaptive FETI-DP for composite material no. 3 with a regular decomposition of the unit cube (cf. Figure 7.7 and Table 7.3). The parts `EPSSolve` and `EPSGetEigenpair` refer to the multiple calls to the corresponding SLEPc functions (timed in total per subdomain).

Table 7.4: *Strong parallel scaling for adaptive FETI-DP (Algorithm Ic (loc. inex.)) with one subdomain per core, stiffness-scaling, and generalized transformation-of-basis approach.* Compressible linear elasticity of composite material no. 1 with $E_1 = 1$ and $N^{2/3}$ beams with $E_2 = 1e+6$ on the unit cube; $\nu = 0.3$ for the whole domain; conforming $\mathcal{P}_2$ finite element discretization with $1/h = 6N^{1/3}$ and irregular partitioning of the domain; see Figure 5.1. Coarse spaces for $\mathrm{TOL} = 50 \log\left(N/n_i\right)^{1/3}$ for each generalized eigenvalue problem. Notation as in Table 7.2.

Adaptive FETI-DP: Algorithm Ic (loc. inex.) (Gen. t.-o.-b. appr.)
1.02e+6 *d.o.f.* – composite material no. 1 – irregular partitioning

N (#cores)	κ	*its*	$\lvert\Pi'\rvert$	$\lvert\Pi\rvert$	*nnz*	*time (min)*	*eff.*
144	52.04	60	6219	3062	5.07e+6	30.50	**100%**
288	63.67	67	12504	3314	7.74e+6	16.67	91%
432	58.44	65	17823	3499	9.60e+6	8.53	119%
576	64.68	61	24090	3433	1.27e+7	5.50	138%
720	61.28	65	29691	3815	1.47e+7	4.61	132%
864	66.14	63	35277	2977	1.63e+7	4.64	110%

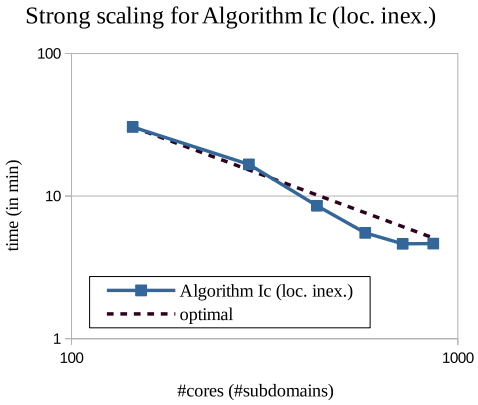

Figure 7.9: *Strong scaling for Algoritm Ic (loc. inex.) with one subdomain per core, stiffness-scaling, and generalized transformation-of-basis approach for compressible linear elasticity.* Plot of the strong scaling of adaptive FETI-DP for composite material no. 1 with an irregular decomposition of the unit cube (cf. Figure 5.1) with approx. one million degrees of freedom, from 144 to 864 cores and subdomains.

Table 7.5: *Strong parallel scaling for adaptive FETI-DP (Algorithm Ic (loc. inex.)) with one subdomain per core, stiffness-scaling, and generalized transformation-of-basis approach.* Compressible linear elasticity of a layered hemisphere with $\mathrm{E}_1 = 1$ and thin layers with $\mathrm{E}_2 = 1e+6$; $\nu = 0.3$ for the whole domain; conforming $\mathcal{P}_2$ finite element discretization with 2.58e+6 d.o.f. and irregular partitioning of the domain; see Figure 7.10. Coarse spaces for $\mathrm{TOL} = 50 \log\left(N/n_i\right)^{1/3}$ for each generalized eigenvalue problem. Notation as in Table 7.2.

Adaptive FETI-DP: Algorithm Ic (loc. inex.) (Gen. t.-o.-b. appr.)
2.58e+6 *d.o.f.* – layered hemisphere – irregular partitioning

N (#cores)	κ	*its*	$\lvert\Pi'\rvert$	$\lvert\Pi\rvert$	*nnz*	*time (min)*	*eff.*
72	100.70	85	1248	4821	3.06e+6	59.20	**100%**
144	74.90	76	3003	9557	6.62e+6	29.42	101%
288	74.31	79	9843	13807	1.34e+7	27.70	53%
576	72.04	74	24033	16262	2.17e+7	11.21	66%

the NETGEN algorithm, the discretization parameter h is only allowed to be in the narrow interval $[0.01, 0.018]$. The entire mesh then is created from the surface mesh by the Gmsh mesh generator [47]. The resulting geometry consists of 2 576 073 degrees of freedom and 581 538 tetrahedral elements.

Our hemisphere consists of five different layers of the Young modulus. As before, we always assume the Young modulus to be constant on each finite element. For each tetrahedron, we calcualte its mass center c_T and set the coefficient on the element to $\mathrm{E}_2 = 1e+6$ if $c_T > 0.98$, $c_T < 0.82$, or $c_T \in (0.89, 0.91)$ and thus obtain thin layers of a stiff material at the boundary and inside the geometry. As a consquence of the unstructured mesh, the layers are not smooth; see Figure 7.10 (left) for the coefficient distribution.

In Table 7.5, we have optimal speedup from 72 to 144 cores. We also see that the gain in speedup from 144 to 288 cores is very low. However, we again have a significant speedup when stepping to 576 cores; see also Figure 7.11 (left). This results from the fact that, although the solution time per eigenvalue problem reduces when chosing 288 instead of 144 cores, the maximum number of local eigenvalue problems increases significantly. From 288 to 576, there is no significant increase in the maximum number of eigenvalue problems per core and the maximum solution time can be reduced from approx. 23 or 21 (for 144 and 288 subdomains, respectively) minutes to approx. nine minutes; see Figure 7.11 (right). We clearly benefit from the superlinear complexicity of the eigensolver and the reduced size of the local problems.

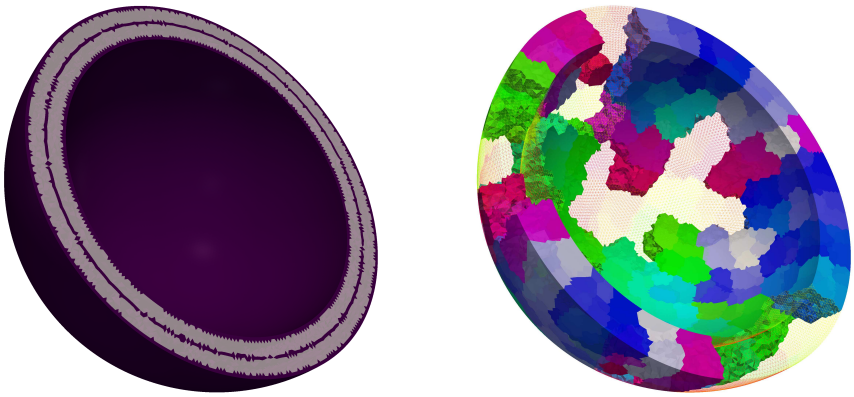

Figure 7.10: *Layered hemisphere with an unstructured mesh (coefficients and irregular partitioning).* Layered hemisphere with thin layers of a stiff material at the boundary and inside the hemisphere with $E_2 = 1e+6$, shown in dark purple, and thicker layers of a soft matrix material with $E_1 = 1$, shown in light, half-transparent gray, (left). Hemisphere geometry for 576 subdomains, certain subdomains shown in different solid colors, for the remaining subdomains the corresponding mesh is shown in different colors (right).

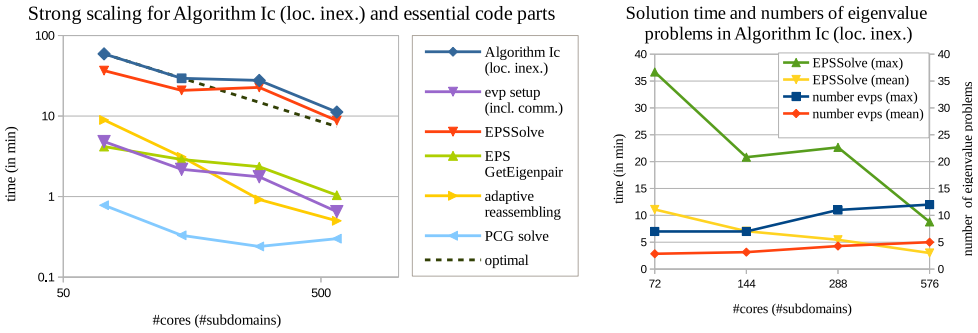

Figure 7.11: *Strong scaling for Algoritm Ic (loc. inex.) with one subdomain per core, stiffness-scaling, and generalized transformation-of-basis approach.* Plot of the strong scaling of adaptive FETI-DP for linear elasticity on a layered hemisphere with an irregular decomposition (cf. Figure 7.10) and approx. 2.58 million degrees of freedom, from 72 to 576 cores and subdomains (left). Details for the maximum and the arithmetic mean of the numbers of local eigenvalue problems and of the summed solution time both per core (right).

Note that, for the considered geometry on the hemisphere, the main memory of the normal computing nodes on magnitUDE (64 GB per node, 2.6 GB per core) might not be sufficient and computing nodes with increased main memory (256 GB per node, 10.6 GB per core) have been requested. For $N \in \{72, 144\}$ subdomains the high memory demand arises from the local generalized eigenvalue problems, which are very large, then. For 72 subdomains and cores, the peak memory consumption is approx. 200 GB per node (8.3 GB per core). For 144 subdomains and cores, the peak memory consumption is about 125 GB per node (5.2 GB per core). For $N = 576$, the increased memory demand comes from the coarse problem, which is already very large, a priori.

8 Conclusion and Future Work

8.1 Conclusion

In this thesis, the nonoverlapping domain decomposition methods FETI-DP and BDDC, to solve large-scale finite element problems, have been considered. These methods are widely-used and highly scalable domain decomposition methods, which have been studied extensively. Depending on the considered problem, which is defined by the underlying partial differential equation, different, sophisticated techniques to obtain fast and robust methods have been introduced in the past.

Important ingredients for fast and robust FETI-DP and BDDC methods are scalings of the variables shared between multiple subdomains as well as coarse space enrichments. In Chapter 4, we have given an overview of popular techniques to implement coarse space enrichements. From a theoretical point of view, it is naturally of interest to have a correspondence between these methods to transfer information of the spectra from one method to the other. In [80], a correspondence between the deflation or balancing approach and the standard transformation-of-basis approach was proven for the case of a constant scaling on any face and any edge. Though, if a nondiagonal or nonconstant scaling and a second set (also *a posteriori* set) of constraints are used, an interaction between dual and primal variables can occur in the deflation and the balancing approach. This interaction can violate the assumptions used in the proofs of FETI-DP and BDDC methods using the standard transformation-of-basis approach. The interaction is generally necessary if scaling-dependent constraints are chosen for the second set of constraints. Allowing for this interaction, the condition number bound can be retained for the transformed and assembled system. For diagonal scalings, the mentioned interaction only occurs for nonnodal constraints. In Section 4.5, we have thus introduced the generalized transformation-of-basis approach, which admits those interactions between dual and primal variables and for which a corresponding deflation or balancing approach can be derived.

If the parameters of the underlying partial differential equation become arbitrarily or highly heterogeneous, classical methods might not converge anymore,

even if sophisticated a priori coarse spaces and scalings are used. A remedy is given by adaptive domain decomposition methods. In these methods, (problem-dependent) eigenvalue problems are solved to set up an additional set of (a posteriori) constraints. In Chapter 5, based on [93, 120, 94, 75], we have introduced a robust adaptive method for three-dimensional problems. We have also presented different strategies to (heuristically) reduce the computational overhead. Then, the adaptive coarse spaces have been implemented by the balancing approach. The extensive set of numerical simulations has shown that the previously known coarse spaces of [93, 120, 94, 75] might not be sufficient to obtain convergence if highly heterogeneous three-dimensional problems are considered. In contrast, our method, which is theoretically proven to be robust, as well as all the heuristical variants introduced here have been found to be robust for any problem setting that was considered. We have seen that the heuristics can reduce the computational overhead of the adaptive methods significantly.

If the considered problem becomes arbitrarily difficult, the coarse space of an adaptive method can become very large. Then, the direct solution of the coarse problem can become impossible due to memory limitations. However, the deflation and the balancing approach are fragile with respect to inexactness of the coarse solution; see, e.g., [80]. The use of partial finite element assembly, after a transformation of basis, is more adequate to implement the constraints. In Chapter 6, we use the generalized transformation-of-basis approach to derive an adaptive algorithm corresponding to the algorithm using the balancing approach. We have presented results to show that the methods using the generalized transformation-of-basis and the balancing approach converge correspondingly at essentially the same costs. We have also presented results for different a priori chosen scalings and shown that the widely-used (diagonal) ρ- and stiffness-scaling, respectively, only produce about 10-15% additional adaptive constraints compared to the popular nondiagonal scalings. It has been shown that the size of the adaptive coarse problem can be reduced significantly if slightly larger condition numbers and larger numbers of iterations are allowed. For the solution of the eigenvalue problem, the user-defined tolerance should not be chosen too small.

In Chapter 7, we have presented an efficient parallel implementation of our adaptive algorithms. We have considered weak and strong parallel scalability of some of our adaptive Algorithm Ic using only rough approximates to the local eigenvectors. Algorithm Ic discards edge eigenvalue problems and edge constraints from face eigenvalue problems if the neighborhood of the edge consists

of an homogeneously soft material; cf. the detailed description in Section 5.2.2. For regular as well as irregular domain decompositions, we have shown good weak parallel scalability of our adaptive algorithm. For regular decompositions, we still achieve an efficiency of 76% if the number of cores and subdomains is increased from 216 to 4096. We have also considered strong parallel scalability for different geometries and irregular domain decompositions. Specifically, we have considered the unit cube with an irregular decomposition as well as an unstructured mesh of a hemisphere and obtained good results for the strong parallel scalability. For the unstructured mesh of the hemisphere with about 2.6 million degrees of freedom, we achieve 66% efficiency if the number of subdomains and cores is increased from 72 to 576.

8.2 Future Work

We have presented an efficient parallel implementation of a robust FETI-DP method for three-dimensional problems. However, we have also shown that a certain load imbalance exists if the eigenvalue problems of pairs of subdomains are solved on the rank of the subdomain with the lower index. More sophisticated ideas for the distribution of the eigenvalue problems, without creating a communication overhead, should be studied.

To further reduce the coarse space dimension and the computation time, additional strategies to detect and discard eigenvalue problems, which do not accelerate the convergence significantly, should be studied. These eigenvalue problems need not to be communicated, set up and solved. Their possible constraints would only enlarge the coarse space unnecessarily and they should not be used.

Another very interesting field of study is that of adaptive Newton-Krylov methods. In these methods, a Newton method is used to compute the solution of a discretized nonlinear partial differential equation. In each Newton step, we can solve a linearized system by the FETI-DP method using the preconditioned conjugate gradient method. Although, theoretically, the adaptive coarse space had to be computed for every single Newton step, a reuse of the coarse space of the previous step or steps is possible; see [71]. Then, the dominating computational costs of the solution of the eigenvalue problems can be saved for several Newton steps while still maintaining enhanced convergence properties for the different calls to the PCG solver.

Bibliography

[1] E. Anderson, Z. Bai, C. Bischof, S. Blackford, J. Demmel, J. Dongarra, J. Du Croz, A. Greenbaum, S. Hammarling, A. McKenney, and D. Sorensen, LAPACK users' guide, third ed., Society for Industrial and Applied Mathematics, Philadelphia, PA, 1999.

[2] Santiago Badia, Alberto F. Martín, and Javier Principe, A highly scalable parallel implementation of balancing domain decomposition by constraints, SIAM J. Sci. Comput. **36** (2014), no. 2, C190–C218.

[3] ———, Multilevel balancing domain decomposition at extreme scales, SIAM J. Sci. Comput. **38** (2016), no. 1, C22–C52.

[4] Satish Balay, Shrirang Abhyankar, Mark F. Adams, Jed Brown, Peter Brune, Kris Buschelman, Lisandro Dalcin, Victor Eijkhout, William D. Gropp, Dinesh Kaushik, Matthew G. Knepley, Lois Curfman McInnes, Karl Rupp, Barry F. Smith, Stefano Zampini, and Hong Zhang, PETSc users manual, Tech. Report ANL-95/11 - Revision 3.8, Argonne National Laboratory, 2017.

[5] Satish Balay, William D. Gropp, Lois Curfman McInnes, and Barry F. Smith, Efficient management of parallelism in object oriented numerical software libraries, Modern Software Tools in Scientific Computing (E. Arge, A. M. Bruaset, and H. P. Langtangen, eds.), Birkhäuser Press, 1997, pp. 163–202.

[6] Lourenço Beirão da Veiga, Luca F. Pavarino, Simone Scacchi, Olof B. Widlund, and Stefano Zampini, Isogeometric BDDC preconditioners with deluxe scaling, SIAM J. Sci. Comput. **36** (2014), no. 3, A1118–A1139.

[7] ———, Adaptive selection of primal constraints for isogeometric BDDC deluxe preconditioners, SIAM J. Sci. Comput. **39** (2017), no. 1, A281–A302.

[8] Adi Ben-Israel and Thomas N. E. Greville, Generalized inverses: Theory and applications, second ed., CMS Books in Mathematics/Ouvrages de Mathématiques de la SMC, 15, Springer-Verlag, New York, 2003.

[9] Petter Bjørstad, Jacko Koster, and Piotr Krzyżanowski, Domain decomposition solvers for large scale industrial finite element problems, Applied Parallel Computing. New Paradigms for HPC in Industry and Academia (Tor Sørevik, Fredrik Manne, Assefaw Hadish Gebremedhin, and Randi Moe, eds.), Lecture Notes in Comput. Sci., vol. 1947, Springer, Berlin, 2001, pp. 373–383.

[10] Petter Bjørstad and Piotr Krzyżanowski, A flexible 2-level Neumann-Neumann method for structural analysis problems, Parallel Processing and Applied Mathematics (Roman Wyrzykowski, Jack Dongarra, Marcin Paprzycki, and Jerzy Waśniewski, eds.), Lecture Notes in Comput. Sci., vol. 2328, Springer, Berlin, 2002, pp. 387–394.

[11] J.-F. Bourgat, Roland Glowinski, Patrick Le Tallec, and Marina Vidrascu, Variational formulation and algorithm for trace operator in domain decomposition calculations, Domain decomposition methods (Los Angeles, CA, 1988), SIAM, Philadelphia, PA, 1989, pp. 3–16.

[12] Christophe Bovet, Augustin Parret-Fréaud, Nicole Spillane, and Pierre Gosselet, Adaptive multipreconditioned FETI: Scalability results and robustness assessment, Computers & Structures **193** (2017), 1–20.

[13] Dietrich Braess, Finite Elemente, 5th, revised ed., Springer-Verlag, Berlin Heidelberg, 2013.

[14] Susanne C. Brenner and L. Ridgway Scott, The mathematical theory of finite element methods, third ed., Texts in applied mathematics, vol. 15, Springer, New York, 2008.

[15] Franco Brezzi and Michel Fortin, Mixed and hybrid finite element methods, Springer Series in Computational Mathematics, vol. 15, Springer-Verlag, New York Berlin Heidelberg, 1991.

[16] Juan G. Calvo, A BDDC algorithm with deluxe scaling for $H(\mathrm{curl})$ in two dimensions with irregular subdomains, Math. Comp. **85** (2016), no. 299, 1085–1111.

[17] Juan G. Calvo and Olof B. Widlund, An adaptive choice of primal constraints for BDDC domain decomposition algorithms, Electronic Transactions on Numerical Analysis **45** (2016), 524–544.

[18] Eric T. Chung and Hyea Hyun Kim, A deluxe FETI-DP algorithm for a hybrid staggered discontinuous Galerkin method for $H(\mathrm{curl})$-elliptic problems, Internat. J. Numer. Methods Engrg. **98** (2014), no. 1, 1–23.

[19] Philippe G. Ciarlet, Mathematical elasticity, volume 1: Three-dimensional elasticity, Studies in mathematics and its applications, vol. 20, Elsevier Science Publishers B.V., Amsterdam New York Oxford, 1988.

[20] Jean-Michel Cros, A preconditioner for the Schur complement domain decomposition method, National Autonomous University of Mexico (UNAM), Mexico City, Mexico, 2003, Proceedings of the 14th International Conference on Domain Decomposition Methods in Science and Engineerung, Cocoyoc, Mexico, January 6-12, 2002; 8 p., pp. 373–380.

[21] Yann-Hervé De Roeck and Patrick Le Tallec, Analysis and test of a local domain-decomposition preconditioner, Fourth International Symposium on Domain Decomposition Methods for Partial Differential Equations (Moscow, 1990), SIAM, Philadelphia, PA, 1991, pp. 112–128.

[22] Clark Dohrmann and Clemens Pechstein, In C. Pechstein, Modern domain decomposition solvers - BDDC, deluxe scaling, and an algebraic approach, Slides to a talk at NuMa Seminar, JKU Linz, December 10th, 2013, `http://people.ricam.oeaw.ac.at/c.pechstein/pechstein-bddc2013.pdf` (2013).

[23] Clark R. Dohrmann, A preconditioner for substructuring based on constrained energy minimization, SIAM J. Sci. Comput. **25** (2003), no. 1, 246–258.

[24] Clark R. Dohrmann and Olof B. Widlund, Some recent tools and a BDDC algorithm for 3D problems in $H(\mathrm{curl})$, Domain decomposition methods in Science and Engineering XX (Randolph Bank, Michael Holst, Olof Widlund, and Jinchao Xu, eds.), Lecture Notes in Computational Science and Engineering, vol. 91, Springer, Heidelberg, 2013, pp. 15–25.

[25] Victorita Dolean, Frédéric Nataf, Robert Scheichl, and Nicole Spillane, Analysis of a two-level Schwarz method with coarse spaces based on local Dirichlet-to-Neumann maps, Comput. Methods Appl. Math. **12** (2012), no. 4, 391–414.

[26] Zdeněk Dostál, Conjugate gradient method with preconditioning by projector, International Journal of Computer Mathematics **23** (1988), no. 3-4, 315–323.

[27] ———, Projector preconditioning and domain decomposition methods, Applied Mathematics and Computation **37** (1990), no. 2, 75–81.

[28] Maksymilian Dryja, Marcus V. Sarkis, and Olof B. Widlund, Multilevel Schwarz methods for elliptic problems with discontinuous coefficients in three dimensions, Numer. Math. **72** (1996), no. 3, 313–348.

[29] Maksymilian Dryja, Barry F. Smith, and Olof B. Widlund, Schwarz analysis of iterative substructuring algorithms for elliptic problems in three dimensions, SIAM J. Numer. Anal. **31** (1994), no. 6, 1662–1694.

[30] Maksymilian Dryja and Olof B. Widlund, Additive Schwarz methods for elliptic finite element problems in three dimensions, Fifth International Symposium on Domain Decomposition Methods for Partial Differential Equations (Norfolk, VA, 1991), SIAM, Philadelphia, PA, 1992, pp. 3–18.

[31] ———, Schwarz methods of Neumann-Neumann type for three-dimensional elliptic finite element problems, Comm. Pure Appl. Math. **48** (1995), no. 2, 121–155.

[32] Erik Eikeland, Leszek Marcinkowski, and Talal Rahman, Overlapping Schwarz methods with adaptive coarse spaces for multiscale problems in 3D, Tech. report, 2016, `https://arxiv.org/abs/1611.00968`.

[33] Lawrence C. Evans, Partial differential equations, second ed., Graduate Studies in Mathematics, vol. 19, American Mathematical Society, Providence, 2010.

[34] Charbel Farhat, Po-Shu Chen, and Jan Mandel, A scalable Lagrange multiplier based domain decomposition method for time-dependent problems, International Journal for Numerical Methods in Engineering **38** (1995), no. 22, 3831–3853.

[35] Charbel Farhat, Po-Shu Chen, Jan Mandel, and François-Xavier Xavier Roux, The two-level FETI method. II. Extension to shell problems, parallel implementation and performance results, Comput. Methods Appl. Mech. Engrg. **155** (1998), no. 1-2, 153–179.

[36] Charbel Farhat, Po-Shu Chen, Franck Risler, and François-Xavier Roux, A unified framework for accelerating the convergence of iterative substructuring methods with Lagrange multipliers, Internat. J. Numer. Methods Engrg. **42** (1998), no. 2, 257–288.

[37] Charbel Farhat, Michael Lesoinne, and Kendall Pierson, A scalable dual-primal domain decomposition method, Numer. Linear Algebra Appl.

7 (2000), no. 7-8, 687–714, Preconditioning techniques for large sparse matrix problems in industrial applications (Minneapolis, MN, 1999).

[38] Charbel Farhat, Michel Lesoinne, Patrick Le Tallec, Kendall Pierson, and Daniel Rixen, FETI-DP: a dual-primal unified FETI method. I. A faster alternative to the two-level FETI method, Internat. J. Numer. Methods Engrg. **50** (2001), no. 7, 1523–1544.

[39] Charbel Farhat and Jan Mandel, The two-level FETI method for static and dynamic plate problems. I. An optimal iterative solver for biharmonic systems, Comput. Methods Appl. Mech. Engrg. **155** (1998), no. 1-2, 129–151.

[40] Charbel Farhat, Jan Mandel, and François-Xavier Roux, Optimal convergence properties of the FETI domain decomposition method, Computer Methods in Applied Mechanics and Engineering **115** (1994), 365–385.

[41] Charbel Farhat and François-Xavier Roux, A method of Finite Element Tearing and Interconnecting and its parallel solution algorithm, Int. J. Numer. Meth. Engrg. **32** (1991), 1205–1227.

[42] Charbel Farhat and François-Xavier Roux, Implicit parallel processing in structural mechanics, Computational Mechanics Advances (John Tinsley Oden, ed.), vol. 2, North-Holland, 1994, pp. 1–124.

[43] Yannis Fragakis and Manolis Papadrakakis, The mosaic of high performance domain decomposition methods for structural mechanics: Formulation, interrelation and numerical efficiency of primal and dual methods, Computer Methods in Applied Mechanics and Engineering **192** (2003), no. 35-36, 3799–3830.

[44] Juan Galvis and Yalchin Efendiev, Domain decomposition preconditioners for multiscale flows in high-contrast media, Multiscale Model. Simul. **8** (2010), no. 4, 1461–1483.

[45] ———, Domain decomposition preconditioners for multiscale flows in high contrast media: reduced dimension coarse spaces, Multiscale Model. Simul. **8** (2010), no. 5, 1621–1644.

[46] Martin J. Gander, Atle Loneland, and Talal Rahman, Analysis of a new harmonically enriched multiscale coarse space for domain decomposition methods, Tech. report, 2015, `https://arxiv.org/abs/1512.05285`.

[47] Christophe Geuzaine and Jean-François Remacle, Gmsh: A 3-D finite element mesh generator with built-in pre- and post-processing facilities, Internat. J. Numer. Methods Engrg. **79** (2009), no. 11, 1309–1331.

[48] Sabrina Gippert, Domain decomposition methods for elastic materials with compressible and almost incompressible components, Ph.D. thesis, Universität Duisburg-Essen, 2012.

[49] Sabrina Gippert, Axel Klawonn, and Oliver Rheinbach, Analysis of FETI-DP and BDDC for linear elasticity in 3D with almost incompressible components and varying coefficients inside subdomains, SIAM J. Numer. Anal. **50** (2012), no. 5, 2208–2236.

[50] ———, A deflation based coarse space in Dual-Primal FETI methods for almost incompressible elasticity, Numerical Mathematics and Advanced Applications - ENUMATH 2013 (Assyr Abdulle, Simone Deparis, Daniel Kressner, Fabio Nobile, and Marco Picasso, eds.), Lecture Notes in Computational Science and Engineering, vol. 103, Springer International Publishing, 2015, pp. 573–581.

[51] Paulo Goldfeld, Luca F. Pavarino, and Olof B. Widlund, Balancing Neumann-Neumann preconditioners for mixed approximations of heterogeneous problems in linear elasticity, Numerische Mathematik **95** (2003), no. 2, 283–324.

[52] Pierre Gosselet and Christian Rey, Non-overlapping domain decomposition methods in structural mechanics, Archives of Computational Methods in Engineering **13** (2006), no. 4, 515–572.

[53] Pierre Gosselet, Christian Rey, and Daniel J. Rixen, On the initial estimate of interface forces in FETI methods, Comput. Methods Appl. Mech. Eng. **192** (2003), no. 25, 2749–2764.

[54] Alexander Heinlein, Axel Klawonn, Jascha Knepper, and Oliver Rheinbach, Multiscale coarse spaces for overlapping Schwarz methods based on the ACMS space in 2D, Tech. report, Technische Universität Bergakademie Freiberg, Fakultät für Mathematik und Informatik, Preprint 2016-09, 2016, `http://tu-freiberg.de/fakult1/forschung/preprints`; Submitted for publication.

[55] V. Hernández, J. E. Román, A. Tomás, and V. Vidal, Krylov-Schur methods in SLEPc, Tech. report, D. Sistemes Informàtics i Computació,

Universitat Politècnica de València, 2007, SLEPc Technical Report STR-07, `http://slepc.upv.es/documentation/reports/str7.pdf`.

[56] Vicente Hernández, Jose E. Román, and Vicente Vidal, SLEPc: A scalable and flexible toolkit for the solution of eigenvalue problems, ACM Trans. Math. Software **31** (2005), no. 3, 351–362.

[57] Intel(R), Intel(R) Math Kernel Library developer reference, `https://software.intel.com/en-us/articles/mkl-reference-manual`, accessed: 2018-01-10, 2018.

[58] Marta Jarošová, Axel Klawonn, and Oliver Rheinbach, Projector preconditioning and transformation of basis in FETI-DP algorithms for contact problems, Math. Comput. Simulation **82** (2012), no. 10, 1894–1907.

[59] George Karypis and Vipin Kumar, Metis, unstructured graph partitioning and sparse matrix ordering system. version 2.0, Tech. report, University of Minnesota, Department of Computer Science, Minneapolis, MN 55455, August 1995.

[60] ———, A fast and high quality multilevel scheme for partitioning irregular graphs, SIAM J. Sci. Comput. **20** (1998), no. 1, 359–392.

[61] David Keyes, Domain decomposition: A bridge between nature and parallel computers, Tech. report, 1992, NASA Contractor Report 189709, ICASE Report No. 92-44, `https://ntrs.nasa.gov/archive/nasa/casi.ntrs.nasa.gov/19930002058.pdf`.

[62] Hyea Hyun Kim, Eric Chung, and Junxian Wang, BDDC and FETI-DP preconditioners with adaptive coarse spaces for three-dimensional elliptic problems with oscillatory and high contrast coefficients, J. Comput. Phys. **349** (2017), 191–214.

[63] Hyea Hyun Kim and Eric T. Chung, A BDDC algorithm with enriched coarse spaces for two-dimensional elliptic problems with oscillatory and high contrast coefficients, Multiscale Model. Simul. **13** (2015), no. 2, 571–593.

[64] Axel Klawonn, Martin Kühn, and Oliver Rheinbach, Adaptive coarse spaces for FETI-DP in three dimensions, SIAM J. Sci. Comput. **38** (2016), no. 5, A2880–A2911.

[65] ———, Using local spectral information in domain decomposition methods–a brief overview in a nutshell, Proc. Appl. Math. Mech. **16** (2016), 729–730.

[66] ———, Adaptive coarse spaces for FETI-DP in three dimensions with applications to heterogeneous diffusion problems, Domain Decomposition Methods in Science and Engineering XXIII (Chang-Ock Lee, Xiao-Chuan Cai, David E. Keyes, Hyea Hyun Kim, Axel Klawonn, Eun-Jae Park, and Olof B. Widlund, eds.), Lecture Notes in Computational Science and Engineering, vol. 116, Springer International Publishing, Cham, 2017, pp. 187–196.

[67] ———, Coarse spaces for FETI-DP and BDDC methods for heterogeneous problems: Connections of deflation and a generalized transformation-of-basis approach, Tech. report, Technische Universität Bergakademie Freiberg, Fakultät für Mathematik und Informatik, Preprint 2017-01, 2017, `http://tu-freiberg.de/fakult1/forschung/preprints`; submitted for publication.

[68] ———, Adaptive FETI-DP and BDDC methods with a generalized transformation of basis for heterogeneous problems, Electronic Transactions on Numerical Analysis (ETNA) **49** (2018), 1–27, submitted July 26, 2017; accepted January 11, 2018. Special volume of ETNA honoring Olof Widlund. Also Preprint 2017-01 at `http://tu-freiberg.de/fakult1/forschung/preprints`.

[69] ———, On a parallel implementation of adaptive FETI-DP with a generalized transformation-of-basis approach, Tech. report, 2018, In preparation.

[70] ———, Preconditioning of iterative eigenvalue problem solvers in adaptive FETI-DP, Springer International Publishing, Cham, 2018, Accepted for publication in the proceedings of the International Conference on Domain Decomposition Methods XXIV, Svalbard, Norway, February 6-10, 2017.

[71] Axel Klawonn, Martin Lanser, Balthasar Niehoff, Patrick Radtke, and Oliver Rheinbach, Newton-Krylov-FETI-DP with adaptive coarse spaces, Domain Decomposition Methods in Science and Engineering XXIII (Chang-Ock Lee, Xiao-Chuan Cai, David E. Keyes, Hyea Hyun Kim, Axel Klawonn, Eun-Jae Park, and Olof B. Widlund, eds.), Lecture Notes in

Computational Science and Engineering, vol. 116, Springer International Publishing, Cham, 2017, pp. 197–205.

[72] Axel Klawonn, Martin Lanser, Patrick Radtke, and Oliver Rheinbach, On an adaptive coarse space and on nonlinear domain decomposition, Domain decomposition methods in Science and Engineering XXI (Jocelyne Erhel, Martin J. Gander, Laurence Halpern, Gèraldine Pichot, Taoufik Sassi, and Olof Widlund, eds.), Lecture Notes in Computational Science and Engineering, vol. 98, Springer, Cham, 2014, pp. 71–83.

[73] Axel Klawonn, Martin Lanser, and Oliver Rheinbach, Toward extremely scalable nonlinear domain decomposition methods for elliptic partial differential equations, SIAM J. Sci. Comput. **37** (2015), no. 6, C667–C696.

[74] Axel Klawonn, Patrick Radtke, and Oliver Rheinbach, FETI-DP methods with an adaptive coarse space, SIAM J. Numer. Anal. **53** (2015), no. 1, 297–320.

[75] ———, A comparison of adaptive coarse spaces for iterative substructuring in two dimensions, Electron. Trans. Numer. Anal. **45** (2016), 75–106.

[76] ———, A comparison of adaptive coarse spaces for iterative substructuring in two dimensions, Tech. report, Technische Universität Bergakademie Freiberg, Fakultät für Mathematik und Informatik, Preprint 2015-05, July 2, 2015, `http://tu-freiberg.de/fakult1/forschung/preprints`.

[77] Axel Klawonn and Oliver Rheinbach, A parallel implementation of dual-primal FETI methods for three-dimensional linear elasticity using a transformation of basis, SIAM J. Sci. Comput. **28** (2006), no. 5, 1886–1906.

[78] ———, Robust FETI-DP methods for heterogeneous three dimensional elasticity problems, Comput. Methods Appl. Mech. Engrg. **196** (2007), no. 8, 1400–1414.

[79] ———, Highly scalable parallel domain decomposition methods with an application to biomechanics, ZAMM Z. Angew. Math. Mech. **90** (2010), no. 1, 5–32.

[80] ———, Deflation, projector preconditioning, and balancing in iterative substructuring methods: connections and new results, SIAM J. Sci. Comput. **34** (2012), no. 1, A459–A484.

[81] Axel Klawonn and Olof B. Widlund, FETI and Neumann-Neumann iterative substructuring methods: connections and new results, Comm. Pure Appl. Math. **54** (2001), no. 1, 57–90.

[82] ———, Dual-primal FETI methods for linear elasticity, Comm. Pure Appl. Math. **59** (2006), no. 11, 1523–1572.

[83] Axel Klawonn, Olof B. Widlund, and Maksymilian Dryja, Dual-primal FETI methods for three-dimensional elliptic problems with heterogeneous coefficients, SIAM J. Numer. Anal. **40** (2002), no. 1, 159–179.

[84] ———, Dual-Primal FETI Methods with face constraints, Recent Developments in Domain Decomposition Methods (Luca F. Pavarino and Andrea Toselli, eds.), Lecture Notes in Computational Science and Engineering, vol. 23, Springer, Berlin Heidelberg, 2002, pp. 27–40.

[85] Andrew V. Knyazev, Toward the optimal preconditioned eigensolver: Locally optimal block preconditioned conjugate gradient method; MATLAB implementation, `https://www.mathworks.com/matlabcentral/fileexchange/48-lobpcg-m`, accessed: 2015-12-09.

[86] ———, Toward the optimal preconditioned eigensolver: Locally optimal block preconditioned conjugate gradient method, SIAM J. Sci. Comput. **23** (2001), no. 2, 517–541.

[87] Martin Lanser, Nonlinear FETI-DP and BDDC methods, Ph.D. thesis, Universität zu Köln, 2015.

[88] Patrick Le Tallec, Domain decomposition methods in computational mechanics, Computational Mechanics Advances (John Tinsley Oden, ed.), vol. 1, North-Holland, 1994, pp. 121–220.

[89] Jing Li and Olof B. Widlund, FETI-DP, BDDC, and block Cholesky methods, International Journal for Numerical Methods in Engineering **66** (2006), no. 2, 250–271.

[90] Jan Mandel, Balancing domain decomposition, Communications in Numerical Methods in Engineering **9** (1993), no. 3, 233–241.

[91] Jan Mandel and Marian Brezina, Balancing domain decomposition for problems with large jumps in coefficients, Math. Comp. **65** (1996), no. 216, 1387–1401.

[92] Jan Mandel, Clark R. Dohrmann, and Radek Tezaur, An algebraic theory for primal and dual substructuring methods by constraints, Appl. Numer. Math. **54** (2005), no. 2, 167–193.

[93] Jan Mandel and Bedřich Sousedík, Adaptive selection of face coarse degrees of freedom in the BDDC and the FETI-DP iterative substructuring methods, Comput. Methods Appl. Mech. Engrg. **196** (2007), no. 8, 1389–1399.

[94] Jan Mandel, Bedřich Sousedík, and Jakub Šístek, Adaptive BDDC in three dimensions, Math. Comput. Simulation **82** (2012), no. 10, 1812–1831.

[95] Jan Mandel and Radek Tezaur, On the convergence of a dual-primal substructuring method, Numer. Math. **88** (2001), no. 3, 543–558.

[96] Tarek P. A. Mathew, Domain decomposition methods for the numerical solution of partial differential equations, Lecture Notes in Computational Science and Engineering, vol. 61, Springer-Verlag, Berlin, 2008.

[97] Reinhard Nabben and Cornelis Vuik, A comparison of deflation and the balancing preconditioner, SIAM J. Sci. Comput. **27** (2006), no. 5, 1742–1759.

[98] Frédéric Nataf, Hua Xiang, and Victorita Dolean, A two level domain decomposition preconditioner based on local Dirichlet-to-Neumann maps, C. R. Math. Acad. Sci. Paris **348** (2010), no. 21-22, 1163–1167.

[99] Frédéric Nataf, Hua Xiang, Victorita Dolean, and Nicole Spillane, A coarse space construction based on local Dirichlet-to-Neumann maps, SIAM J. Sci. Comput. **33** (2011), no. 4, 1623–1642.

[100] Roy A. Nicolaides, Deflation of conjugate gradients with applications to boundary value problems, SIAM J. Numer. Anal. **24** (1987), no. 2, 355–365.

[101] Duk-Soon Oh, Olof B. Widlund, Stefano Zampini, and Clark R. Dohrmann, BDDC Algorithms with deluxe scaling and adaptive selection of primal constraints for Raviart-Thomas vector fields, Math. Comp. **87** (2018), no. 310, 659–692.

[102] Luca F. Pavarino, Olof B. Widlund, and Stefano Zampini, BDDC preconditioners for spectral element discretizations of almost incompressible elasticity in three dimensions, SIAM J. Sci. Comput. **32** (2010), no. 6, 3604–3626.

[103] Clemens Pechstein and Clark R. Dohrmann, A unified framework for adaptive BDDC, Electron. Trans. Numer. Anal. **46** (2017), 273–336.

[104] Clemens Pechstein and Robert Scheichl, Analysis of FETI methods for multiscale PDEs, Numer. Math. **111** (2008), no. 2, 293–333.

[105] ———, Analysis of FETI methods for multiscale PDEs. Part II: interface variation, Numer. Math. **118** (2011), no. 3, 485–529.

[106] ———, Weighted Poincaré inequalities, IMA J. Numer. Anal. **33** (2013), no. 2, 652–686.

[107] Kendall Hugh Pierson, A family of domain decomposition methods for the massively parallel solution of computational mechanics problems, Ph.D. thesis, University of Colorado, 2000.

[108] Alfio Quarteroni and Alberto Valli, Numerical approximation of partial differential equations, second printing ed., Springer Series in Computational Mathematics, vol. 23, Springer-Verlag, Berlin Heidelberg, 2008.

[109] Patrick Radtke, Adaptive coarse spaces for FETI-DP and BDDC methods, Ph.D. thesis, Universität zu Köln, 2015.

[110] Oliver Rheinbach, Parallel scalable iterative substructuring: Robust exact and inexact FETI-DP methods with applications to elasticity, Ph.D. thesis, Universität Duisburg-Essen, 2006.

[111] Andre Ribes and Christian Caremoli, Salome platform component model for numerical simulation, 31st Annual International Computer Software and Applications Conference (COMPSAC 2007), vol. 2, July 2007, pp. 553–564.

[112] Daniel J. Rixen and Charbel Farhat, A simple and efficient extension of a class of substructure based preconditioners to heterogeneous structural mechanics problems, Internat. J. Numer. Methods Engrg. **44** (1999), no. 4, 489–516.

[113] J. E. Román, C. Campos, E. Romero, and A. Tomás, SLEPc users manual, Tech. Report DSIC-II/24/02 - Revision 3.8, D. Sistemes Informàtics i Computació, Universitat Politècnica de València, 2017.

[114] Yousef Saad, Iterative methods for sparse linear systems, 2nd ed., Society for Industrial and Applied Mathematics, Philadelphia, PA, USA, 2003.

[115] Marcus V. Sarkis Martins, Schwarz preconditioners for elliptic problems with discontinuous coefficients using conforming and non-conforming elements, Ph.D. thesis, New York University, 1994.

[116] O. Schenk, K. Gärtner, and W. Fichtner, Efficient sparse *LU* factorization with left-right looking strategy on shared memory multiprocessors, BIT **40** (2000), no. 1, 158–176.

[117] Lisa Scheunemann, Daniel Balzani, Dominik Brands, and Jörg Schröder, Design of 3D statistically similar representative volume elements based on Minkowski functionals, Mechanics of Materials **90** (2015), 185–201, Proceedings of the IUTAM Symposium on Micromechanics of Defects in Solids.

[118] Joachim Schöberl, NETGEN an advancing front 2D/3D-mesh generator based on abstract rules, Computing and Visualization in Science **1** (1997), no. 1, 41–52.

[119] Barry Smith, Petter Bjørstad, and William Gropp, Domain decomposition: Parallel multilevel methods for elliptic partial differential equations, Cambridge University Press, Cambridge, 1996.

[120] Bedřich Sousedík, Comparison of some domain decomposition methods, Ph.D. thesis, Czech Technical University in Prague, 2008.

[121] ———, Adaptive-multilevel BDDC, Ph.D. thesis, University of Colorado Denver, 2010.

[122] Bedřich Sousedík, Jakub Šístek, and Jan Mandel, Adaptive-multilevel BDDC and its parallel implementation, Computing **95** (2013), no. 12, 1087–1119.

[123] Nicole Spillane, Méthodes de décomposition de domaine robustes pour les problèmes symétriques définis positifs, Ph.D. thesis, École Doctorale Paris Centre, 2014.

[124] Nicole Spillane, An adaptive multipreconditioned conjugate gradient algorithm, SIAM J. Sci. Comput. **38** (2016), no. 3, A1896–A1918.

[125] Nicole Spillane, Victorita Dolean, Patrice Hauret, Frédéric Nataf, Clemens Pechstein, and Robert Scheichl, Abstract robust coarse spaces

for systems of PDEs via generalized eigenproblems in the overlaps, Numer. Math. **126** (2014), no. 4, 741–770.

[126] ———, Achieving robustness through coarse space enrichment in the two level Schwarz framework, Domain decomposition methods in Science and Engineering XXI (Jocelyne Erhel, Martin J. Gander, Laurence Halpern, Gèraldine Pichot, Taoufik Sassi, and Olof Widlund, eds.), Lecture Notes in Computational Science and Engineering, vol. 98, Springer, Cham, 2014, pp. 447–455.

[127] Nicole Spillane and Daniel J. Rixen, Automatic spectral coarse spaces for robust finite element tearing and interconnecting and balanced domain decomposition algorithms, Internat. J. Numer. Methods Engrg. **95** (2013), no. 11, 953–990.

[128] G. W. Stewart, A Krylov-Schur algorithm for large eigenproblems, SIAM J. Matrix Anal. Appl. **23** (2001/02), no. 3, 601–614.

[129] Patrick Le Tallec, Yann-Hervé De Roeck, and Marina Vidrascu, Domain decomposition methods for large linearly elliptic three-dimensional problems, Journal of Computational and Applied Mathematics **34** (1991), no. 1, 93–117.

[130] Andrea Toselli and Olof B. Widlund, Domain Decomposition Methods - Algorithms and Theory, Springer Series in Computational Mathematics, vol. 34, Springer-Verlag, Berlin Heidelberg New York, 2005.

[131] Lubomír Říha, Tomáš Brzobohatý, Alexandros Markopoulos, Ondřej Meca, and Tomáš Kozubek, Massively parallel hybrid total FETI (HTFETI) solver, Platform for Advanced Scientific Computing Conference, PASC, ACM, 2016.

[132] Jakub Šístek, Jan Mandel, and Bedřich Sousedík, Some practical aspects of parallel adaptive BDDC method, Applications of mathematics 2012, Acad. Sci. Czech Repub. Inst. Math., Prague, 2012, pp. 253–266.

[133] Kesheng Wu and Horst Simon, Thick-restart Lanczos method for large symmetric eigenvalue problems, SIAM J. Matrix Anal. Appl. **22** (2000), no. 2, 602–616.

[134] Stefano Zampini, PCBDDC: a class of robust dual-primal methods in PETSc, SIAM J. Sci. Comput. **38** (2016), no. 5, S282–S306.

[135] Stefano Zampini and Xuemin Tu, Multilevel balancing domain decomposition by constraints deluxe algorithms with adaptive coarse spaces for flow in porous media, SIAM J. Sci. Comput. **39** (2017), no. 4, A1389–A1415.

[136] O.C. Zienkiewicz, R.L. Taylor, and David Fox, The finite element method for solid and structural mechanics, seventh ed., Butterworth-Heinemann, Oxford, 2014.

Erklärung

Ich versichere, dass ich die von mir vorgelegte Dissertation selbständig angefertigt, die benutzten Quellen und Hilfsmittel vollständig angegeben und die Stellen der Arbeit – einschließlich Tabellen, Karten und Abbildungen –, die anderen Werken im Wortlaut oder dem Sinn nach entnommen sind, in jedem Einzelfall als Entlehnung kenntlich gemacht habe; dass diese Dissertation noch keiner anderen Fakultät oder Universität zur Prüfung vorgelegen hat; dass sie – abgesehen von unten angegebenen Teilpublikationen – noch nicht veröffentlicht worden ist, sowie, dass ich eine solche Veröffentlichung vor Abschluss des Promotionsverfahrens nicht vornehmen werde. Die Bestimmungen der Promotionsordnung sind mir bekannt. Die von mir vorgelegte Dissertation ist von Herrn Prof. Dr. Axel Klawonn betreut worden.

Teilpublikationen

- **A. Klawonn, M. Kühn, O. Rheinbach**, "Adaptive Coarse Spaces for FETI-DP in Three Dimensions", SIAM J. Sci. Comput., Vol. 38(5), pp. A2880–A2911. Verfügbar in modifizierter Form als Technical Report: TU Bergakademie Freiberg Preprint 2015-11; `http://tu-freiberg.de/fakult1/forschung/preprints`

- **A. Klawonn, M. Kühn, O. Rheinbach**, "Using Local Spectral Information in Domain Decomposition Methods – A Brief Overview in a Nutshell", Proc. Appl. Math. Mech., 16: 729–730 (2016).

- **A. Klawonn, M. Kühn, O. Rheinbach**, "Adaptive coarse spaces for FETI-DP in three dimensions with applications to heterogeneous diffusion problems", Domain Decomposition Methods in Science and Engineering XXIII (Chang-Ock Lee, Xiao-Chuan Cai, David E. Keyes, Hyea Hyun Kim, Axel Klawonn, Eun-Jae Park, and Olof B. Widlund, eds.), Lecture Notes in Computational Science and Engineering, vol. 116, Springer International Publishing, Cham, 2017, pp. 187-196.

- **A. Klawonn, M. Kühn, O. Rheinbach**, "Preconditioning of iterative eigenvalue problem solvers in adaptive FETI-DP", Akzeptiert zur Publikation in den Proceedings der International Conference on Domain Decomposition Methods XXIV, Svalbard, Norway, February 6-10, 2017. Springer International Publishing, Cham, 2018.

- **A. Klawonn, M. Kühn, O. Rheinbach**,"Adaptive FETI-DP and BDDC methods with a Generalized Transformation of Basis for Heterogeneous Problems", Electronic Transactions on Numerical Analysis (ETNA) 49 (2018), pp. 1-27. Publiziert im Special Volume von ETNA zu Ehren von Olof Widlund. Verfügbar in modifizierter Form als Technical Report: TU Bergakademie Freiberg Preprint 2017-04; `http://tu-freiberg.de/fakult1/forschung/preprints`

- **A. Klawonn, M. Kühn, O. Rheinbach**, "Coarse spaces for FETI-DP and BDDC methods for heterogeneous problems: Connections of deflation and a generalized transformation-of-basis approach". Zur Publikation eingereicht. Verfügbar in modifizierter Form als Technical Report: TU Bergakademie Freiberg Preprint 2017-01; `http://tu-freiberg.de/fakult1/forschung/preprints`

Ort, Datum Unterschrift (M. Kühn)